Vol. 57 DECEMBER, 1953 No. 9

THE JOURNAL OF PHYSICAL CHEMISTRY

(Registered in U. S. Patent Office)

Founded by Wilder D. Bancroft

Marvin F. L. Johnson and Herman E. Ries, Jr.: The Structure of Cobalt Catalysts Supported on Diatomaceous Earth 865
K. Bril and P. Krumholz: The Polarographic Determination of Relative Formation Constants of Metal Complexes of Ethylenediaminetetraacetic Acid 874
S. Bywater: Thermal Degradation of Polymethyl Methacrylates 879
L. M. Watt and W. O. Milligan: X-Ray Diffraction Studies in the System BeO-In_2O_3 883
W. O. Milligan and C. R. Adams: Sorption-Desorption Studies in the System BeO-In_2O_3 885
J. Bromilow and P. A. Winsor: The Structure and Electrical Conductivity of Hydrocarbon-Based Solutions of the "Soluble Oil" Type. A Comparable Aqueous System 889
Cecil V. King and Ruth Kimmelman Schochet: The Adsorption of Silver Salts on Silver 895
Lawrence M. Kushner and Willard D. Hubbard: On the Determination of Critical Micelle Concentrations by a Bubble Pressure Method 898
H. H. G. Jellinek and J. R. Urwin: The Hydrolysis of Picolinamide and Isonicotinamide in Concentrated Hydrochloric Acid Solutions 900
J. Erskine Hawkins and James W. Vogh: The Rate of Thermal Isomerization of β-Pinene in the Vapor Phase 902
Roger L. Jarry, Fred D. Rosen, Charley F. Hale and Wallace Davis, Jr.: Liquid-Vapor Equilibrium in the System Uranium Hexafluoride-Hydrogen Fluoride 905
S. Chu Liang: On the Calculation of Thermal Transpiration 910
J. J. Chessick, F. H. Healey and A. C. Zettlemoyer: Adsorption Studies on Metals. II. Absolute Entropies of Adsorbed Molecules on Molybdenum 912
C. M. Judson, A. A. Lerew, J. K. Dixon and D. J. Salley: Radiotracer Study of Sulfate Ion Adsorption at the Air/Solution Interface in Solutions of Surface-Active Agents 916
H. M. Scholberg, R. A. Guenthner and R. I. Coon: Surface Chemistry of Fluorocarbons and their Derivatives 923
R. J. Orr and H. Leverne Williams: Kinetics of the Reactions between Iron(II) and Hydroperoxides Based upon Cumene and Cyclohexane 925
G. B. Alexander and R. K. Iler: Colloidal Silica—Determination of Particle Sizes 932
Hugo Fricke: The Maxwell-Wagner Dispersion in a Suspension of Ellipsoids 934
Mino Green and Paul H. Robinson: The Refractive Index of Germane 938
Ellis R. Lippincott, Philip Mercier and Marvin C. Tobin: The Vibrational Spectra of Some Tin and Germanium Halogen Metalorganic Compounds 939
F. Wm. Cagle, Jr., and Henry Eyring: An Application of the Absolute Rate Theory to Phase Changes in Solids 942
M. K. B. Day and V. J. Hill: The Thermal Transformations of the Aluminas and their Hydrates 946
E. Matijević and B. Težak: Coagulation Effects of Aluminum Nitrate and Aluminum Sulfate on Aqueous Sols of Silver Halides *in Statu Nascendi*. Detection of Polynuclear Complex Aluminum Ions by Means of Coagulation Measurements 951
Chester T. O'Konski and Henry C. Thacher, Jr.: The Distortion of Aerosol Droplets by an Electric Field 955
H. Benoit and P. Doty: Light Scattering from Non-Gaussian Chains 958
Harry Letaw, Jr., and Armin H. Gropp: Polarographic Studies in Formamide Solutions 964
Raymond T. Davis, Jr., and Robert W. Schiessler: Vapor Pressures of Perdeuterobenzene and of Perdeuterocyclohexane 966
Monroe H. Waxman, Benson R. Sundheim and Harry P. Gregor: Studies on Ion Exchange Resins. VI. Water Vapor Sorption by Polystyrenesulfonic Acid 969
Benson R. Sundheim, Monroe H. Waxman and Harry P. Gregor: Studies on Ion Exchange Resins. VII. Water Vapor Sorption by Cross-linked Polystyrenesulfonic Acid Resins 974

THE JOURNAL OF PHYSICAL CHEMISTRY will appear monthly in 1954
After January 1, 1954, Notes and Communications to the Editor
will be accepted for publication.

Founded by Wilder D. Bancroft

THE JOURNAL OF PHYSICAL CHEMISTRY

(Registered in U. S. Patent Office)

Published monthly (except July, August and September) by the American Chemical Society at 20th and Northampton Sts., Easton, Pa.

Entered as second-class matter at the Post Office at Easton, Pennsylvania.

The *Journal of Physical Chemistry* is devoted to the publication of selected symposia in the broad field of physical chemistry and to other contributed papers.

Manuscripts originating in the British Isles, Europe and Africa should be sent to F. C. Tompkins, The Faraday Society, 6 Gray's Inn Square, London W. C. 1, England.

Manuscripts originating elsewhere should be sent to W. Albert Noyes, Jr., Department of Chemistry, University of Rochester, Rochester 3, N. Y.

Correspondence regarding accepted copy, proofs and reprints should be directed to Assistant Editor, Allen D. Bliss, Department of Chemistry, Simmons College, 300 The Fenway, Boston 15, Mass.

Business Office: American Chemical Society, 1155 Sixteenth St., N. W., Washington 6, D. C.

Advertising Office: American Chemical Society, 332 West 42nd St., New York 36, N. Y.

Articles must be submitted in duplicate, typed and double spaced. They should have at the beginning a brief Abstract, in no case exceeding 300 words. Original drawings should accompany the manuscript. Lettering at the sides of graphs (black on white or blue) may be pencilled in, and will be typeset. Figures and tables should be held to a minimum consistent with adequate presentation of information. Photographs will not be printed on glossy paper except by special arrangement. All footnotes and references to the literature should be numbered consecutively and placed on the manuscript at the proper places. Initials of authors referred to in citations should be given. Nomenclature should conform to that used in *Chemical Abstracts*, mathematical characters marked for italic, Greek letters carefully made or annotated, and subscripts and superscripts clearly shown. Articles should be written as briefly as possible consistent with clarity and should avoid historical background unnecessary for specialists.

Symposium papers should be sent in all cases to Secretaries of Divisions sponsoring the symposium, who will be responsible for their transmittal to the Editor. The Secretary of the Division by agreement with the Editor will specify a time after which symposium papers cannot be accepted. The Editor reserves the right to refuse to publish symposium articles, for valid scientific reasons. Each symposium paper may not exceed four printed pages (about sixteen double spaced typewritten pages) in length except by prior arrangement with the Editor.

Remittances and orders for subscriptions and for single copies, notices of changes of address and new professional connections, and claims for missing numbers should be sent to the American Chemical Society, 1155 Sixteenth St., N. W., Washington 6, D. C. Changes of address for the *Journal of Physical Chemistry* must be received on or before the 30th of the preceding month.

Claims for missing numbers will not be allowed (1) if received more than sixty days from date of issue (because of delivery hazards, no claims can be honored from subscribers in Central Europe, Asia, or Pacific Islands other than Hawaii), (2) if loss was due to failure of notice of change of address to be received before the date specified in the preceding paragraph, or (3) if the reason for the claim is "missing from files."

Subscription Rates: to members of the American Chemical Society, $8.00 for 1 year, $15.00 for 2 years, $22.00 for 3 years; to nonmembers, $10.00 for 1 year, $18.00 for 2 years, $26.00 for 3 years. Postage free to countries in the Pan American Union; Canada, $0.40; all other countries, $1.20. Single copies, $1.25; foreign postage, $0.15; Canadian postage, $0.05.

The American Chemical Society and the Editors of the *Journal of Physical Chemistry* assume no responsibility for the statements and opinions advanced by contributors to THIS JOURNAL.

The American Chemical Society also publishes *Journal of the American Chemical Society*, *Chemical Abstracts*, *Industrial and Engineering Chemistry*, *Chemical and Engineering News*, *Analytical Chemistry*, and *Journal of Agricultural and Food Chemistry*. Rates on request.

(Continued from first page of cover)

F. E. Harris, E. W. Haycock and B. J. Alder: Pressure Dependence of the Dielectric Constant of Water and the Volume Contraction of Water and *n*-Butanol upon Addition of Electrolyte 978
Additions and Corrections 980
Author Index 981
Subject Index 986

THE JOURNAL OF PHYSICAL CHEMISTRY

Founded by Wilder D. Bancroft

VOL. LVII

1953

EASTON, PA.
MACK PRINTING COMPANY
1953

THE JOURNAL OF PHYSICAL CHEMISTRY

(Registered in U. S. Patent Office) (Copyright, 1954, by the American Chemical Society)

Founded by Wilder D. Bancroft

VOLUME 57 JANUARY 4, 1954 NUMBER 9

THE STRUCTURE OF COBALT CATALYSTS SUPPORTED ON DIATOMACEOUS EARTH[1]

BY MARVIN F. L. JOHNSON AND HERMAN E. RIES, JR.

Sinclair Research Laboratories, Inc., Harvey, Illinois

Received January 24, 1953

Various points are presented as evidence for the existence of catalyst-support interaction in the case of cobalt oxide precipitated in the presence of a diatomaceous earth support. A complex is believed to form which has the following properties: (1) a high surface area in small pores; (2) a sintering temperature distinct from those of cobalt oxide or silica gel; and (3) a resistance toward reduction by hydrogen to cobalt metal. The characteristic adsorption–desorption isotherms for nitrogen are discussed in terms of pore structure. The surface area of this complex increases with decreasing cobalt content and increasing support area, within certain limits. Preliminary results with supported iron oxide show some indication of the same type of pore structure while in the case of chromia the presence of support hinders the normal shrinkage during drying, leading to a large-pore structure resembling aerogels.

Introduction

In an earlier study of the effect of support structure on the structure of supported catalysts it was shown that a diatomaceous earth (Celite 337) was the most effective support insofar as the catalyst area was several times that of the unsupported catalyst.[2] It was the objective of the present investigation to obtain additional information about the structure of unreduced cobalt catalysts supported on diatomaceous earth by means of various applications of physical adsorption techniques and by a study of the degree of reduction. Anderson, Hall, Hewlett and Seligman[3] have made a somewhat similar study of unreduced cobalt catalysts. However, the structures of their catalysts more closely resemble the "unsupported-type" catalyst, such as those precipitated in the presence of non-porous titania[2] than they do the diatomaceous earth supported catalysts of the present study. It is believed that these differences may be attributed to differences in method of preparation. The differences, as well as the evidence for interaction of catalyst and support in the preparations of this Laboratory, are presented in the following discussion.

(1) Presented before the Petroleum Division of the American Chemical Society in Milwaukee in April, 1952.

(2) H. E. Ries, Jr., M. F. L. Johnson and J. S. Melik, THIS JOURNAL, **53**, 638 (1949).

(3) R. B. Anderson, W. K. Hall, H. Hewlett and B. Seligman, *J. Am. Chem. Soc.*, **69**, 3114 (1947).

Experimental

Extent of Reduction.—Measurements were made of the extent of reduction chiefly by following changes in ferromagnetism. Four to nine grams of catalyst was placed in a sample tube 3″ long provided with an inlet and an outlet for hydrogen. The tube was surrounded by a rigid coil of 30 turns of silver-plated Invar wire. This induction coil was wound upon a ceramic support provided with rigid electrical leads; the whole was placed in a non-inductively wound furnace with three heating coils, three variacs, and four thermocouples to eliminate temperature gradients. Care was taken to ensure that the top and bottom of the catalyst bed coincided with the induction coil extremities. The coil was connected in parallel with two variable condensers and in series with a high frequency resonance circuit. The adjustment of the coarse variable condenser was not altered during an experiment. The dial of the other condenser was graduated in arbitrary units of 0–300; readings of the coil inductance could be taken by increasing the dial reading to the point at which the current in the external circuit reached a minimum, the resonance point, after which there was a sharp increase. The system was calibrated by introducing a test-tube containing weighed quantities of cobalt powder mixed with diatomaceous earth into the coil, and observing the change in readings. A smooth curve was obtained, and indicated that a dial increment of 100 corresponded roughly to 1.3 g. of cobalt metal.

Dial readings, which are averages of a number of consecutive readings, were taken at room temperature before reduction of the catalyst. Reductions were carried out at the specified temperatures (Table IV) by passage of a rapid flow of purified hydrogen through the catalyst bed until the inductance readings indicated that no further changes were taking place; reduction was continued for one to two hours more. At the end of the reduction period, the catalyst was cooled in an atmosphere of flowing hydrogen. Dial read-

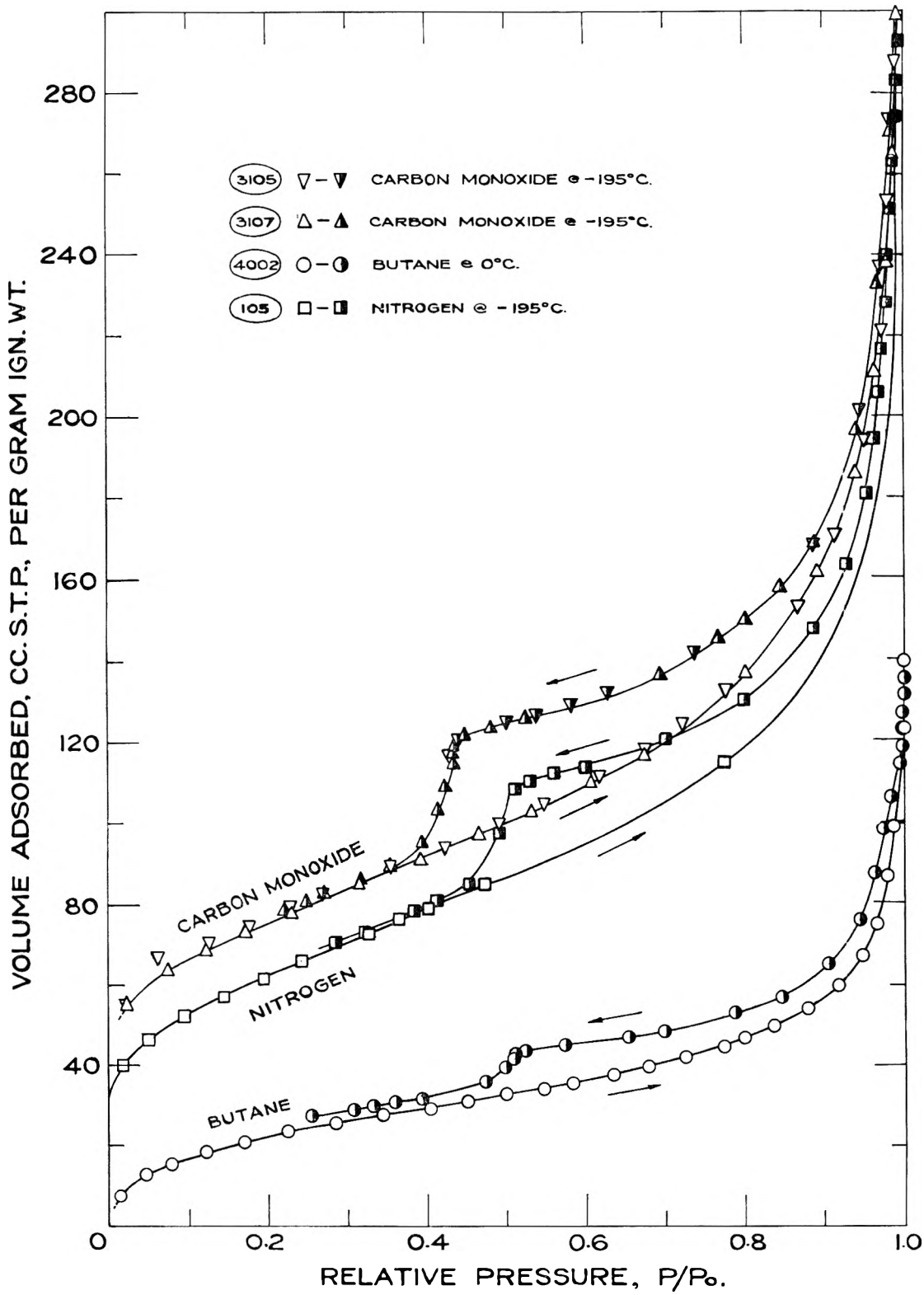

Fig. 1.—Adsorption–desorption isotherms for nitrogen, carbon monoxide and butane on H-G catalyst.

ings were again taken at room temperature. From the dial reading increment, the weight of catalyst in the coil, and the cobalt analysis, the percentage reduction of cobalt to cobalt metal was calculated.

In addition, measurements were made of hydrogen consumption. A volumetric apparatus was used, similar to that used for gas adsorption measurements, with the exception that the hydrogen was continually circulated over the catalyst and through a drying tube by means of a double Toepler pump.[4] The catalyst temperature was controlled at 358° by means of a mercury-vapor bath, at 400° by means of a Wood's metal bath in a furnace controlled by a Wheelco Potentiotrol. The pressure was held manually at one at-

(4) M F. L. Johnson and J. A. Glover, *Anal. Chem.*, **22**, 204 (1950).

TABLE I

ADSORPTION DATA FOR NITROGEN, AMMONIA, CARBON MONOXIDE AND BUTANE ON H–G CATALYST[a]

Sample age, months[b]	2	4	18	18	20	24
Adsorbate	N_2	NH_3	CO	N_2	C_4H_{10}	N_2
Temp., °C.	−195	−34	−195	−195	0	−195
B.E.T. area, sq. m./g.	267	284	263	247	179	242
H–J area, sq. m./g.	268	...	...	...	276	...
V_s, cc. S.T.P./g.[c]	344	506	340	...	116	...
P_g, cc./g.[d]	0.532	0.563	0.522	...	0.501	...
V_B, cc. S.T.P./g.[e]	130	199	120	...	42	...
P_g', cc./g.[f]	0.201	0.222	0.184	...	0.18	...
P_g-P_g', cc./g.	0.331	0.341	0.338	...	0.32	...

[a] 40% Co on Celite 337. [b] Each new sample taken from the same bottle. [c] V_s = volume adsorbed at saturation. [d] P_g = total pore volume, by conversion of V_s to liquid volume. [e] V_B = volume adsorbed at the sharp break in the desorption curve. [f] P_g = small-pore volume, by conversion of V_B to liquid volume.

TABLE II

PORE VOLUME–AREA RELATIONSHIPS

Catalyst[a]	Support	B.E.T. area, sq. m./g.	V_B, cc.[b] S.T.P./g.	P_g',[b] cc./g.	V_s,[b] cc. S.T.P./g.	P_g, cc./g.	P_g(He),[c] cc./g.
A	Alumina	173	...	...	273	0.422	0.40
S	Silica	410	160	0.248	232	.359	.54
T	Anatase	79	...	...	192	.297	.28
H–A	Celite 337	120	72	.111	338	.523	.52
H–G	Celite 337	268	130	.201	344	.532	...
Used H–G	Celite 337	62.5	31.5	.049	249	.385	...
H–I	Celite 337	217	118	.182	(329)	(.51)	.50
H–L	Celite 337	309	135	.209	443	.686	.69
Used H–L	Celite 337	86	(44)	(.068)	332	.514	.53
O-16	Celite 337	136	103	.159	308	.477	.48
M-19	Celite 337	197	111	.172	237	.367	.36
H-161	Celite 337	56.5	37.5	.058	304	.471	.47
P-79	Celite 337	188	105	.163	358	.555	.56
P-83	Celite 337	148	88	.136	(354)	(.55)	.51
P-89	Celite 337	85	47	.073	299	.463	.51
P-114	Celite 337	278	124	.192	423	.655	.71

[a] 40–42% Co on indicated support. [b] See footnotes, Table I. [c] Pore volumes determined by helium–mercury displacement.

mosphere by adjusting the bulb-buret settings, and the level of mercury in the manometer; the side of the manometer connected to the system was calibrated in units of 0.01 cc. Hydrogen consumption was plotted as a function of time. At the end of about 20 hours a straight line was obtained; the slope of this line was essentially the same for all runs, and equalled the slope obtained for a blank run with no catalyst. It was believed that this represented permeation through Pyrex; therefore, the hydrogen consumption was obtained by extrapolation to zero time.[5] This value was further corrected for the reduction of carbon dioxide (from residual carbonates) to methane by means of a mass spectrometric analysis of the residual gas. No correction was made for chemisorption. The corrected hydrogen consumption (cc. S.T.P. per gram) was converted to per cent. reduction from the weight of sample and cobalt analysis by assuming trivalent cobalt.

Adsorption Measurements.—The apparatus and technique used in this Laboratory for the determination of nitrogen adsorption–desorption isotherms have been fully described.[2,6] The adsorption measurements with carbon monoxide (−195.8°) and butane (0°) were obtained in the same manner, with the exception that for butane an apparatus with mercury-sealed stopcocks lubricated by means of a starch–mannitol–glycerol grease was necessary, in addition to an ice-water bath. Carbon monoxide was prepared by dropping formic acid into 85% phosphoric acid at 175°. The gas was purified by passage through concentrated sulfuric acid, potassium hydroxide pellets, and phosphorus pentoxide, and then stored in an evacuated reservoir. Butane from the Ohio Chemical Company was repeatedly condensed in liquid nitrogen, and non-condensable material was pumped off before admission of the butane to an evacuated reservoir. Mass spectrometer analyses of all gases used showed a minimum purity of 99.9%. For nitrogen and carbon monoxide, perfect gas law corrections of 5% at 760 mm. were used in dead space calculations; for butane the corrections were 10.8% at 0° and 3.2% for the room temperature portion of the gas.[7] In all cases, vapor pressure thermometers filled with adsorbate were employed to measure p_0, the saturation pressure, for each point of the isotherm. Adsorptions are expressed as cc. S.T.P./g. of sample, using the ignited weights of the samples.

The preparation of H–G catalyst has previously been described[2]; all other supported catalysts were prepared in essentially the same manner under the supervision of Dr. L. E. Olson.[8] It should be noted that this involves the addition of a hot cobalt salt solution to a hot slurry of support in sodium carbonate solution; the precipitates were washed, dried at 110°, formed into 1/8" pellets and calcined at 340°. This is in sharp contrast to the procedure employed by Anderson, *et al.*,[3] in which the support was added *during* or *after* the precipitation of cobalt. Results of the present study indicate that this difference in preparational procedure may be responsible for the difference in catalyst structure.

(5) The absolute rate of hydrogen permeation at 358° was 0.37 cc. (S.T.P.)/hr., from a sample bulb consisting of a 30-mm. length of 13 mm. Pyrex tubing plus a concentric preheat coil consisting of seven turns of 5 mm. tubing.

(6) H. E. Ries, Jr., R. A. Van Nordstrand and J. W. Teter, *Ind. Eng. Chem.*, **37**, 311 (1945).

(7) S. Brunauer and P. H. Emmett, *J. Am. Chem. Soc.*, **59**, 1553 (1937).

(8) J. W. Teter, U. S. Patent 2,381,473 (August 7, 1945); *C A.*, **39**, 5253 (1945).

Results and Discussion

Pore Structure and Area Relationships.—The nitrogen[2,6] and ammonia[9] adsorption–desorption isotherms for H–G have previously been published. In Fig. 1 are shown the isotherms for carbon monoxide and butane on the same catalyst; that for nitrogen is again included. The data for all four adsorbates are given in Table I, and area values calculated by both the Brunauer–Emmett–Teller (B.E.T.)[10a] and Harkins–Jura[10b] methods are included. The following molecular areas were used in calculating B.E.T. areas: for N_2[10a] and CO, 16.2 Å.^{2}; for C_4H_{10}, 32.1 Å.^{2} [10a]; for NH_3, 12.9 Å.^{2} [9] Unfortunately, the adsorption measurements were made over a period of several months, as indicated in Table I, during which time a loss of surface area occurred. For this reason the determinations with different adsorbates are not strictly comparable; it is believed, nevertheless, that conclusions drawn from the data are valid.

In Table II are listed data obtained from nitrogen isotherms for a number of catalysts, most of which are supported on diatomaceous earth. In all cases, nitrogen adsorption–desorption isotherms for diatomaceous earth supported cobalt catalysts exhibit the characteristics of the nitrogen and carbon monoxide isotherm plotted in Fig. 1; it is for this reason that the other plots were omitted. The characteristic feature of this type of isotherm is the sharp break in the desorption curve in the neighborhood of $p/p_0 = 0.5$; this implies a narrow pore distribution in this range. The amount adsorbed at this break point on the desorption curve is designated V_B, and is believed to represent the volume filling the small pores primarily responsible for surface area, just as the adsorption at $p/p_0 = 1$ represents the total pore volume. For the titania- and alumina-supported catalysts T and A (Table II), and for an unsupported catalyst no break appears in the desorption curve[2]; the point V_B only occurs for cobalt catalysts supported on siliceous material. On the other hand, there is but slight evidence for the appearance of the V_B point in the isotherms of Anderson, *et al.*,[3] for unreduced cobalt supported on diatomaceous earth; in the latter case, the support was added during or after the precipitation of cobalt, while in the present case the support was added prior to precipitation.

The adsorption curves of Fig. 1 appear to be type II isotherms, according to the classification of Brunauer, Deming, Deming and Teller,[11] while the desorption curves are a combination of type II and type IV. However, it has recently been observed[12] that severe grinding of a catalyst with a type IV isotherm (horizontal approach to p_0) can lead to the formation of a "tail" on the isotherm due to interparticle condensation. The similarity between the two cases is such as to suggest that for the present catalysts, adsorption at higher relative pressures, approaching p_0 asymptotically, is merely interparticle condensation. While this may be multilayer adsorption, there is some correlation between the volume adsorbed at higher relative pressures and catalyst permeability. In addition, the upper portions of the isotherms are very much like that of the non-porous, unsupported catalyst.[2] It appears, therefore, that the catalysts studied consist of extremely small particles whose pores contribute the major portion of the surface area, and which are held together in aggregates within which interparticle condensation takes place. The necessity for postulating the presence of aggregates arises from the fact that pelleting causes no change in pore volume.[13] These aggregates, therefore, are the powder particles which are actually compressed together in the pelleting operation.

For all adsorbates and all Celite-supported cobalt catalysts, V_B occurs at a relative pressure which yields, by application of the Kelvin equation, values of 21–22 Å. for the pore radius or platelet separation, with the assumption of two adsorbed layers; if one adsorbed layer is assumed, the values are 17–18 Å. The steep drop in adsorption below V_B indicates a narrow pore distribution. Therefore all of these catalysts have the same pore size. From the relationship $r = 2\ V/A$ in which A is equal to the area, V is equal to the pore volume, a proportionality between pore volume and area is expected. The truth of this is shown by the plot of Fig. 2, showing a linear relationship between V_B and area, the slope of which corresponds to $r = 17$ Å. The points of Fig. 2 were obtained from isotherms for Celite-supported cobalt catalysts; some were deactivated by use, while for others the preparation procedures were varied subsequent to precipitation. The break in the curve at higher area shows that certain catalysts with greater areas have smaller pores.

Pore volumes calculated from V_B values (P_g') for the four adsorbates on H–G catalyst agree well among themselves in spite of the fact that the B.E.T. area for butane, using 32.1 Å.^{2} for the butane molecular area, is much lower than those of the others (Table I). The low B.E.T. area obtained with butane cannot be explained by a screening effect, because of the agreement in pore volume, but rather must be attributed to a poor choice of molecular area.[14,15] The area calculated by the Harkins–Jura[10b] method for butane agrees quite well with the other data.

The agreement in total pore volume, calculated from V_s, which is the adsorption at p_0, is also good for different adsorbates, while that for the difference between total pore volume and P_g' is excellent. The interpretation of V_s as corresponding to a filling of pores has been amply verified by use of a number of adsorbates, including butane.[15,16] In addition, there is good agreement in many cases, and fair agreement in most, between pore volumes

(9) H. E. Ries, Jr., R. A. Van Nordstrand and W. E. Kreger, *J. Am. Chem. Soc.*, **69**, 35 (1947).

(10) (a) S. Brunauer, P. H. Emmett and E. Teller, *ibid.*, **60**, 309 (1938); (b) W. D. Harkins and G. Jura, *ibid.*, **66**, 1366 (1944).

(11) S. Brunauer, L. S. Deming, W. E. Deming and E. Teller, *ibid.*, **62**, 1723 (1940).

(12) R. A. Van Nordstrand, W. E. Kreger and H. E. Ries, Jr., THIS JOURNAL, **55**, 621 (1951).

(13) H. E. Ries, Jr., R. A. Van Nordstrand, M. F. L. Johnson and H. O. Bauermeister, *J. Am. Chem. Soc.*, **67**, 1242 (1945).

(14) S. Brunauer and P. H. Emmett, *ibid.*, **59**, 2682 (1937).

(15) P. H. Emmett and M. R. Cines, THIS JOURNAL, **51**, 1248 (1947).

(16) P. H. Emmett and T. W. DeWitt, *J. Am. Chem. Soc.*, **65**, 1253 (1943)

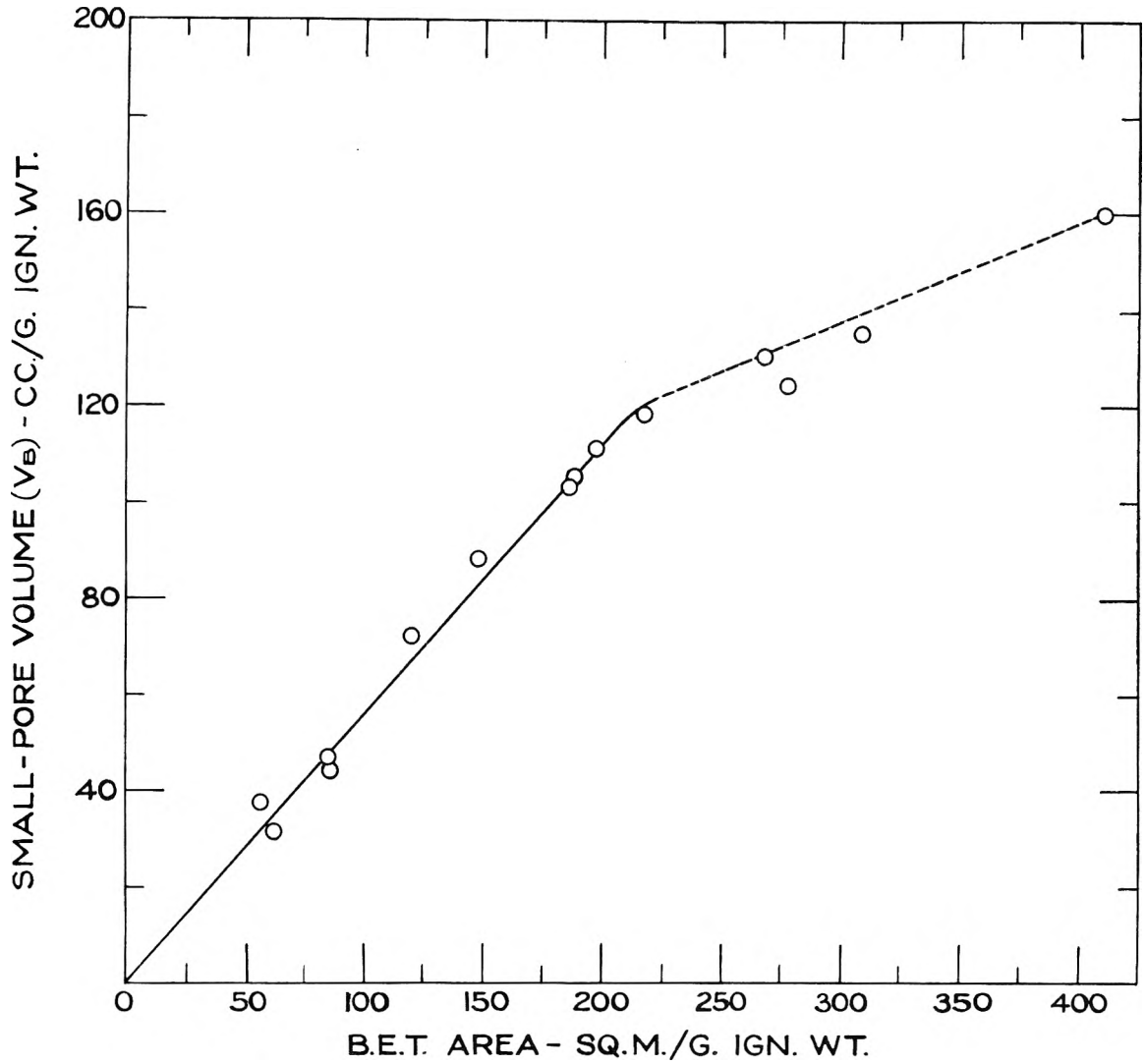

Fig. 2.—Variation of small-pore volume (V_B) with area for Celite supported cobalt oxide catalysts.

determined by helium–mercury displacement and those calculated from nitrogen adsorption at p_0. For asymptotic curves the latter were obtained from the point at which a break from p_0 occurs on desorption.[13] The He–Hg measurements have been found to be precise to 0.003 cc./g., and could be expected to include volume in very large pores, to which isotherm data are not sensitive.

In contrast to the characteristic isotherms of Celite-supported cobalt are those of supported chromia and iron oxide shown in Fig. 3 along with that of a chromia gel. Failure of adsorption–desorption curves joining below $p/p_0 = 0.4$ is attributed to accumulated error. The curve for iron is somewhat similar to that for cobalt; the point corresponding to V_B is less well-defined, and occurs at about 0.75 relative pressure. The effect of the support on chromia, however, was quite different. The area per gram of chromia remained approximately the same, as did the pore volume per gram of catalyst. The average pore size increased from 22 to 40 Å., as calculated from the pore volume and area, leading to an isotherm resembling aerogels.[17] In some way, therefore, the presence of the Celite added to the hydrogel before drying hindered shrinkage of the hydrogel to a xerogel during the drying step.

The fact that a characteristic small-pore structure with a high surface area is produced in the H–G type of catalyst implies a different composition from that of the catalysts prepared by Anderson and his co-workers,[3] which do not have this small-pore structure. For Anderson's catalysts the area is not much greater than that expected from an additive combination of support and unsupported catalysts areas; for the catalysts of the present study, the area is much more than additive.[2] This high area is believed to be the result of an interaction between colloidal silica and cobalt ion. A similar interaction was postulated by Visser for the nickel–kieselguhr system.[18] Because the present catalysts were prepared by the addition of a solution of a cobalt salt to a hot slurry of diatomaceous earth and sodium carbonate solution, the possibility exists that an attack by the alkaline solution upon the silica produced sodium silicate before addition of the cobalt. This possibility does not exist in the case of the Anderson

(17) S. S. Kistler, THIS JOURNAL, **36**, 52 (1932).

(18) G. H. Visser, *Chem. Weekblad*, **42**, 127 (1945).

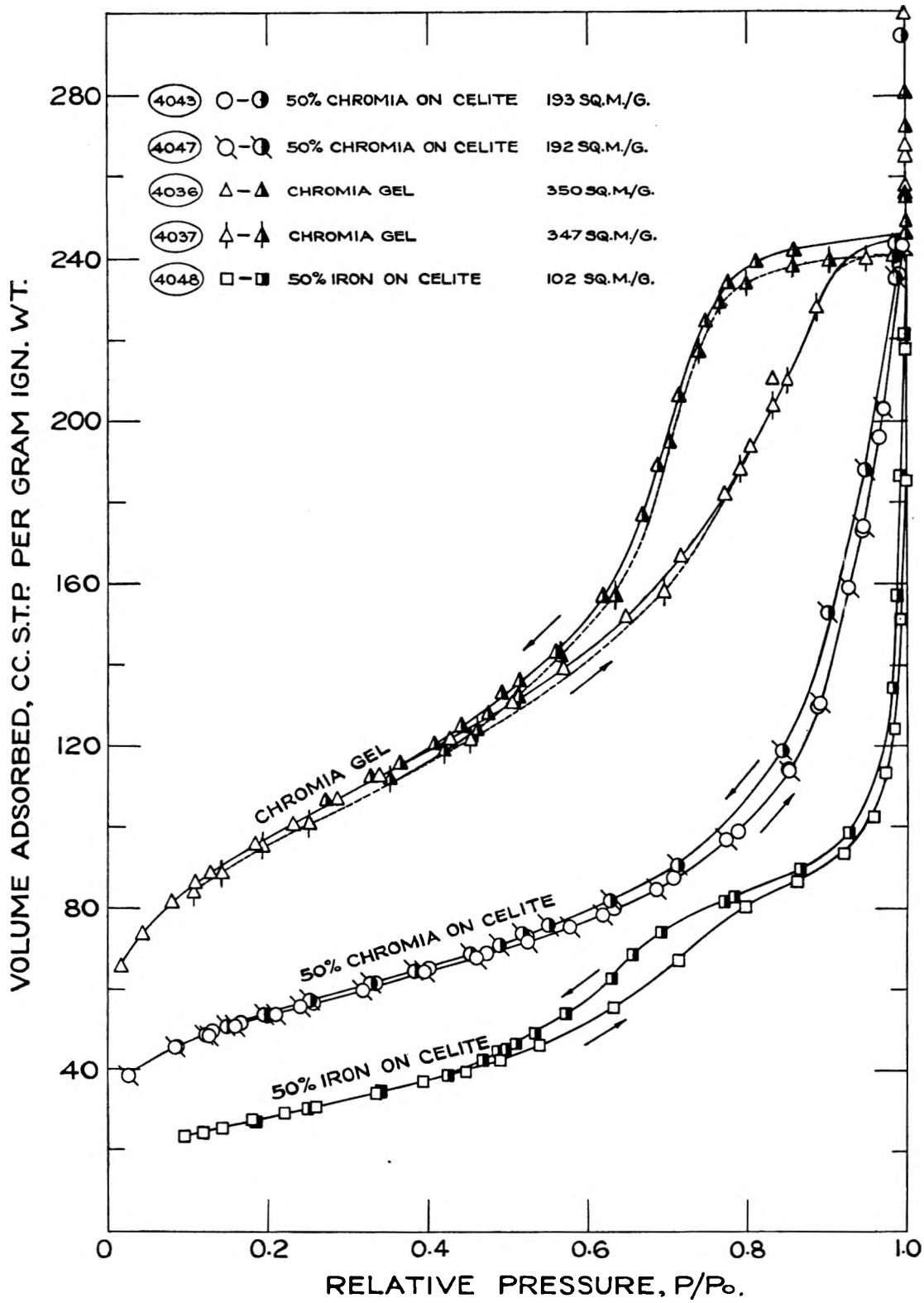

Fig. 3.—Nitrogen adsorption–desorption isotherms for Celite-supported chromia and iron, and unsupported chromia.

catalysts which were prepared by adding diatomaceous earth during or after precipitation. This explanation will account for the observation that a support such as titanium dioxide (area = 10 sq. m./g.) leads to a low area catalyst with no small-pore structure.

Several catalysts were prepared to test the hypothesis by exaggerating the conditions of preparation.

(1) Catalyst 0–16 (Table II) with an area of 186 sq.m./g., may be considered to be a typical example of a normal small-scale preparation, since the cobalt solution was added to the alkaline slurry as soon as possible. In large-scale preparations, such

as H–G or H–L, contact between Celite and hot sodium carbonate solution was maintained for several hours, or overnight, before addition of cobalt; in these cases, areas of 250–300 sq.m./g. were obtained in the unreduced state.

(2) In one small-scale preparation the Celite was stirred for several hours with boiling sodium carbonate solution before precipitation; the resulting catalyst had an area of 257 sq.m./g. Boiling after precipitation led to an area of only 207 sq.m./g.

(3) On the other hand, whereas the area of the unsupported catalyst "U" was 91 sq.m./g., a sample prepared by boiling sodium carbonate solution with Celite, and subsequently filtering before addition of the cobalt salt to the *filtrate*, contained 33.5% silica, and had an area of 181 sq.m./g. Sufficient silica was present in the filtrate to form a complex with cobalt, leading to the higher area.

(4) Substitution of silica as sodium silicate for 5% of the Celite led to a catalyst with an area of 273 compared to 186 sq.m./g. for 0–16.

(5) Precipitation of cobalt on Celite with ammonium hydroxide led to a thermally unstable sample with an area of 104 sq.m./g. in the uncalcined state, 77 after calcination at 350°. X-Ray diffraction patterns showed the presence of $Co(OH)_2$ and Co_3O_4, respectively; Celite supported samples gave no crystalline pattern.

(6) The areas of Celite-supported catalysts degassed at 100° and without calcination are approximately equal to those of the calcined samples. Thus, the area does not arise from the high temperature treatment, as has been suggested.[19]

A number of small catalyst preparations was made in order to determine the effect on catalyst area of variations in cobalt support ratio, and in area and type of support. The results are listed in Table III. The maximum catalyst area was obtained with about 38% cobalt. A more adequate criterion is the area per gram of catalyst material. This figure essentially represents the area per unit of cobalt; it is calculated from the relationship

$$A_m = \frac{(A_c - A_s)S}{1 - S}$$

where A_m = area per gram of metal, A_c = total catalyst area, A_s = area per gram of support, and S = % SiO_2/100. It is assumed that % SiO_2 represents % support. This concept is the equivalent of the cobalt complex area employed by Anderson, Hall, Hewlett, and Seligman.[3] It will be observed that the area per gram of catalyst material increases markedly with decreasing % Cobalt, down to 40% Co, after which it tends to level off. Furthermore, it may be observed that catalyst area increases with support area, with per cent. cobalt approximately constant.

Some of these diatomaceous earths have been examined under the electron microscope by Anderson, McCartney, Hall and Hofer.[20] Dicalites SF and HSC appear to differ from the others in having much larger pores. With the exception of these two, a correlation is found to exist in these data (Table III) such that catalyst material area increases with total support area (= area/g. of support × % support); this is contrary to the findings of Anderson, *et al.*,[3] for their type of catalysts, in which there is apparently little or no catalyst-support interaction. The support action, therefore, increases with increasing support area/wt. % cobalt ratio, when using diatomaceous earth supports. Support action is here defined as that action which increases catalyst material area.

TABLE III

AREA AND COMPOSITION DATA FOR CATALYSTS SUPPORTED ON DIATOMACEOUS EARTH

Diatomaceous earth support	Support area, sq. m./g.	Analysis of catalyst,[a] % Cobalt	Silica	Catalyst B.E.T. area, sq. m./g.	Area per g. catalyst material, sq. m./g.[b]
Celite 337	26	16.2	70.5	124	364
Celite 337	26	32.9	51.1	172	303
Celite 337	26	38.1	42.3	200	330
Celite 337	26	40.7	41.3	190	308
Celite 337	26	42.1	40.8	186	298
Celite 337	26	44.4	36.5	167	250
Celite 337	26	47.2	32.2	148	207
Celite 337	26	60.9	16.7	125	145
Celite 545	0.9	37.5	43.7	92	162
JM HSC	2.2	36.9	44.4	91	162
Dicalite SF	4.8	37.8	40.9	164	273
Dicalite SF	4.8	37.8	44.9	113	202
Dicalite SF	4.8	39.4	40.7	128	212
Dicalite 1	28	40.7	41.4	232	375
Dicalite 911	49	37.8	46.0	274	467

[a] Wet analyses. [b] Calculated on the assumption that the support contributes its maximum area, and that % SiO_2 = % support.

Sintering Curves.—Further evidence for the existence of a cobalt silicate complex may be derived from sintering curves, which show that the high area is not silica gel area, and from reduction studies, which show that the cobalt is not reducible in the supported catalysts, but is reducible to metal when unsupported.

The sintering curves shown in Fig. 4 were obtained by area measurements after 12-hour evacuations at successively increasing temperatures. Sintering curves of this type apparently characterize a material much as melting points do pure compounds. Data are shown only for one of a number of typical Celite-supported catalysts whose sintering curves were determined; in all cases sharp decreases in area were observed after 650° evacuation. Catalyst "S" supported on silica gel, was quite similar. However, the area of silica gel itself remained high at 650° and did not approach zero area until a temperature of 1050° was reached. Evidently the areas of these supported catalysts are not simply silica gel area as such, but are related to a complex.

Extent of Reduction.—Two methods were employed for measuring the extent of reduction: changes in ferromagnetism and hydrogen consumption, described in the Experimental Section. Typical results are given in Table IV. The two methods agree only qualitatively; the extent of

(19) R. B. Anderson, W. K. Hall and L. J. E. Hofer, *J. Am. Chem. Soc.*, **70**, 2465 (1948). The formation of high-area material is clearly related to silica sol produced by alkaline attack of the support.

(20) R. B. Anderson, J. T. McCartney, W. K. Hall and L. J. E. Hofer, *Ind. Eng. Chem.*, **39**, 1618 (1947).

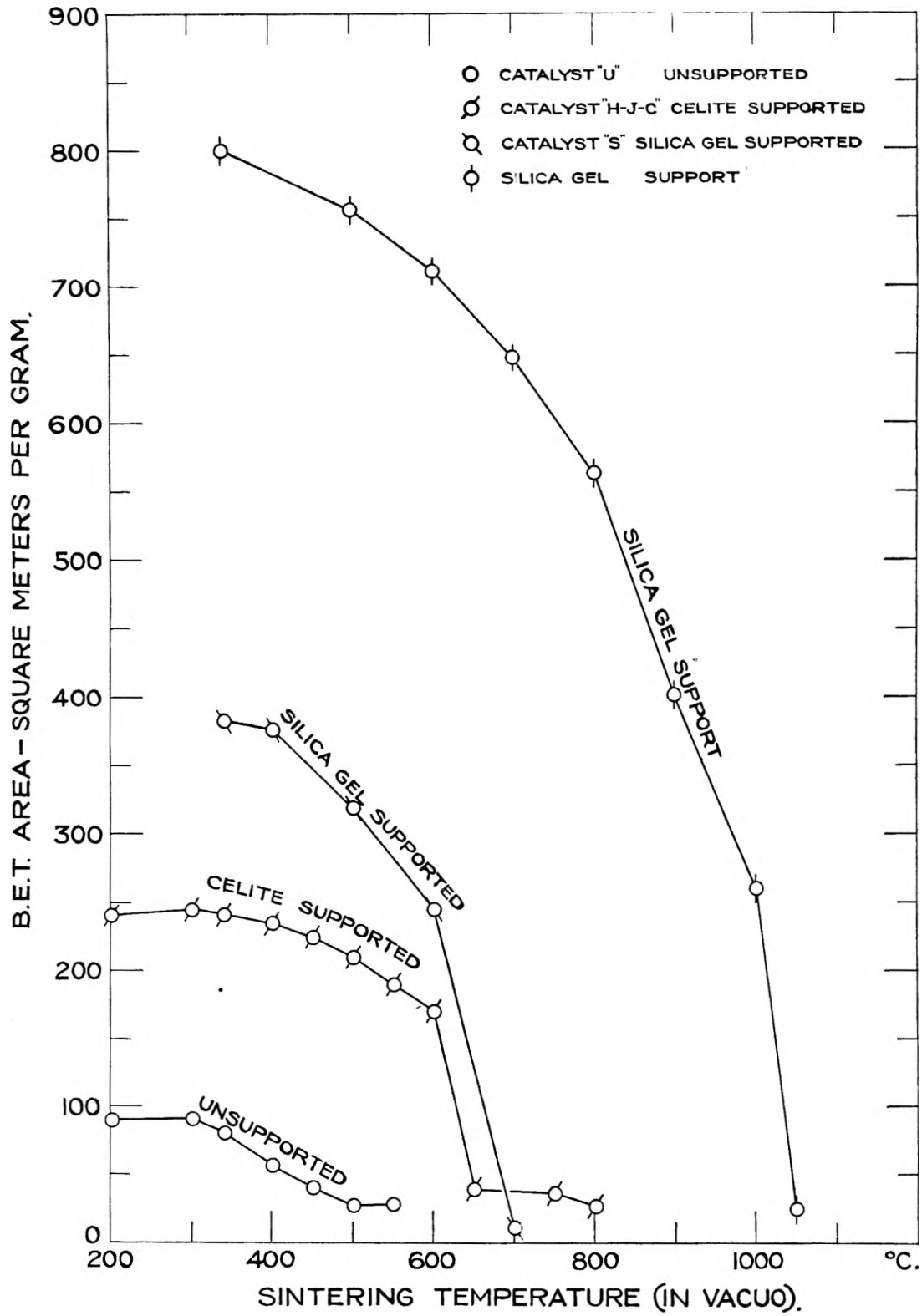

Fig. 4.—Sintering curves for supported and unsupported cobalt oxide and silica gel.

reduction as measured by hydrogen absorption is usually higher, due possibly to the complication of chemisorption. It is evident that the unsupported catalyst is reduced almost completely, while cobalt from catalyst "S" made from silica gel is reduced only a negligible amount. At intermediate levels, the degree of reduction appears to be in concordance with support action, as previously defined. Reduction of the catalyst supported on titania goes nearly to completion, as is to be expected from the lack of support action. Among the three catalysts supported on different diatomaceous earths, the high area "H–L" (on Celite 337) is reduced only 4–13% at 350° as measured by ferromagnetism.

TABLE IV

EXTENT OF REDUCTION OF COBALT CATALYSTS

Catalyst[a]	Support	Ferromagnetism Temp., °C.	Ferromagnetism Reduction,[b] %	Hydrogen absorption Temp., °C.	Hydrogen absorption Reduction,[b] %	B.E.T. areas[c] (sq. m./g.) Before reduction	B.E.T. areas[c] (sq. m./g.) After reduction
"U"	None	...	...	400	97	91	6
"O-6-1" +	None	340	71				
Celite 337		400	78	400	72	56	28
(Mech. mixt.)		450	78				
"O-17"	TiO_2	350	74	358	89	40	20
				400	92	40	19
"O-53"	Celite 545	350	39				
		400	45–49	400	70	92	60.5
"Q-2"	Dicalite SF	350	42	...	...	128	...
		400	54	...	...	128	...
"H-L"	Celite 337	350	4–13	358	24	309	304
		400	26	400	27	309	254
		460	52				
Uncalcined	Celite 337	350	14–22	...	...	...	...
"H-L"		400	27	...	...	...	...
"S"	SiO_2	...	...	358	2.6	410	374

[a] Supported catalysts contain 40–42% Co. [b] After no further change appeared to be taking place. [c] Areas measured before and after hydrogen absorption measurements.

"Q-2" and "O-53" were prepared from low-area supports (Table IV) and were more easily reduced. A mechanical mixture of Celite 337 with unsupported catalyst appears to hinder reduction, possibly by a solid–solid reaction between the support and cobalt oxide at the temperature of reduction.

It will be noted that severe area losses accompany reduction, in agreement with the findings of Anderson, Hall and Hofer.[15] Area losses are slight, however, when little reduction takes place ("H-L" and "S"). Upon increasing the temperature of reduction, further reduction is found to take place, and the surface area is decreased correspondingly. It has not been determined whether sintering makes reduction possible, or whether the loss of area occurs after reduction to metal. The former hypothesis seems to be more probable, since metals are not to be found as high area gels.

It might be added that the chemisorption of carbon monoxide at liquid nitrogen temperatures, according to the technique of Brunauer and Emmett,[21] amounts to 1–2 cc. S.T.P./g. for most of these catalysts after reduction at 350°. This corresponds to 35% of the total surface of "O–17" which is supported on titania, but only 2–3% of the total surface of catalysts supported by Celite 337.

Acknowledgment.—The authors are indebted to E. J. Martin for permission to publish this paper, to J. W. Teter for valuable suggestions and advice, to J. S. Melik for part of the experimental adsorption work, to R. A. Van Nordstrand for X-ray diffraction work which has assisted in the interpretation of the data, to R. D. Duncan for the preparation of the figures, and to Paul Bender and S. H. Bauer for the design and construction of the resonance circuit for measurement of changes in ferromagnetism.

(21) S. Brunauer and P. H. Emmett, *J. Am. Chem. Soc.*, **57**, 1754 (1935).

THE POLAROGRAPHIC DETERMINATION OF RELATIVE FORMATION CONSTANTS OF METAL COMPLEXES OF ETHYLENEDIAMINETETRAACETIC ACID

BY K. BRIL AND P. KRUMHOLZ

Contribution from the Research Laboratory of Orquima S. A., São Paulo, Brasil

Received February 18, 1953

The relative formation constants of the cadmium, copper, lead, nickel and zinc complexes of ethylenediaminetetraacetic acid have been determined by means of the polarographic method using the conventional dropping mercury electrode as well as the streaming mercury electrode. The reliability of the method was shown by the concordance of directly determined and indirectly calculated values of the relative formation constants and by comparison of such values with those obtained by different methods. The influence of ion pair formation on the equilibria studied is discussed.

Introduction

Schwarzenbach and colleagues[1] have studied extensively the stabilities of metal complexes with ethylenediaminetetraacetic acid (Enta) using essentially electrometric methods. Relative formation constants of some of these complexes were investigated, photometrically, by Martell and colleagues,[2] using the following displacement equilibrium

$$Me^{2+}_{(1)} + Me_{(2)}Y^{2-} \rightleftharpoons Me^{2+}_{(2)} + Me_{(1)}Y^{2-} \quad (1)$$

where Y represents the tetravalent ion of Enta.

We investigated the reaction 1 involving the ions of cadmium, zinc, copper, lead and nickel, by the polarographic technique.

The conventional polarographic determination of the concentration of a metal ion in an equilibrium mixture as 1 is possible only if the rate of formation of this ion from its complex is so low, that the amount produced during the lifetime of a mercury drop is negligibly small as compared with its equilibrium concentration. Otherwise the limiting current has a measurable kinetic contribution.[3] At the streaming mercury electrode[4] this kinetic contribution is greatly decreased[4a] as compared with the dropping mercury electrode. This is due to the fact that the diffusion layer at the jet surface is renewed much faster than at the drop surface. Indeed, Koessler and Koryta[5] have shown that the streaming electrode may be suitable for the study of some complex equilibria, where, due to kinetic factors, consistent results cannot be obtained using the dropping mercury electrode.

In the case of the stable complexes of Enta with transition metals reaction rates are apparently slow enough to justify the use of the dropping mercury electrode[6] for the determination of the equiiibrium concentrations.

In the present work we adopted both polarographic techniques. The complete concordance of values obtained on both types of electrodes can be taken as a full proof that the limiting current, in this special case, has no kinetic contribution and that true equilibrium concentrations have been measured. At the same time we hope to have shown that the streaming mercury electrode, up to now used rather sporadically, is a valuable analytical tool; its precision and reliability compares favorably with the classical techniques using a dropping mercury electrode.

From the measured equilibrium concentration of the metal $Me_{(2)}$ and the known total analytical concentrations $(\ )_0$, the equilibrium constant K^2_1 of the reaction 1 may be calculated according to

$$K^2_1 = \frac{(Me_{(1)})(Me_{(2)}Y)}{(Me_{(2)})(Me_{(1)}Y)} = \frac{\{(Me_{(1)})_0 - (Me_{(2)})\}\{(Me_{(2)}Y)_0 - (Me_{(2)})\}}{(Me_{(2)})^2} \quad (2)$$

assuming that the dissociation of both metal complexes and their reaction with hydrogen ions can be neglected. According to Schwarzenbach's values of the dissociation constants of Enta[7] and the stability constants of the MeY complexes investigated here[8] this assumption is valid at a *p*H higher than 4.

Experimental Part

Materials.—Enta was used in the form of the dihydrate of its disodium salt, C.P. grade, as supplied by the Bersworth Chem. Co. The solution was standardized by amperometric titration[9] with a solution of cadmium nitrate prepared from a previously weighed amount of C.P. cadmium metal. The metal nitrate solutions were prepared from C.P. salts and standardized in a similar manner against the solution of Enta. In the titration of lead, zinc and cadmium the supporting electrolyte was a 0.1 *m* acetate buffer 1:1, 1.0 *m* in respect to potassium nitrate. In the case of copper and nickel it was 1.5 *m* ammonia and 0.5 *m* in respect to ammonium nitrate.[10] A manual polarograph and a dropping mercury electrode were used for the determination, the precision of which was 0.5% or better.

Solutions of the MeY complexes were prepared by mixing the components in exactly equimolar proportions, the solutions being controlled polarographically not to contain more than 0.5% of the free components.

Apparatus.—The streaming mercury electrode vessel is of 50-ml. capacity, all surrounded by a water jacket. Water from a thermostat, maintained constant within ±0.1°, is circulated through the jacket. The bottom of this vessel is provided with a ground glass joint with a fitting in capillary tube, of about 0.1 mm. orifice diameter, directed up-

(1) G. Schwarzenbach and colleagues, *Helv. Chim. Acta* (1945–1953).

(2) R. C. Plumb, A. E. Martell and F. C. Bersworth, THIS JOURNAL, **54**, 1208 (1950).

(3) See I. M. Kolthoff and J. J. Lingane, "Polarography," 2nd ed., Interscience Publishers, Inc., 1952, Chap. XV.

(4) (a) J. Heyrovsky and J. Forejt, *Z. physik. Chem.*, **193**, 77 (1943); (b) J. Heyrovsky, *Chem. Listy*, **40**, 22 (1946); (c) A. Rius and J. Llopis, *Anales Fis. y Quim. (Madrid)*, **42**, 617 (1946).

(5) I. Koessler and J. Koryta, *Experientia*, **6**, 136 (1950); *Collection Czechoslov. Chem. Communs.*, **15**, 241 (1950).

(6) H. Ackermann and G. Schwarzenbach, *Helv. Chim. Acta*, **35**, 485 (1952), use the dropping mercury electrode for the study of the kinetics of the copper-cadmium-Enta displacement reaction.

(7) G. Schwarzenbach and H. Ackermann, *ibid.*, **30**, 1798 (1947).

(8) G. Schwarzenbach and E. Freitag, *ibid.*, **34**, 1503 (1951).

(9) See R. Pribil and B. Matyska, *Chem. Listy*, **44**, 305 (1950).

(10) See W. E. Alsopp and F. E. Arthur, *Anal. Chem.*, **23**, 1883 (1951).

wards at an angle of about 30° against a movable vertical glass knife edge.[5] The distance between the capillary orifice and the glass knife was adjusted to about 3 mm.[11] The rate of mercury outflow was about 0.015 ml. per second. The solutions were deaerated by a stream of pure nitrogen. The mercury which accumulates at the bottom of the vessel is maintained at a constant level by means of an overflow. This mercury pool is used as the anode. The head of mercury is held constant by means of Miller's[12] device. The potential of the jet electrode is measured against a saturated calomel electrode connected to the vessel by means of a potassium nitrate salt bridge, using an electronic potentiometer. Both the diffusion current and the potential of the jet electrode are of good stability and reproducibility, the fluctuations of the former being about 1% of its value,[13] of the latter about 2 mv. A manual polarograph was used as a measuring device. The galvanometer had a sensitivity of about 5×10^{-8} amp. per division and an internal resistance of about 50 ohms.

A manual polarograph also was used for measurements with the dropping mercury electrode. The galvanometer had a sensitivity of 7.00×10^{-9} amp. per division and an internal resistance of about 400 ohms. It was provided with a damping circuit according to Philbrook and Grubb.[14] The capillary characteristics were determined in 0.1 *m* potassium nitrate at 20.0° in open circuit: $m = 3.46$ mg./sec., $t = 2.16$ sec., $m^{2/3}t^{1/6} = 2.81$. A saturated calomel electrode was used as an external anode. The measuring vessel was of 25-ml. capacity, all surrounded by a water jacket.

Measurements and Calibrations.—Solutions of the copper-Enta complex containing an excess of the copper ion show two distinct polarographic waves[16] the first being due to the reduction of the copper ion, the second to the reduction of the complex. In well buffered solutions the half wave potential of the second wave depends upon the *p*H shifting toward more positive values with increasing acidity; we found for a 10^{-3} *m* copper-Enta solution in 0.5 *m* potassium nitrate at the jet electrode $E_{1/2} = -0.482$ at a *p*H 5.5 and $E_{1/2} = -0.350$ at a *p*H 3.5. In unbuffered solutions the wave of the complex is split in the *p*H range 3.5–5 into two distinct waves. A similar split is observed at *p*H higher than 5 in the presence of all bivalent metals studied with the exception of nickel.[16] The separation of the copper wave was in all cases clean enough to allow an unambiguous copper determination. No similar waves of the nickel–, zinc–, lead– or cadmium–Enta complexes could be found.

Figure 1 shows a typical polarogram of the copper–copper–Enta complex system as obtained on the jet mercury electrode. In the case of lead and cadmium the polarograms obtained had exactly the same shape as those obtained with a dropping mercury electrode, at the same metal concentration the limiting current at the jet electrode being about 20 times greater than at the dropping electrode. At jet potentials suitably chosen[17] the limiting current of the three metal ions is within the experimental error of 1–2% proportional to their concentration. This was also the precision of the measurements using the dropping mercury electrode.

The diffusion current constant (at a given potential) depends upon the total composition of the solution. The diffusion current of $Me_{(2)}$ was not affected by the presence of the competing metal $Me_{(1)}$ if the concentration of the latter was lower than 20% of the total electrolyte concentration. The influence of the concentration of the supporting electrolyte (potassium nitrate) as well as that of the Enta complex of the metal to be determined has to be taken into account.

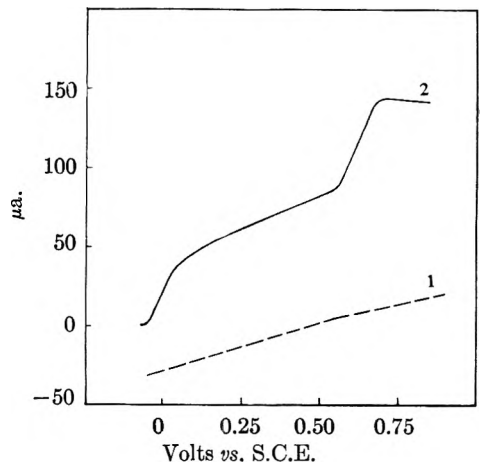

Fig. 1.—Copper–Enta–copper polarogram in unbuffered 0.10 *m* KNO_3, 20°. 1, residual current; 2, Cu = 0.4; CuY = 0.6 millimole/l.; *p*H 5.1 (cor. for the residual current).

Individual calibrations were performed, using both types of electrodes, at 20° in the range of 10^{-5} to 10^{-3} *m* for copper, lead and cadmium. Total nitrate concentration was varied from 0.05 to 1.0 *m*. As measurements of the competition reactions were made at constant total analytical concentration of the metal to be determined ($Me_{(2)}$), the same condition was maintained in the calibrations by suitable addition of $Me_{(2)}Y$. The total analytical concentration of $Me_{(2)}Y$ was varied between 2×10^{-4} and 3×10^{-3}. The *p*H of the solutions was maintained between 4.8 and 5.4 by careful addition (potentiometric control) of nitric acid or potassium hydroxide. Residual currents were determined in solutions containing all components of the calibration solutions except the free metal $Me_{(2)}$ ion.

For the equilibrium measurements of the displacement reactions, solutions were prepared containing varying proportions of the $Me_{(2)}Y$ complex ($Me_{(2)}$ = copper, lead and cadmium) and of the metal $Me_{(1)}$. Total nitrate concentration was maintained constant by a suitable addition of potassium nitrate. Total nitrate concentration rather than ionic strength was maintained constant: the displacement reaction 1 being charge symmetrical in all cases studied here, the constant K^2_1 should not depend to a great extent on the ionic strength. The *p*H of the solutions was adjusted to 5.1 ± 0.3. With suitable precautions the *p*H before and after the polarographic measurement was found to be unchanged within ±0.1 *p*H. Variations of the experimental values of the competition constants in the *p*H range 4.5 to 5.5 were found to be within the experimental error.

The equilibria of the competition reactions studied are not instantaneously reached.[18] The velocities of these reactions vary widely according to the system investigated. Thus in the system cadmium–Enta–zinc at 20° and in the concentration range investigated (see below) equilibrium is reached within a few minutes, but only in several hours in the system copper–Enta–nickel. All solutions were left before the measurement for 24 hr. in the thermostat at 20.0°, except in the case of the system nickel–copper–Enta where measurements were made three days after the solution had been prepared.

Experimental Results

The following systems have been investigated at 20° and total nitrate concentration of 0.1 and 0.5 *m:* copper–Enta with nickel, lead, cadmium and zinc; cadmium–Enta with zinc and lead–Enta with zinc. The last system was investigated over a

(11) The natural length of the mercury jet, all other conditions being constant, depends upon the jet potential. It presents a minimum length at the maximum of the capillary curve of mercury in the particular solution.[4c] The distance between the capillary orifice and the knife edge (about 3 mm.) must be shorter than this minimum length as otherwise large current fluctuations may occur. We found that the ratio between the residual current and the limiting current (for a given metal concentration) also depends upon the proper choice of the knife edge position in respect to the jet. A position can be found, by trial and error, where this ratio is minimum, representing optimal working conditions.

(12) A. R. Miller, *Ind. Eng. Chem., Anal. Ed.*, **12**, 171 (1940).

(13) With the particular electrode used about 0.3% of the metal to be determined was electrolyzed per minute. The time necessary for the measurement seldom exceeded 1–2 minutes.

(14) G. E. Philbrook and H. M. Grubb, *Anal. Chem.*, **19**, 7 (1947).

(15) See ref. 6, p. 487: W. Furness, P. Crowshaw, and W. C. Davies, *Analyst*, **74**, 629 (1949); R. E. Pecsok, *J. Chem. Ed.*, **29**, 597 (1952).

(16) In a forthcoming paper we shall report on this peculiar behavior of the copper–Enta system in full detail.

(17) 0.15–0.20 volt *vs.* S.C.E. for copper; 0.5–0.7 volt *vs.* S.C.E., for lead and 0.7–0.9 volt *vs.* S.C.E. for cadmium.

(18) See ref. 6 and 7; see also S. S. Jones and F. A. Long, THIS JOURNAL, **56**, 25 (1952).

wider range of nitrate concentration, 0.05 to 1.0 *m* (see below). The concentrations of the complex $(Me_{(2)}Y)_0$ were 4×10^{-4}, 10^{-3} and 3×10^{-3} *m*. The concentration of the competing metal ($Me_{(1)}$) was varied between 10^{-4} and 3×10^{-2} *m*, more than a hundred-fold. Parallel measurements were executed using the dropping and the streaming mercury electrodes; most of the measurements were duplicated. Admitting a calibration error of 1–2% and an error of ±0.5% on the total analytical concentrations the equilibrium constants calculated according to 2 should be consistent within ±5%. Table I shows the result of about 50 individual measurements in the copper–Enta–nickel system at 20.0° and in 0.1 *m* potassium nitrate. The constants are consistent within the predicted error of ±5%, with very few exceptions. Table I shows also that the value of the competition constant K^2_1, in the concentration range investigated and

TABLE I

COPPER–ENTA–NICKEL SYSTEM AT 20° AND 0.10 *m* POTASSIUM NITRATE, *p*H RANGE 4.8–5.3

$(CuY)_0 \times 10^{-3}$ *m*	0.400		1.00		3.00	
$(Ni)_0 \times 10^{-3}$ *m*	K^2_1 as obtained with the {jet / drop} electrode					
	Jet	Drop	Jet	Drop	Jet	Drop
0.129			1.45	1.71		
.258	1.85	1.78	1.74	1.78		
.387			1.77	1.78	1.75	1.75
.516	1.86	1.83	1.84	1.86		
.645			1.73	1.81	1.70	1.76
.903	1.88	1.84	1.75	1.79	1.68	1.79
1.29			1.76	1.82	1.70	1.80
1.935	1.88	1.73	1.80	1.87		
2.58			1.79	1.91	1.71	1.61
5.16	1.95	1.70	1.87	1.90	1.71	
9.03		1.75				
12.9		1.74	1.86	1.86		

within the experimental error, is a true equilibrium concentration constant independent of the copper–Enta and nickel concentrations. The same was found to be true for the system cadmium–Enta–zinc. In the system copper–Enta–zinc the competition "constant" K^2_1 increases by about 10% in the zinc concentration range up to 3×10^{-2} *m*, showing however, within the experimental error, no dependence upon the copper–Enta concentration.

In all other systems investigated, especially in those involving lead, K^2_1 depends strongly upon the concentrations of both $Me_{(2)}Y$ and $Me_{(1)}$. This is clearly shown by Figs. 2–4.

Theoretical considerations (see below) make it highly probable that the K^2_1 values, extrapolated for zero concentrations of $Me_{(2)}Y$ and $Me_{(1)}$, give the true equilibrium constants, K^2_1, at the given total nitrate concentration. Thus K^2_1, as obtained at constant $(Me_{(2)}Y)_0$ and varying $(Me_{(1)})_0$, was first extrapolated to $(Me_{(1)})_0$ equal zero ($K^2_{1=0}$). The $K^2_{1=0}$ values thus obtained were then extrapolated to $(Me_{(2)}Y)_0$ equals zero ($K^{2=0}_{1=0}$).

Table II shows the values so obtained for all systems investigated, at a total nitrate concentration 0.1 *m* and 20°. The reliability of the constants reported is shown by comparison of the experimental values with those calculated from the relations between other constants involving the ion pair in question. As shown by Table II the agreement is excellent and concordant with the assumption that the error of the experimental constants as obtained by our method should not exceed ±5%.

TABLE II

t = 20.0°, NITRATE 0.1 *m* SOLUTIONS

$K^{2=0}_{1=0}$	K^{Cu}_{Ni}	K^{Cu}_{Pb}	K^{Cu}_{Cd}	K^{Cu}_{Zn}	K^{Pb}_{Zn}	K^{Cd}_{Zn}
Exptl. values	1.78	5.0	315	340	71	1.05
Calcd. values	..	4.8	320	350	70	1.08
Constants combination used for the calculation	$\frac{K^{Cu}_{Zn}}{K^{Pb}_{Zn}}\frac{K^{Cu}_{Zn}}{K^{Cd}_{Zn}}K^{Cu}_{Pb}$		$\times K^{Pb}_{Zn}\frac{K^{Cu}_{Zn}}{K^{Cu}_{Pb}}\frac{K^{Cu}_{Zn}}{K^{Cu}_{Cd}}$			

For the systems copper–Enta–zinc and copper–Enta–nickel the constants $K^{2=0}_{1=0}$ are within the experimental error identical at 0.1 and at 0.5 *m* potassium nitrate. This confirms our assumption that the charge symmetrical equilibrium 1 may be considered, in a first approximation, as independent of ionic strength.

The constants $K^{Zn=0}_{Cu=0}$ and $K^{Cu=0}_{Cd=0}$ increase by about 10% when passing from 0.1 to 0.5 *m* potassium nitrate. In all systems involving lead a very pronounced dependence upon the total nitrate concentration was found. This will be discussed below.

Discussion

The dependence of the numerical values of the "constants" K^2_1, calculated according to 2 upon the concentrations of $Me_{(2)}Y$, $Me_{(1)}$ and nitrate, shows clearly that the simplified treatment of the equilibria investigated, as outlined in the introduction, is insufficient. At the high ionic concentrations encountered throughout this work, the influence of ion pair formation[19] on the equilibrium of the displacement reactions studied must be considered and, as shown below, may account for most of the effects observed.

MeY–H.—As pointed out by Schwarzenbach[7,8] heavy metal Enta complexes are rather strong acids with *pK* values greater than 10[3]. The formation of these hydrogen complexes can thus be practically neglected at *p*H values greater than 4.5.

Me–OH.—Among all metals investigated here, copper forms the most stable hydroxo-ion pair.[20] Titration of a 5×10^{-3} *m* solution of copper nitrate in 0.1 *m* potassium nitrate with potassium hydroxide, shows that at *p*H 5.5 about 1% only of the total copper is bound into hydroxo-ion pairs. Thus in the *p*H range studied here, hydrolysis of metal ions can be neglected even in the case of copper.

MeY–Me.—The pronounced dependence of the "constants" calculated according to equation 2 upon the concentrations of both the complexed and free metal ion, makes it probable that rather stable ion pairs are formed between the bipositive metal ions and the binegative complex ions MeY. Simi-

(19) N. Bjerrum, *Kgl. Danske Vidensk. Selskab.*, **7**, no. 9 (1926); R. M. Fuoss and C. Kraus, *J. Am. Chem. Soc.*, **55**, 21, 476, 1019 (1933).

(20) H. S. Britton, *J. Chem. Soc.*, **125**, 2124 (1927); **127**, 2110 (1925); I. M. Kolthoff and T. Kameda, *J. Am. Chem. Soc.*, **53**, 832 (1931); W. Feitknecht and E. Haeberli, *Helv. Chim. Acta*, **33**, 922 (1950); S. Chaberek and A. E. Martell, *J. Am. Chem. Soc.*, **74**, 5052 (1952); K. H. Gayer and L. Wootner, *ibid.*, **74**, 1436 (1952); H. Freiser, R. G. Charles and W. D. Johnston, *ibid.*, **74**, 1383 (1952).

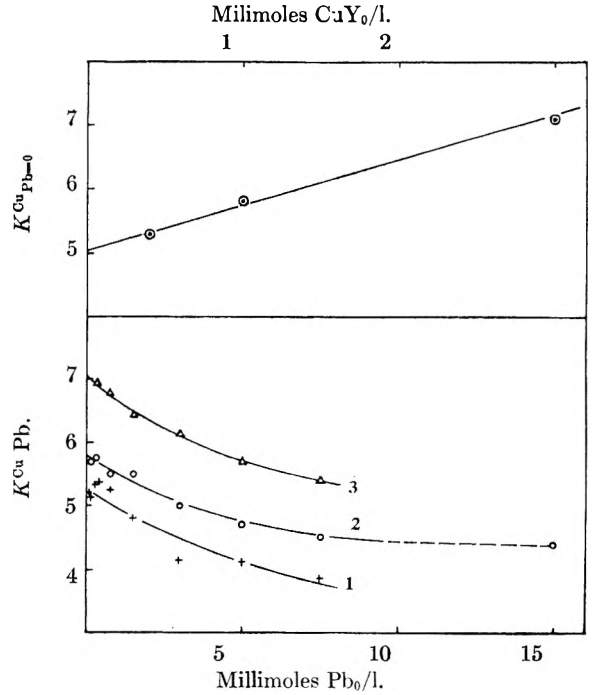

Fig. 2.—Copper–Enta–lead system at 20°, KNO_3 0.10 *m*, *p*H 4.9–5.3, lower graph, CuY_0 in millimoles/l.: 1, 0.400; 2, 1.00; 3, 3.00; upper graph, extrapolation to $K^{Cu=0}{}_{Zn=0}$.

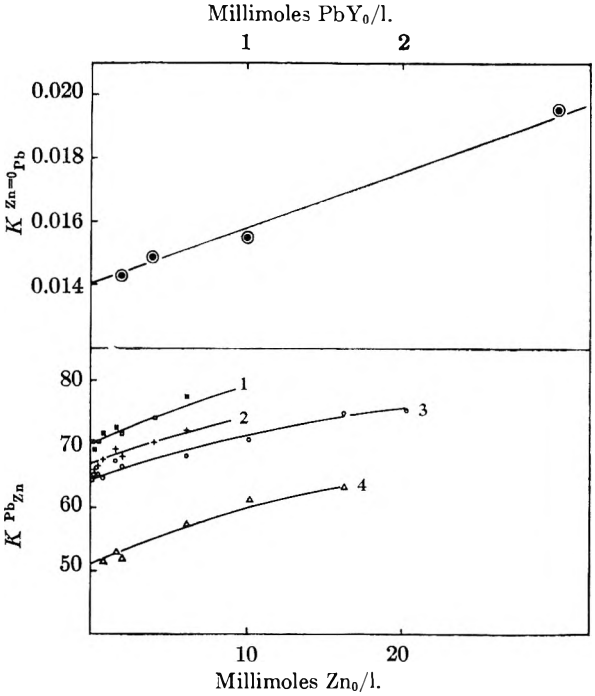

Fig. 3.—Lead–Enta–zinc system at 20°, KNO_3 0.10 *m*, *p*H 4.9–5.3, lower graph, PbY_0 in millimoles/l.: 1, 0.200; 2, 0.400; 3, 1.00; 4, 3.00; upper graph, extrapolation to $K^{Zn=0}{}_{Pb=0}$.

lar, rather stable ion pairs (pK values up to 3) were found by Schwarzenbach[21] in the case of calcium complexes with higher homologs of Enta. No evidence, however, was found by those authors for the formation of this type of ion pairs between transition metals and Enta.[7]

(21) G. Schwarzenbach and H. Ackermann, *Helv. Chim. Acta*, 31, 1029 (1948).

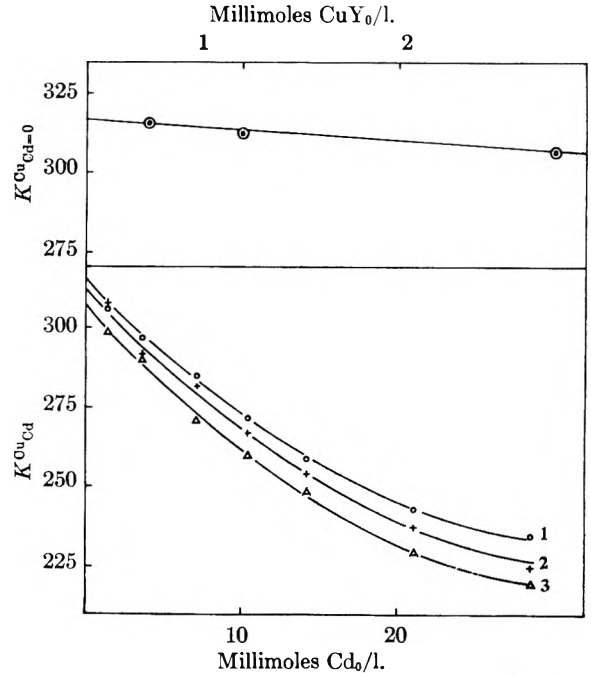

Fig. 4.—Copper–Enta–cadmium system at 20°, KNO 0.10 *m*, *p*H 4.9–5.3, lower graph, CuY_0 in millimoles/l.: 1, 0.400; 2, 1.00; 3, 3.00; upper graph, extrapolation to $K^{Cu=0}{}_{Cd=0}$.

$MeNO_3$.—The existence of metal nitrate ion pairs was first pointed out by Davies and his coworkers.[22] In the case of lead and cadmium thermodynamic ion pair formation constants were reported[22] at 18°.

Admitting the existence of MeY–Me and $MeNO_3$ ion pairs, the following (concentration) formation constants must be considered

$$K_1 = \frac{(Me_{(2)}Y - Me_{(1)})}{(Me_{(2)}Y)(Me_{(1)})} \quad K_2 = \frac{(Me_{(2)}Y - Me_{(2)})}{(Me_{(2)}Y)(Me_{(2)})}$$

$$K_3 = \frac{(Me_{(1)}Y - Me_{(2)})}{(Me_{(1)})(Me_{(2)})} \quad K_4 = \frac{(Me_{(1)}Y - Me_{(1)})}{(Me_{(1)}Y)(Me_{(1)})} \quad (3)$$

$$K_5 = \frac{(Me_{(1)} - NO_3)}{(Me_{(1)})(NO_3)} \quad K_6 = \frac{(Me_{(2)} - NO_3)}{(Me_{(2)})(NO_3)}$$

The following stoichiometric relations are easily found

$$\begin{aligned} (Me_{(1)})_0 &= \alpha(Me_{(1)}) + \beta(Me_{(1)}Y) \\ (Me_{(2)}Y)_0 &= (Me_{(2)})_0 = \gamma(Me_{(2)}) + \delta(Me_{(2)}Y) = \\ &= (Y)_0 = \epsilon(Me_{(1)}Y) + \eta(Me_{(2)}Y) \end{aligned} \quad (4)$$

Here

$$\begin{aligned} \alpha &= 1 + K_1(Me_{(2)}Y) + K_5(NO_3) \\ \beta &= 1 + K_3(Me_{(2)}) + 2K_4(Me_{(1)}) \\ \gamma &= 1 + K_3(Me_{(1)}Y) + K_6(NO_3) \\ \delta &= 1 + K_1(Me_{(1)}) + 2K_2(Me_{(2)}) \\ \epsilon &= 1 + K_3(Me_{(2)}) + K_4(Me_{(1)}) \\ \eta &= 1 + K_2(Me_{(2)}) + K_1(Me_{(1)}) \end{aligned} \quad (5)$$

Then the competition constant of 2 is

$$\overline{K^2}_1 = \frac{\{(Me_{(1)})_0 - \theta\beta/\kappa\,(Me_{(2)})\}\,\{(Me_{(2)})_0 - \gamma(Me_{(2)})\}}{(Me_{(2)})^2} \times \frac{\kappa}{\theta\epsilon\delta} \quad (6)$$

(22) E. C. Righellato and C. W. Davies, *Trans. Faraday Soc.*, 26, 592 (1930); H. S. Harned and B. B. Owen, "The Physical Chemistry of Electrolytic Solutions," 2nd ed., Reinhold Publ. Corp., New York, N. Y., 1950, p. 147.

Here

$$\theta = 1 + K_2(Me_{(2)}Y) + K_5(NO_3) \quad (7)$$
$$\kappa = 1 + K_4(Me_{(1)})$$

Making the reasonable assumption that the first wave observed (see Fig. 1) is due to the reduction of the free or (and) weakly complexed (by ion pair formation) metal ion $Me_{(2)}$, the measured concentration of $Me_{(2)}$ ($= (Me_{(2)})^*$) is

$$(Me_{(2)})^* = (Me_{(2)})\{1 + K_2(Me_{(2)}Y) + K_3(Me_{(1)}Y) + K_5(NO_3)\} = \lambda(Me_{(2)}) \quad (8)$$

Thus the equation 6 becomes

$$\overline{K_1}^2 = \frac{\{(Me_{(1)})_0 - \theta\beta/\kappa\lambda(Me_{(2)})^*\}\{(Me_{(2)})_0 - \gamma/\lambda\,(Me_{(2)})^*\}}{(Me_{(2)})^{2*}} \frac{\lambda^2\kappa}{\theta\alpha\delta} \quad (9)$$

Using proper K_i values, equation 9 allows, at least qualitatively, for all experimental facts observed. It is, however, not suitable for quantitative estimation of the individual stability constants, because of the great number of parameters involved.

Extrapolating 9 for $(Me_{(1)}) \rightarrow 0$ and thus $(Me_{(2)}) \rightarrow 0$ $(Me_{(1)}Y) \rightarrow 0$ and $(Me_{(2)}Y) \rightarrow (Me_{(2)}Y)_0$ we get

$$\overline{K^2}_1 = \frac{\{(Me_{(1)})_0 - (Me_{(2)})^*\}(Me_{(2)})_0}{(Me_{(2)})^{2*}} \frac{\lambda}{\alpha} = K^2_{1=0} \frac{1 + K_2(Me_{(2)}Y)_0 + K_5(NO_3)}{1 + K_1(Me_{(2)}Y)_0 + K_5(NO_3)} \quad (10)$$

where $K^2_{1=0}$ is obviously the apparent formation constant as calculated according to 2 for $(Me_{(1)}) \rightarrow 0$.

It can be seen that $K^2_{1=0}$ will increase (see Fig. 3) or decrease (see Figs. 2 and 4) with increasing $(Me_2Y)_0$ according to whether $K_1 > K_2$ or $K_1 < K_2$. If $K_1 = K_2$, or if both of them are very small, $< K^2_{1=0}$ will not depend upon $(Me_{(2)}Y)_0$ within the experimental errors.

Equation 10 shows also that the effect of $(Me_{(2)}Y)_0$ upon $K^2_{1=0}$ can be masked by high nitrate concentration[23]; this conclusion was experimentally confirmed.

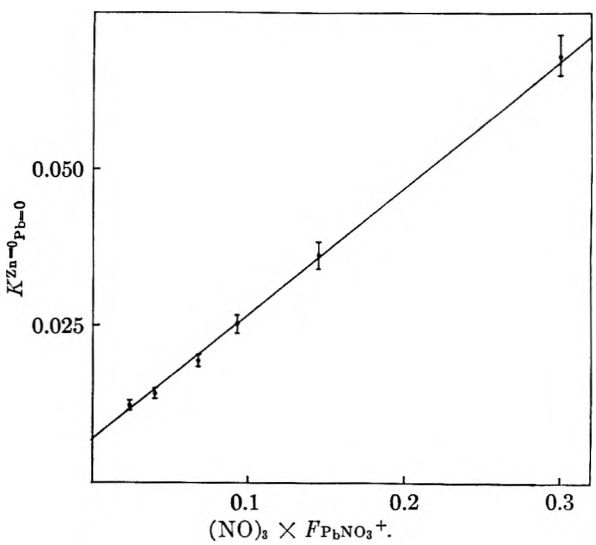

Fig. 5.—Graphical estimation of the equilibrium constant $\overline{K}^{Pb}_{Zn}$

(23) This effect is also in part due to the fact that K_1 and K_2 decrease with increasing ionic strength (see equation 5).

Extrapolating 10 for $(Me_{(2)}Y)_0 \rightarrow 0$ we get

$$\overline{K^2}_1 = K^{2=0}_{1=0} \frac{1 + K_5(NO_3)}{1 + K_5(NO_3)} \quad (11)$$

Equation 11 can basically be used to evaluate both the nitrate ion pair formation constants and the equilibrium constants $\overline{K^2}_1$, which in the charge symmetrical case may be considered, in first approximation, as a thermodynamic equilibrium constant. For that purpose the concentration constants K_5 and K_6 must be expressed in terms of the corresponding thermodynamic constants and ionic activity coefficients, giving

$$\overline{K^2}_1 = K^{2=0}_{1=0} \frac{1 + \overline{K}_5 F_5(NO_3)}{1 + \overline{K}_5 F_5(NO_3)} \quad (12)$$

where

$$F = \frac{\gamma_{Me^{++}}\gamma_{NO_3^-}}{\gamma_{MeNO_3^+}}$$

It is actually impossible to make an exact evaluation of the constants involved in 12, because of the lack of data as to the values of the activity coefficients at high ionic strengths. Using, however, approximate values as calculated from an extended Debye–Hückel equation,[24] a semi-quantitative calculation can be tried.

The accuracy of eq. 12 is best tested on the system lead Enta–zinc, because the $K^{Pb=0}_{Zn=0}$ values show a most pronounced variation with total nitrate concentration ($K^{Pb=0}_{Zn=0} = 14.5$ and 80.5 at total nitrate concentration 0.050 and 1.0 m, respectively). The small increase of $K^{Zn=0}_{Cd=0}$ with increasing nitrate concentration (see experimental results) indicates, according to 12, that $\overline{K}_{ZnNO_3}$ is smaller than $\overline{K}_{CdNO_3}$. As Davies[22] found $\overline{K}_{CdNO_3} = 2.5$ (at 18°) $\overline{K}_{ZnNO_3}$ should be about 1. The activity coefficient F_{ZnNO_3} in the ionic strength's range 0.1 to 1 is probably about 0.3. Thus for the lead–Enta–zinc system the numerator of 12 will not differ greatly from unity, and as expressed by

$$\frac{1}{K^{Pb=0}_{Zn=0}} = K^{Zn=0}_{Pb=0} \backsimeq \overline{K}^{Zn}_{Pb} + \overline{K}^{Zn}_{Pb}\,\overline{K}_{PbNO_3}(NO_3)F_{PbNO_3} \quad (13)$$

the experimental $K^{Zn=0}_{Pb=0}$ values should be roughly proportional to the product, $(NO_3) \times F_{PbNO_3}$. Figure 5 confirms this conclusion. From the slope of the straight line obtained, a value of about 25 can be calculated for the thermodynamic ion pair formation constant of $PbNO_3$, using for $\overline{K}^{Zn}_{Pb}$ the intercept value at nitrate concentration zero. Davies[22] found $\overline{K}_{PbNO_3} = 15.5$ (at 18°). In view of the very drastic approximations used here, especially concerning the activity coefficients at high ionic strengths, the difference between the two values is not unreasonably high.

The linear relation 13 may be used, for the extrapolation of the equilibrium constants obtained at different nitrate concentrations (see, *i.e.*, Table II) to zero nitrate concentration. True thermodynamic equilibrium constants should thus be obtained. Table III contains equilibrium constants for all systems investigated here, obtained, where

(24) $pF = 2.04\sqrt{\mu}/(1 + 1.645\sqrt{\mu}) - 0.25\mu$. This equation was shown to fit very well the experimental data for the $CuCl^+$ ion pair; see R. Näsänen, *Acta Chem. Scand.*, **4**, 140 (1950).

TABLE III

THERMODYNAMIC EQUILIBRIUM CONSTANTS AT 20° COMPARED WITH SCHWARZENBACH[7] VALUES AS OBTAINED AT 20°, μ = 0.100, CHLORIDE SOLUTIONS

$\bar{K}^2_1$	K^{Cu}_{Ni}	K^{Cu}_{Pb}	K^{Cu}_{Cd}	K^{Cu}_{Zn}	K^{Pb}_{Zn}	K^{Cd}_{Zn}
Our values	1.78	2.2	300	340	140	1.1
Schwarzenbach values[7]	1.2	1.5	80	170	110	2.1

necessary, by similar extrapolation. The possible error of those "thermodynamic" constants is, of course, greater than the error of the "concentration" constants given in Table II and valid at 0.10 *m* total nitrate concentration only. This is essentially due to the nature of the approximations introduced in eq. 13. However, even for systems showing a great variation of K^2_1 with total nitrate concentration (systems involving lead) the values given in Table III should be correct within ±25%.

For comparison Table III gives also equilibrium constants as calculated from the concentration formation constants of the individual complexes obtained by Schwarzenbach[7] by an entirely different technique. The differences between both sets of values are in most cases greater than the experimental error of the methods employed. It is possible that the agreement could be improved if Schwarzenbach values could be corrected for the formation of MeY–Me and similar ion pairs.

The present study shows clearly the experimental difficulties in obtaining true values of formation constants of metal complexes even in apparently simple systems. The interference of the MeY–Me and similar ion pairs is to be expected in all cases where polyvalent cations and (or) anions are present in a complex equilibrium. Although the influence of those ion pairs on the complex equilibria may be quite large, it has been, up to now, considered only in a few cases (see ref. 21). Still greater may be the interference of the "neutral" electrolytes as potassium chloride and nitrate and especially of complexing admixtures as acetates, phosphates, etc., commonly used as buffer solutions. Only few formation constants of weak ion pairs are known exactly. Their numerical application to experimental data obtained at high ionic strengths (0.1 up to 1), can be, with our present knowledge of thermodynamics of concentrated solutions, only very approximate. Measurements at low ionic strengths ($\mu << 0.1$) will be required to enable the performance of the necessary extrapolations with a reasonable precision.

Special care should be taken when using stability constants other than thermodynamic ones for the discussion of numerical relations between formation constants and structural properties of complexes.

THERMAL DEGRADATION OF POLYMETHYL METHACRYLATES

BY S. BYWATER

National Research Council, Applied Chemistry Division, Ottawa, Canada

Received February 19, 1953

Experiments are described on the thermal decomposition *in vacuo* of thin films of polymethyl methacrylate. The investigation covers a series of sharply fractionated samples over a large molecular weight range. The results are interpreted in terms of a free radical mechanism for thermal breakdown.

Very little work of a quantitative nature has been reported on the thermal breakdown of polymers. This work describes the thermal breakdown of polymethyl methacrylate, a polymer which is known qualitatively to break down almost exclusively to monomer.[1]

Experimental

The rate of breakdown of the polymer was measured by the increase in pressure in a closed system due to monomer evolution. The pressure increase was measured on a Pirani gage, calibrated with monomer vapor at the same time as vapor pressure measurements[2] were being made. The total volume of the cell and Pirani to the first stopcock was 126 cc. so that very small rates could be measured.

The polymer in the form of thin film (0.0005″ thick) was cut into 2 discs using a No. 12 cork-borer and was placed on each side of a copper block and held in place by copper rings. This assembly was held in a glass cup inside a cylindrical cell around which a furnace could be lowered. Temperatures were measured by means of a copper–constantan thermocouple element in a well drilled into the block and held in contact by a small copper wedge. The leads were brought out of the cell by soldered joints through kovar-glass seals. The cell could be evacuated to a pressure of 10^{-5} mm. by means of a mercury diffusion pump backed by a rotary oil pump.

Except for preliminary measurements carried out with a benzoyl peroxide-catalyzed polymer, the samples used were all Fe^{++}–H_2O_2 initiated samples produced in aqueous solution. The higher molecular weight fractions were those described by Baxendale, Bywater and Evans[3] (their Table IV) and were the results of a double fractionation. The lower fractions were produced by separating a lower molecular weight Fe^{++}–H_2O_2 catalyzed polymer into twenty-five fractions. Thin films were formed by dissolving the polymer in benzene, placing the solution in a glass ring on a mercury surface and allowing the benzene to evaporate. Preliminary drying was carried out by heating in a vacuum desiccator for two days at ~ 80°.

Viscosity measurements were made in reagent grade benzene solution at 20° using an Ostwald viscometer whose flow time for benzene was 380 seconds. Molecular weights were determined from the extrapolated (η_{sp}/C) *vs.* C curves using the relation between molecular weight and intrinsic viscosity of Baxendale, Bywater and Evans.[4]

In all cases a preliminary rapid heating of the sample to 180–200° with the pumps running was found to be necessary to remove the last traces of solvent from the film. The measurements could then be taken reproducibly over a range of temperatures. Since the Pirani detects minute traces of monomer, measurements of the rate of monomer evolution at a series of temperatures could be made without appreci-

(1) S. L. Madorsky, *J. Polymer Sci.*, 9, 133 (1952).

(2) S. Bywater, *ibid.*, 9, 417 (1952).

(3) J. H. Baxendale, S. Bywater and M. G. Evans, *Trans. Faraday Soc.*, 42, 675 (1946).

(4) J. H. Baxendale, S. Bywater and M. G. Evans, *J. Polymer Sci.*, 1, 237 (1946).

ably changing the amount of polymer in the cell with most samples. For the investigation of rates at various extents of reaction, it was necessary to heat the material to between 200–300° with the pumps running for a controlled time. On quickly cooling, the rate of monomer evolution could then be studied over a lower temperature range without further changing the residual amount of polymer. A preliminary heating to 180° caused no measurable loss in weight of the polymer (< 1%), except in the case of very low molecular weight polymers. The sample was brought to a steady temperature with continuous pumping. For a rate measurement at each temperature, the pumps were cut off and the pressure increase was followed by Pirani measurements for several minutes. The sample was continuously pumped except for these short periods. During a measurement the pressure of monomer vapor never exceeded 2×10^{-3} mm. so that repolymerization should be negligible. The rate of monomer formation was always found to be a linear function of time over the small time ranges studied.

In order to check on the reliability of the apparatus rates of monomer evolution were measured with various amounts of a low molecular weight polymer film on the block. The rate of monomer production was directly proportional to the amount of material as expected.

At the low temperature used in all these experiments, the question arises as to whether monomer diffuses out of the film fast enough, that the results are not vitiated by repolymerization in the highly viscous medium. This problem has been treated by Cowley and Melville, who found that in the photochemical degradation of polymethyl methacrylate results below 160° were unreliable due to slow diffusion of monomer out of the film. The experimental arrangement used here was very similar to that of Cowley and Melville[5] except that the films were somewhat thinner and rates of monomer evolution much lower (2×10^{-8} to 5×10^{-7} g./sec./ml. at the lowest temperatures). These factors make reliable measurements below 160° possible. Calculations using the formula given by Cowley and Melville show that the rates measured even at 100° (the lowest temperature ever used), where diffusion of the monomer will be slowest, should not be complicated by retention of monomer in the polymer film.

Results

The over-all activation energy was found to be independent of extent of reaction (up to 20% monomer loss) for the whole range of molecular weights as measured on fractionated samples. The rate of reaction at any temperature falls off rapidly with increasing conversion (Fig. 1).

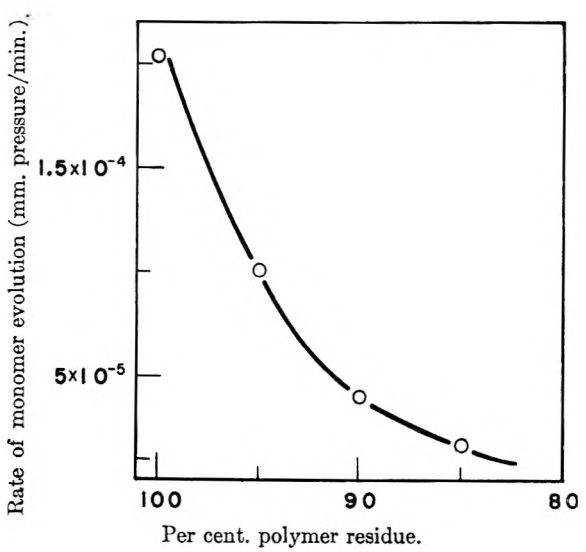

Fig. 1.—Variation of rate of monomer evolution with extent of reaction at a given temperature (M = 322,000).

(5) P. R. E. J. Cowley and H. W. Melville, *Proc. Roy. Soc.* (*London*), A210, 461 (1951).

The over-all rate and activation energy for thermal breakdown was found to be influenced markedly by the molecular weight of the fraction (Fig. 2). Since the rate drops rapidly with extent of reaction, attempts were made to measure all rates at essentially zero conversion. This was

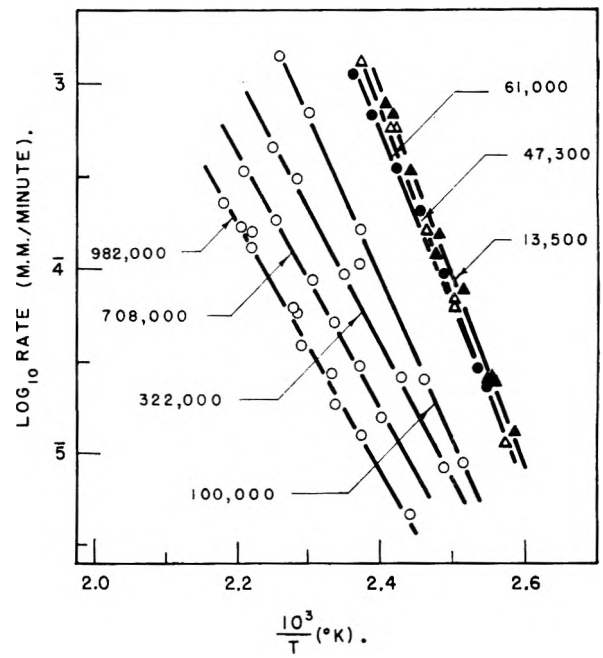

Fig. 2.—Arrhenius plots for the decomposition of fractionated polymers of different molecular weights. The numbers indicate the molecular weight of each fraction (10-mg. samples).

accomplished for all specimens except those of molecular weight 61,000 (95% residue) and 47,300 and 13,500 (90% residue) where reaction was so rapid that the preliminary heating to remove volatiles also produced appreciable degradation. For comparison with the other curves these should be transposed toward the right-hand side of the figure. The variation of activation energy with molecular weight is shown in Fig. 3. Two distinct regions of constant activation energy can be seen with an intermediate zone.

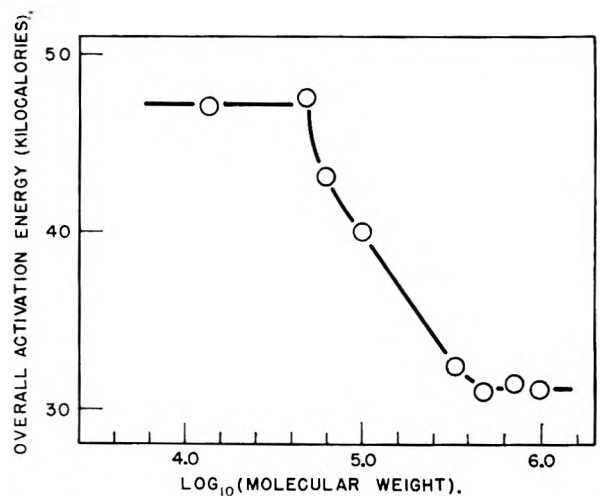

Fig. 3.—Variation of activation energy with molecular weight (fractionated samples).

The behavior of a sample heterogeneous with respect to molecular weight ($\bar{M}_v$ = 89,000) is to be contrasted with the above behavior (Fig. 4). Here the over-all rate and activation energy drop with increasing conversion. This, of course, is to be expected since the work on fractionated samples shows that the lower molecular weight fraction will react preferentially and, as it is removed, the higher molecular weight constituents will degrade with a progressively lower activation energy.

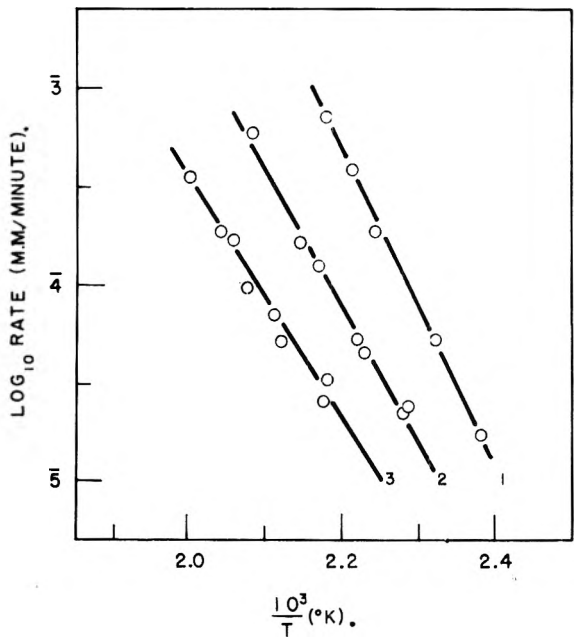

Fig. 4.—Arrhenius plots for the decomposition of a heterogenous polymer at various extents of decomposition: 1, <1%; 2, 14%; 3, 29% (10-mg. samples).

Molecular weights of the polymer residue were measured viscometrically in several cases. There was insufficient specimen to measure viscosities over a range of concentrations but since the solution concentration used was of the order of 0.05%, the (η_{sp}/C) values do not differ appreciably from intrinsic viscosity values. Figure 5 shows the variation of viscosity average molecular weight (of the polymer residue in the cell) with increasing extents of reaction at different molecular weights. The highest fraction alone shows a drop in average molecular weight, but it can be safely assumed that since the viscosity average molecular weight is not unduly sensitive to the presence of a small amount of short chain material, then shorter chain polymers may be present in the polymer residue even with the medium molecular weight fractions.

Discussion

The results presented here show a number of contrasts with those presented by Grassie and Melville,[6] but are still explainable in terms of the same general mechanism. The differences are due to the use of fractionated samples, the use of lower reaction temperatures and to the use of polymer containing a different end grouping. The molecular weight data presented here together with the

(6) N. Grassie and H. W. Melville, *Proc. Roy. Soc. (London)*, A199, 1 (1949).

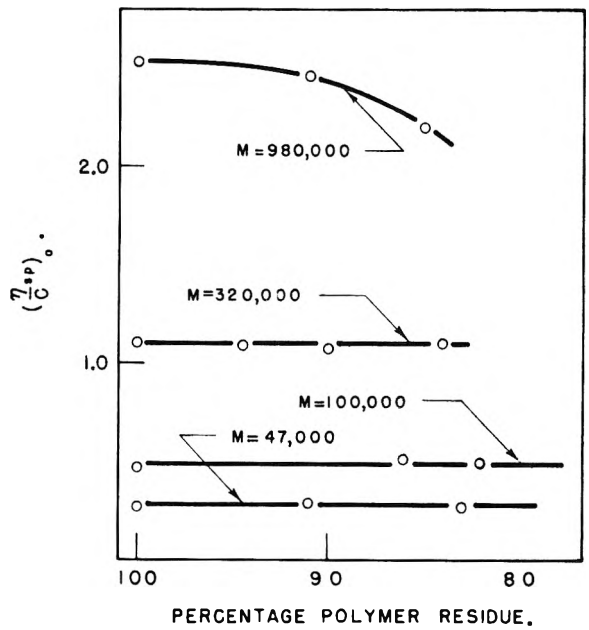

Fig. 5.—Variation of intrinsic viscosity of the polymer residue at various extents of decomposition.

osmotic work of Grassie and Melville show that the initial bond break must occur at the end of the chains. A free radical ending thus produced enables a rapid elimination of monomer to take place by the reverse of the normal polymerization propagation step.

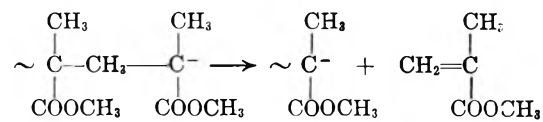

The radical is regenerated allowing the reaction to repeat many times, and this step is of low activation energy (E_D) due to the energy gain on forming the monomer double bond. In fact, numerically, $E_D = \Delta H + E_p$ where ΔH is the heat of polymerization and E_p the activation energy for the normal polymerization propagation step.

Thus if the molecular chain is short, it is possible for each polymer chain undergoing decomposition to degrade completely to monomer without the intervention of a chain termination step. The over-all rate would remain unchanged if a chain transfer reaction consisting of abstraction of a hydrogen atom at random from a neighboring chain would occur. This process must occur very infrequently otherwise the mean molecular weight of the residue would drop rapidly due to the accumulation of shorter chains terminated in this way.

With higher molecular weight polymers the molecular chain length is likely to be higher than the kinetic chain length and chain termination by radical interaction is likely to occur before the molecules are completely degraded. In this case the residual average molecular weight of the polymer would decrease, with increasing conversion, and the over-all rate would be lower because of a lower chain initiation rate due to the smaller number of chain endings per unit mass.

This sharp change in mechanism which would

occur when kinetic and molecular chain lengths were equal, depends on the final one unit radical produced by complete degradation of short chain polymers being incapable of a transfer reaction with a neighboring chain. This is only possible if the radical is capable of isomerization to a stable molecule or if it is rapidly removed from the seat of reaction. Isomerization does not seem likely in the present case, but it seems reasonable that the final one, and possibly two, monomer unit radicals would be volatile enough to be removed into the gas phase. No polymerization of the monomer already there is possible since polymer radicals are unstable at the reaction temperature, so slow recombination is likely. The calculations mentioned above showed that monomer volatilizes rapidly enough so that interaction with radicals is not important; it seems possible that the small radicals could volatilize rapidly enough so as not to react with polymer. A definite proof would be difficult to obtain, but it is clear that a very low chain transfer rate is implied.

Alternative mechanisms involving recombination of radicals with samples of all molecular weights make it necessary to assume a sharp change of initiation or termination mechanisms on increasing the molecular weight of the sample. It seems very reasonable to assume that the depolymerization propagation reaction is unchanged in all cases. This change would involve a difference in activation energy of about 36 kcal. between low and high molecular weight materials in either chain initiation or termination steps. It is difficult to suggest a plausible scheme which would produce this change.

The present data conform to the above scheme if it is assumed that the final one unit radical does not react further due to one of the causes mentioned above. This implies that the kinetic chain length is around 10^3 since the sharp mechanism change occurs at molecular weights between 50,000 and 200,000.

Application of the usual steady state treatment to the concentration of the various radicals, assuming that transfer or terminated polymer chains do not appreciably decompose since due to the low conversions used, the original polymer is in large excess, then the rate of monomer production at low conversions is given by the equations

$$\text{Low mol. wt. polymers } \frac{d[M]}{dt} = \frac{k_i}{M_0} \times P_w \qquad (1)$$

$$\text{High mol. wt. polymers } \frac{d[M]}{dt} = k_D \frac{k_i^{1/2}}{k_t^{1/2}} \sqrt{\frac{P_w}{NM_0}} \qquad (2)$$

where P_w is the original weight of polymer, N is the molecular chain length, M_0 is the monomer molecular weight and k_i, k_D, k_t, are the rate constants for chain initiation, depropagation and mutual termination, respectively. Use of these equations yields values of 48 kcal. for E_i and 22 kcal. for E_T using the extreme experimental over-all activation energies for low and high molecular weights and a value of 18.5 kcal. for E_p.[5] The value of E_i appears low in comparison with known bond dissociation energies in simpler molecules, but there exist no data on larger molecules for an accurate comparison. The value of E_T must correspond to a diffusion controlled recombination of polymer radicals in the viscous polymer melt. It is in reasonable agreement with the E_T value found by Cowley and Melville in photochemical degradation studies at about the same temperatures. The results of Grassie and Melville were obtained at much higher temperatures where E_T was apparently zero due to a melt viscosity of a different order of magnitude. This fact explains the main differences in experimental results. Thus, using the same scheme for the kinetics of depolymerization, due to the particular E_i and E_T values in their case, little change in activation energy is predicted between low and high molecular weight samples, and none in fact was found.

Since a limiting over-all activation energy is obtained at high molecular weights in this work, this implies that E_T does not change over a limited range of polymer viscosities, since the absolute viscosity of the polymer must have varied between the 322,000 and 982,000 molecular weight samples. This perhaps is understandable since Fox and Flory[7] have shown that in a series of polystyrene melts of different molecule weights the absolute viscosity changes somewhat, but the activation energy for viscous flow is unchanged with molecular weight over roughly the same temperature interval. The diffusion of polymer radicals in the polymer is a related phenomenon and hence E_T would probably change very little in these experiments.

Chain initiation exclusively at the ends of the original polymer would explain the unchanged activation energy up to 20% conversion. Grassie and Melville observed an increase in activation energy as reaction proceeded and supposed this to be due to the presence of two types of chain ending in the polymer. No change would be expected with the polymers used here, since the studies on their polymerization[3] suggested identical —OH groups on each end of the polymer chain. Recent studies[8,9] on the kinetics of polymerization of methyl methacrylate by Arnett have corroborated this evidence.

The rapid drop in rate up to 20% conversion is difficult to explain on the basis of the above simple mechanism. An extensive transfer reaction would rapidly reduce the number of original type chain endings, and hence could produce a rapid drop in over-all rate, but would also produce a noticeable drop in the molecular weight of the residue. No such effect was noticeable with low molecular weight polymers. It must be concluded that the mechanism is undoubtedly more complex than the simple scheme suggested above. The limitations imposed by working with a thin polymer film are great and, for example, make it impossible to investigate the effect of polymer concentration and produce uncertainties due to unknown diffusion rates. The simple scheme above does explain many of the observed experimental facts, but cannot be regarded as entirely satisfactory.

(7) T. G. Fox and P. J. Flory, *J. Am. Chem. Soc.*, **70**, 2384 (1948).
(8) L. M. Arnett and J. H. Peterson, *ibid.*, **74**, 2031 (1952)
(9) L. M. Arnett, *ibid.*, **74**, 2027 (1952).

X-RAY DIFFRACTION STUDIES IN THE SYSTEM $BeO-In_2O_3$[1]

BY L. M. WATT AND W. O. MILLIGAN

The Rice Institute, Houston, Texas

Received March 2, 1953

Marked mutual protection against crystallization was observed in the system $BeO-In_2O_3$. The composition ranges over which the two zones of mutual protection extend vary with the temperature level at which the gels are heated. Heat treatment of the dual oxide gels for two hours at 700 or 800° results in interstitial solid solution in the In_2O_3 structure of as much as 90 mole per cent. beryllium oxide.

Introduction

The phenomenon of mutual protective action[2] in dual systems of hydrous oxides has been previously observed in the following systems: $CuO-Fe_2O_3$,[3] $NiO-Al_2O_3$,[4] $Fe_2O_3-Cr_2O_3$,[5] and $BeO-Al_2O_3$, $ZrO_2-Al_2O_3$ and $SnO_2-Al_2O_3$.[6] An examination of the ternary systems $NiO-Cr_2O_3-ZrO_2$[7] and $Al_2O_3-SnO_2-TiO_2$[8] revealed a similar behavior. In each of these systems each oxide prevents or retards the crystallization of the other. The degree of mutual protection varies from system to system and also depends upon the temperature level at which the dual gels have been heated.

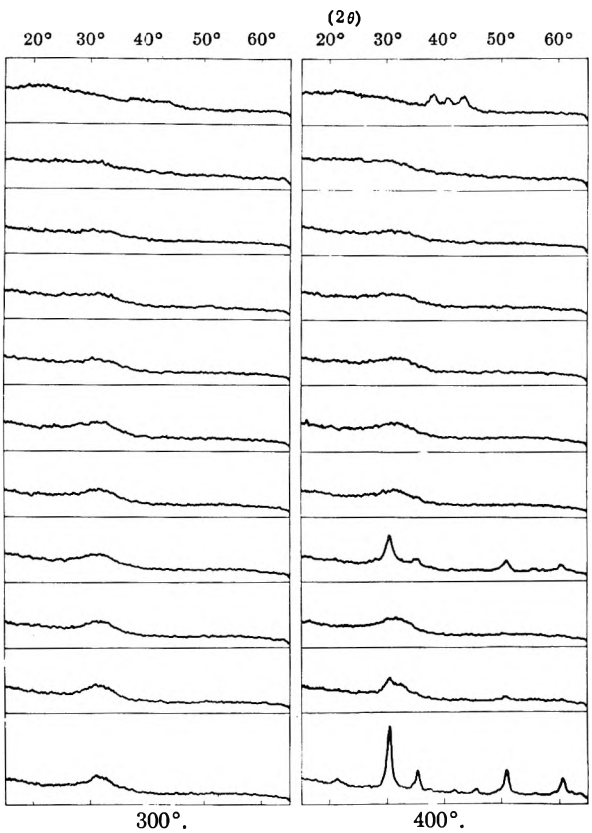

Fig. 1.—X-Ray spectrometer tracings of $BeO-In_2O_3$ gels heat treated at 300 and 400°.

Similar studies are reported here for the system $BeO-In_2O_3$, chosen for the distinctively different crystal structures of the two oxides.

Experimental

Appropriate portions of beryllium and indium nitrate solutions (0.71 *M* with respect to the anhydrous oxides) were mixed together and precipitated with a slight excess of ammonium hydroxide (*ca.* 5.0 *M*) to form eleven mixed hydrous oxide gels containing 0, 10, 20, 30, 40, 50, 60, 70, 80, 90 and 100 mole per cent. In_2O_3. After being washed in a centrifuge with distilled water and dioxane until nitrate free, the gels were poured into evaporating dishes and allowed to dry in air at room temperature. Small portions of the air-dried gels were heated for two hour periods in an electric furnace at 300, 400, 500, 600, 700 and 800°.

X-Ray diffraction patterns of the air-dried and the heat-treated samples were obtained using CuK_α X-radiation and a Norelco 90° recording X-ray spectrometer. Tracings of some of the 77 X-ray spectrometer curves are given in Figs. 1–2 for samples heat treated at 300, 400, 500 and 600°. The results at the higher temperatures are given in chart form in Figs. 3–4.

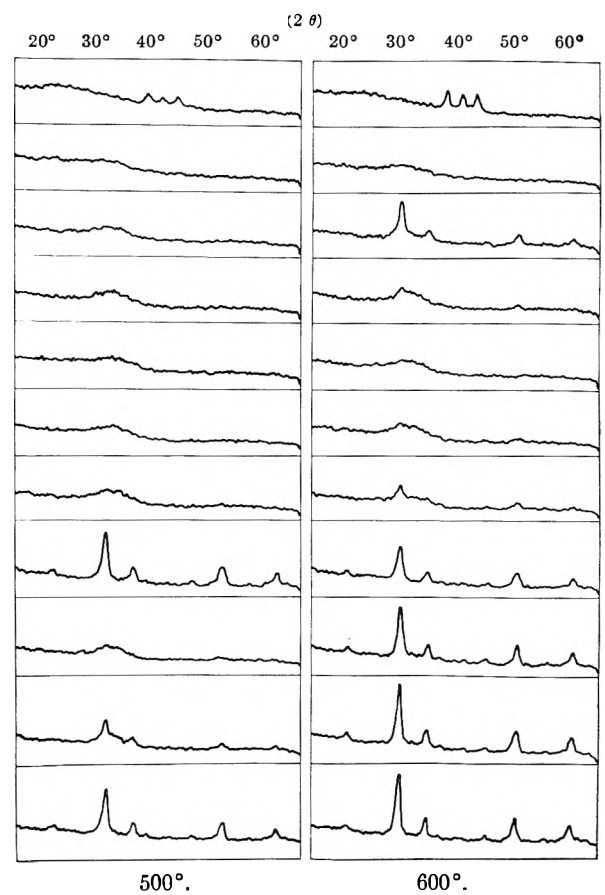

Fig. 2.—X-Ray spectrometer tracings of $BeO-In_2O_3$ gels heat treated at 500 and 600°.

(1) Preliminary results were presented before the 2nd Texas Regional Meeting of the American Chemical Society, Dallas, Texas, December, 1946.

(2) W. O. Milligan, THIS JOURNAL, 55, 497 (1951).

(3) W. O. Milligan and J. Holmes, *J. Am. Chem. Soc.*, 63, 149 (1941).

(4) W. O. Milligan and L. Merten, THIS JOURNAL, 50, 465 (1946).

(5) W. O. Milligan and L. Merten, *ibid.*, 51, 521 (1947).

(6) H. B. Weiser, W. O. Milligan and G. A. Mills, *ibid.*, 52, 942 (1948).

(7) W. O. Milligan and L. M. Watt, *ibid.*, 52, 230 (1948).

(8) W. O. Milligan and B. G. Holmes, *ibid.*, 57, 11 (1953).

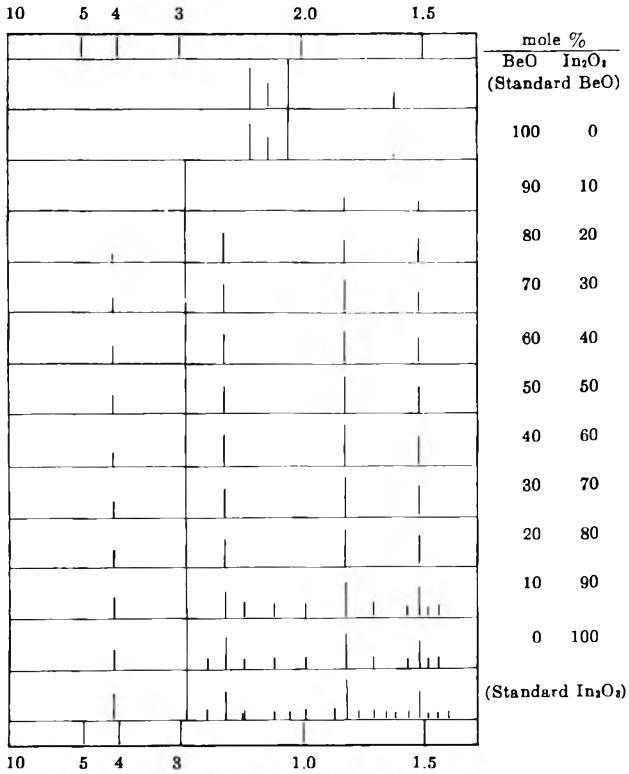

Fig. 3.—Chart of X-ray diffraction patterns of $BeO-In_2O_3$ gels heat treated at 700°.

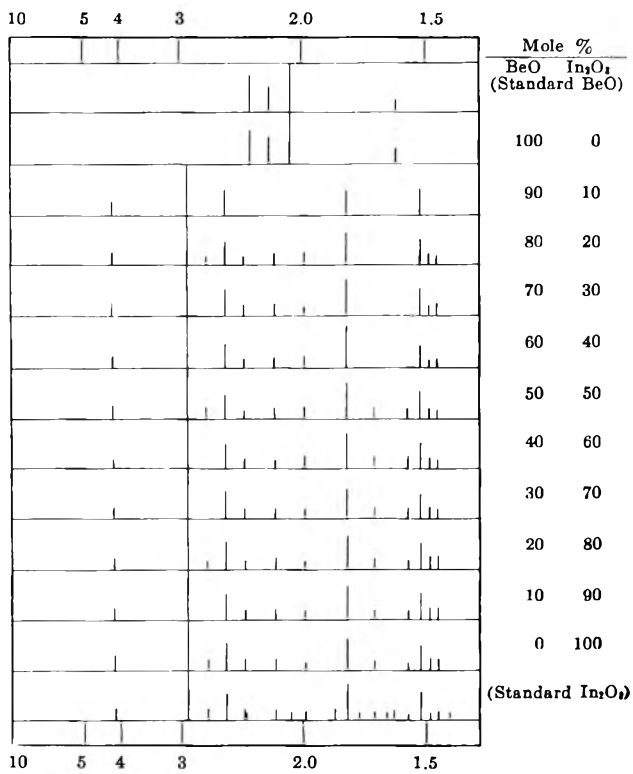

Fig. 4.—Chart of X-ray diffraction patterns of $BeO-In_2O_3$ gels heat treated at 800°.

Discussion

The air-dried samples were amorphous to X-rays, and heat treatment at 300° did not increase the crystallinity appreciably.

The series of samples heated for two hours at 400° and that heated for two hours at 500° exhibited very similar X-radiograms. At these temperatures the mutual protection phenomenon was clearly visible. The samples containing 100 and 90 mole per cent. In_2O_3 gave the standard cubic In_2O_3 pattern; the 80 mole per cent. In_2O_3 sample was amorphous to X-rays; the X-radiogram of the 70% In_2O_3–30% BeO sample also exhibited lines of the standard In_2O_3 pattern; all samples containing 60 through 90 mole per cent. In_2O_3 were again amorphous; and the pure BeO sample gave the standard hexagonal BeO pattern. Thus, two zones of mutual protection against crystallization were observed, one between 90 and 70 mole per cent. In_2O_3 and another between 70 and 0 mole per cent.

Heat treatment at 600° shifted these regions of mutual protection. Figure 2 shows that after two hours at this higher temperature all samples containing 100 through 60 mole per cent. In_2O_3 contain In_2O_3 crystals; the 50 and 40 mole per cent. In_2O_3 samples are amorphous; the 30 and 20 mole per cent. In_2O_3 samples are crystalline; and the 10 mole per cent. sample is also amorphous. The pure BeO sample is again crystalline. In this series of samples the zones of mutual protection lie between 60 and 30 mole per cent. In_2O_3 and 20 and 0 mole per cent.

The samples heated at 700° and at 800° were all crystalline (Figs. 3 and 4), the latter set giving sharper patterns indicating greater crystallinity. All of the dual samples exhibited the diffraction pattern of In_2O_3 alone, instead of the anticipated patterns showing the presence of a mixture of hexagonal BeO crystals and cubic In_2O_3 crystals. The pattern of In_2O_3 alone was observed even when 90 mole per cent. BeO and only 10 mole per cent. In_2O_3 was present. The positions of the diffraction lines did not change appreciably with the addition of increasing amounts of beryllium oxide. The results are in general agreement with some recent observations of Ensslin and Valentiner.[9]

Solid solutions of the lattice substitution type exhibit with a change in composition a change in lattice constants caused by the replacement of ions of one kind by ions of another having different effective radii. The deformation of the unit cell resulting from such substitutions is revealed in the X-ray diagrams by a shift in the positions of the diffraction lines and has been observed in other dual oxide systems such as that of the ferric and chromic oxides.[5]

However, if the packing of the ions in a crystalline compound leaves large enough holes between its ions, small incoming ions foreign to the original substance might fit into these holes without greatly disturbing the structure about them. This would result in an interstitial solid solution. In such an instance an appreciable shift of the lines of the diffraction pattern should not occur. Also, if this distribution of the incoming ions among the holes was entirely

(9) F. Ensslin and S. Valentiner, *Z. Naturforsch.*, 26, 5 (1947).

random, no coherent scattering of the X-rays would be expected, and hence new diffraction lines would not appear.

The small radius of the beryllium ion compared to that of the oxygen and indium ions and the lack of a detectable shift in the observed cubic In_2O_3 lines (Fig. 4) make this type of interstitial solid solution a likely explanation of the crystal structures giving rise to the X-radiograms obtained of the $BeO–In_2O_3$ system.

SORPTION–DESORPTION STUDIES IN THE SYSTEM $BeO–In_2O_3$[1]

BY W. O. MILLIGAN AND C. R. ADAMS

The Rice Institute, Houston, Texas

Received March 2, 1953

Water vapor sorption–desorption isotherms at 2 and 12° have been obtained for a series of eleven heat-treated (2-hour periods) gels selected at every 10 mole per cent. in the system $BeO–In_2O_3$. Two zones of enhanced adsorption occur at compositions of about 40–60 and 90 mole per cent. BeO, in a plot of specific adsorptive capacity at constant p/p_0 as a function of composition. Plots of BET surface area as a function of composition lead to the same conclusion. The two zones of enhanced adsorptive capacity correspond to the zones of mutual protection against crystallization previously detected by X-ray diffraction methods. Isosteric differential and integral heats of adsorption are likewise higher in the regions of mutual protection. The observed enhanced composition zones of amount of adsorption and the enhanced heats of adsorption confirm a prediction set forth in an earlier paper. The most frequent uncorrected Kelvin pore radii computed from the desorption isotherms are 125 Å. for pure In_2O_3 and 25 Å. for pure BeO. As the amount of BeO is increased the pore radii decrease regularly, the greatest changes occurring at compositions of 10 and 90 mole per cent. BeO.

Introduction

In a previous report from this Laboratory[2] a systematic X-ray diffraction study of dual hydrous oxide gels in the system $BeO–In_2O_3$ demonstrated the existence of two composition zones of mutual protection against crystallization. In an earlier investigation[3] the prediction was made that such zones of protection may correspond to regions of maximum surface, and which, therefore, may exhibit enhanced adsorptive properties.

The purpose of this present paper is to report the results of an extensive sorption–desorption study of gels in the system $BeO–In_2O_3$ which have been heat treated at 500°.

Experimental

Preparation of Samples.—The samples employed in this investigation were prepared similarly to those previously used in X-ray diffraction experiments.[2] Freshly prepared solutions of beryllium and indium nitrate (0.5 *M* with respect to the anhydrous oxides) in 0.01 *N* nitric acid were coprecipitated at a *p*H value of 9.4 in a rapid mixing device[4] by the addition of a previously determined quantity of dilute freshly distilled ammonium hydroxide. The amounts of the beryllium and indium nitrate solutions were selected so that the eleven gels corresponded to 0, 10, 20, 30, 40, 50, 60, 70, 80, 90 and 100 mole per cent. In_2O_3. The carefully washed[2] gels were dried in air at room temperature, and then were heat treated at 500° for a period of two hours. After the heat treatment the samples were allowed to attain equilibrium with water vapor in the atmosphere, in order that samples for sorption-desorption isotherms and aliquot portions for water analysis would be identical in composition.

X-Ray Analysis.—In order to ensure that the samples were closely similar to the ones used earlier in X-ray diffraction studies,[2] monochromatic X-radiograms were obtained, using chromium $K\alpha$ X-radiation from a sodium chloride crystal monochromator. "No-Screen" X-ray film was employed, and the exposure time was 60 hours.

Sorption–Desorption Isotherms.—The isotherms were obtained in a multiple sorption–desorption apparatus, fully described elsewhere.[5] The temperature was held constant during each isotherm to approximately ±0.001°.[5] At the same time that the adsorption samples were placed in the apparatus, aliquot portions were weighed and then ignited to constant weight at 750°. The loss in weight upon ignition was attributed to the loss of water, inasmuch as these samples had previously been heated at 500°, at which temperature essentially all of the possible foreign volatile matter would have been lost.

Complete sorption–desorption isotherms were obtained at 12°, employing water vapor as the adsorbate. Barium chloride dihydrate, carefully degassed at liquid nitrogen temperature, was used as the source of water vapor. Water vapor was made available to the samples, while the temperature was being lowered from that of the room to 12° in order to maintain true equilibrium, after which the apparatus was evacuated at 10^{-6} mm. before the commencement of the isotherms. Upon completion of the isotherms at 12°, the temperature was lowered to 2°, again in the presence of excess water vapor. Complete sorption–desorption isotherms were then obtained at 2°, following the same procedure as at 12°.

Results and Conclusions

X-Ray Analysis.—The results of X-ray diffraction analysis were similar to those obtained previously[2] at a temperature level of 500 or 600°. Samples in a wide region of composition were found to be amorphous to X-rays: namely, the region lying between 70% In_2O_3–30% BeO and 10% In_2O_3–90% BeO. The samples containing 30% or less BeO gave only the pattern of In_2O_3 with a decrease in crystallinity as the amount of BeO increased. The X-ray results will not be discussed in detail here.

Isotherms.—The sorption–desorption isotherms are plotted in Figs. 1–22. All of the samples gave similarly shaped isotherms, with the exception of the sample consisting of pure BeO. The isotherms for the ten samples containing In_2O_3 show that a considerable amount of water vapor is taken up at low relative pressures and that only a small amount of water vapor is taken up thereafter, until the relative pressure reaches a rather high value. At

(1) Preliminary results presented before the Division of Colloid Chemistry at the 122nd meeting of the American Chemical Society in Atlantic City, N. J., September 14–19, 1952.

(2) L. M. Watt and W. O. Milligan, THIS JOURNAL, 57, 883 (1953).

(3) H. B. Weiser, W. O. Milligan and G. A. Mills, *ibid.*, 52, 942 (1948).

(4) H. B. Weiser and W. O. Milligan, *ibid.*, 40, 1075 (1936).

(5) W. O. Milligan, W. C. Simpson, G. L. Bushey, H. H. Rachford, Jr., and A. L. Draper, *Anal. Chem.*, 23, 739 (1951).

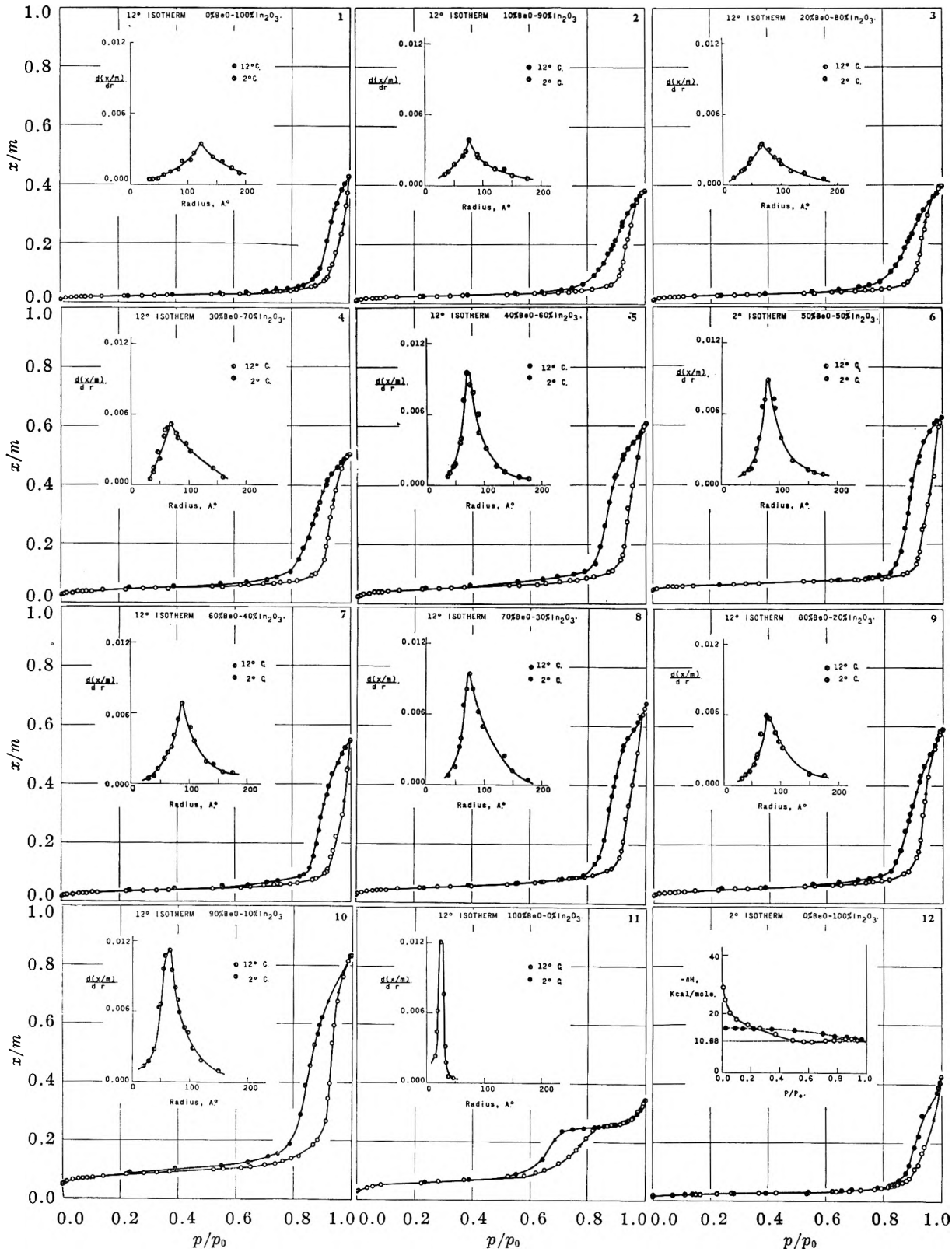

Figs. 1–11.—Sorption–desorption isotherms at 12° and Kelvin pore distributions at 2 and 12° for In_2O_3–BeO mixtures:

Fig.	1	2	3	4	5	6	7	8	9	10	11
BeO, mole %	0	10	20	30	40	50	60	70	80	90	100

Fig. 12.—Sorption–desorption isotherms at 2° and differential (solid line) and integral (dashed line) heats of adsorption at 7° for 100 mole % In_2O_3.

high relative pressures a large amount of vapor is adsorbed, and marked hysteresis occurs.

The sample consisting of pure BeO gives a decidedly different type of isotherm. The amount ad-

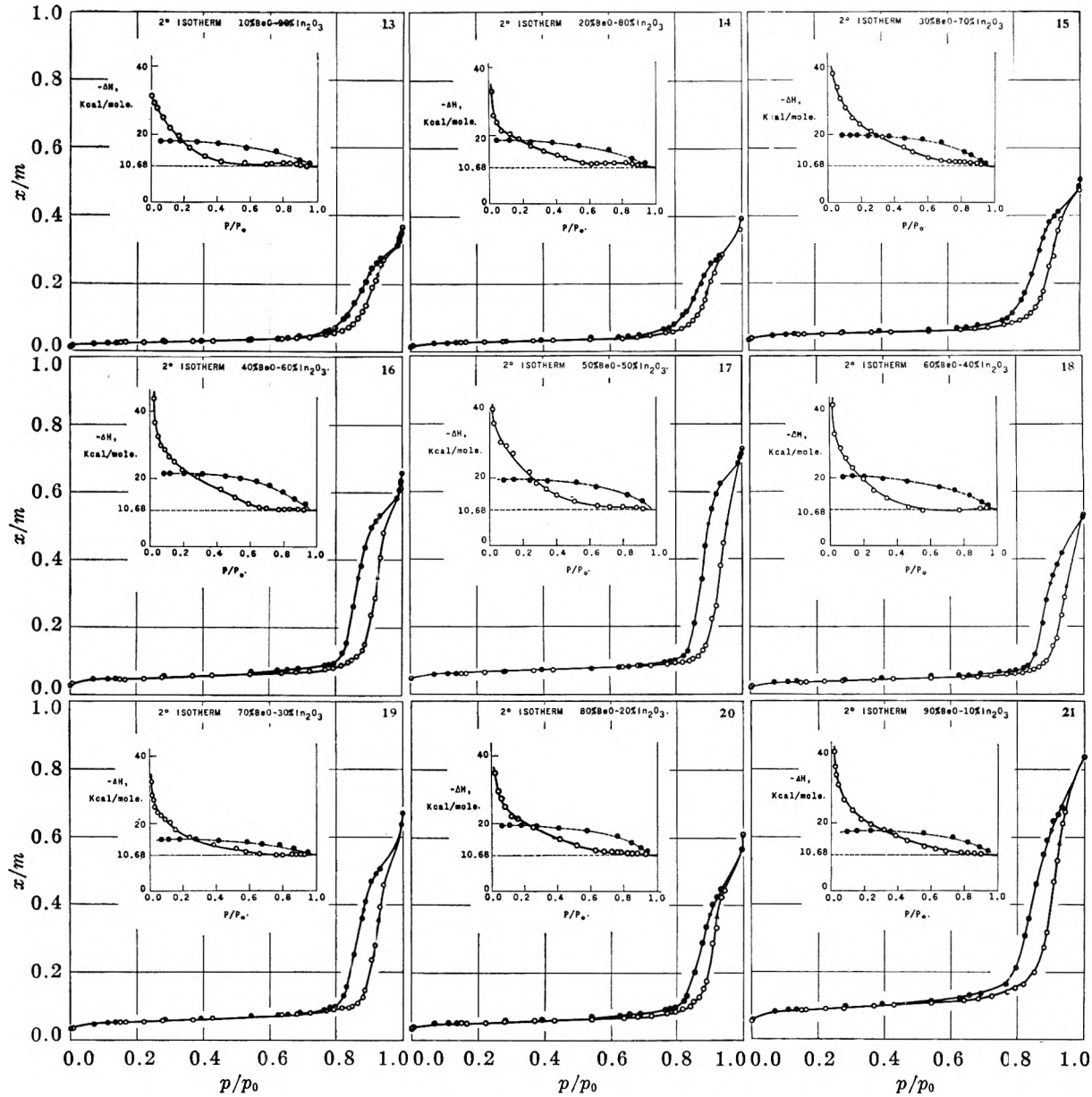

Figs. 13–21.—Sorption–desorption isotherms at 2° and differential (solid line) and integral (dashed line) heats of adsorption at 7° for In_2O_3–BeO mixtures:

Fig.	13	14	15	16	17	18	19	20	21
BeO, mole %	10	20	30	40	50	60	70	80	90

sorbed increases more rapidly in the middle pressure region than for the other ten samples. Also it is noted that, whereas hysteresis in the other ten samples continues up to the saturation pressure, there is a definite region near saturation where adsorption is reversible, and that the hysteresis occurs at a much lower relative pressure, indicating the the absence of large pores.

The results bear out the conclusions reached from X-ray diffraction studies: namely, that the effect of BeO upon the properties of In_2O_3 is not nearly equivalent to the effect of In_2O_3 upon the properties of BeO. The addition of a large amount of BeO to In_2O_3 has relatively little effect upon the properties of the latter, whereas only a small amount of In_2O_3 added to BeO changes its characteristics drastically.

Specific Adsorptive Capacity.—In Fig. 23 the amount of water vapor adsorbed at two different relative pressures is shown as a function of composition. From these two curves it is noted that there are two major regions of increased specific adsorptive capacity, at a region corresponding to 40–60% BeO and at a region corresponding to 90% BeO. These are the same composition regions where maximum mutual protection against crystallization has been observed.

The enhanced adsorptive capacity may be explained on the basis of mutual protection against crystallization.[3] If one oxide acts as a protective colloid for another oxide in the solid state, the protective action serves to prevent growth in the solid phase into the ordered crystal state. It follows that if oxide A is adsorbed by oxide B, it will inhibit

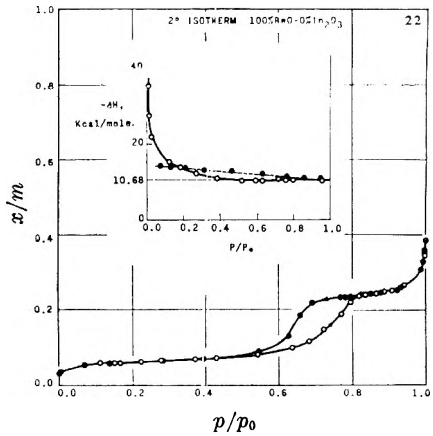

Fig. 22.—Sorption–desorption isotherm at 2° and differential (solid line) and integral (dashed line) heats of adsorption at 7° for 100 mole % BeO.

the crystallization of B, and if oxide B is adsorbed by oxide A, it will inhibit the crystallization of A. The mutual protective action of the two oxides on each other will result in two composition zones of maximum protection against crystallization (one in which oxide A is in excess, and a second in which oxide B is in excess) and three zones of maximum crystallization (in which B is in large excess, a second in which A is in large excess, and a third in which both A and B are present in proportionately large amounts). In the zones of protection, the gels are amorphous to X-rays or consist of extremely finely divided crystals which may correspond to regions of maximum surface and which, therefore, exhibit enhanced adsorptive properties.

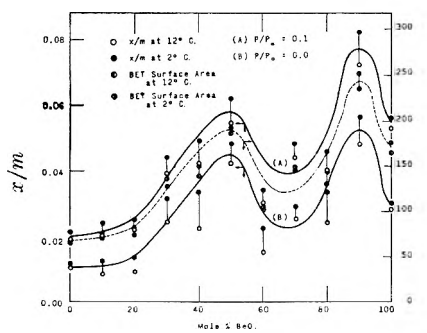

Fig. 23.—Specific adsorptive capacities and surface areas in the system BeO–In_2O_3.

The adsorption data were converted to the BET function and were found to give good straight lines within the range of relative pressures from 0.05 to 0.3, where experience has shown that the BET equation is usually applicable. Surface areas, as calculated by fitting the data to the BET equation by means of the method of least squares, are shown as a function of composition in Fig. 23. They are plotted with the x/m values corresponding to monolayer coverage on the same scale as the x/m values at $p/p_0 = 0.0$ and 0.1. It is noticed that this curve parallels quite closely the curve of x/m *vs.* composition at $p/p_0 = 0.1$. A discussion of the surface areas would lead to the same conclusions as those reached above in connection with enhanced specific adsorptive capacities.

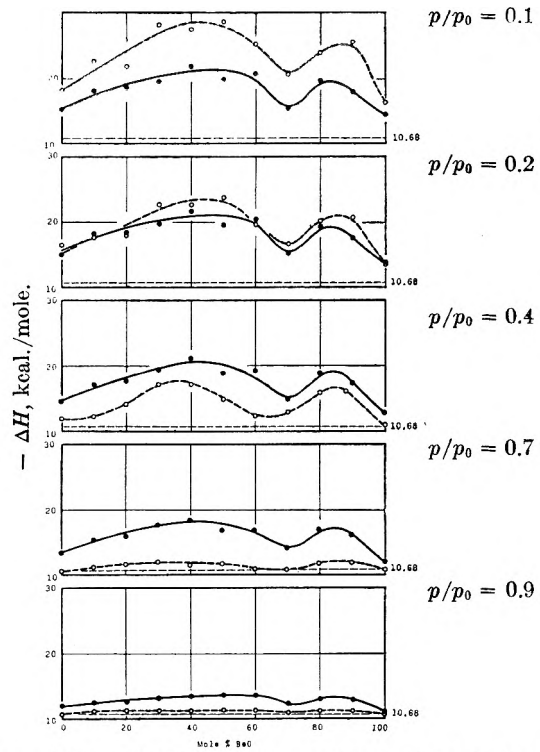

Fig. 24.—Differential (dashed line) and integral (solid line) heats of adsorption in the system BeO–In_2O_3.

Pore Size Distribution.—The hysteresis effects often observed in sorption–desorption isotherms may be interpreted on the basis of the pore structure of the adsorbent.[6] The curves in the insets of Figs. 1–11 give the uncorrected pore distribution for each of the samples as obtained by means of the Kelvin equation, assuming complete wetting.[7] This assumption is justifiable, since the walls of the pores already are wetted by at least a monolayer of water. The maximum point of these curves represents the most frequent uncorrected pore radius. It will be noticed that the pore distributions at the two different temperatures agree closely. This internal consistency of the results supports the view that the Kelvin equation is applicable, inasmuch as several temperature dependent variables are involved.

The most frequent pore radius for 100% In_2O_3 is about 125 Å. The addition of 10 mole per cent. BeO decreases this value to about 80 Å. The average pore radius does not change by more than ±10 Å. upon the addition of more BeO until a composition of 90% BeO is reached. Here the average pore radius is about 64 Å., a decrease attributed to the effect of a high concentration of BeO. The pure BeO shows a very sharp distribution at about 25 Å.

Differential and Integral Isosteric Heats of Adsorption.—The isosteric differential heats of adsorption at 7° obtained by means of the classical Clausius–Clapeyron equation are given in the insets in Figs. 12–22. The integral heat of adsorption

(6) W. O. Milligan and H. H. Rachford, Jr., THIS JOURNAL, **51**, 33 (1947).

(7) W. O. Milligan and H. H. Rachford, Jr., *J. Am. Chem. Soc.*, **70**, 2922 (1948).

was also computed, at constant spreading pressure, employing methods described in the literature.[8] The integral heats are also included in Figs. 12–22.

The differential heats of adsorption at 7° obtained by means of the classical Clausius–Clapeyron equation are quite high at low p/p_0 values where the water vapor is being adsorbed on the bare oxide surface. However, by the completion of the second layer the heats have dropped off to approximately the heat of liquefaction of water.

The integral heats of adsorption at 7° are of lower magnitude in the lower relative pressure regions and show a much smaller decrease with increasing pressure. This is probably due to the particular shape of the adsorption isotherm; there is very little increase in adsorption for a long increase of pressure after a value of $0.1p/p_0$ is reached. The integral heats hold practically constant until pressures of 0.6 to $0.7p/p_0$, at which point they progress regularly toward the heat of liquefaction of bulk water. The pressures at which the integral heats of adsorption show an appreciable reduction correspond with the incidence of capillary condensation.

In Fig. 24 are shown plots of the differential and integral heats of adsorption as a function of composition at various values of the relative pressure. Within the limits to which one would expect the surface properties of one sample to compare with those of another, the two types of curves show a great similarity. Two maxima exist, one between 30% BeO and 60% BeO, the other between 80% BeO and 90% BeO. These are essentially the same composition ranges in which there is mutual protection against crystallization[2] and an increase in surface area and adsorptive capacity (Fig. 23). It will be noted that the two types of heat of adsorption curves cross, as is required.[8] Although there appear to be some additional systematic small maxima, it is the opinion of the authors that they are not to be considered significant at the present time.

(8) T. L. Hill, P. H. Emmett and L. G. Joyner, *ibid.*, **73**, 5102 (1951).

THE STRUCTURE AND ELECTRICAL CONDUCTIVITY OF HYDROCARBON-BASED SOLUTIONS OF THE "SOLUBLE OIL" TYPE. A COMPARABLE AQUEOUS SYSTEM

BY J. BROMILOW AND P. A. WINSOR

Shell Petroleum Co., Ltd., P. O. Box 1, Chester, Great Britain

Received March 6, 1953

The variations in electrical conductivity with gradual modification of the composition of a number of "soluble oils" based on Aerosol OT/undecane-3 sodium sulfate mixtures, on monoethanolamine laurate or on monoethanolamine oleate have been examined. It has been found that a qualitative interpretation of the results obtained may be given on the basis of the intermicellar equilibrium indicated in Fig. 1 which has been used previously in interpreting the electrical conductivity and phase relationships shown by aqueous "solubilized systems" and in accounting for the X-ray diffraction patterns obtained from solutions of detergents. The completely analogous form of the conductivity behavior and phase relationships of the "soluble oil" systems and of a series of wholly aqueous solutions in which the sodium ion of sodium hendecane-3 sulfate is progressively replaced by the cyclohexylammonium ion has been demonstrated. It is concluded that an intermicellar equilibrium of the kind indicated in Fig. 1 is operative in all solutions of amphiphilic substances from the completely aqueous to those based completely on hydrocarbon.

Introduction

In a series of papers published elsewhere[1–3] observations have been described of the phase transitions and electrical conductivity changes which accompany variations of the composition and temperature of a number of solubilized systems. In these systems, containing various amphiphilic salts as "solubilizing agents" or "co-solvents," water and organic liquid were usually present in approximately equal proportions although in some cases water was the major constituent. It was found that a consistent interpretation of the results obtained could be given on the hypothesis of a very mobile intermicellar equilibrium of the type illustrated by Fig. 1. It was also shown[4] that such an equilibrium was in agreement with the published X-ray measurements on detergent solutions.

Systems of the type discussed earlier but of lower water content, or even containing no water at all, are technically of much importance as water-dispersible or "soluble" oils for use in metal working and as textile assistants, etc. The present paper describes an investigation of systems of this type. It will be seen that the phase changes and conductivity variations now recorded are analogous to those found earlier with the more aqueous systems.

To complete the picture, analogous results obtained with an aqueous system in the complete absence of an organic liquid are given (Fig. 6). It thus appears that the intermicellar equilibria and the associated phase transitions shown in Fig. 1 may be realized over the entire range of solutions containing amphiphilic electrolytes from those based completely on hydrocarbon, to those based completely on water.

Experimental

Apparatus.—The apparatus and procedure used for the determination of the electrical conductivities were those described earlier.[3]

(1) P. A. Winsor, *Trans. Faraday Soc.*, **44**, 376 (1948).
(2) P. A. Winsor, *ibid.*, **44**, 451 (1948).
(3) P. A. Winsor, *ibid.*, **46**, 762 (1950).
(4) P. A. Winsor, THIS JOURNAL, **56**, 391 (1952)

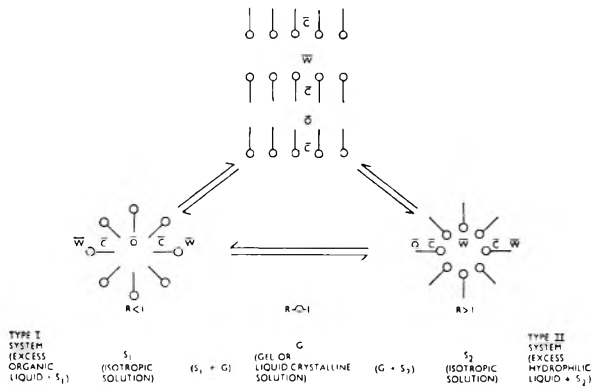

Fig. 1.—Intermicellar equilibrium and associated phase changes: $\overline{\overline{W}}$ = hydrophilic section of micelle; $\overline{C}$ = amphiphilic section of micelle; $\overline{O}$ = lipophilic section of micelle; R = ratio of dispersing tendencies on lipophilic; and hydrophilic faces of $\overline{C}$ respectively.

Materials.—The organic liquids (*n*-hexane, cyclohexane, octanol-1, cyclohexanol) used were middle fractions from the redistillation of pure grade laboratory reagents. Specific resistances (S.R.) > 10^7 ohms.

The undecane-3 sodium sulfate solution, prepared as described earlier,[3] was substantially free from inorganic salt and unsulfated organic matter, had d^{20}_{20} 1.051, undecane-3 sodium sulfate content 26.8% w. (28.2% w./total volume of solution).

The Aerosol OT[5] was the pure compound from General Metallurgical and Chemical Co. Ltd. Its 15% w/total volume solution in *n*-hexane had d^{20}_{20} 0.748, and that in cyclohexane had d^{20}_{20} 0.815.

Monoethanolamine, redistilled, d^{20}_{20} 1.018, n^{20}_{D} 1.4537, equivalent 60.5 (theory 61.0), S.R. 20,500 ohms.

Lauric acid ("Distec," pure), setting point 42.7°, equivalent, found 202 (theory 200).

Oleic acid, cloud point *ca.* 4°, d^{20}_{20} 0.899; n^{20}_{D} 1.4631, equivalent, found 282 (theory 282).

Cyclohexylammonium chloride, colorless crystals, equivalent, found 134.3 (theory 135.5).

Phase Analyses.—The phase compositions recorded in Tables I and II were calculated from the analyses of the S_1- and S_2-phases, the densities of these phases, the relative volumes of the phases measured after complete settling and the synthetic composition of the total systems.

The S-phases of Table I were analyzed as follows: (1) (Aerosol OT + undecane-3 sodium sulfate) by dry wt.; (2) (Aerosol OT/undecane-3 sodium sulfate) by sulfated ash/dry weight, and also by methylene blue titration[6]/dry weight; (3) water by Karl Fischer method; (4) hydrocarbon by difference.

The compositions of the liquid crystalline ("gel") phases were calculated by difference.

In Table II likewise the S-phases were analyzed and the composition of the G-phases calculated by difference. Monoethanolamine was titrated in the presence of water using methyl orange, which is unaffected by lauric acid, as indicator. The lauric acid was titrated in alcoholic solution using as indicator phenolphthalein which is unaffected by monoethanolamine under these conditions.

Graphs.—The wide range of the resistance measurements makes the presentation of the graphs somewhat difficult. Figures for points which could not be conveniently plotted have therefore been indicated at the top of the graphs.

Discussion

A. Aerosol OT–Undecane-3 Sodium Sulfate Systems (Figs. 2 and 3). (1) Conductivity Measurements and Phase Transitions.—In Fig. 2 the specific-resistance/composition curve indicates that the equilibrium, initially in favor of the S_2-micelle, which is the predominant form in solutions of Aerosol OT in hydrocarbon,[7,8] is progressively shifted in favor of the G- and S_1-micelles by addition of the aqueous solution of undecane-3 sodium sulfate ((1) Methods IIa and IIc). A similar curve is obtained with cyclohexane as solvent. The displacement of the intermicellar equilibrium to the left is accompanied by the typical series of phase transitions (S_2 → (S_2 + G) → G → (G + S_1) → S_1 → Type I system) and the changes in electrical resistance are similar to those discussed earlier[3] for more aqueous systems. As with the earlier systems the phase transitions and resistance changes may be reversed by addition of an oil soluble alkanol, *e.g.*, with octanol-1 as shown in Fig. 3. The more water-soluble cyclohexanol produces a similar but less sharp rise in resistance than does the less water-soluble octanol-1.[9]

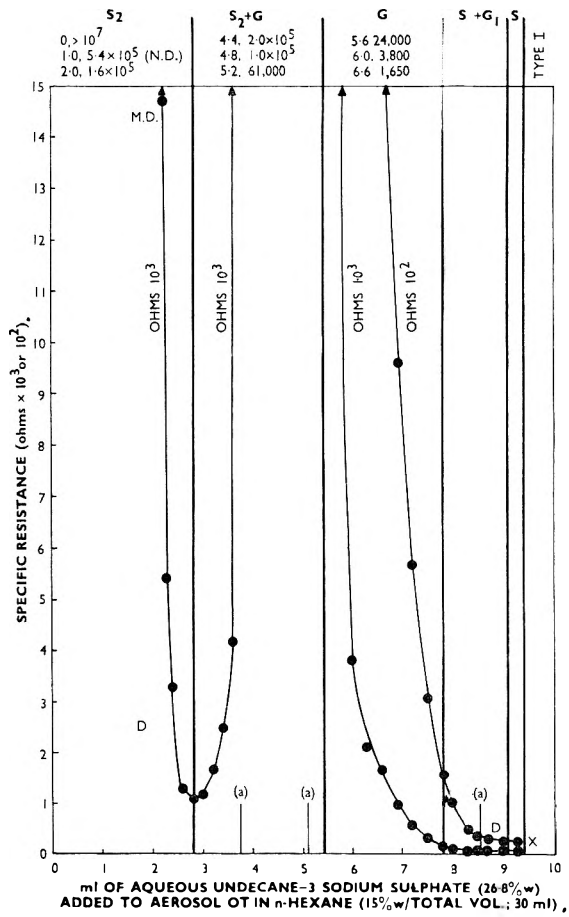

Fig. 2.—Specific resistance changes in Aerosol OT./*n*-hexane systems: D = Opalescent dispersion in water; M.D. = Milky dispersion in water; N.D. = No dispersion; (X) See Fig. 3. (a) Compositions in Table I.

(2) Composition of Equilibrium Phases.—When the lamellar micelle in equilibrium with the S_1- and S_2-micelles reaches a certain concentration and stability, separation of a liquid crystalline phase in equilibrium with a residual S_1- or S_2-phase occurs. It seems likely that this "Gel" phase consists entirely of lamellar micelles which have the com-

(5) The sodium bisulfite adduct of diisoöctyl maleate.

(6) S. R. Epton, *Trans. Faraday Soc.*, 44, 226 (1948)

(7) R. W. Mattoon and M. B. Mathews, *J. Chem. Phys.*, 17, 496 (1949).

(8) W. Philippoff, *J. Colloid Sci.*, 5, 947 (1950).

(9) P. A. Winsor, *Trans. Faraday Soc.*, 46, 768, Fig. 4 (1950).

TABLE I

COMPOSITION OF EQUILIBRIUM S- AND G-PHASES FORMED ON ADDITION OF AQUEOUS UNDECANE-3 SODIUM SULFATE SOLUTION (26.8% w.; 28.2% w./total vol.) TO AN (Aerosol OT + *n*-hexane) SOLUTION (15% w./total vol.; 20 ml.)

$C_{11}H_{23}SO_4Na$ solution, ml.	2.5[a]		3.4[a]		5.7[a]	
Nature of phases	S_2	G	S_2	G	S_1	G
Phase vol., ml.	4.8	17.7	2.4	21.0	11.8	13.9
Specific gravity (D^{20}_{20})	0.732	0.798[b]	0.758	0.780[b]	0.773	0.925[b]
Specific resistance, ohms	4.47×10^5	..	[c]	..	40.0	..
Composition of phases (S_2%w.; G%w./total vol.)						
$C_{11}H_{23}SO_4Na$, %	9.7	2.1	4.7	4.2	9.6	5.3
Aerosol OT, %	2.7	16.5	1.5	14.3	6.9	17.1
n-Hexane, %	79.6	51.9	82.4	48.0	64.3	51.1
Water, %	8.0	9.3	11.4	11.5	19.2	19.0
$C_{11}H_{23}SO_4Na$/Aerosol OT (w./w.)	3.5	0.13	3.3	0.29	1.4	0.31
n-Hexane/water (w./w.)	10.0	5.57	7.25	4.18	3.3	2.7

[a] Compare Fig. 2, subscript *a*. [b] Computed by adding w./total vol. percentages. [c] Insufficient material for determination.

position of the bulk phase and fill it completely.[4,10] A comparison of the composition of the lamellar and equilibrium S-phases should give some idea of the limiting extent of the fluctuations of composition which are osmotically permissible within the individual S-phases. Such comparisons are made in Table I. Entirely analogous results are obtained with comparable systems containing cyclohexane.

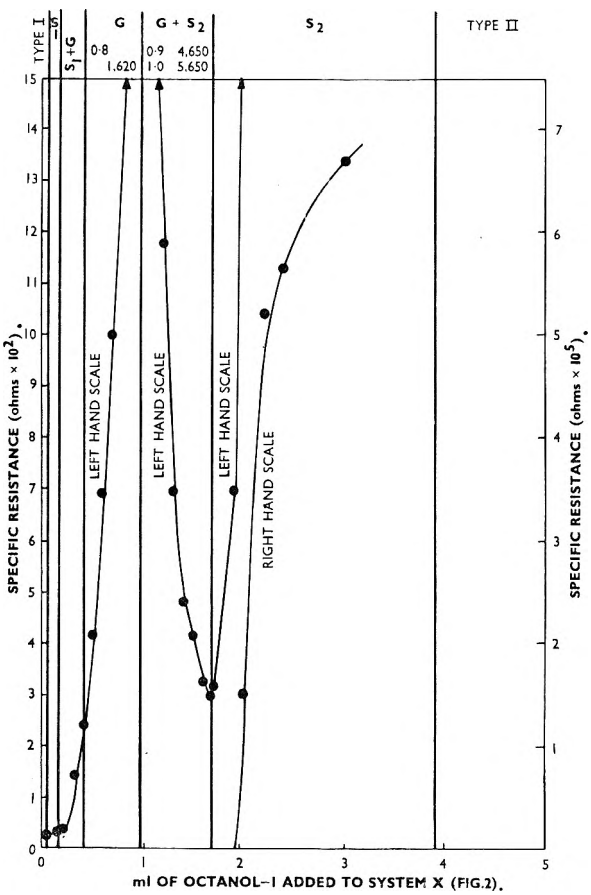

Fig. 3.—Specific resistance changes in Aerosol OT./*n*-hexane systems.

It will be seen that although the equilibrium phases contain significant concentrations of all the components (in contrast to the excess hydrocarbon or water phases in Type I or Type II systems[1]) the divergence in composition is considerable. In spite of this, however, since the phases are in equilibrium the colligative properties of each constituent must be the same in both phases.

An interesting and somewhat surprising feature of Table I is the marked concentration of Aerosol OT relative to undecane-3 sodium sulfate in the liquid crystalline phase whether this is in equilib-

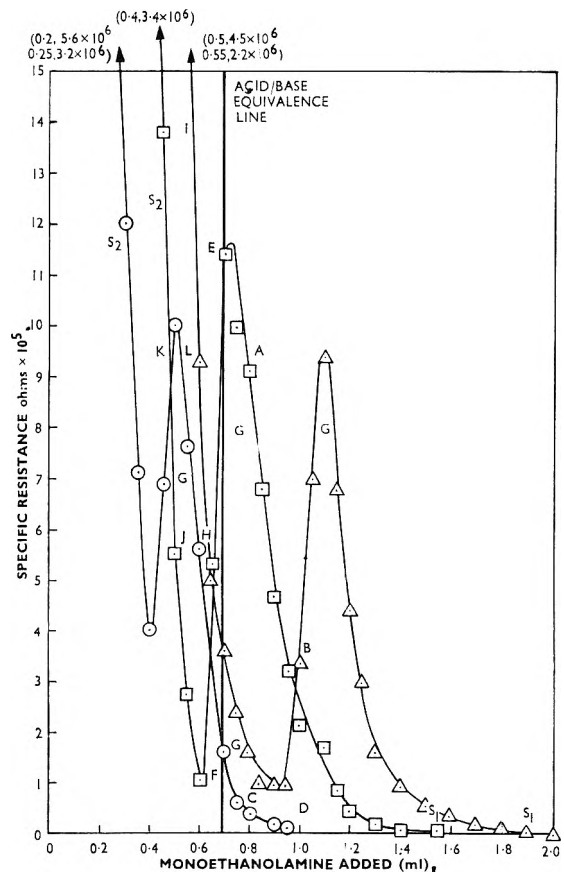

Fig. 4.—Phase transitions and accompanying specific resistance changes on adding monoethanolamine to 25 ml. of a solution of lauric acid (10 g.) in cyclohexane (100 ml.): ⊡, in the presence of 0.15 ml. water; ⊙, in the presence of 0.15 ml. of water and 0.75 ml. of methanol; △ in the presence of 1.00 ml. of water.

(10) A. P. Brady, THIS JOURNAL, 53, 947 (1949).

TABLE II

COMPOSITION OF EQUILIBRIUM S- AND G-PHASES FORMED ON ADDITION OF MONOETHANOLAMINE[a] TO 25 ML. OF A SOLUTION[b] OF LAURIC ACID (10 G. IN CYCLOHEXANE[c] (100 ML.)) IN THE PRESENCE OF WATER (0.15 ML.)

Monoethanolamine added, ml.	0.65		1.10		1.80	
Nature of phases	S_2	G	S_1	G	S_1	Excess cyclohexane
Phase vol., ml.	6.2	19.6	10.4	15.85	23.95	3.0
Specific gravity (20°/20°)	0.782	0.814[d]	0.777	0.837[d]	0.826[d]	0.774
Compositions of phases						
Lauric acid, g.	0.084	2.21	0.008	2.28	2.29	trace
Monoethanolamine, g.	0.021	0.64	0.002	1.12	1.80	only
Cyclohexane, g.	4.70	13.00	8.07	9.63	15.39	2.31

[a] Specific gravity (20°/20°) 1.018. [b] Specific gravity (20°/20°) 0.800. [c] Specific gravity (20°/20°) 0.772. [d] Calculated.

rium with either S_2 or S_1. This may be connected with the relative intolerance of the G-phase for inorganic ions.[4]

B. Hydrocarbon Systems of Lauric (or Oleic) Acid + Monoethanolamine.—Although the systems described under A are of low water content, it was thought worthwhile to determine whether similar phase changes could be realized in almost, or completely anhydrous systems. Results for such systems are recorded in Figs. 4 and 5. In the lauric acid/monoethanolamine systems (Fig. 4) a trace of water was found necessary to inhibit crystallization. It was thought that this was probably due to the high crystallizing tendency of the *n*-fatty acid soap rather than to the necessity for the presence of traces of water for the constitution of the liquid (soap/hydrocarbon) phases. This view was confirmed by the preparation of the oleic acid systems illustrated by Fig. 5. In the latter series all ingredients were carefully dried by entrainment distillation of water before use.

In the hydrocarbon solutions of fatty acid, the acids, presumably, will be dispersed initially as bimolecular units. On increasing the polarity of the carboxyl groups by gradual conversion to monoethanolammonium salts, their tendency to segregation is enhanced and the size of the units will increase giving, at first, a solution with micelles predominantly in the S_2-form. On further gradual addition of monoethanolamine, as is evidenced by comparison of Fig. 4 with Figs. 2 and 3 discussed under A above and with those reported earlier[3] the micellar equilibrium is progressively shifted in favor of the G-(lamellar) and S_1-micelles. This displacement is accompanied by the usual phase transitions and conductivity changes.

(i) **Lauric Acid–Monoethanolamine Systems.**—The most remarkable feature shown by the phase analyses in Table II is that in both the heterogeneous regions $S_2 + G$ and $G + S_1$, the monoethanolamine and lauric acid are very largely confined to the liquid crystalline phase.

In Fig. 4 the further addition of monoethanolamine to the $G + S_1$ mixtures gives first, over a rather narrow range, of compositions, homogeneous S_1 solutions, which break down at the right hand terminations of the conductivity curves into Type I systems (S_1 + excess hydrocarbon) as indicated by the phase analyses in the last two columns of Table II.

The occurrence in these low-water-content systems of rather highly conductive S_1-solutions, and of their breakdown in the above manner is especially interesting. In these S_1-solutions, which are spontaneously emulsifiable in water, the monoethanolammonium carboxylate groups must apparently be associated together, forming (with the small amount of excess monoethanolamine and the water present) a virtually continuous conductive network enclosing the $C_{11}H_{23}$-chains with their associated C_6-hydrocarbon molecules. In the formation of the Type I systems with further addition of monoethanolamine, the increased tendency toward concavity (R (*cf.* Fig. 1) becoming progressively smaller) toward the hydrocarbon side of the network causes extrusion of hydrocarbon as a separate phase.

The formation of the liquid crystalline phase does not correspond to the formation of a definite stoichiometric compound of the lauric acid and the monoethanolamine present. Thus the position of the resistance peaks in Fig. 4 is much affected by the amount of water present and by the addition of methanol. Replacement of cyclohexane with *n*-hexane gives a maximum displaced somewhat to the right.

(ii) **Oleic Acid–Monoethanolamine Systems.**—These systems (Fig. 5) although completely anhydrous show entirely similar behavior to the lauric acid–monoethanolamine systems containing approximately 0.6% water.

In the refractive index/composition curve included in Fig. 5 a maximum in refractive index occurs in the region of homogeneous liquid crystalline systems. This indicates a contraction on the formation of liquid crystal of the order of 1%.[9,11] It is remarkable that this inflexion of the R.I. curve, which is also shown by the monoethanolammonium laurate systems containing 0.15 ml. of water (Fig. 4), is obtained only in the presence of a small amount of water and is absent with the completely anhydrous systems. In a complementary manner no inflection was observed for the completely aqueous systems in Fig. 6 but on addition of 2.5 ml. of cyclohexane (10%) a pronounced maximum appeared as shown. The constitutional significance of these results is not yet clear.

C. Aqueous Systems of Undecane-3 Sodium Sulfate and Undecane-3 Cyclohexylammonium Sulfate.—In the preceding sections A and B it has been shown that the micellar equilibria and associated phase transitions, studied in detail in earlier papers with systems usually containing approxi-

(11) K. Hess, H. Kiessig and W. Philippoff, *Kolloid Z.*, **88**, 48 (1939).

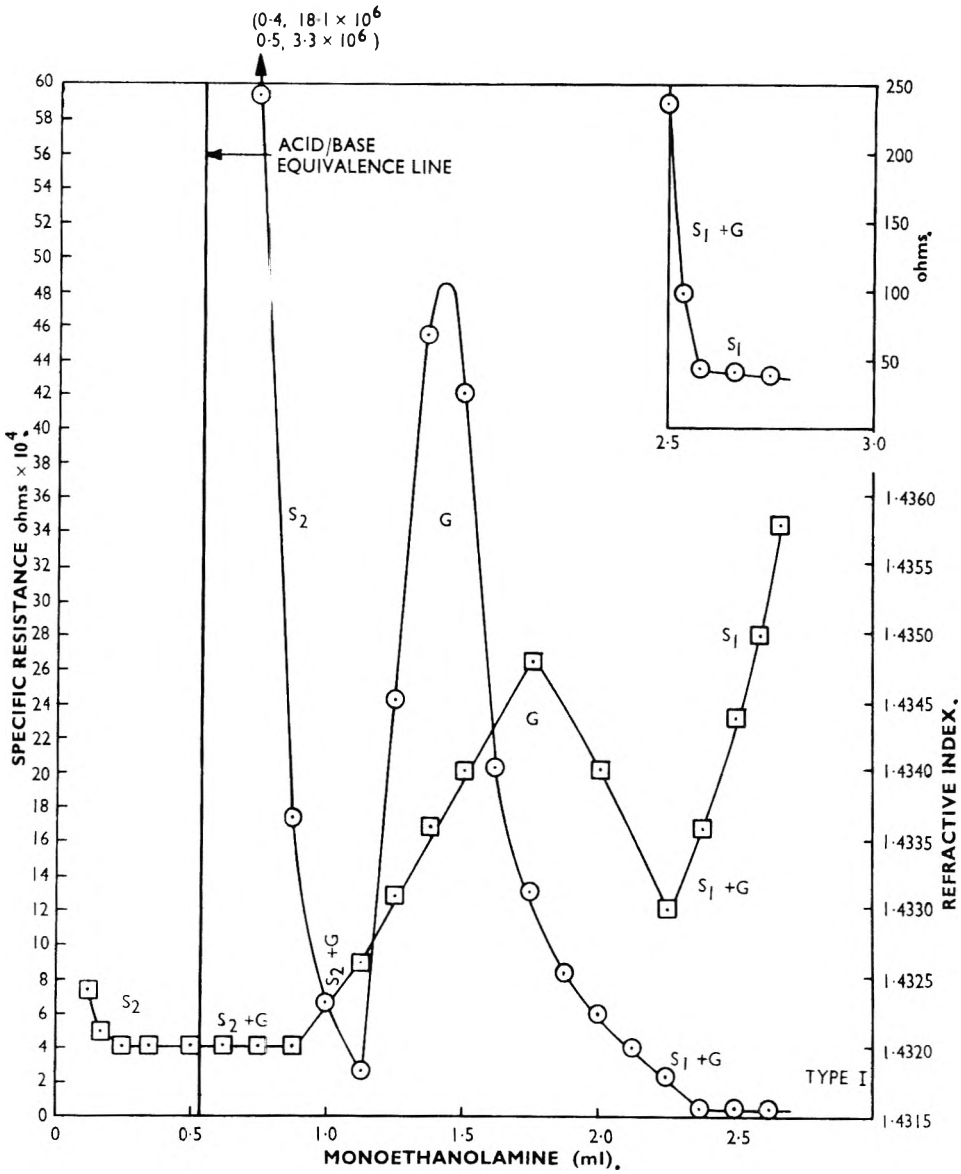

Fig. 5.—⊙, phase transitions and accompanying specific resistance changes on adding monoethanolamine to 25 ml of a 9.90% w./v. solution of oleic acid in cyclohexane; ⊡, corresponding refractive index changes in the presence of 0.25 ml. of water.

mately equal amounts of hydrocarbon and water, are also found with systems based almost or wholly on hydrocarbon. The same equilibria and phase transitions are also observable in wholly aqueous systems (*cf.* ref. 1, 12).

An exact aqueous counterpart to the sequence described under B, *viz.*

$$\text{hydrocarbon soln. of fatty acid} \xrightarrow{\text{mono-ethanolamine}} S_2 \longrightarrow (S_2 + G) \longrightarrow G \longrightarrow (G + S_1) \longrightarrow S_1 \rightarrow \text{Type I system}$$

would be

$$\text{aqueous solution of monoethanolamine} \xrightarrow{\text{fatty acid}} S_1 \longrightarrow (S_1 + G) \longrightarrow G \longrightarrow (G + S_2) \longrightarrow S_2 \longrightarrow \text{Type II system}$$

Attempts were made to study this sequence using lauric acid and oleic acid but, as is usual in systems containing water (± hydrocarbon) with alkane-1 salts in conjunction with alkane-1 polar derivatives,[13] the range of compositions in which liquid crystal G is present was very large. Also these liquid crystalline or partially liquid crystalline systems were very viscous, entrained air bubbles readily and were generally unsuitable for use in conductivity experiments. A much more experimentally convenient series was obtained starting with a 10% w. aqueous solution of undecane-3 sodium sulfate and displacing the intermicellar equilibrium to the right by gradual replacement of Na^+ with cyclohexylammonium$^+$ according to the reaction $C_{11}H_{23}SO_4^-Na^+ + C_6H_{11}\cdot NH_3^+Cl^- \rightleftarrows C_{11}H_{23}SO_4^-C_6H_{11}NH_3^+ + Na^+Cl^-$ (ref. 1, method Ic).

This reaction involves the introduction of NaCl into the system but this should also tend to shift the intermicellar equilibrium to the right (ref. 1 method Id). It should, however, by introducing

(12) J. W. McBain and S. Ross, *J. Am. Chem. Soc.*, **68**, 296 (1946)

(13) P. A. Winsor, *Trans. Faraday Soc.*, **44**, 397, 467 (1948).

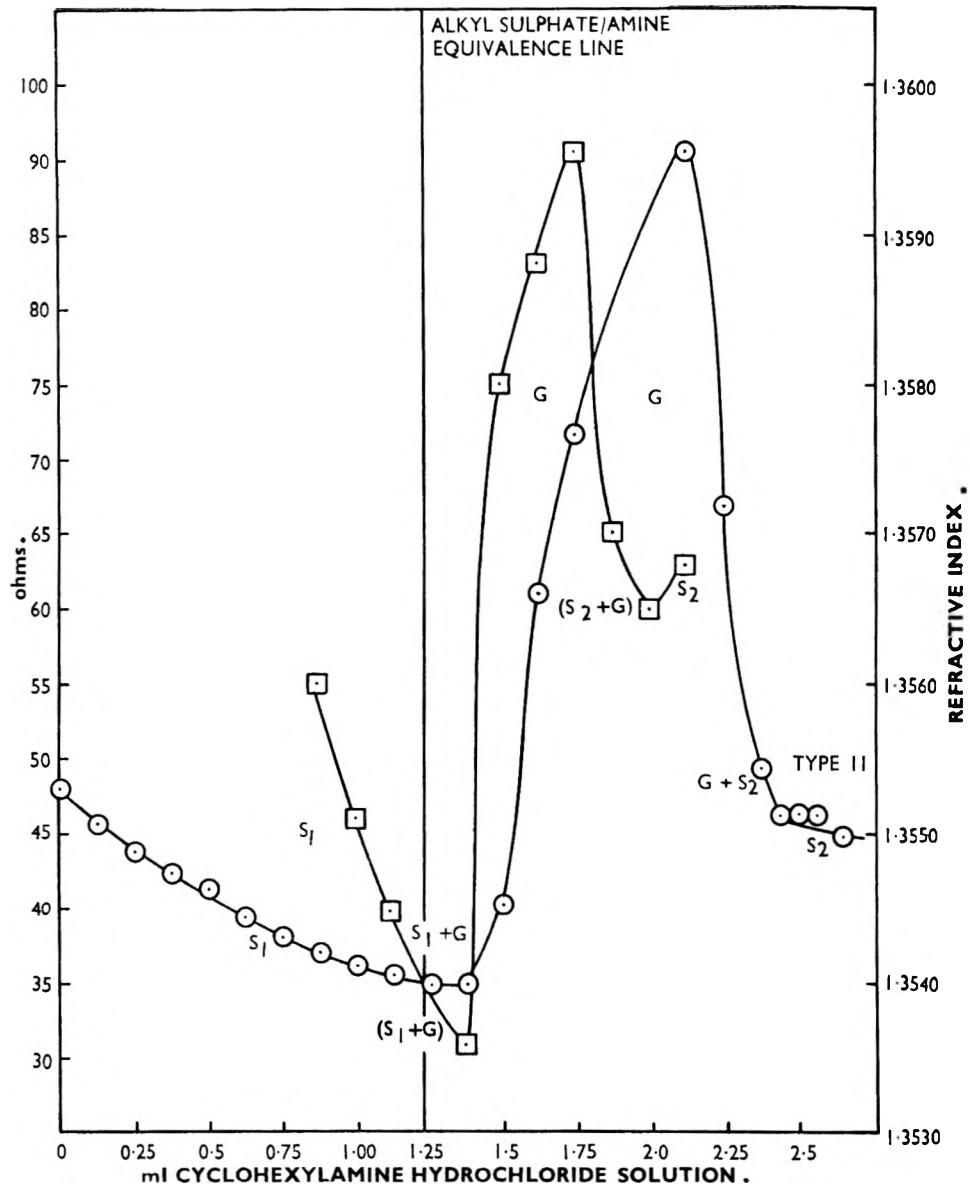

Fig. 6.—⊙, phase transitions and accompanying specific resistance changes on adding cyclohexylamine hydrochloride solution (48.6% w./total volume) to 25 ml. of undecane-3 sodium sulfate solution (10% w.); ⊡, corresponding refractive index changes in the presence of 2.5 ml. of cyclohexane.

additional ions, superimpose a progressive increase in conductivity on the general reduction in conductivity due to the displacement of the intermicellar equilibrium to the right. The phase transitions and accompanying conductivity changes observed are shown in Fig. 6 and appear to be completely analogous to those found with the hydrocarbon and (hydrocarbon + water) systems.

When the clear aqueous gels or liquid crystalline solutions obtained according to Fig. 6 are drawn into a capillary they show birefringence at 45° angle to crossed polaroid sheets and not at angles normal to the crossed polaroids. This behavior, which has been described by Schulman[14] in the case of gels from mixtures containing fatty alcohol/ethylene oxide condensate, water and hydrocarbon, also occurs with the hydrocarbon/monoethanolamine/oleic acid liquid crystalline phase indicated in Fig. 5, with the liquid crystalline 20% aqueous sodium tetradecane-7 sulfate solution,[15] and with other G-phases.

Conclusions

The results described in A, B and C above in conjunction with those reported earlier indicate that the intermicellar equilibrium illustrated by Fig. 1 is operative over the whole range of amphiphilic salt compositions from water-based aqueous soap solutions to hydrocarbon-based "soluble oils."

The considerable conductivity of the G- and S_1-phases in the hydrocarbon systems shows that electrical conduction can occur along the amphiphilic layers which, in these phases, virtually form a many-layer sandwich or quasi-cellular structure enclosing the hydrocarbon. The much higher conductivity of the S_2-phases in aqueous systems even close to the Type II region, probably indicates

(14) J. H. Schulman, *Trans. Faraday Soc.*, **1A**, 3341 (1951).

(15) P. A. Winsor, *ibid.*, **44**, 463 (1948).

that electrical conduction can also readily occur across the amphiphilic electrolyte layers which, in this case, virtually form a quasi-cellular structure enclosing the water.

The progressive change in conductivity with composition or temperature[3] in the S_1- or S_2-phases indicates that the relative abundance of the more and less-conducting micellar forms changes gradually with changing conditions, *i.e.*, that the different forms co-exist in equilibrium and are mutually transformable.

The discontinuous form of the conductivity curve in the region of the existence of the liquid crystalline phase G indicates, when taken with the other special properties of this phase, that its micellar organization is fundamentally different from that of the S_1- and S_2-phases. The variation in structure between the latter two phases is however continuous in character.

Acknowledgment.—The writers wish to thank the Shell Petroleum Co., Ltd., for permission to publish this paper.

THE ADSORPTION OF SILVER SALTS ON SILVER[1]

By Cecil V. King and Ruth Kimmelman Schochet

Department of Chemistry, New York University, New York

Received March 20, 1953

The amount of adsorption of silver nitrate, perchlorate and sulfate on crystalline silver powder, from aqueous solutions, has been measured. The results at 25°, when the metal surface has received no special treatment, indicate less than monolayer adsorption. If the metal has been washed with dilute nitric acid, much larger amounts of silver salt can be taken up. A few measurements have been made at 0°. The results are compared with measurements found in the literature.

The amount of silver nitrate adsorbed on silver (and gold) was first determined by v. Euler and his co-workers.[2-5] The first measurements were made with very fine precipitated silver (particle diameter 0.6–0.8 μ). The values found were consistent, but the authors were not satisfied with their estimation of surface area. Rudberg and v. Euler employed silver sheet, and found several times as much adsorption per unit of apparent area.

Experiments by Proskurnin and Frumkin,[6] designed to find the concentration of silver ion which would make silver a "null electrode," allow calculation of the amount of adsorption of silver nitrate on sheet silver. The values cover an extreme range and are not very self-consistent, which is probably to be explained by the method of surface preparation employed.

Experiments intended to be similar to those of v. Euler and Hedelius, using fine precipitated silver, have been reported by Tartar and Turinsky.[7] These authors concluded that any apparent adsorption was really due to reaction with traces of reducing agent left in the silver. However, in most cases their ratio of silver to solution volume was too small to detect adsorption, and their results are inconclusive.

Work in this Laboratory on the rate of dissolution of silver in ferric sulfate[8] and perchlorate[9] solutions has shown that silver salts, whether formed in the reaction or added separately, have a pronounced inhibiting effect. Equations based on surface coverage following isotherms of the Langmuir type were used to express the dissolution rates. A few adsorption experiments with silver perchlorate on reduced silver[9] were found to follow approximately a Langmuir isotherm, and the adsorption per unit apparent area, extrapolated to infinite concentration ($1/c = 0$), was about twice that estimated from the values of Rudberg and v. Euler for silver nitrate.

Because of the great discrepancies in published values, and to find more about the influence of the anion, it was thought desirable to make quantitative measurements of the adsorption of silver nitrate, perchlorate and sulfate on the metal.

Experimental

The Silver.—In order to adsorb appreciable amounts of the salt, it is necessary to have a large silver surface area in contact with the solutions, and for this reason precipitated silver was employed. Most of the measurements reported here were made with one lot of Mallinckrodt silver. The analysis indicated 0.005% other metals, a similar per cent. of chloride, and 0.05% sulfate.

Preliminary measurements were done with the lot of silver used by King and Lang,[9] which was prepared as described by Walden, Hammett and Edmonds.[10] Both samples were similar in appearance under the microscope, consisting originally of quite uniform rectangular particles whose dimensions could be measured easily. After some use the particles were in general less uniform, the edges and corners were less sharp, and the estimated area had increased as much as 15%. About 80 particles were examined to calculate the area.

Another lot of Mallinckrodt silver was purchased, but not used in the experiments. The particles were smaller and less uniform in size. The estimated area was 1780 $cm.^2/g.$; low temperature nitrogen adsorption[11] gave an area of 2380 $cm.^2/g.$ If the true areas of all the samples are considered to have this ratio to the microscopic area, the adsorption values given below should be multiplied by 0.75.

(1) Based on a Ph.D. thesis submitted by Ruth Kimmelman Schochet to the Graduate School of New York University. Work done under U. S. Atomic Energy Commission Contract No. AT (30-1)-816 with New York University.

(2) H. v. Euler and A. Hedelius, *Arkiv Kemi, Mineralogi Geologi*, **7**, No. 31 (1920).

(3) H. v. Euler and G. Zimmerlund, *ibid.*, **8**, No. 14 (1921).

(4) E. G. Rudberg and H. v. Euler, *Z. Physik*, **13**, 275 (1923).

(5) H. v. Euler, *Z. Elektrochem.*, **28**, 446 (1922).

(6) M. Proskurnin and A. Frumkin, *Z. physik. Chem.*, **155A**, 29 (1931).

(7) H. V. Tartar and O. Turinsky, *J. Am. Chem. Soc.*, **54**, 580 (1932).

(8) H. Salzberg and C. V. King, *J. Electrochem. Soc.*, **97**, 290 (1950).

(9) C. V. King and F. S. Lang, *ibid.*, **99**, 295 (1952).

(10) G. H. Walden, L. P. Hammett and S. M. Edmonds, *J. Am. Chem. Soc.*, **56**, 350 (1934).

(11) Courtesy of Sylvania Electric Products, Inc.

The Measurements.—Bottles containing silver and solution were rotated in a thermostat at 25 ± 0.02° except for a few experiments done in an ice-bath. It is essential to have a silver surface–solution volume ratio which will result in a reasonable concentration change. King and Lang used 10 g. of silver, estimated area 500 cm.²/g., with 25 ml. of silver perchlorate solution, and found 4–10% loss from the solution. When the same silver was used with silver sulfate solution in the present work, the concentration change was found to be 2% or less; with silver nitrate the change was even smaller. The discrepancy was later traced to treatment of the silver with dilute nitric acid before use by King and Lang. This apparently "activates" the surface in some way, and the effect is not permanent.

Without such activating treatment, it was found necessary to increase the amount of silver to 55 g. with 25 ml. of solution. This was the largest amount which would move about freely when the bottles were rotated slowly. This resulted in a loss of 4–12% silver sulfate from solution, somewhat less perchlorate and nitrate.

All of the silver powder was used in preliminary runs, so that it had been in contact with silver salt solution for several hours before use in final experiments; this should be effective in removing less noble metals from the surface, and possibly in reducing local cell action. Before each experiment the silver was washed very thoroughly with water, rinsed with alcohol and fat-free ether, and dried with air on a glass filter.

Since surface contamination with oxide or sulfide was feared, a few samples were rinsed with 5% potassium cyanide before washing with water and drying. There was no pronounced effect on the adsorption measurements.

The time necessary to ensure equilibrium was explored thoroughly. Two hours was sufficient for the nitrate and sulfate; perchlorate was taken up very slowly for a much longer time, and the experiments reported were continued for 72 hours.

Analysis of the Solutions.—Analytical grade potassium bromide was used as the primary standard, and titrations were made with Rhodamine 6 G as adsorption indicator. Successive samples of approximately 10 ml., delivered carefully from a pipet, could be titrated with a precision approaching one part per thousand. Samples of original and final solutions were titrated in succession with the same bromide solution to obtain maximum accuracy in measuring the concentration changes.

From two to six samples were run at each concentration, and the results averaged. The average deviation in amount of adsorption was ordinarily 1 to 6%, in only two experiments above 10%.

Results

The amount of adsorption of the three salts is represented in Fig. 1 in terms of the reciprocal of equivalents per cm.² apparent area[12] *vs.* the reciprocal of equivalent concentration; this is a convenient way of extrapolating to "infinite concentration" ($1/c = 0$). Since silver sulfate is not very soluble, the concentration range for this salt is limited. The other salts were used to the highest practical concentrations to assist in the extrapolation.

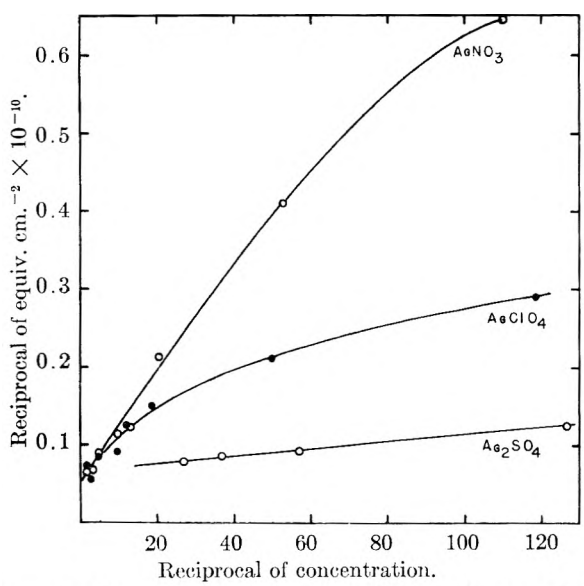

Fig. 1.—The adsorption of silver salts on silver at 25°.

To find whether dilute nitric acid treatment was responsible for the much larger sorption values found for silver perchlorate by King and Lang, silver samples were washed with 4.5% nitric acid (7 ml. commercial acid per 100 ml.) as was done by them. Brief rinsing on a suction filter had little effect, and the silver treatment was repeated as follows: 30-g. samples were washed with six to eight 50-ml. portions of acid, allowing 2 or 3 minutes each time before applying suction to remove the acid. The silver was then washed and dried as usual. Measurements are given in Table I, and are to be compared with values ranging from 3.5 to 18 × 10^{-10} equiv./cm.² plotted in Fig. 1.

TABLE I

SORPTION OF $AgClO_4$ ON NITRIC ACID TREATED SILVER AT 25°

10.0 g. silver, area 675 cm.²/g., bottles rotated 72 hr.

C orig., *N*	*C* final, *N*	Equiv. cm.$^{-2}$ × 10^{10}
0.0226	0.02075	68
.0496	.0458	141
.0606	.0561	167
.2585	.2495	330
.447	.437	360

Rudberg and v. Euler reported no significant difference in the adsorption of silver nitrate on gold between 0 and 50°, but did not carry out similar experiments with silver. A few experiments with silver nitrate at 0° are given in Table II. The bottles were immersed in an ice- and water-bath and were shaken frequently during the day.

TABLE II

ADSORPTION OF $AgNO_3$ ON SILVER AT ~0°

25 ml. solution, 55.0 g. silver, area 615 cm.²/g., two samples each concentration

Hours in ice-bath	*C* orig., *N*	*C* final, *N*	Equiv. cm.$^{-2}$ × 10^{10}
8	0.01885	0.01855	2.3
25	.01922	.01730	14.1
25	.09825	.08715	82

It is well known that silver ion in solution undergoes exchange with silver metal, to such an extent that penetration to the depth of several atomic layers, or its equivalent in surface electrolysis or recrystallization must be assumed.[13] A few adsorption experiments were carried out with silver nitrate containing a small amount of radioactive Ag^{110} in order to measure the adsorption and exchange simultaneously. Samples were titrated as

(12) R. B. Dean, THIS JOURNAL, **55**, 611 (1951), has proposed that 10^{-10} mole cm.$^{-2}$ be regarded as an adsorption unit and called the Gibbs.

(13) B. V. Rollin, *J. Am. Chem. Soc.*, **62**, 86 (1940); C. C. Coffin and I. I. Tingley, *J. Chem. Phys.*, **17**, 502 (1949); H. Gerischer and W. Vielstich, *Z. Elektrochem.*, **56**, 380 (1952); M. Anta and M. Cottin, *Compt. rend.*, **234**, 1686 (1952).

usual, and 2-ml. samples of initial and final solutions were placed in small Petri dishes and counted with an end window GM tube. The initial count of each solution was about 800 per minute above background. Two and three duplicates at each concentration gave the usual agreement in amount adsorbed (~5%) and similar agreement in amount of exchange. The removal of silver nitrate and of radioactivity from the solutions is shown in Table III.

TABLE III

ADSORPTION AND EXCHANGE WITH $AgNO_3$ CONTAINING Ag^{110} ON SILVER AT 25°

25 ml. solution, 55.0 g. silver, area 675 cm.²/g., bottles rotated 20–25 hours

C orig., N	$AgNO_3$ removed, %	Activity removed, %	Adsorption, equiv. cm.$^{-2}$ × 10^{10}	Exchange + adsorption, equiv. cm.$^{-2}$ × 10^{10}
0.01876	2.03	63	2.6	79
.04855	1.55	60	5.1	196
.09875	0.81	77	5.4	510

Discussion

A Langmuir adsorption isotherm can be put in the form

$$\frac{1}{x} = \frac{a}{c} + \frac{1}{x_0}$$

Where x = amount adsorbed per unit area, a is a constant, c = concentration and x_0 is the saturation adsorption. In Fig. 1, values for silver sulfate and for more concentrated nitrate solutions are in reasonable agreement with such isotherms, while values for the perchlorate approach those for the nitrate at higher concentrations. It is significant that the three curves extrapolate to about the same value, near 0.05, at $1/c = 0$, indicating saturation adsorption near 20×10^{-10} equivalents per cm.².

A single atomic layer in the (100) plane of the silver crystal contains 19.9×10^{-10} gram atoms per cm.², while the reticular density of other principal planes is somewhat smaller. Since the true area is almost certainly not less than the measured area, we can say that the adsorption at 25° on silver not treated with nitric acid is always less than monolayer in nature. One is inclined to believe that, with precipitated silver crystals which have been in contact with silver salt solution for several hours, the real area is not much different from the apparent area, and that the limiting amount of adsorption is a monolayer.

The measurements of v. Euler and Hedelius with silver nitrate on precipitated silver have been plotted in the same manner in the upper part of Fig. 2. The straight line has been drawn arbitrarily to an intersection of 0.05×10^{10}, but could hardly be drawn much differently. While the authors felt uncertain of the area within ±50%, it seems more than coincidence that the extrapolated value agrees with ours. However adsorption at the low concentrations employed by these authors, while representing less than a monolayer, is much greater than was found in the present experiments with silver nitrate. To make the two sets of data overlap in the dilute range, one of the area estimations would have to be in error by a factor of 13 times. This is rather unlikely, especially since our

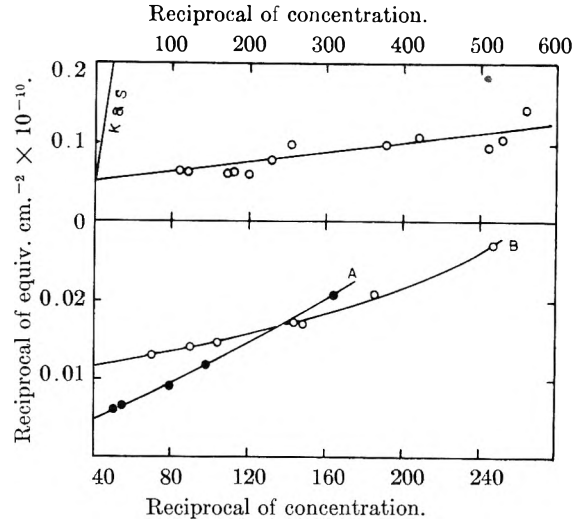

Fig. 2.—The adsorption of silver nitrate and perchlorate on silver: upper curve, v. Euler and Hedelius, precipitated silver; lower curves, A, King and Lang; B, Rudberg and v. Euler, silver sheet.

values for silver sulfate are in the same range as those of v. Euler and Hedelius for the nitrate, and both extrapolate to similar values at $1/c = 0$. It seems more probable that a factor such as surface cleanness is involved, with other adsorbed materials being displaced most easily by the sulfate, but by the other salts at sufficiently high concentrations.

While the measurements discussed above seem to indicate that a simple adsorption process occurs normally, other results show that more complicated sorption can take place under suitable conditions. Curves A and B of Fig. 2 show the measurements of King and Lang on nitric acid treated precipitated silver, and of Rudberg and v. Euler on sheet silver. These curves extrapolate to 87 and 200×10^{-10} equiv./cm.², and the smallest value measured is about 40×10^{-10}. If the silver used by King and Lang had not failed to give similar sorption in later use, we should ascribe the large values to enhanced surface area. The silver used by Rudberg and v. Euler was treated with steam and alcohol vapor, rinsed with water and dried at 100°. Mechanical polishing or nitric acid etching (presumably followed by the above treatment) did not affect the results by more than the experimental error (about 25%).

Cooling to 0° certainly does not affect the surface area, but can have a pronounced effect on the sorption (Table II). The surface treatments mentioned above probably do not increase the real area to 5 or 10 times the apparent area but, instead, favor multilayer sorption. Consistent measurements then demand consistent surface treatment, and each experimenter finds different values.

According to the measurements of Proskurnin and Frumkin,[6] silver acquires a positive charge in solutions containing its ion in concentrations above 10^{-5} N. The charge density on the metal results in an electrical double layer capacity in the neighborhood of 20 microfarads per cm.². Since the potential difference between metal and solution is only a few tenths of a volt, this would require less

adsorption of silver ion alone than any of the values give above; substitution in the relation between capacity, charge and potential

$$20 \times 10^{-6} = \frac{96500x}{0.1}$$

gives $x = 0.2 \times 10^{-10}$ equiv./cm.^{2} per 0.1 volt. Consequently adsorption is specific, involving attachment of both anions and cations to the surface, and not merely a process of charging the double layer.

We may assume that silver ions are adsorbed first, but become a part of the metal lattice; the positive charge carried does not remain localized. To obtain the equivalent of monolayer adsorption, it would not be necessary that silver ions deposit over the whole surface but, rather, that anions become intimately attached in a monolayer. If the anions should be bound approximately as rigidly as in the salt lattice, further sorption might reasonably be expected to occur. The process would not continue indefinitely, because the effect of extra charge on the metal and the lattice forces would be balanced by thermal agitation and dissolution forces acting on the outer layer.

One can understand why low temperatures might favor such multilayer sorption, but we have no explanation for the effect of nitric acid too dilute to etch the surface, or possibly the alcohol vapor treatment of Rudberg and v. Euler.

Exchange experiments show that the surface atoms of a metal, to a depth of several atomic layers at least, have a great deal of mobility. The experiments of Table III show that 60 to 77% of the silver ions originally in solution become part of the metal in some 20 hours, while an equal amount of the original metal dissolved. Exchange in depth may be aided by local cell action, but there is probably the equivalent of an abnormally large self diffusion coefficient in the surface layers, as postulated by Gerischer and Vielstich.[13] The mobility should be an aid in establishing adsorption equilibrium and especially in the displacement of less firmly adsorbed substances. The tremendously rapid exchange must serve to repair minor irregularities of the surface when the metal is immersed in a solution of its own ions. The true area would tend to become equal to the measured area unless the metal is actually porous or has major faults such as abrasion marks, corroded areas, etc.

ON THE DETERMINATION OF CRITICAL MICELLE CONCENTRATIONS BY A BUBBLE PRESSURE METHOD

BY LAWRENCE M. KUSHNER AND WILLARD D. HUBBARD

Surface Chemistry Section, Division of Chemistry, National Bureau of Standards, Washington 25, D. C.

Received March 23, 1953

Bubble pressure measurements have been made on aqueous solutions of pure and commercial grade sodium dodecyl sulfate. The curves obtained with the commercial material have considerable structure depending on the bubbling rate. The curves for the pure samples are what one might expect on the basis of the surface tension of the solutions. The interpretation of bubble pressure and conductance data for solutions of impure surface active materials is discussed.

Introduction

In a recent publication,[1] Brown, *et al.*, have described a bubble pressure method for the determination of the critical micelle concentration of surface active agents in aqueous solution. The method involves measurement of the air pressure necessary to maintain a stream of bubbles from a small diameter tube immersed in the detergent solution. Plots of bubble pressure *versus* concentration of detergent, at different rates of bubbling, show distinct and reproducible irregularities at particular concentrations. The electrical conductances of the same solutions show sudden, small changes at some of these concentrations.

Brown, *et al.*, interpret these effects as indicating more than one critical micelle concentration and also feel that the data present a strong argument for the existence of more than one micellar species in these dilute solutions. They do however point out that all of the surface active compounds used were commercial grade, and suggest that some of the effects noted may be due to the presence of impurities. Since their apparatus is easily reproduced, it was decided to make bubble pressure measurements of this type on a sample of commercial sodium dodecyl sulfate and a sample of pure sodium dodecyl sulfate which had been synthesized in this Laboratory for an earlier research.[2]

Experimental

Materials.—The commercial material[3] was used as received. The pure sodium dodecyl sulfate was synthesized, as described by Shedlovsky,[4] from a vacuum-distilled sample of *n*-dodecyl alcohol. The chlorosulfonic acid for the synthesis was distilled immediately before use. All other reagents and subsequent purification conformed with American Chemical Society specifications. The final step in the purification procedure consisted of extracting the detergent crystals with diethyl ether for about 8 hours in a Soxhlet extractor.

Apparatus and Procedure.—The apparatus design and procedure were the same as described by Brown, *et al.*[1] A 20-gage hypodermic needle was used for all the measurements reported here.

Results and Discussion

Typical plots of bubble pressure *versus* concentration of detergent for both pure and commercial grade sodium dodecyl sulfate are shown in Fig. 1.

(1) A. S. Brown, R. U. Robinson, E. H. Sirois, H. G. Thibault, W. McNeill and A. Tofias, THIS JOURNAL, **56**, 701 (1952).

(2) L. M. Kushner, B. C. Duncan and J. I. Hoffman, *J. Research Natl. Bur. Standards*, **49**, No. 2, 85 (1952), RP 2346.

(3) Obtained from the Fisher Scientific Co., Silver Spring, Md., under the label, Sodium Lauryl Sulfate, U.S.P.

(4) L. Shedlovsky, *Ann. N. Y. Acad. Sci.*, **46**, 427 (1946).

For both samples the upper curve corresponds to a bubbling rate of about 10 bubbles in 4 seconds, the lower to 10 bubbles in 10 seconds.

It is to be noted that whereas the commercial material shows two regions of peculiar behavior (the effects being larger as the bubbling rate is increased, as observed by Brown, *et al.*), the pure sample shows only a rather sudden leveling off of the curve in the region 0.008 to 0.009 *M*. This, it is true, is quite close to the region of micelle formation for sodium dodecyl sulfate, but it is also the region in which the surface tension of these solutions becomes essentially constant.[4] Since, at very low bubbling rates, there is a direct proportionality between surface tension and the maximum bubble pressure during bubble formation and detachment, one would expect an interdependence between the two phenomena even at higher rates of bubbling. Thus, the observed behavior with the pure sample is reasonable without considering the formation of micelles.

Further, the behavior of the commercial material in the region around 0.008 *M* may also be associated with the surface tension rather than micellar effects. Shedlovsky[4] has observed, in this region, a minimum in the surface tension *versus* concentration curve for solutions of sodium dodecyl sulfate which have been deliberately contaminated with dodecanol, an expected impurity in the commercial product.

The break in the curve at 0.03 to 0.04 *M* for the commercial sodium dodecyl sulfate must also, on the basis of the data presented here, be ascribed to the presence of an impurity.

The breaks in the molar conductance *versus* $\sqrt{M}$ curves observed by Brown, *et al.*, at concentrations higher than that expected for micelle formation, are probably due to the nature of the impurity. In the case of lauryl pyridinium chloride and Santomerse No. 3 (used by Brown, *et al.*), the presence of a lower homolog of the major constituent would probably result in the appearance of a second region of micelle formation at a concentration somewhat higher than that of the major constituent. The effect at the higher concentration, however, may be the result of the solubilization of an impurity by the micelles of the major constituent. Such behavior has been observed in this Laboratory with commercial grade sodium dodecyl sulfate. If the impurity were to contribute to the conductance of the solution, such a process could explain the conductivity data.

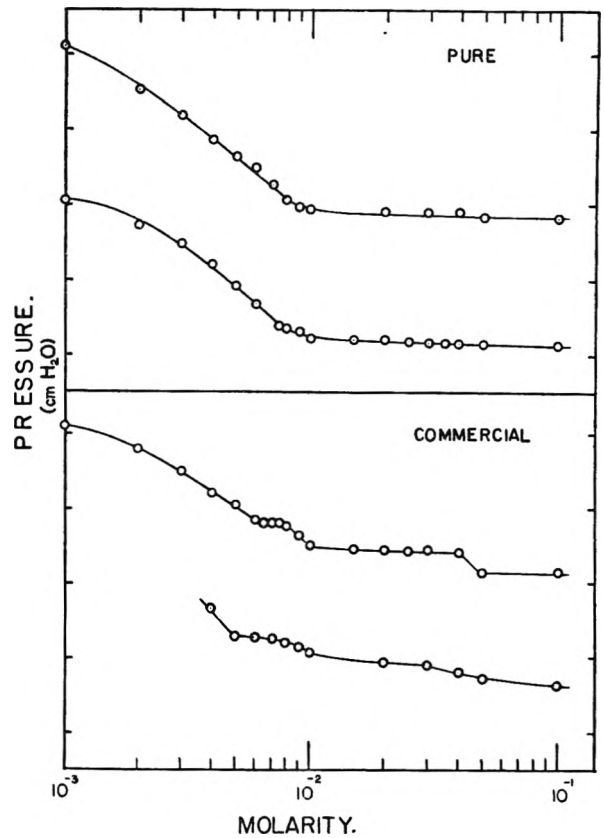

Fig. 1.—Comparison of the concentration dependence of bubble pressure for pure and commercial grade sodium dodecyl sulfate. For each sample, the upper curve corresponds to a bubbling rate of 10 bubbles in 4 seconds, the lower, 10 bubbles in 10 seconds.

Additional work should clarify these points and aid in the evaluation of a bubble pressure technique for the determination of critical micelle concentrations. Of particular interest would be bubble pressure measurements on a pure and impure sample of a surface active material which does not form micelles. It would appear however that the interpretation of a surface effect, as is bubble pressure, is risky in the presence of even a small amount of impurity. Further, one must be extremely cautious in interpreting a surface effect in terms of any bulk property of a solution, such as micelle formation.

THE HYDROLYSIS OF PICOLINAMIDE AND ISONICOTINAMIDE IN CONCENTRATED HYDROCHLORIC ACID SOLUTIONS

BY H. H. G. JELLINEK AND J. R. URWIN

Department of Chemistry, The University, Adelaide, South Australia

Received March 24, 1953

The hydrolyses of picolinamide and isonicotinamide were investigated over a range of hydrochloric acid concentrations from 0.1 to 8 *N*. The experimental first-order rate constants do not pass through maxima with increasing hydrochloric acid concentration. The Arrhenius equations at a number of hydrochloric acid concentrations were determined. The energies of activation and the *A* factors increase with hydrochloric acid concentration.

The hydrolysis of amides in concentrated acid solutions was studied by a number of workers.[1] The first-order rate constants pass through maxima in all cases with increasing acid concentrations. Various theories were advanced to account for these maxima; however, none can be considered satisfactory.

Recently, Jellinek and Gordon[2] investigated the hydrolysis of nicotinamide. In contrast to all the other amides, the rate constants for this heterocyclic amide do not pass through a maximum, but increase steadily with the acid concentration.

The present paper extends the work to other heterocyclic amides, such as picolin- and isonicotinamide. It is shown that these amides behave in a similar way to nicotinamide. A study also has been made of the parameters of the Arrhenius equation as functions of the acid concentration. Both the energies of activation and frequency factors, the latter divided by the respective acid concentrations, increase with the acid concentration. In the case of the non-heterocyclic amides, only the energies of activation increase, whereas the frequency factors remain constant.[1]

The differences in the hydrolyses of the three heterocyclic amides are only small, indicating that the position of the amido group on the ring does not exert a significant influence on the reaction.

As in the previous work on nicotinamide,[2] the polarograph was used to analyze the reaction mixtures. The analysis was based on the fact that the polarographic waves of the acids corresponding to the amides disappear at high *p*H values.

Experimental

Materials.—The preparation of picolinamide (m.p. 106.5°) and isonicotinamide (m.p. 156.0°) is described elsewhere.[3] Hydrochloric acid, sodium hydroxide, borax and disodium hydrogen phosphate were Analar reagents.

Technique.—The hydrolyses were carried out in sealed glass tubes, immersed in an oil thermostat, kept constant within ±0.5°. The tubes (Hy-sil glass) were cleaned with chromic acid mixture, thoroughly rinsed with distilled water and dried. Tubes were withdrawn from the thermostat at definite time intervals, rapidly cooled and analyzed as described below.

Calibration curves for the polarographic analysis were prepared for picolinamide and isonicotinamide over a range of concentrations from 0.2×10^{-3} to 2×10^{-3} *M*. These solutions were obtained from stock solutions of the amide in 0.1 *N* hydrochloric acid diluted with 0.1 *N* hydrochloric acid to give a range of amide concentration. Ten-ml. portions of these solutions were made up to 50 ml. with a phosphate buffer. The *p*H values were 11.5 ± 0.1 as determined with a Cambridge *p*H meter in conjunction with an "Alki" glass electrode. The buffer consisted of 100 ml. of *M*/20 $Na_2HPO_4 \cdot 2H_2O$ plus 86.4 ml. of 0.1 *N* sodium hydroxide; this solution made up to 200 ml. with water gave a *p*H value of 12.0.

The diffusion current was found to be a linear function of the amide concentration in the range of concentrations indicated above. It was also ascertained that hydrolysis did not take place in the buffer over several hours at 25°.

The reaction mixtures, after hydrolysis for definite time intervals, were buffered as described above, with the exception of those reaction mixtures which had concentrations of hydrochloric acid of 1 *N* or above. In these instances, the reaction mixtures were first diluted to make them 1 *N* with respect to hydrochloric acid. Ten ml. samples were then almost neutralized with 2 *N* sodium hydroxide and made up to 50 ml. with the phosphate buffer. All final solutions had *p*H values of 11.5 ± 0.2.

Experimental Results

(a) **Hydrolyses as a Function of the Temperature.**—The hydrolyses in 0.1 *N* hydrochloric acid were carried out over a range of temperatures from 79.5 to 139.3° for picolinamide and from 70 to 130° for isonicotinamide. In both cases the reactions follow a first-order law. Table I gives the initial concentrations of the amides in moles/liter at the various temperatures and the corresponding rate constants in reciprocal seconds. The last column shows these rate constants corrected for thermal expansion of the solutions from room temperature to the respective reaction temperatures. These corrections were made by first calculating the hydrochloric acid concentrations at the respective reaction temperatures. The rate constants were then adjusted linearly to the same hydrochloric acid concentration (*i.e.*, 1/10 *N*) for all reaction

TABLE I

HYDROLYSIS OF PICOLINAMIDE AND ISONICOTINAMIDE IN 0.1 *N* HYDROCHLORIC ACID

Temp., °C.	Initial concn. of amide, mole/l. ($\times 10^3$)	Rate constants, sec.$^{-1}$ ($\times 10^4$)	Cor. rate constants, sec.$^{-1}$ ($\times 10^4$)
	Picolinamide		
79.5	5.02	0.0213	0.0216
90.5	5.02	0.0807	0.0836
99.5	5.02	0.155	0.161
119.5	4.98	0.685	0.725
129.5	4.98	1.46	1.56
139.5	5.05	2.53	2.73
	Isonicotinamide		
70.0	5.00	0.0266	0.0271
79.5	5.00	0.0576	0.0587
98.3	5.03	0.238	0.248
120.3	4.96	1.163	1.23
130.0	5.00	2.24	2.39

(1) B. S. Rabinovitch and C. A. Winkler, *Can. J. Research*, **20B**, 73 (1942), contain references to earlier work.

(2) H. H. G. Jellinek and A. Gordon, THIS JOURNAL, **53**, 966 (1949).

(3) H. H. G. Jellinek and J. R. Urwin, not yet published.

temperatures. The assumption of linearity is justified for small concentration ranges.

Figure 1 shows the experimental results for picolinamide; isonicotinamide gives very similar straight lines. The first-order law for these amides is obeyed up to about 80% conversion.

Hydrolyses were also investigated in 1, 3 and 8 *N* hydrochloric acid over a range of temperatures. Table II gives the relevant initial concentrations of amide and rate constants.

TABLE II

HYDROLYSIS OF PICOLINAMIDE AND ISONICOTINAMIDE IN 1, 3 AND 8 *N* HYDROCHLORIC ACID

HCl, *N*	Temp., °C.	Initial concn. of amide, moles/l. ($\times 10^2$)	Rate constants, sec.$^{-1}$ ($\times 10^4$)	Cor. rate constants, sec.$^{-1}$ ($\times 10^4$)
		Picolinamide		
1.00	85.0	5.07	0.392	0.405
1.00	102.0	5.07	1.56	1.63
1.00	113.0	5.20	3.47	3.66
3.04	70.5	15.0	0.368	0.376
3.04	85.0	15.0	1.43	1.48
3.04	100.0	15.0	4.72	4.92
8.08	54.5	30.2	0.232	0.235
8.08	69.5	30.4	1.095	1.12
8.08	85.0	30.0	5.18	5.35
		Isonicotinamide		
1.00	68.0	5.00	0.373	0.380
1.00	90.5	5.05	2.21	2.23
1.00	100.0	5.05	4.80	5.00
1.00	105.0	5.04	6.78	7.10
3.04	55.5	15.10	0.375	0.380
3.04	68.0	14.90	1.29	1.32
3.04	83.0	14.85	4.75	4.89
8.08	41.0	29.3	0.294	0.296
8.08	55.5	29.8	1.43	1.45
8.08	68.0	30.8	4.52	4.61

The Arrhenius equations for the hydrolyses in 0.1, 1, 3 and 8 *N* hydrochloric acid were derived from plots of the logarithms of the corrected rate constants against the reciprocal of the absolute temperatures:

PICOLINAMIDE

0.1 *N* HCl $k = 6.5 \times 10^7 e^{-21500/RT}$ sec.$^{-1}$
1.0 *N* HCl $k = 7.6 \times 10^8 e^{-21800/RT}$ sec.$^{-1}$
3.0 *N* HCl $k = 8.45 \times 10^9 e^{-22200/RT}$ sec.$^{-1}$
8.0 *N* HCl $k = 3.80 \times 10^{11} e^{-23800/RT}$ sec.$^{-1}$

ISONICOTINAMIDE

0.1 *N* HCl $k = 2.7 \times 10^7 e^{-20500/RT}$ sec.$^{-1}$
1.0 *N* HCl $k = 9.2 \times 10^8 e^{-20900/RT}$ sec.$^{-1}$
3.0 *N* HCl $k = 7.9 \times 10^9 e^{-21100/RT}$ sec.$^{-1}$
8.0 *N* HCl $k = 7.4 \times 10^{10} e^{-21700/RT}$ sec.$^{-1}$

(b) **Rate Constants as a Function of the Hydrochloric Acid Concentration.**—Hydrolyses were carried out over a range of hydrochloric acid concentrations from 1.0 to 8 *N* at 85° for picolinamide and at 68° for isonicotinamide. A first-order law is obeyed for either substance over the whole range of hydrochloric acid concentrations. As can be seen from Table III, the rate constants increase steadily with the hydrochloric acid concentrations. The rate constants for 0.1 *N* hydrochloric acid were calculated from the corresponding Arrhenius equations.

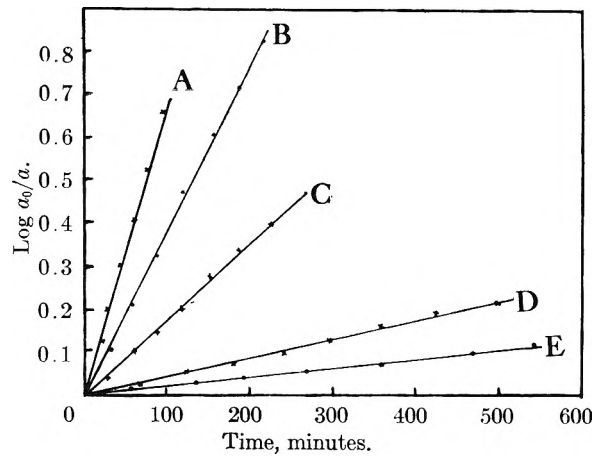

Fig. 1.—Hydrolyses of picolinamide in 0.1 *N* hydrochloric acid over a range of temperatures: A, 139.5°; B, 129.5°; C, 119.5°; D, 99.5°; E, 90.5°.

TABLE III

RATE CONSTANTS AS FUNCTION OF THE HYDROCHLORIC ACID CONCENTRATION

HCl, *N*	Cor. $k_{expt.}$, sec.$^{-1}$ $\times 10^4$	HCl, *N*	Cor. $k_{expt.}$, sec.$^{-1}$ $\times 10^4$
Picolinamide at 85°		Isonicotinamide at 68°	
0.100	0.058	0.100	0.020
0.970	0.392	0.980	0.373
1.94	0.875	1.96	0.775
2.94	1.43	2.98	1.29
3.86	1.85	3.91	1.83
5.73	3.28	5.02	2.56
6.85	4.35	5.80	3.18
7.83	5.18	7.92	4.52

Discussion

It is of interest to consider the energies of activation and frequency factors of the Arrhenius equations as functions of the hydrochloric acid concentration for the non-heterocyclic[1] and heterocyclic amides.

Whereas, the energies of activation rise steadily for all amides with increasing acid concentration, the frequency factors divided by the respective acid concentrations, remain practically constant for the non-heterocyclic amides, but rise continuously for the heterocyclic amides. In the latter case, the increase in the energies of activation is just about compensated by the increase in the $A/[HCl]$ factors. The logarithms of the $A/[HCl]$ factors plotted against the respective energies of activation give straight lines for picolin- and isonicotinamide, as is shown in Fig. 2.

A satisfactory mechanism has not yet been advanced to account for the maxima in the rate constant *versus* acid curves for non-heterocyclic amides, though a number of suggestions have been made by various authors.[1] The occurrence of these maxima has been ascribed repeatedly to salt or complex formation.[4-6] The reason for the different behavior of the heterocyclic amides is not clear and it would be premature to offer any suggestions at this stage of the work.

(4) T. W. J. Taylor, *J. Chem. Soc.*, 2741 (1930).
(5) V. K. Krieble and K. A. Holst, *J. Am. Chem. Soc.*, **60**, 2976 (1938).
(6) A. Benrath, *Z. anorg. allgem. Chem.*, **151**, 53 (1926).

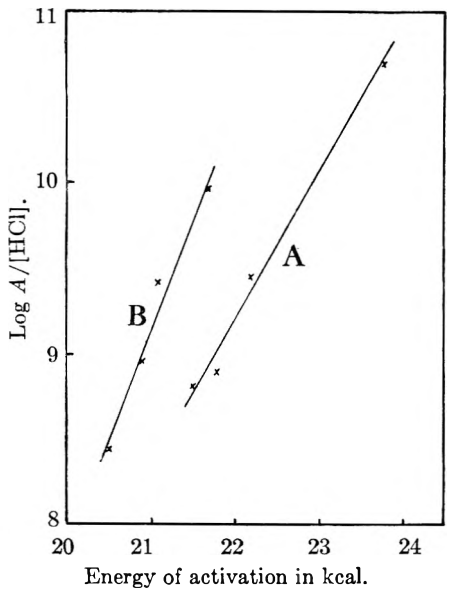

Fig. 2.—Log $A/[HCl]$ values as a function of corresponding energies of activation for picolinamide (A) and isonicotinamide (B).

A mechanism for the hydrolysis of nicotinamide was presented in a previous paper.[2] However, it is difficult to decide whether such a mechanism is really operative because of medium effects. The experimental results indicate that at low hydrochloric acid concentrations the experimental rate constants are proportional to the first power of the acid concentration and not to the second power as the mechanism, proposed previously, would require. A first power law would be obtained by assuming the following reaction to take place

$$H^+RCONH_3^+ + H_2O \longrightarrow H^+RCOOH + NH_4^+$$

The experimental rate constants, not considering medium effects, should then be given by

$$k_{expt} = k_2[H_2O]\frac{K_3[H_3O^+]}{1 + K_3[H_3O^+]} \qquad (1)$$

If K_3 is small, k_{expt} is proportional to the first power of the hydrogen ion concentration, which is the case up to about 2 N hydrochloric acid for the three heterocyclic amides. Any deviations can then be ascribed to medium effects. k_2 in equation 1 is a rate constant and K_3 an equilibrium constant pertaining to the dissociation of the amide.[2,7]

A detailed discussion of mechanisms will be reserved until more data are available for dilute solutions, the main purpose of the present paper being to ascertain the dependence of the experimental rate constants and the parameters of the Arrhenius equation on hydrochloric acid in concentrated solutions.

The three heterocyclic amides do not show very pronounced differences amongst themselves. The energies of activation for picolinamide are higher than those for the other two amides. It may also be mentioned that the energies of activation for the three amides plotted against the logarithms of their experimental rate constants for any one hydrochloric acid concentration do not give straight lines with slopes of magnitude $2.303RT$, as was the case for other amides.[1]

(7) H. H. G. Jellinek and M. G. Wayne, THIS JOURNAL, 55, 173 (1951).

THE RATE OF THE THERMAL ISOMERIZATION OF β-PINENE IN THE VAPOR PHASE[1]

BY J. ERSKINE HAWKINS AND JAMES W. VOGH

Contribution from the Department of Chemistry, University of Florida

Received March 30, 1953

The rate of the thermal isomerization of β-pinene in the vapor phase has been determined in the range 350–400°. Sufficient variation in pressure, temperature and extent of decomposition was obtained to calculate the order of the reaction and the energies of activation for the formation of myrcene and *l*-limonene and for the decomposition of β-pinene. The rate constants for the first-order reactions are equal to $10^{17.7}e^{-49,900/RT}$, $10^{15.3}e^{-45,100/RT}$ and $10^{17.4}e^{-48,800/RT}$ min.$^{-1}$, respectively. Two minor products of the reaction were found but have not been identified. A discussion of the mechanism of the reaction is included.

The rate of the thermal isomerization of β-pinene in the liquid phase has been reported by Hunt and Hawkins.[2] It was shown that the presence of quinoline, hydroquinone and dipentene diluent had no effect upon the pyrolysis reactions. Myrcene polymers and *l*-limonene were the products. The activation energies for the formation of myrcene and *l*-limonene were found to be 47 and 50 kcal./mole, respectively, in the temperature range 220 to 235°. Other thermal isomerizations of β-pinene in the vapor phase have been carried out but no rates of the reactions were measured. The first work of this type was that of Arbuzov,[3] who stated, apparently erroneously, that β-pinene partially isomerized to alloöcimene at 345 to 350°. Goldblatt and Palkin[4,5] and Savich and Goldblatt[6] have shown the pyrolysis products to be *l*-limonene, myrcene and myrcene polymers and have discussed Arbuzov's work.[3] The conditions they used were 5 seconds

(1) The material included in this paper is based upon a partial abstract of a dissertation presented to the Graduate Council of the University of Florida by James W. Vogh in partial fulfillment of the requirements for the degree of Doctor of Philosophy, June, 1953.

(2) H. G. Hunt and J. E. Hawkins, *J. Am. Chem. Soc.*, 72, 5618 (1950).

(3) B. A. Arbuzov, *J. Gen. Chem.* (*U.S.S.R.*), 6, 297 (1936).

(4) L. A. Goldblatt and S. Palkin, *J. Am. Chem. Soc.*, 63, 3517 (1941).

(5) L. A. Goldblatt and S. Palkin, U. S. Patent 2,420,131 (May 6, 1947).

(6) T. R. Savich and L. A. Goldblatt, U. S. Patent 2,507,546 (May 16, 1950).

contact time at 405°[5] and 0.004 second contact time at 725 to 750°.[6] At the higher temperature the yield was 85% myrcene and 0.8% polymer. Nothing else was reported. This virtual absence of polymer correlates with the small contact time, which does not permit the formation of the high boiling compounds, α-camphorene or other polymers.[4]

Experimental

Preparation of Materials.—Commercial *l*-β-pinene was distilled in a Lecky and Ewell column of about 60 plates under the conditions of operation. The β-pinene used in these studies was distilled from a single batch in order to ensure uniformity of the physical properties of the pinene and the pyrolysis products. The constants for the β-pinene were: b.p. 59.5° (20 mm.), $n^{25}D$ 1.4768, d^{25}_4 0.8669 and $[\alpha]^{25}D$ −21.35.

Myrcene was prepared according to the procedure of Goldblatt and Palkin.[4] Approximately three liters of carefully distilled β-pinene was pyrolyzed. Myrcene was obtained from the product of distillation and the constants were: b.p. 65.5° (20 mm.), $n^{25}D$ 1.4682, d^{25}_4 0.7921, and $[\alpha]^{25}D$ 0.

l-Limonene was prepared by distillation of the same pyrolysis mixture and the constants found for it were: b.p. 71.5° (20 mm.), $n^{25}D$ 1.4710, d^{25}_4 0.8385 and $[\alpha]^{25}D$ −107.91.

Separate redistillation of the fractions obtained prior to the myrcene and after the limonene produced two more components. Neither of these compounds was identified.

Apparatus and Procedure.—All experimental runs reported in this paper were carried out in a pyrolysis train of the usual type. The pyrolysis tube consisted of four sections of 1.25-cm. Pyrex tubing, each 36 cm. in length. These were connected by narrow-bore U-bends, about 4-mm. inside diameter. This design was found satisfactory since replacement of the upper half of the first section with a narrow tube had no effect on the calculated reaction rates. The volume determined for the pyrolysis tube was corrected for the calculated expansion at the operating temperature. The correction was approximately 0.7 cc. for the total volume of 200 cc.

The tube was heated to the operating temperature in an electrically heated thermostat which contained a fused mixture of $LiNO_3$, 27.3 wt. %; $NaNO_3$, 18.2 wt. % and KNO_3, 54.5 wt. %.

Three iron–constantan thermocouples were placed in the bath: one near the bottom, one near the top and one halfway down. Temperature control was attained by the use of a thermoregulator of the design given by Benedict.[7] A nickel resistance thermometer was used to operate the thermoregulator. When in use the bath was found to have a maximum difference in temperature throughout the whole length of less than 0.2° at all times.

The products of the reaction were discarded through a side arm until a steady rate was obtained. The drop rate into the receiver was noted in order to ascertain that the steady rate of production of pyrolysate was maintained. At the completion of the timed runs the samples were weighed and stored at 0° under nitrogen.

Analysis of Pyrolysate.—The determination of the rate of pyrolysis was carried out assuming that the amounts of materials other than β-pinene, myrcene and *l*-limonene present in the product could be neglected. This was done since the complete decomposition of β-pinene under the conditions of the experiment produced no more than 0.5 wt. % of material other than myrcene and *l*-limonene. Density and optical rotation measurements were made for analysis of the product using the relations

$$1/d_p = w_\beta/d_\beta + w_M/d_M + w_L/d_L + 0.0044\, w_\beta w_M \quad (1)$$

$$[\alpha_p] = [\alpha_\beta]w_\beta + [\alpha_L]w_L \quad (2)$$

$$1 = w_\beta + w_M + w_L \quad (3)$$

The symbols have the definitions: d = density, $[\alpha]$ = specific rotation at 25°, w = weight fraction. The subscripts p, β, L and M refer to the pyrolysis mixture, β-pinene, *l*-limonene and myrcene, respectively. The relations were based upon the density and optical rotation values for β-pinene–myrcene mixtures and *l*-limonene–myrcene mixtures.

In a supplementary test of the validity of this analytical method it was found that the average discrepancy between the known and calculated values of weight fractions for the three components of three mixtures was 0.002 unit. These known mixtures were prepared to correspond to the compositions of typical pyrolysis products.

There appeared to be no polymers in the pyrolysis product. Successive simple distillations of 30 cc. of fresh pyrolysis samples left less than 0.1 g. of residue in each case.

Results and Discussion

The constants found for the component boiling at 78° (20 mm.) were: $n^{25}D$ 1.4836, $n^{20}D$ 1.4862, d^{25}_4 0.8557, d^{20}_{20} 0.8612, $[\alpha]^{25}D$ −0.35. Iskenderov[8] reported the following values for 1(7),8(9)-*p*-menthadiene prepared by dehydration of $\Delta^{8,9}$-dihydroperillic alcohol: b.p. 65–66° (11 mm.), d^{20}_{20} 0.8735, $n^{20}D$ 1.4870. When this b.p. is corrected to 20 mm. pressure by the method of Hass[9] it becomes 77.3–78.3°. The mechanism (Fig. 1) for the thermal isomerization of β-pinene permits the formation of 1(7),8(9)-menthadiene. However, the infrared spectrum of the compound isolated in this work does not indicate its presence.[10]

Another unidentified component was obtained in a mixture with β-pinene at 59–60° (20 mm.). Although only a partial separation could be made, the physical constants were estimated to be: b.p. 59–60° (20 mm.), $n^{25}D$ 1.4661, d^{20}_4 0.833, $[\alpha]^{25}D$ 0.

Since the combined amount of the unidentified substances was less than 0.5% of the products, their structures were not investigated further.

Table I contains the data of the several experimental runs.

TABLE I

CONDITIONS OF PYROLYSIS AND RATE CONSTANTS FOR FORMATION OF MYRCENE AND *l*-LIMONENE

Experiment no.	Temp., °C.	Pressure, mm.	Contact time, min.	k_M, min.$^{-1}$	k_L, min.$^{-1}$
1	350.1	35.1	0.304	1.72	0.35
2	350.1	80.3	.482	1.62	0.33
3	364.8	20.3	.1519	4.17	0.79
4	364.8	50.4	.1732	4.08	0.78
5	378.7	35.7	.0617	9.72	1.70
6	378.5	36.3	.0457	9.69	1.72
7	378.5	50.3	.1444	9.55	1.70
8	378.4	80.4	.1143	9.34	1.63
9	395.0	20.4	.0736	24.58	3.97
10	395.5	35.5	.0508	25.59	4.11
11	395.1	50.5	.0581	24.56	3.95
12	409.5	35.3	.0397	53.0	8.0
13	409.0	20.5	.0438	48.7	7.4

First-order reaction rate constants for the reactions were calculated according to the equations

$$k_{dec} = \frac{2.303}{t} \log w_B \quad (4)$$

$$k_M = \frac{w_M/w_L}{1 + w_M/w_L} k_{dec} \quad (5)$$

$$k_L = k_{dec} - k_M \quad (6)$$

The symbols k_{dec}, k_M and k_L are the rate constants for the decomposition of β-pinene, the formation of myrcene and the formation of *l*-limonene, respec-

(7) M. Benedict, *Rev. Sci. Instruments*, **8**, 252 (1937).

(8) M. A. Iskenderov, *J. Gen. Chem.* (*USSR*), **1**, 1435 (1937).

(9) H. B. Hass, *J. Chem. Education*, **13**, 490 (1936).

(10) R. L. Webb and J. P. Bain, *J. Am. Chem. Soc.*, **75**, 4279 (1953).

tively. w_M and w_L are the weight fractions of myrcene and *l*-limonene, respectively. The contact time is t, minutes, and the other symbols have meanings previously designated. Table I contains the rate constants for the formation of myrcene and *l*-limonene.

When log k's for the decomposition of β-pinene, for the formation of myrcene, and for the formation of *l*-limonene are plotted against $10^3/T$, straight lines result.

Activation energies for the decomposition of β-pinene and for the formation of myrcene and *l*-limonene were determined from the slope of these plots and were found to be 48,800, 49,900 and 45,100 cal./mole, respectively. The dependence of the rate of these reactions may be expressed by

$$\begin{aligned} k_{dec} &= 10^{17.4}e^{-24600/T}\ \text{min.}^{-1} \\ k_M &= 10^{17.7}e^{-25100/T}\ \text{min.}^{-1} \\ k_L &= 10^{15.3}e^{-22700/T}\ \text{min.}^{-1} \end{aligned} \qquad (7)$$

The above relations indicate that the rate of the reaction is independent of pressure, contact time and amount of β-pinene decomposed within the ranges covered.

The preferred mechanism for this reaction in the vapor phase is the diradical scheme proposed by Burwell[11] which is shown in Fig. 1. This mechanism is in agreement with the findings of Hunt and Hawkins[12] that the liquid phase pyrolysis of β-pinene was not affected by the presence of quinoline, hydroquinone or dipentene.

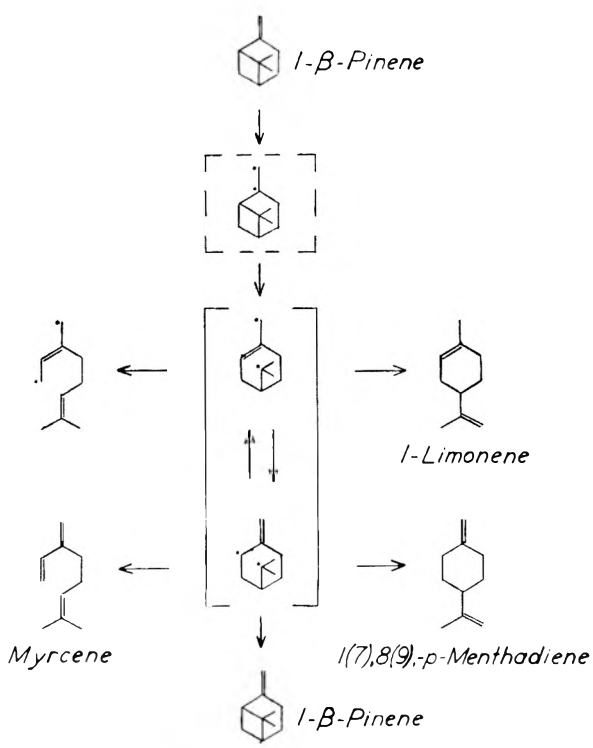

Fig. 1.—The mechanism of the thermal isomerization of β-pinene in the vapor phase.

The pyrolysis of cyclobutane to ethylene by Genaux and Walters[13] was found to be homogeneous and first order and to be unaffected by the presence of propene or nitric oxide. This reaction is analogous to the breaking of the cyclobutane ring in β-pinene during the formation of myrcene. The formation of the menthadienes from β-pinene is best explained by an intramolecular exchange of hydrogen as suggested by Burwell.[11] The possibility that there is an exchange of hydrogen between the biradical and a stable molecule and a resulting complex mechanism is lessened by the fact that the reaction is first order and the rate constant is unaffected by a change of pressure within the range in which this work was carried out.

On the basis of the proposed mechanism the following steps may be set up for the pyrolysis reactions where B, R, L and M are the symbols for β-pinene, the biradical shown in Fig. 1, *l*-limonene, and myrcene, respectively.

$$B \xrightarrow{k_1} R \qquad (8)$$

$$R \xrightarrow{k_2} B \qquad (9)$$

$$R \xrightarrow{k_3} L \qquad (10)$$

$$R \xrightarrow{k_4} M \qquad (11)$$

The corresponding reactions have been observed in the pyrolysis of α-pinene by Fuguitt and Hawkins.[14] The rate constant for the racemization of α-pinene was shown to be about one-tenth that of the sum of the rate constants for the formation of dipentene and alloöcimene and the activation energy of the racemization to be 1.5 kcal. greater than that for alloöcimene formation. If the same relation of rate constants and activation energies occurs in the pyrolytic reactions of β-pinene the reaction R → B may be omitted without introducing a great error. Appropriate treatment of the rate equations and the energies of activation of the reactions in 8, 9, 10 and 11 lead to the conclusion that

$$E_{dec} = E_1 \qquad (12)$$

where E_1 is the activation energy for reaction 8.

Since w_M/w_L is not independent of temperature, neither E_L nor E_M can be expected to be independent of temperature. However, temperature dependence could not be observed in the data available.

E_3 and E_4, the energies of activation for the reactions in equations 10 and 11, could not be determined from the information available. However, the difference may be shown to be

$$E_M - E_L = E_4 - E_3 \qquad (13)$$

Reaction 8 represents dissociation of the 6–8 bond. The activation energy of this reaction can be taken as equivalent to the dissociation energy of the 6–8 bond of the β-pinene with the resulting formation of the biradical. No direct comparison with reported dissociation energies can be made. Sehon and Szwarc[15] found a bond dissociation energy of 61.5 kcal. for the 3–4 bond of 1-butene. The difference between this and the experimentally

(11) R. L. Burwell, *J. Am. Chem. Soc.*, **73**, 4461 (1951).
(12) H. G. Hunt and J. E. Hawkins, *ibid.*, **72**, 5618 (1950).
(13) C. T. Genaux and W. D. Walters, *ibid.*, **73**, 4497 (1951).
(14) R. E. Fuguitt and J. E. Hawkins, *ibid.*, **69**, 319 (1947).
(15) A. H. Sehon and M. Szwarc, *Proc. Roy. Soc.* (*London*), **A202**, 263 (1950).

determined activation of 48.8 kcal. may be attributed to the strained nature of the cyclobutene ring of the β-pinene, to the hyperconjugation effect due to the two methyl groups on carbon 8, to the fact that the distance between the unpaired electrons of the biradical is restricted by the molecular dimensions of the biradical, and to the fact that the two resonance forms shown are not symmetrical.

The only mechanism other than that suggested by Burwell which completely agrees with the kinetic behavior and products observed is that of Hunt.[16] While the possibility of the occurrence of a chain reaction mechanism, particularly in the formation of the menthadienes, cannot be excluded on the basis of the information available, several possible chain mechanisms were analyzed but none fitted the experimental observations in a satisfactory manner.

(16) H. G. Hunt, "The Kinetics of the Thermal Isomerization of the Pinenes," Ph.D. Dissertation, Department of Chemistry, University of Florida, June, 1950, p. 32.

LIQUID–VAPOR EQUILIBRIUM IN THE SYSTEM URANIUM HEXAFLUORIDE–HYDROGEN FLUORIDE[1]

BY ROGER L. JARRY, FRED D. ROSEN, CHARLEY F. HALE AND WALLACE DAVIS, JR.

Contribution from the K-25 Laboratory Division, Carbide and Carbon Chemicals Company, Oak Ridge, Tennessee

Received April 4, 1953

Liquid–vapor equilibrium in the system uranium hexafluoride–hydrogen fluoride has been determined over the whole range of compositions in the temperature interval 40 to 105°. In this temperature range, and considerably beyond, the system is one of maximum pressure at constant temperature. Vapor–liquid separation factors, activity coefficients and other pertinent functions have been calculated with respect to a formula weight of hydrogen fluoride of 20.01. This procedure is convenient and practical, but it is not in agreement with molecular weights of hydrogen fluoride calculated from vapor density measurements. These weights vary from 60 to 100 in the temperature range 60 to 40° for saturated vapor in contact with solutions.

In a recent publication[2] the nature of condensed phase equilibria of the binary system uranium hexafluoride–hydrogen fluoride was presented. The purpose of the present paper is to submit data on liquid–vapor equilibrium. Two factors should be noted concerning this system, as follows: first, a miscibility gap extends from 61.2 to 101°; second, since the manner in which the molecular weight of hydrogen fluoride varies with temperature, pressure and concentration is not known, the system cannot be expressed in terms of molar quantities. Formula quantities have been used in this paper for convenience, although such units introduce very extensive distortions in graphical representation of this binary system.

Experimental

Equilibrium Still.—The equilibrium still used to obtain data for this paper has been described in a previous communication,[3] as has the vapor pump.[4] Briefly, it consisted of a pot, an overhead vapor column that could be isolated from the pot, and a pump to force vapor through the liquid. This whole unit, with its pressure transmitter, was contained in one side of a two-compartment air thermostat; the other compartment contained the sampling manifold. One portion of this unit not previously described in adequate manner is the liquid pipet. It was formed by major modeling of two Hoke M 342 valves which were welded to the bottom of the pot, as shown in Fig. 1.

The still was controlled at one of eight temperatures by mercury regulator-electronic relay circuits. Temperatures were measured by means of a calibrated copper–constantan thermocouple and a Leeds and Northrup Portable Potentiometer. Vapor and liquid temperatures were maintained equal within 0.1 to 0.2°.

Pressures were measured by use of a Booth–Cromer pressure transmitter[5] and one of two Bourdon gages, each of which was calibrated against a dead weight gage.[6] One, used in most of the experiments, had a 7-in. diameter scale of 0 to 160 p.s.i.g. in 2 pound increments; the second had a 4-in. diameter scale of 0 to 300 p.s.i.g. in 1 pound increments.

Gas Density Flask.—This flask was made of spun nickel, about 10 mils thick, and had a volume of about 535 cc. With its light weight, right angle, metal valve (monel metal body, Z nickel stem, modified from Hoke type 431) this unit weighed less than 200 g. It was connected to the sampling manifold through a 1/4 in. compression fitting in which the copper gasket was replaced by one made of Fluorothene.

Materials.—Uranium hexafluoride used in these experiments contained less than 0.015 wt. % impurity,[2] the impurity being principally hydrogen fluoride. Hydrogen fluoride, whose purification has been described previously,[3] was about 99.74 mole % pure.

Procedure.—The pot (A, Fig. 1, ref. 3) was charged with a mixture of hydrogen fluoride and uranium hexafluoride, and then heated to one of the 8 different temperatures used in this work. Vapor was circulated through the solution while the materials were heating and until constant temperature and pressure had been obtained. The pump was then stopped and the vapor and liquid materials valved off from each other. A sample of the vapor was obtained by cracking a valve between the vapor volume and the sampling manifold. The pressure and temperature of this sample as expanded into the gas density flask was taken, the flask closed, and then, along with a counterpoise, removed from the thermostat for weighing.

A sample of the solution was obtained by use of the solution pipet of Fig. 1. After collecting liquid between valves V-1 and V-2, valve V-1 was closed and valve V-2 rapidly and completely opened. By this operation all the liquid in the pipet was completely vaporized, without fractionation, into a part of the gas sampling manifold (Fig. 1, ref. 3) which included a re-evacuated and retared vapor density flask. It should be noted that the counterpoise was taken through the same heating and cooling cycles as was the gas density flask.

In three experiments the complete vapor sample was condensed from the isolated vapor volume into a weighing flask

(1) This work was performed for the U. S. Atomic Energy Commission by Union Carbide and Carbon Corporation at Oak Ridge, Tennessee.

(2) G. P. Rutledge, R. L. Jarry and W. Davis, Jr., THIS JOURNAL, 57, 541 (1953).

(3) R. L. Jarry and W. Davis, Jr., *ibid.*, 57, 600 (1953).

(4) F. D. Rosen, *Rev. Sci. Instruments*, 24, in press (1953).

(5) S. Cromer, "The Electronic Pressure Transmitter and Self-Balancing Relay," MDDC-803 (1947).

(6) W. B. Kay, *J. Am. Chem. Soc.*, 69, 1273 (1947).

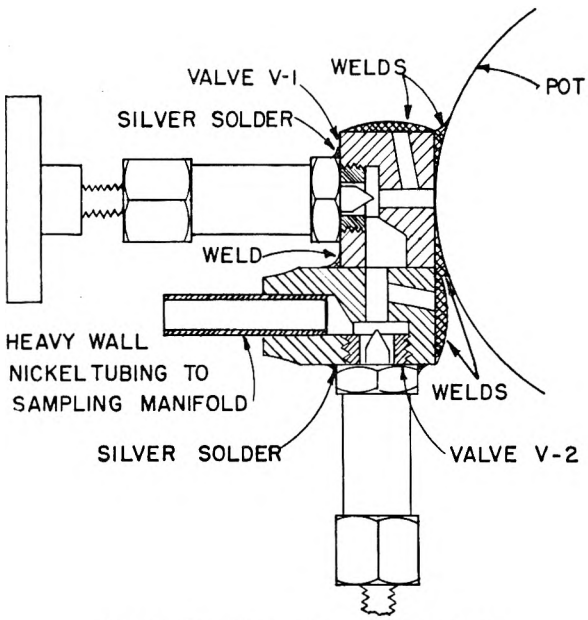

Fig. 1.—Liquid sample pipet (top view).

by liquid nitrogen condensation. These experiments were performed to provide values of the apparent molecular weight of hydrogen fluoride under specific conditions.

Standardization.—Vapor density analyses of mixtures of uranium hexafluoride and hydrogen fluoride present somewhat unusual aspects; first, because the former reacts with nickel and, second, because hydrogen fluoride polymerizes, at least at relative pressures much in excess of 0.1. Because of this a number of standardization tests were made on the gas density method of analysis. First, to check the potential errors due to technique, the molecular weight of nitrogen was calculated, in two tests, using the ideal gas law, pressure, volume, weight and temperature data. The values were 27.89 and 28.06. These and all other tests were run at about 80°, a temperature chosen as being high enough to minimize hydrogen fluoride polymerization at pressures below one atmosphere. Second, in four determinations with hydrogen fluoride at pressures of 400 to 650 mm., the molecular weight was found to be 20.35 with a standard deviation of 0.15. Third, in six determinations with uranium hexafluoride at pressures of 100 to 400 mm., the molecular weight was found to be 349.3 with a standard deviation of 3.0. Finally, to check the possible time dependence of probable chemical reaction of uranium hexafluoride with metal, as well as to check the accuracy of analyses of mixtures, a synthetic gas mixture was made and sampled during a period of two days. Results of this test, summarized in Fig. 2, indicate that during the few minutes maximum, while these gases were contained in the transfer lines, little reaction of uranium hexafluoride would occur, and that accuracy within about 1 to 1.5% of the apparent molecular weight could be expected.

Results

Liquid–vapor equilibrium data, separation factors and activity coefficients are presented in Table I while Table II contains data on the degree of polymerization of hydrogen fluoride in vapor over

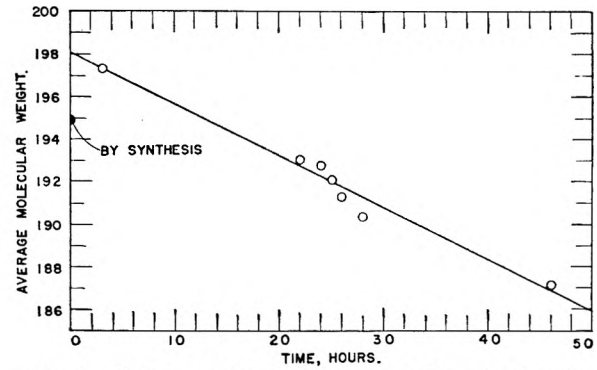

Fig. 2.—Effects of chemical reaction in the metal system on the average molecular weight of a synthetic gas mixture of HF and UF_6.

the saturated solution. Explicit meanings of the headings of these tables are given in equations 3–6, the following definitions applying throughout: $f^{v}_{UF_6}$, $f^{l}_{UF_6}$, f^{v}_{HF}, f^{l}_{HF} are formula fractions of uranium hexafluoride and hydrogen fluoride, superscripts v and 1 referring to vapor and liquid phases, respectively; P is the measured pressure, $P^{\circ}_{UF_6}$ the vapor pressure of pure[7] UF_6 and P°_{HF} the vapor pressure of pure hydrogen fluoride[3]; $n^{v}_{UF_6}$ is the number of moles of UF_6 per unit volume in the vapor phase and $N^{v}_{UF_6}$ is the "true" mole fraction of UF_6; n^{v}_{i} is the number of moles of $(HF)_i$ in the vapor phase per unit volume; $Z^{v} = \Sigma i n^{v}_{i}/\Sigma n^{v}_{i}$ is the association number of hydrogen fluoride; $\bar{M}$ is the average molecular weight of material in the vapor phase as determined by gas analysis; and W is the weight of the gas sample taken for analysis. Equation 3 follows directly from the assumption that P–V–T relations of mixtures of UF_6 and the various hydrogen fluoride polymers $(HF)_i$ may be described adequately by ideal gas laws at the sampling conditions of relatively low pressure and high temperature. This assumption is contained in equations 1 and 2 wherein the ratio $20.01\ \Sigma i n^{v}_{i}/\Sigma n^{v}_{i}$ is assumed to have the same value of 20.35 for UF_6–HF mixtures as it did for pure HF.

$$n^{v}_{UF_6} + \sum_{i=1}^{m} n^{v}_{i} = \frac{PV}{RT} = \frac{W}{\bar{M}} \qquad (1)$$

$$352.07\ n^{v}_{UF_6} + 20.01 \sum_{i=1}^{m} i n^{v}_{i} = W \qquad (2)$$

$$f^{v}_{UF_6} = \frac{\bar{M} - 20.35}{337.7 - 0.017\bar{M}} \qquad (3)$$

$$\text{Separation factor} = \alpha = \frac{f^{v}_{HF}}{f^{l}_{HF}} \Big/ \frac{f^{v}_{UF_6}}{f^{l}_{UF_6}} \qquad (4)$$

$$\gamma_{UF_6} = \frac{P f^{v}_{UF_6}}{P^{\circ}_{UF_6} f^{l}_{UF}} \qquad (5)$$

$$\gamma_{HF} = \frac{P f^{v}_{HF}}{P^{\circ}_{HF} f^{l}_{HF}} \qquad (6)$$

As mentioned previously, this work was performed at a series of constant temperatures, one of these being 104.7°. Liquid–vapor equilibrium data were not taken over the full composition range at this temperature since the maximum pressure, about 220 p.s.i.a., was somewhat beyond the safe limits of

(7) G. D. Oliver, H. T. Milton and J. W. Grisard, *J. Am. Chem. Soc.*, 75, 2827 (1953).

TABLE I

LIQUID–VAPOR EQUILIBRIUM DATA FOR THE SYSTEM URANIUM HEXAFLUORIDE–HYDROGEN FLUORIDE

Temp., °C.	Pressure, cm.	Composition, formula %UF_6[a] Liquid	Vapor	Separation factor, $\frac{(HF)_V/(UF_6)_V}{(HF)_L/(UF_6)_L}$	Activity coefficient in sol. γ_{UF_6}	γ_{HF}
40.89	156.0	0.00	0.00	...	..	1.000
40.89	179.6	2.74	6.85	0.383	8.76	1.103
40.89	51.3	100.00	100.00	...	1.00	..
50.90	214.0	0.00	0.00	...	..	1.000
50.90	244.7	2.47	7.45	0.315	10.03	1.085
50.90	258.3	3.81	9.09	0.396	8.37	1.141
50.90	73.6	100.00	100.00	...	1.00	..
59.66	275.0	0.00	0.00	...	..	1.000
59.56	314.4	1.64	7.54	0.205	14.62	1.075
59.75	343.8	5.78	11.59	0.468	6.97	1.173
59.66	98.9	100.00	100.00	...	1.00	..
66.87	340.0	0.00	0.00	...	..	1.000
66.99	382.7	1.89	7.17	0.249	11.66	1.065
67.01	412.7	4.07	12.48	0.298	10.16	1.107
66.92	429.6	7.40	14.01	0.491	6.53	1.173
66.97	431.1	..	13.99	...	..	..
66.79	424.5	7.42	13.96	0.494	6.41	1.160
66.97	430.5	7.67	15.14	0.466	6.82	1.164
66.83	428.3	8.27	14.40	0.536	5.99	1.176
66.87	423.1	77.72	15.33	19.27	0.670	4.73
66.85	422.6	78.86	14.96	21.21	0.643	5.00
66.74	360.8	91.45	24.70	32.61	0.782	9.35
66.81	360.1	92.53	25.10	36.96	0.784	10.62
..	..	91.93	..	33.99	0.789	9.83
66.92	262.0	98.50	46.73	74.86	0.998	27.4
66.87	124.5	100.00	100.00	...	1.000	..
72.47	396.0	0.00	0.00	...	..	1.000
72.48	442.5	1.83	7.38	0.234	12.82	1.054
72.28	442.8	2.55	8.00	0.301	9.41	1.056
72.50	482.6	4.26	13.13	0.294	10.07	1.106
72.48	498.4	7.44	15.04	0.454	6.82	1.155
72.48	503.6	10.84	16.15	0.629	5.19	1.191
72.48	499.8	73.48	16.40	14.12	0.755	3.98
72.62	494.7	77.62	16.93	17.02	0.731	4.64
72.28	409.1	93.57	28.40	36.69	0.841	11.50
72.62	286.7	98.43	51.15	59.88	1.009	22.5
72.47	147.7	100.00	100.00	...	1.000	..
84.46	538.0	0.00	0.00	...	..	1.000
84.45	597.3	1.55	6.07	0.244	11.21	1.059
84.49	652.1	3.60	11.60	0.285	10.08	1.112
84.40	681.9	7.36	16.00	0.417	7.11	1.149
84.47	688.2	11.05	17.75	0.517	5.30	1.183
84.38	688.6	11.32	17.81	0.589	5.20	1.186
84.38	686.6	65.78	17.80	8.88	0.892	3.07
84.55	678.4	73.12	17.56	12.77	0.782	3.87
84.53	543.5	93.74	33.33	29.95	0.927	10.8
84.53	364.7	98.96	58.75	66.81	1.039	26.9
84.46	208.5	100.00	100.00	...	1.000	..
92.30	656.0	0.00	0.00	...	..	1.000
92.28	718.8	1.50	6.15	0.232	11.45	1.044
92.28	789.2	3.50	11.22	0.287	9.83	1.111
92.30	830.5	6.91	16.95	0.364	7.91	1.129
92.30	840.6	11.24	18.51	0.558	5.38	1.176
92.30	837.9	61.67	18.70	6.99	0.987	2.71
92.37	821.8	71.17	19.19	10.40	0.861	3.51
92.30	637.6	93.94	35.45	28.23	0.935	10.4
92.28	421.1	99.53	62.43	127.4	1.026	51.3
92.30	257.5	100.00	100.00	...	1.000	...
104.74	886.0	0.00	0.00	...	..	1.000
104.77	962.4	1.18	5.24	0.216	12.13	1.042
104.73	1051.3	3.22	10.73	0.277	9.93	1.095
104.60	804.6	94.92	40.85	27.06	0.983	10.6
104.87	524.8	99.56	66.44	114.3	0.993	45.2
104.74	352.5	100.00	100.00	...	1.000	..

[a] Compositions were calculated on the basis of association of hydrogen fluoride in samples equivalent to a molecular weight of 20.35.

the apparatus. However, pressure *vs.* composition data for this temperature are plotted in Fig. 3; experimental and extrapolated points are appropriately differentiated.

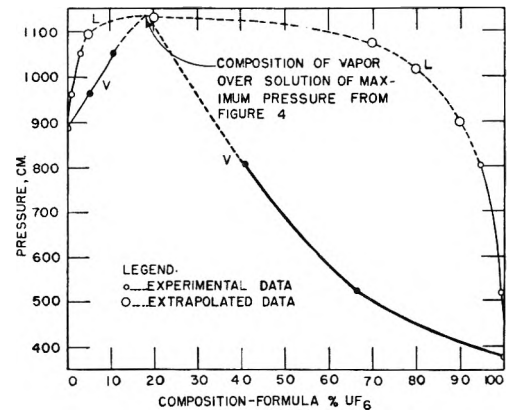

Fig. 3.—Liquid–vapor equilibrium in the system UF_6–HF at 104.7 ± 0.1°.

Discussion

Comparison of results obtained in this research with previous work from this Laboratory[2] is possible mainly in the region of the miscibility gap of the system uranium hexafluoride–hydrogen fluoride. The equilibrium still was run with 200 to 400 cc. of liquid and the liquid pipet was located so close to the bottom of the pot that only the lower (UF_6 rich) of the two phases could be sampled when two liquid phases were present. Analyses of liquid phases consistently agreed with previous results[2] and scattered only to a small extent about the heavy-lined miscibility curve—or solubility curve—shown in Fig. 4. This figure also summarizes liquid–vapor equilibrium data at a series of pressures. Data points and dashed lines to connect liquid composition curves through the miscibility gap have been omitted to keep the figure legible. It is obvious that this system is one of minimum boiling point at temperatures considerably beyond the range studied, *i.e.*, 40 to 105°.

Extensive deviations of solutions of uranium hexafluoride and hydrogen fluoride from ideal or "real"[8] solution theory have previously been reported[2]; this is indicated quantitatively by the activity coefficients of Table I. However, these coefficients are based on *formula* weights, rather than mole quantities, and accentuate deviations of the system from ideality. In order to obtain some estimate of the distortion produced by use of the formula weight, the density as well as formula composition of saturated vapor in equilibrium with saturated solution was determined at 3 temperatures below the four phase invariant temperature of 61.2°. Using the definitions given above we may write equations 7 and 8. The second equality of equation 7 can be written only in the event that solid UF_6 is present in the system.

$$N^{V}_{UF_6} = P^{vap}_{UF_6}/P = \frac{n^{V}_{UF_6}}{n^{V}_{UF_6} + \sum_{i=1}^{m} n^{V}_{i}} \qquad (7)$$

$$f^{V}_{UF_6} = \frac{n^{V}_{UF_6}}{n^{V}_{UF_6} + \sum_{i=1}^{m} i n^{V}_{i}} \qquad (8)$$

(8) J. H. Hildebrand and R. L. Scott, "Solubility of Non-Electrolytes," Third Edition, Reinhold Publ. Corp., New York, N. Y., 1950.

TABLE II

APPARENT MOLECULAR WEIGHT OF HYDROGEN FLUORIDE

Temp., °C.	Vapor press. of solid UF_6, cm.	Total press. over satd. UF_6–HF sol., cm.	Mole frac. UF_6 in vapor (eq. 5), $N^v_{UF_6}$	Formula frac. UF_6 in vapor (Table I), $f^v_{UF_6}$	HF association no. (eq. 5 and 6)	Av. mol. wt. of HF Vapor over sol.	Av. mol. wt. of HF Vapor over Pure HF[a]
40.89	51.1	179.6	0.283	0.0685	5.37	107	64
50.90	73.5	258.3	.285	.0909	3.99	80	60
59.66	98.8	343.8	.287	.1159	3.07	61	56

[a] See ref. 3.

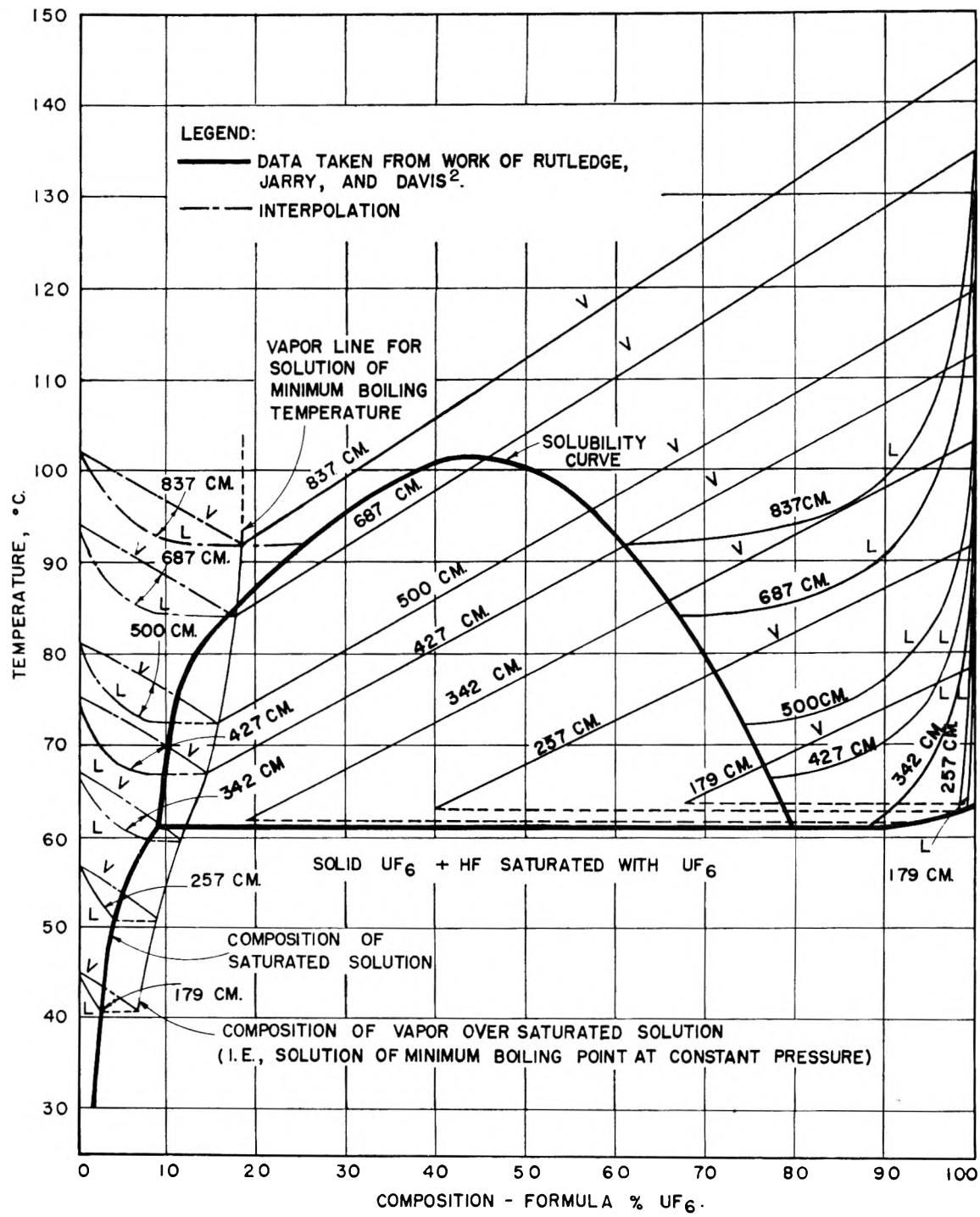

Fig. 4.—Summary of liquid–vapor equilibrium in the system UF_6–HF.

Assuming the ideal gas laws and no association of UF_6, the vapor phase association numbers ($Z^v = \Sigma i n_i^v / \Sigma n_i^v$) of hydrogen fluoride have been calculated from data and presented in Table II. In

terms of average molecular weight this association has been compared with association in pure hydrogen fluoride vapor.[3] Such data indicate the complexity of this binary system but are of little value in terms of solution theory unless it is safe to assume that saturated liquid and saturated vapor have approximately the same degree of association of hydrogen fluoride.

The azeotropic nature of the system UF_6–HF, in the temperature region studied, is shown in the X–Y plot of Fig. 5. This figure gives a quantitative expression to the ease of removing "small" (less than 75 formula %) amounts of HF from UF_6, either in a simple still or by a "flashing" procedure. Use of "flashing", or pumping, at −80° to remove HF has been described by Katz and Rabinowitch.[9]

By use of data of Table I the effect of temperature on the vapor pressure of a solution of fixed composition may be obtained. Plots of log P *vs.* $1/T$ yield nearly straight lines; considering deviations therefrom as within experimental error, data have been expressed in Table III in terms of the analytical equation

$$\log P = A - B/T \qquad (9)$$

TABLE III

VAPOR PRESSURE EQUATION CONSTANTS FOR UF_6–HF SOLUTIONS

Sol. comp., formula % UF_6	Expt. temp. range, °C.	A[a]	B, °K.$^{-1}$	BR ln 10, cal./mole[b]
5	54– 94	6.906	1460	6680
10–60	66– 94	6.864	1440	6590
70	72– 94	6.474	1300	5950
80	66– 94	6.423	1290	5900
90	66– 94	6.295	1260	5760
95	66–105	6.344	1300	5950
96	66–105	6.322	1300	5950
97	66–105	6.298	1300	5950
98	66–105	6.233	1290	5900

[a] Pressures are in cm. [b] The term *mole* is here used with considerable reservation.

In addition to values of A and B, the apparent heats of vaporization, BR ln 10, where R is the gas constant, have been listed for comparison with (1) the molar heat of vaporization of pure[7] UF_6 and (2) Z^v times the formula heat of vaporization of hydrogen fluoride (Z^v here is the association factor of saturated hydrogen fluoride vapor in contact with liquid). $Z^v\Delta H_{vap,HF}$, where $\Delta H_{vap,HF}$ is the heat of vaporization of 20.01 g. of hydrogen fluoride,[3] is the heat that must be added to this liquid material to produce vapor containing 1 total mole (not 1 formula weight) of the species $(HF)_i$. By analogy and within limits imposed by assuming that the various molecular species in the gas phase obey ideal gas laws, the term BR ln 10 is that quantity of heat which when added to a UF_6–HF solution at constant temperature and pressure will lead to the formation of saturated vapor that contains 1 mole (not 1 formula weight) of a mixture of UF_6 and $(HF)_i$. Comparative numbers are ΔH_{vap} = 6500–6900 cal./mole[7] for UF_6 and $Z^v\Delta H_{vap,HF}$ = 6400 to 6300 cal./mole vapor,[3] these values applying to the temperature interval 90 to 60°. It is evident that, from HF-rich solution, heats required to form vapor containing 1 mole of mixture are less than those for pure hydrogen fluoride or pure uranium hexafluoride. It should be noted that the weight of 1 mole of vapor is not known and that this weight varies with temperature.

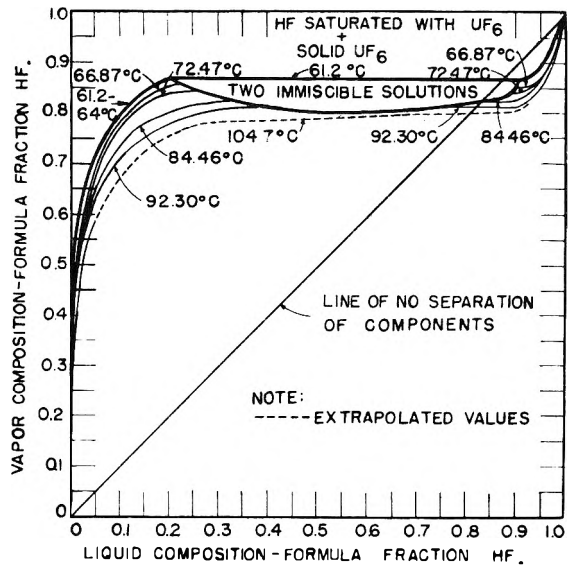

Fig. 5.—Liquid *vs.* vapor composition diagram.

Acknowledgments.—The authors wish to acknowledge many helpful discussions with Drs. E. J. Barber and H. A. Bernhardt and Mr. G. P. Rutledge during the course of this work.

(9) J. J. Katz and E. Rabinowitch, "The Chemistry of Uranium, Part I. The Element, Its Binary and Related Compounds," McGraw-Hill Book Co., Inc., New York, N. Y., 1951.

ON THE CALCULATION OF THERMAL TRANSPIRATION

BY S. CHU LIANG[1]

Division of Applied Chemistry, National Research Council, Ottawa, Canada

Received April 4, 1953

The empirical constants used for the calculation of thermal transpiration have been more accurately determined, and a new correlation between the pressure shifting factor and the gas collisional diameter becomes possible. Helium has been adopted as the new standard to replace nitrogen.

Introduction

When a temperature difference exists between the pressure measuring device and the part of the system to be measured, such as in the cases of low temperature adsorption and vapor pressure measurements, the pressure measured differs from that desired because of thermal transpiration. For the calculation of this thermal transpiration effect R, an equation was introduced,[2] where p_1 and p_2 are

$$R = p_1/p_2 = [\alpha(X/f)^2 + \beta(X/f) + R_m]/[\alpha(X/f)^2 + \beta(X/f) + 1] \quad (1)$$

the true and measured pressures; α and β the empirical constants; $X = p_2 d$, d being the diameter of the connecting tube; $R_m = (T_1/T_2)^{1/2}$, T_1 and T_2 being the temperatures (°K.) of the system to be measured and of the measuring device; and f the pressure shifting factor with f for nitrogen arbitrarily defined as unity; the empirical relationship

$$f_2/f_1 = 1 + 4[(r_1/r_2) - 1] \quad (2)$$

was suggested later on for the estimation of the R values of one gas from those of another, through the use of their collisional diameters r_1 and r_2.[3] In the earlier communication, in addition to the obvious error that f_1/f_2 appeared where f_2/f_1 should, the condition $r_1/r_2 \geqslant 1$ was, unfortunately, left out. Without this condition, eq. 2 would require r_1/r_2 to have a fixed value. The constants α, β and f's have since been more accurately determined, and a more reliable correlation between r and f becomes possible. It is felt that the new information is useful enough to be reported.

Experimental

The measurements were made by the "relative method" described in detail elsewhere.[2] Briefly, the system to be measured was connected with two tubes of different diameters, one narrow and one wide, to two pressure gages. The "measured pressure" p_2 was that measured through the narrow tube. The "true pressure" p_1 was represented by that measured through the wide tube of such a diameter $d/\lambda > 10^3$ to 10^4, λ being the mean free path of the gas, so that the thermal transpiration effect became unimportant. Thus, the larger the diameter of the wide tube, the more accurate the measurements may be made at lower pressures. In the present study, a 90 mm. i.d. tube was used as the wide tube. Two capillaries of 1.2 and 2.6 mm. i.d. were used as the narrow tubes. The pressure gage temperature was constant at 296 ± 2°K. The cold bath temperature was at 195°K. (Dry Ice–acetone) and 77.5 ± 0.1°K. for two sets of measurements.

The gases measured included helium, neon, hydrogen, argon, nitrogen, krypton, xenon and ethylene. The ethylene was withdrawn from a commercial tank and purified by fractionation, the final gas was found to be at least 99.9% pure by mass spectrometric analysis. All the other gases were obtained from Linde Air Products.

(1) Research Laboratory, Dominion Tar & Chemical Co., 3547 Allard Street, Ville LaSalle, P. Q., Canada.

(2) S. C. Liang, *J. Applied Phys.*, **22**, 148 (1951).

(3) S. C. Liang, THIS JOURNAL, **56**, 660 (1952).

Results and Discussion

In the earlier works, nitrogen was chosen arbitrarily as the standard. It has now been found that the thermal transpiration effect is important in a much wider region than then anticipated, and the choice of standard cannot be made arbitrarily without causing inconvenience in the future. Helium has thus been decided upon as the new standard. Because helium has the smallest collisional diameter of all the gases, it has the largest thermal transpiration effect under the same conditions. Therefore, its effect can be measured most accurately. Furthermore, by redefining a new pressure shifting factor ϕ, eq. 1 takes a new form more convenient for calculation

$$R = p_1/p_2 = [\alpha_{He}(\phi_g X)^2 + \beta_{He}(\phi_g X) + R_m]/[\alpha_{He}(\phi_g X)^2 + \beta_{He}(\phi_g X) + 1] \quad (3)$$

The relationship between f and ϕ may be expressed, for a gas, $\phi_g = f_{He}/f_g$. In the present form, ϕ has a minimum value of unity.

The results obtained are summarized in Table I, where the previously published f values are also included and f_{He}/f_g evaluated to compare with the newly determined ϕ_g values. Also included are the collisional diameters r of the various gases. It is of interest to note that, with the exception of nitrogen and krypton, a higher r is associated with a higher ϕ.

TABLE I

PRESSURE SHIFTING FACTORS AND COLLISIONAL DIAMETERS

Gas	He	Ne	H_2	A	N_2	Kr	Xe	C_2H_4
Old factor f (f_{N_2} = 1)	2.80	2.0	2.20	1.25	1.0000	..	..	0.5
f_{He}/f_g	1.0000	1.40	1.27	2.24	2.80	..	..	5.60
New factor ϕ (ϕ_{He} = 1)	1.0000	1.41	1.52	2.93	3.28	3.90	6.87	7.2
Collisional diam. r, Å.	2.58	2.80	2.90	3.41	3.70	3.60	4.1	4.5

In Fig. 1 are plotted ϕ *vs.* r (in Å.), both on a logarithmic scale. The straight line relationship

$$0.27 \log \phi = \log r - 0.41 \quad (4)$$

is indicated. At present the ϕ values can be determined only with 5% uncertainty, with the exception of that of helium which is defined as unity. The r values are not yet very well defined, and a 5% uncertainty is used for illustration. The cross on each point represents such uncertainties.

It should be mentioned that the molecular diameters used are those calculated from the viscosity data by the Lennard-Jones 12:6 potential method. It has been suggested to the author that the "equivalent elastic-sphere diameters"[4] given by Kennard should be used, because the krypton molecule under

(4) E. H. Kennard, "Kinetic Theory of Gases," McGraw-Hill Book Co., Inc., New York, N. Y., 1938, p. 149.

such considerations, has a larger diameter than nitrogen. Since a universally accepted method for the calculation of molecular diameter is not available, and a discussion of the relative merit of different methods is out of the province of this communication, we shall leave this point out. This action may be justified because eq. 4 is only an empirical relationship (the true relationship is unknown) for the *estimate* of the thermal transpiration effect of a gas for which no experimental measurements have been made, and accuracy is unimportant. Accurate values, if desired, should be obtained experimentally, or calculated from eq. 3 if ϕ-value is obtainable by some other more accurate method.

We wish to emphasize, however, although we are not convinced of the accuracy of the Kennard molecular diameter values, we agree that krypton should have a larger diameter than nitrogen. The thermal transpiration effect of nitrogen has been determined several times. The constants α and β for nitrogen obtained previously are compared with those obtained during the present study in Table II. The difference is very small indeed. In fact, it coincides almost exactly with the results of Los and Fergusson.[5] All these indicate that the existence of serious experimental errors is unlikely. In the case of krypton, our results agree well with those of Fergusson[6a] and also those of Holmes and Kington,[6b] and ϕ_{Kr} is unmistakably larger than ϕ_{N_2}, suggesting that krypton may have a collisional diameter larger than nitrogen, in fact, by some 6–7%. When krypton and nitrogen were used for surface area measurement by the adsorption method, it was always necessary to assign krypton a cross-sectional area some 15% higher than that of nitrogen, or 7.5% in terms of diameter.[7] The Kennard values indicate a 10% difference.

TABLE II

CONSTANTS FOR NITROGEN

Cold end temp., °K.	α Previous	α New ($\alpha_{He}\phi_{N_2}^2$)	β Previous	β New ($\beta_{He}\phi_{N_2}$)
195	22.76	27.1	5.00	4.79
77.3	29.5	27.1	12.5	12.4

In the earlier studies, the f values were thought to be a function of the cold end temperatures; this is now known to be not the case. The ϕ (and therefore f) values are independent of temperature. The constants α_{He} and β_{He} are found to be: (1) $\alpha_{He} = 2.52$, independent of cold end temperature, and (2) $\beta_{He} = 7.68\,(1 - R_m)$, with $R_m \leqslant 1$; when pressure and tube diameter are measured in mm. Hg and mm., respectively.

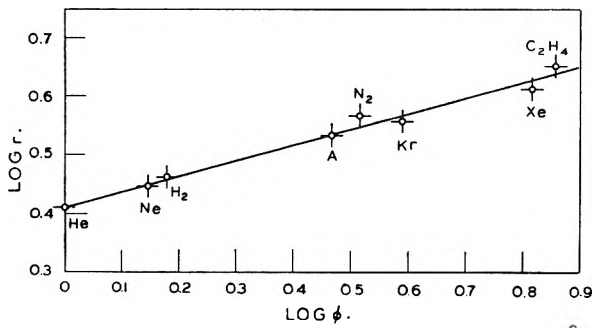

Fig. 1.—Correlation between collisional diameter r (in Å.) and the pressure shifting factor ϕ.

Although some difference is noted between the f_{He}/f_g and ϕ_g values in Table I, it remains to be pointed out that the actual change in R values in most cases is small. Thus, for example, $f_{He}/f_{C_2H_4} = 5.60$, whereas $\phi_{C_2H_4} = 7.2$, an almost 30% difference; the effect on the thermal transpiration is illustrated in the following.

The results of previous vapor pressure measurements[3] are summarized in Table III.

TABLE III

VAPOR PRESSURE MEASUREMENT OF ETHYLENE

Tube diameter →	1.6 mm. Exptl., μ	1.6 mm. Cor., μ	32 mm. Exptl., μ	32 mm. Cor., μ
77.5°K.	1.04	0.53 ± 0.01	0.77	0.55 ± 0.03
90°K.	36	30	30	30

Equation 3 may be conveniently written in the form

$$(p_2 - p_1)/p_2 = \Delta p/p_2 = (1 - R_m)/(\alpha_{C_2H_4}X^2 + \beta_{C_2H_4}X + 1)$$

$$\alpha_{C_2H_4} = \alpha_{He}\phi^2_{C_2H_4} = 131$$

At 77.5°K.: $R_m = 0.510$, $\beta_{C_2H_4} = \beta_{He}\phi_{C_2H_4} = 27.1$

$d = 1.6$ mm. $\Delta p = 0.488\mu$ $p_1 = p_2 - \Delta p = 0.55\mu$

$d = 32$ mm. $\Delta p = 0.216\mu$ $p_1 = p_2 - \Delta p = 0.55\mu$

At 90°K.: $R_m = 0.550$, $\beta_{C_2H_4} = 24.9$

$d = 1.6$ mm. $\Delta p = 5.64\mu$ $p_1 = 30\mu$

$d = 32$ mm. $\Delta p = 0.092\mu$ $p_1 = 30\mu$

The vapor pressure data of ethylene are therefore not materially affected.

(5) J. M. Los and R. R. Fergusson, *Trans. Faraday Soc.*, **48**, 730 (1952).

(6) (a) and (b) both unpublished.

(7) R. A. Beebe, J. B. Beckwith and J. M. Honig, *J. Am. Chem. Soc.*, **67** 1554 (1945).

ADSORPTION STUDIES ON METALS. II. ABSOLUTE ENTROPIES OF ADSORBED MOLECULES ON MOLYBDENUM[1,2]

BY J. J. CHESSICK, F. H. HEALEY AND A. C. ZETTLEMOYER

Contribution from the Surface Chemistry Laboratory, Lehigh University, Bethlehem, Penna.

Received April 7, 1953

Adsorption measurements for A, N_2, O_2 and CO on molybdenum powder were extended from multilayer coverages at high relative pressures to pressures of one-tenth of a micron of mercury. Little or no physical adsorption data for metal surfaces has previously been reported down to such low pressures. Thermal transpiration corrections applied to the low pressure data modified the calculated heats of adsorption by about 200 cal. at the lowest pressure measured. Further evidence for the surface heterogeneity of a reduced molybdenum sample was revealed by heat of adsorption data. The initial heat value for argon on the reduced metal was about 0.9 kcal. greater than the respective value on the unreduced sample. Nitrogen and carbon monoxide had similar isosteric heat values, *ca.* 3.5 kcal., at low surface coverages. Argon and oxygen heat values were very close at all coverages with an initial value of about 3.1 kcal. The absolute entropies of the adsorbed phase have been calculated. These data were compared with theoretical entropy values obtained from statistical mechanical considerations.

Introduction

The results of a study of the physical and chemical adsorption of gases at low temperatures on molybdenum powders in the pressure range which extends roughly from 1 to 76 cm. were reported recently.[3] From these studies important information concerning the physical and chemical heterogeneities of molybdenum surfaces was obtained.

The more fundamental objective of the present work was the obtainment of accurate, low pressure adsorption data in the range 1×10^{-4} to 10 mm. These data together with the high pressure data allow the various thermodynamic quantities recently developed by Hill[4] to be calculated. The most important of these is the absolute entropy of the adsorbed molecules, which can be used for the interpretation of absorbate behavior by comparison with simple statistical mechanical models.

Little or no adsorption data for metal surfaces has previously been reported for such a wide range of pressures. In a recent comprehensive search of the literature, Honig and Reyerson[5] found only six instances of adsorption measurements for the physical adsorption of gases on solids which included the low pressure region of the isotherm. Prominent among these was the work of Jura and Harkins[6] who measured the adsorption of nitrogen on anatase at pressures as low as 5×10^{-3} mm. through use of a wide bore mercury manometer and a traveling microscope.

Further, the effect of thermal transpiration corrections of low pressure physical adsorption data on calculated thermodynamic quantities has been evaluated. In low pressure adsorption work, correction for this effect has seldom been made heretofore.

Experimental

Apparatus and Procedure.—The pretreatment of the molybdenum powders and the purification of the gases used in the adsorption measurements have been reported previously.[3] Low pressure adsorption measurements were determined in an apparatus described by Orr.[7] However, in this work absolute pressures rather than differential pressures were measured. The oil manometer used allowed adsorption pressures to be measured in the range 0.10 to 50 mm. Apiezon "B" was used in the manometer. This oil has a very low vapor pressure and did not dissolve measurable amounts of the gases used. Pressures below the oil manometer range were read on a calibrated McLeod gage. The well known BET volumetric apparatus was used to obtain adsorption measurements in the higher relative pressure range.

McLeod Gage.—In initial studies, data for the adsorption of nitrogen on unreduced molybdenum were obtained at −183 and −195°. The isosteric heats of adsorption were calculated by means of the Clausius–Clapeyron equation. Although adsorption pressures as low as 0.1 mm. were measured using an oil manometer, it was found that reliable heat data below a V/V_m value of 0.4 could not be obtained because a large fraction of the surface was already covered below 0.1 mm. After a thorough study of the various pressure gages available, it was decided that a modified McLeod offered the best possibilities for adequate pressure measurements below the range of the oil manometer.

The McLeod gage consisted of a series of bulbs joined by capillary tubing. The gage volumes were determined both gravimetrically and volumetrically. The method of calibration and the accuracy obtained will be discussed in a forthcoming publication. An accuracy of approximately 4% was obtained for the lowest pressure measured: 5×10^{-4} mm.

At least 1.5 hours were required for equilibrium to be attained in the low pressure region at −195°. A slightly lesser time interval was necessary at −183°.

Calculations

Heats of Adsorption.—The heat term most useful in explaining adsorption phenomena is defined by the equation developed by Hill.[4]

$$\left(\frac{\mathrm{d} \ln p}{\mathrm{d} T}\right)_{\varphi} = \frac{H_G - H_S}{RT^2} = \frac{Q_{eq}}{RT^2}$$

where the subscripts S and G refer to the adsorbed and gaseous phase, respectively. The independent variables are: the temperature, T; pressure of the gas, p; and the spreading pressure, φ, the difference in free surface energy between the clean solid and the film covered solid. The heat term, Q_{eq}, is the equilibrium heat of adsorption defined by Hill. R is the molar gas constant.

In order to calculate the equilibrium heat, use was made of the fundamental Gibbs equation for the spreading pressure

$$\varphi = \frac{RT}{\Sigma V} \int_0^p \left(\frac{v}{p}\right) \mathrm{d} \ln p$$

(1) This work was used as part of a thesis submitted by J. J. Chessick in partial fulfillment of the requirements for the degree of Doctor of Philosophy.

(2) Presented at the Fall, 1952, meeting of the American Chemical Society, Atlantic City, New Jersey.

(3) F. H. Healey, J. J. Chessick and A. C. Zettlemoyer, THIS JOURNAL, **57**, 178 (1953).

(4) T. L. Hill, *J. Chem. Phys.*, **17**, 520 (1949).

(5) J. M. Honig and L. H. Reyerson, THIS JOURNAL, **56**, 140 (1952).

(6) G. Jura and W. J. Harkins, *J. Am. Chem. Soc.*, **66**, 1356 (1944).

(7) W. J. C. Orr, *Proc. Roy. Soc.* (*London*), **173A**, 349 (1939).

The undefined terms introduced are the molar volume of the adsorbate V, the volume adsorbed v, and the surface area of the adsorbent Σ. Since no simple relationship exists between v and p, the spreading pressure must be calculated by graphical integration. Large scale plots of v/p *vs.* p were made for the two temperatures employed. These were graphically integrated to obtain the area under the curve between definite pressure intervals. For the calculation of the spreading pressure from 0 to $p(p < 10^{-3}$ mm.) the following procedure was used. The experimental values for v were plotted against the low pressure values on large graph paper and a smooth curve was drawn through these points to the lowest measured pressure. A straight line, $v = kp$, was used as an analytical expression for the lowest pressures. The equilibrium heat values were then calculated according to the method described by Hill.[4]

Entropies of Adsorption.—Assuming no entropy change for the adsorbent, the integral entropy of the adsorbed molecule, S_S, was calculated from the equilibrium heats and a knowledge of the entropy of a gas as a function of the equilibrium pressure. Since the adsorption process is an equilibrium process the following expression holds

$$\frac{Q_{eq}}{\bar{T}} = \frac{H_G - H_S}{\bar{T}} = S_G - S_S$$

and

$$S_S = S_G - \frac{Q_{eq}}{\bar{T}}$$

From the third law of thermodynamics one obtains the expression for the absolute entropy of a gas as a function of pressure

$$S_G = S_G^0 - \int_{P_{eq}}^{p\ =\ 1\ atm.} d \ln p$$

where S_G^0 is the absolute entropy of the gas at 1 atm. and the average temperature $\bar{T}$.

Thermal Transpiration Corrections.—Reynolds[8] first pointed out the necessity for applying thermal transpiration corrections to low pressure measurements for a system and gage operating at widely differing temperatures. Tompkins and Wheeler[9] determined values for the pressure ratio $R = (P_1/P_2)$, where P_1 is the pressure of the system at $-183°$ and P_2 is the pressure observed on the gage at room temperature using hydrogen gas. Once values of R for hydrogen were available, corresponding values for nitrogen and argon were obtained through use of a proper factor. For example Liang[10] has shown that for the four gases employed in his investigation (H_2, He, A and N_2) plots of R *vs.* P_2 could be reduced to a single curve by changing the pressure scale. Unfortunately no "pressure shifting" factors were determined for oxygen and carbon monoxide.

Values of R for nitrogen and argon for systems at -195 and 25°, respectively, were taken directly from the data of Liang.

(8) O. Reynolds, see Maxwell, "Scientific Papers," Vol. 2, 1890, p. 708.

(9) F. S. Tompkins and D. E. Wheeler, *Trans. Faraday Soc.*, 29, 1248 (1933).

(10) S. Chu Liang, *J. Appl. Phys.*, 22, 148 (1951).

Discussion

Isosteric and Equilibrium Heats of Adsorption, Unreduced Molybdenum.—The heats of adsorption as a function of the fraction of surface covered, θ, were calculated using the Clausius-Clapeyron equation in the form

$$\log \left(\frac{p_1}{p_2}\right)_V = \frac{-\Delta H}{2.303R}\left(\frac{1}{T_1} - \frac{1}{T_2}\right)$$

where ΔH is the isosteric heat evolved per mole of gas adsorbed at a given equilibrium pressure. The heat values thus obtained fall steadily with increasing θ to the latent heat of vaporization or sublimation of the gases employed. The results are plotted in Fig. 1.

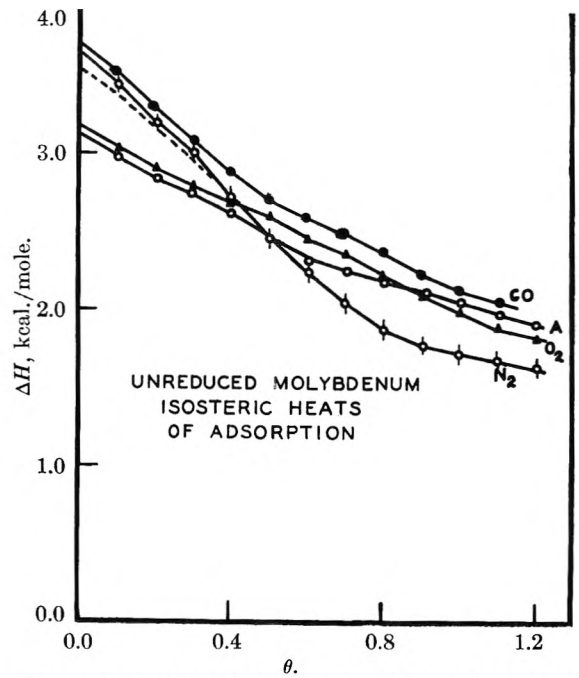

Fig. 1.—Isosteric heats of adsorption for a variety of gases adsorbed on unreduced molybdenum; average temperature, $T = -189.4°$.

The similarity of the argon and oxygen heat curves is not surprising. Orr[7] pointed out the marked resemblance between the potential energy curves for two argon atoms and two oxygen molecules as derived from virial coefficient data. Further, the diameters of the argon atom and the oxygen molecule derived from liquid densities are about the same. Thus, it is reasonable to expect the behavior of these gases to be similar under the influence of relatively weak van der Waals forces. Because of its lower heat of vaporization, one would expect lower energies of adsorption for nitrogen than those found for argon and oxygen. This is contrary to experimental findings. Morrison and Drain[11] have recently successfully correlated the differences in the adsorption heats of a variety of gases on rutile by considering the effect of electric quadrupole moments of these molecules on adsorption.

Roberts and Orr[12] carried out detailed calcula-

(11) Private communication from L. E. Drain and J. A. Morrison, National Research Council, Ottawa, Canada.

(12) J. K. Roberts and W. J. C. Orr, *Trans. Faraday Soc.*, 34, 1346 (1938).

tions for the energies of adsorption at equilibrium distances for an argon atom at various positions on a potassium chloride surface. Similar considerations hold for the adsorption of other non-polar atoms or molecules on smooth surface of crystals. For example, the polar van der Waals energy for the adsorption of argon on the smooth surface of MoO_2 calculated from the equation of Hückel[13] amounts merely to 0.25 kcal. per mole and must, therefore, play only a minor role in the adsorption process. Unfortunately, the molybdenum samples used were not smooth surfaces but rather polycrystalline in nature. Furthermore, data concerning the oxides of molybdenum necessary for calculation of the more important non-polar van der Waals energies of adsorption are not available. Thus a comparison of theoretical and experimental heat quantities is not possible. As a consequence, advantage must be taken of the availability of equilibrium heats of adsorption and the entropies calculable from them to gain knowledge of the behavior of the adsorbed phase.

Before proceeding further, it should be pointed out that the transpiration corrections applied to the pressures used in calculating the isosteric heat values did not change these values greatly. This is illustrated in Fig. 1 where both corrected (solid line) and uncorrected (dotted line) heat curves for nitrogen are plotted. Since the temperatures em-

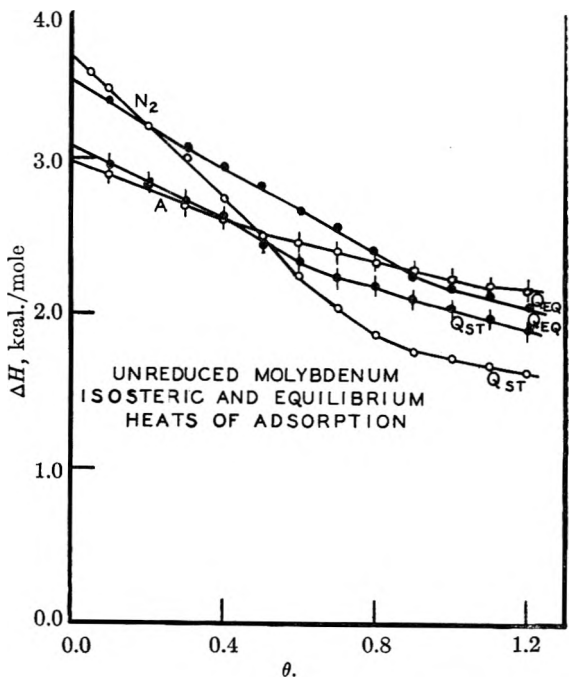

Fig. 2.—Isosteric and equilibrium heats of adsorption for argon and nitrogen adsorbed on unreduced molybdenum. $T = -189.4°$.

ployed in the adsorption studies differed only by approximately 12°, it is not surprising that the corrections applied to the measured pressures did not differ much at these two temperatures. Nonetheless, these corrections are important for the obtainment of true values for the absolute entropies of the adsorbed molecules. The equilibrium heat values obtained for the adsorption of argon and nitrogen on unreduced molybdenum are shown in Fig. 2 plotted as a function of the fraction of surface covered, θ.[14] The heat values at low coverage start below the isosteric heat values and fall less rapidly than the latter as θ increases. The condition set forth by Hill that the isosteric heat be RT (167 cal.) greater than the equilibrium heat at $\theta = 0$ is met.

Isosteric and Equilibrium Heats, Reduced Molybdenum.—The isosteric heat values obtained for the adsorption of argon on the reduced surface are plotted in Fig. 3 as a function of θ. The curve is about 0.9 kcal. greater at $\theta = 0$ than the corresponding one found for the adsorption of this gas on the oxide surface. The argon curve falls rapidly and essentially equals that for the unreduced metal at monolayer coverage. The larger adsorption heats found at small coverages for adsorption on the metal surface are not surprising. This sample of molybdenum had been subjected to only one reduction and should have the maximum of physical imperfections on the surface, since sintering effects are at a minimum here. Evidence for physical heterogeneities on a reduced molybdenum surface has been reported previously.[2]

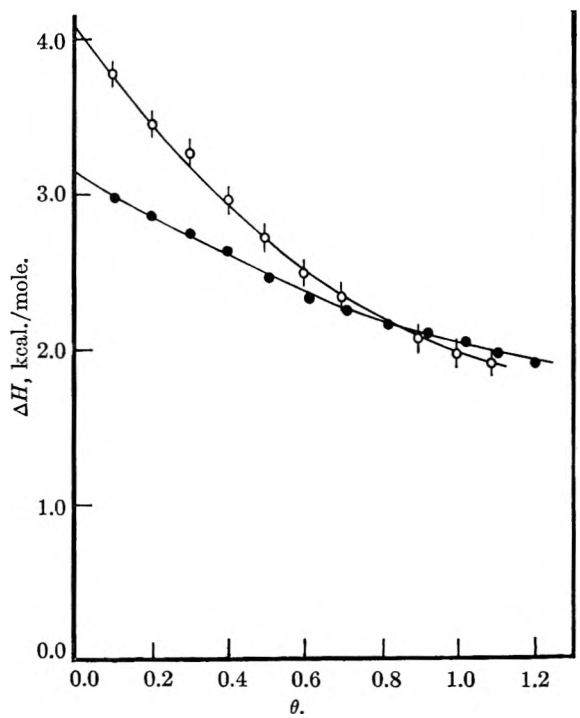

Fig. 3.—Isosteric heats of adsorption for argon adsorbed on reduced (ϕ) and unreduced (●) molybdenum; $T = -189.4°$.

Integral Entropies of Adsorption.—The integral entropy curves determined from equilibrium heat data are shown in Fig. 4 for the adsorption of nitrogen, argon and oxygen gases on unreduced molybdenum. The absolute entropies per mole of the adsorbed phase are given assuming the thermodynamic properties of the solid are not changed by the adsorbed molecules. The figure also contains

(13) E. Hückel, "Adsorption und Kapillarkondensation," Akad. Verlagsgesellschaft, Leipzig, 1928, p. 126.

(14) The pressures of nitrogen and argon used to calculate these heat values are corrected for transpiration effects. Oxygen pressures are not corrected.

for comparative purposes curves representing the theoretical entropy, S_T, of a perfect two-dimensional gas which has lost one degree of translational freedom. The theoretical values were calculated according to the equation developed by Kemball[15]

$$S_T = (R \ln MTa + 65.80 + S_{rot} + S_{el})$$

where a is the area available per molecule, S_{rot} the rotational entropy term and S_{el} the electronic entropy term.[16]

For immobile adsorption there will be a configurational term in the entropy associated with the number of ways of distributing the molecules over the surface. If the fraction of surface covered is $1/X$, the distribution of N molecules among NX sites gives an entropy

$$S = Rx \ln x - (X - 1) \ln (X - 1)$$

Thus a mole of argon adsorbed on a uniform surface at $\theta = 0.5$ would have an additional entropy of about 1.8 e.u. over that for the completely covered surface providing the adsorbed phase has the properties of solid argon. The configurational curve for solid argon is labeled S_c.

It is of interest also to compare the integral entropy values with those for the bulk three-dimensional phases of the adsorbates. The absolute entropies of all the gases studied were obtained from the NBS–NCA Tables of Thermal Properties of Gases.[17] The entropies of solid nitrogen and oxygen at 78.5°K. were taken from the work of Kingston, *et al.*[18] The entropy of solid argon was obtained from its heat of sublimation and the knowledge of its saturation pressure at 83.5°K. The liquid entropies were obtained from heats of liquefaction.

All the integral entropy curves approach ∞ as $\theta \rightarrow 0$ since

$$S_S = S_G - \Delta S$$

and ΔS is finite while the entropy of the gas S_G is infinite at $\theta = 0$. The entropy of adsorbed oxygen decreases rapidly and then remains close to the entropy of liquid oxygen over a large range of surface coverage. The nitrogen curve is similar except that the entropy values fall slightly below that for solid nitrogen. The argon curve on the other hand is slightly below the theoretical, S_c, curve which was obtained by adding the configurational entropy terms to that for solid argon. The theoretical, S_c, type of curve might well be explained on the basis of: (1) immobile adsorption on a uniform surface with no lateral interaction between adsorbed molecules and (2) a high configurational entropy since the atoms favor all sites equally and have a large choice of sites. It is highly improbable that the surface of unreduced molybdenum would exhibit behavior typical of a uniform surface especially in the region of low pressures where heterogeneities of the surface must play an important role in the adsorption process. Furthermore, if the configurational entropy terms are added to the entropy of solid nitrogen, it is evident from an inspection of Fig. 4 that these values will be higher than those found experimentally for nitrogen. This is in agreement with the concept that adsorption takes place on a non-uniform surface.

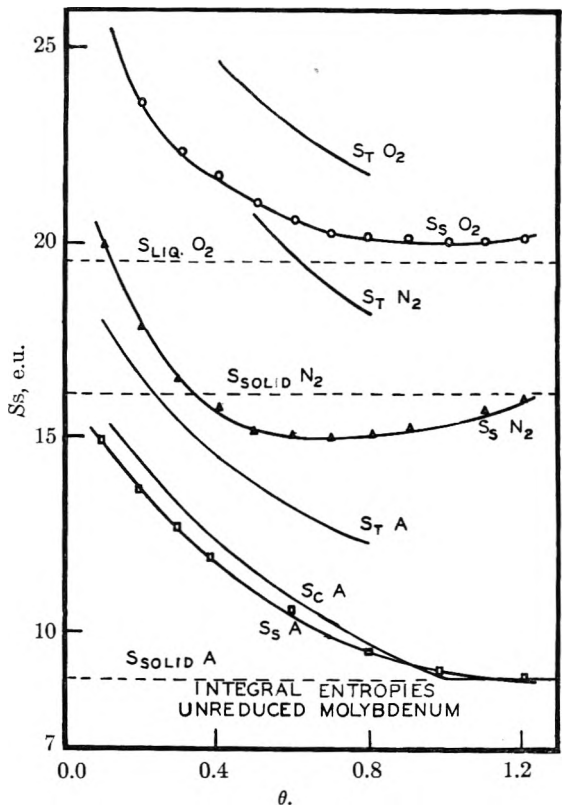

Fig. 4.—Integral entropies of adsorption for a variety of gases adsorbed on unreduced molybdenum; $T = -189.4°$.

A comparison of the experimental values with those calculated from statistical mechanics reveals that a standard state of $\theta = 0.5$ the integral entropy of adsorbed oxygen is about 2.0 e.u. lower than S_T, the entropy of gaseous oxygen minus one degree of translational freedom. Adsorbed nitrogen, however, is about 5.0 e.u. lower than the value expected for a perfect two-dimensional gas which would indicate more restriction on the adsorbate than is the case with oxygen.

Argon suffers about the same entropy loss as oxygen. In view of the similarity of the heat of sublimation of argon and the heat of vaporization of oxygen it is not surprising that while the absolute entropy of adsorbed oxygen is close to that of the liquid the adsorbed argon has an entropy very much like the solid.

Acknowledgment.—This research has been carried out under Contract N8onr-74300 with the Office of Naval Research. The authors are happy to acknowledge this aid and are grateful to this agency for the support.

(15) C. Kemball, "Advances in Catalysis," Vol. II, Academic Press, Inc., New York, N. Y., 1950, p. 233.

(16) The rotational entropy of argon is, of course, zero. Those for nitrogen and oxygen at 83.5°K. are calculated to be 7.52 and 7.96 e.u., respectively. In addition oxygen has an electronic entropy amounting to 2.17 e.u., resulting from allowable transitions between the two lowest lying electronic levels.

(17) The Tables 9.10, 11.10 and 19.10 may be obtained from the National Bureau of Standards, Washington, D. C.

(18) G. C. Kington, R. A. Beebe, M. H. Polley and W. R. Smith, *J. Am. Chem. Soc.*, **72**, 1780 (1950).

RADIOTRACER STUDY OF SULFATE ION ADSORPTION AT THE AIR/SOLUTION INTERFACE IN SOLUTIONS OF SURFACE-ACTIVE AGENTS

BY C. M. JUDSON, A. A. LEREW, J. K. DIXON AND D. J. SALLEY

Stamford Research Laboratories, American Cyanamid Company, Stamford, Conn.

Received April 8, 1953

Radioactive tracer methods have been used to measure the adsorption of sulfate at the air/solution interface in solutions containing sulfate with various cationic, anionic and non-ionic agents. Measurements of sulfate adsorption with solutions of Aerosol[1] SE Cationic Agent indicate that there is a surface hydrolysis which can be explained in terms of competition between sulfate and hydroxyl gegenions. It also has been shown that sulfate gegenions replace chloride gegenions with the replacement substantially complete in the presence of a moderate excess of sulfate. At high concentrations it was found that multilayers of gegenion were adsorbed. Multilayer adsorption of sulfate, up to an equivalent of about 200 monolayers, was also found in solutions containing sodium sulfate with anionic and non-ionic agents. It appears that when a layer of surface-active agent is present at the surface, electrolyte which may be present in the solution tends to accumulate in the region adjacent to the surface in an amount which is proportional to the concentration of the electrolyte. Multilayers of surface-active electrolyte apparently form in the same way as multilayers of any other electrolyte, in spite of the fact that long chain ion micelles may be involved as well as small ions.

Introduction

Adsorption of surface-active agents at the air/solution interface can be conveniently measured by methods using radiotracers.[2-6] It appeared that, since the number of gegenions adsorbed should be equivalent to the number of long chain ions, measurement of gegenion adsorption would offer a relatively simple method of estimating adsorption of a number of different surface-active agents without requiring the synthesis of each agent in the radioactive form. Some measurements of the adsorption of sulfate ions from solutions of cationic and anionic surface-active agents have been reported in preliminary notes.[7] The data presented from the study of cationic agents[7(a)] indicated: that multilayers of considerable depth are formed at the surface of these solutions; that at low concentrations the adsorbed species is the hydrolyzed form; and that although chloride gegenions are replaced by sulfate gegenions on the addition of sodium sulfate to the cationic chloride, substantial replacement by sulfate does not occur with trace amounts of sulfate as has been suggested.[8] The data reported from the study of anionic agents[7b] indicated that small ions of the same sign as the long chain ion are adsorbed as well as ions of the opposite sign (gegenions). It is seen that sulfate gegenion adsorption can be used to measure long chain ion adsorption in cationic agents, but that the concentration of long chain ion and of sulfate ion must both be large enough so that the adsorption of other ions can be neglected.

The data which have been obtained for the adsorption of sulfate ions from solutions containing sulfate with cationic, anionic and non-ionic agents are presented in detail below.

(1) Registered trademark, American Cyanamid Company.

(2) J. K. Dixon, A. J. Weith, Jr., A. A. Argyle and D. J. Salley, *Nature*, **163**, 845 (1949).

(3) D. J. Salley, A. J. Weith, Jr., A. A. Argyle and J. K. Dixon, *Proc. Roy. Soc. (London)*, **A203**, 42 (1950).

(4) G. Aniansson and O. Lamm, *Nature*, **165**, 357 (1950).

(5) G. Aniansson, THIS JOURNAL, **55**, 1286 (1951).

(6) E. Hutchinson, *J. Coll. Sci.*, **4**, 599 (1949).

(7) (a) C. M. Judson, A. A. Argyle, J. K. Dixon and D. J. Salley, *J. Chem. Phys.*, **19**, 378 (1951); (b) C. M. Judson, A. A. Lerew, J. K. Dixon and D. J. Salley, *ibid.*, **20**, 519 (1952).

(8) D. Reichenberg, *Trans. Faraday Soc.*, **43**, 467 (1947).

Experimental

Method.—Sulfate adsorption measurements were made by the surface count method of Salley, Weith, Argyle and Dixon.[2,3] This method depends on the use of a soft β-emitter as a label, the radiation above a solution of a surface active agent being greater than over a solution at which no surface adsorption occurs, because radiation from the molecules at the surface is not self-absorbed in the solution. The procedure used was essentially that previously described,[3] except that the specific activity at the surface of the solution was corrected for the geometry of the counting arrangement by determining the specific activity as a function of radius from the counter tube axis, and integrating over the area of the sample. This method of correcting the specific activity has been developed independently by Aniansson,[5] and the procedure used was essentially that reported by him except that the integration was made graphically. As in the previous measurements,[3] the surface count was followed with time until constant values were obtained.

Some measurements of adsorption were also made by the film method developed by Hutchinson,[6] using a platinum ring of 1.5 cm. radius to draw the film of surface-active agent from the solution.

Materials.—Radioactive sodium sulfate was prepared from neutron bombarded potassium chloride obtained from the Oak Ridge National Laboratories on allocation by the U.S. Atomic Energy Commission. Barium sulfate was precipitated and was converted to sulfur dioxide according to the procedure previously described.[3] The sulfur dioxide was then dissolved in a calculated amount of sodium hydroxide and the solution was treated with hydrogen peroxide to obtain sodium sulfate.

Aerosol[1] OTN Anionic Agent (di-*n*-octylsodium sulfosuccinate, referred to below as A-OTN) was prepared by reaction of di-*n*-octyl maleate with sodium bisulfite.[9] The product was recrystallized from an alcohol–water mixture. Aerosol SE Cationic Agents[1] (γ-stearamidopropyl-2-hydroxyethyldimethylammonium chloride and sulfate, referred to below as A-SE chloride and A-SE sulfate, respectively) were prepared by neutralizing γ-stearamidopropyldimethylamine with acid and treating the amine salt with ethylene oxide.[10] The chloride, prepared using hydrochloric acid, was recovered by precipitating with ether and recrystallizing from acetone. In the preparation of the sulfate the intermediate γ-stearamidopropyldimethylamine was recrystallized from an alcohol–water mixture and the quaternary salt, obtained using sulfuric acid, was recovered by concentrating on the steam-bath and then pumping off the remaining solvent, and was used without further purification. Solutions of A-SE sulfate were also prepared by adding a calculated amount of silver sulfate to solutions of A-SE chloride and removing the silver chloride by filtration. Aerosol[1] NL-10 Non-ionic Agent (referred to below as A-NL-10) was prepared by condensing 10 mols. of ethylene

(9) A. O. Jaeger, U. S. Patent 2,028,091 (Jan. 14, 1936).

(10) E. W. Cook and P. H. Moss, U. S. Patent 2,589,674 (March 18, 1952).

oxide with one mol of N-(2-hydroxyethyl)-lauramide. The product obtained was bleached with hydrogen peroxide and was used without further purification. American Cyanamid Company 100% Aerosol[1] OT Anionic Agent (di-2-ethylhexylsodium sulfosuccinate, referred to below as A-OT), and Edwal Laboratories cetylpyridinium chloride were also used in these experiments.

Results

Competition between Sulfate and Chloride Gegenions.—The competition between sulfate and chloride gegenions is illustrated by sulfate adsorption measurements in solutions containing cetyl pyridinium chloride and sodium sulfate. The data obtained are shown in Fig. 1 as a function of sodium sulfate concentration at constant cetyl pyridinium chloride concentration, and in Fig. 2 as a function of cetyl pyridinium chloride concentration at constant sodium sulfate concentration.

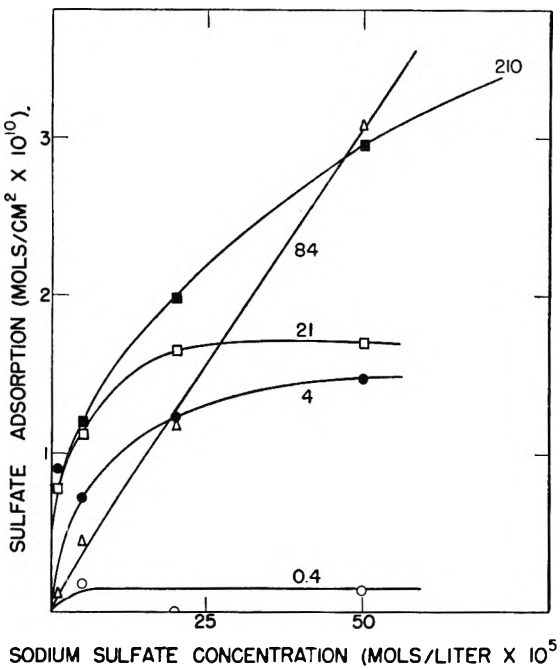

Fig. 1.—Adsorption of sulfate from solutions of cetyl pyridinium chloride containing sodium sulfate; measured at constant cetyl pyridinium chloride concentrations: △, 210 × 10^{-5} M; ■, 84 × 10^{-5} M; □, 21 × 10^{-5} M; ●, 4.0 × 10^{-5} M; ○, 0.4 × 10^{-5} M. Critical concentration, 100 × 10^{-5} M, lower with added sodium sulfate.

Figure 1 indicates that the sulfate adsorption increases with sulfate concentration but tends to level off at sulfate concentrations somewhat greater than the long chain ion concentration. It appears that on addition of sulfate ions to these solutions, the monovalent gegenions which are present in the surface layer (chloride ions or, if the agent is hydrolyzed at the surface, hydroxyl ions) are replaced by sulfate gegenions. In solutions containing a moderate excess of sulfate the monovalent gegenions in the surface layer are substantially replaced by sulfate gegenions.

Figure 2 indicates that the sulfate adsorption increases with increasing concentration of cationic chloride, reaches a maximum, and then decreases at higher concentrations of cationic chloride. The increase in sulfate adsorption with increase in concentration of cationic chloride observed at low concentrations is apparently due to the increase in adsorption of long chain ion with increasing concentration of long chain ion. The decrease in sulfate adsorption at higher concentrations is apparently due to replacement of sulfate gegenions by chloride gegenions with increasing concentration of chloride ion.

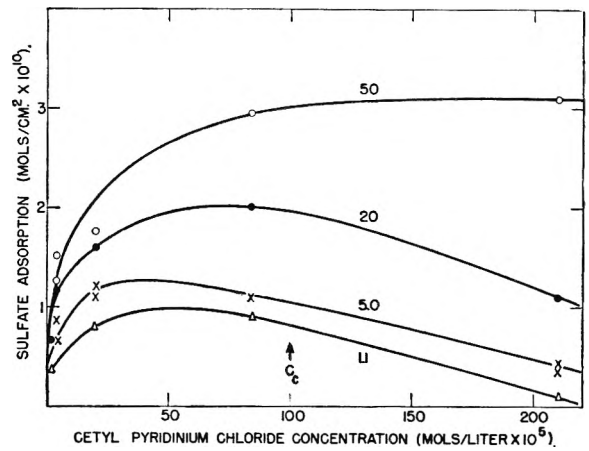

Fig. 2.—Adsorption of sulfate from solutions of cetyl pyridinium chloride containing sodium sulfate; measured at constant sodium sulfate concentration: ○, 50 × 10^{-5} M; ●, 20 × 10^{-5} M; ×, 5.0 × 10^{-5} M; △, 1.1 × 10^{-5} M. Critical concentration, 100 × 10^{-5} M, lower with added sodium sulfate.

Data qualitatively similar to the foregoing were obtained with solutions of A-SE chloride and sodium sulfate. At constant A-SE chloride concentrations of 10 × 10^{-5} and 100 × 10^{-5} M, the monovalent gegenions in the surface layer were substantially replaced by sulfate when the sulfate concentrations were roughly 15 × 10^{-5} and 200 × 10^{-5} M, respectively. Likewise, at constant sodium sulfate concentrations of 5 × 10^{-5}, 10 × 10^{-5} and 20 × 10^{-5} M, maxima were observed in the curves of sulfate adsorption *vs.* A-SE chloride concentration.

Reichenberg,[8] in attempting to explain the minima sometimes observed in the surface tension *vs.* concentration curves, has suggested that trace amounts of sulfate ions would completely replace the monovalent gegenions at the surface. The present data for cetyl pyridinium salts (one of the specific instances considered by Reichenberg) show that the monovalent gegenions are not substantially replaced by sulfate gegenions in the presence of trace amounts of sulfate. Although the quantitative treatment given by Reichenberg is not applicable, these results do not necessarily mean that his qualitative explanation of surface tension minima as being due in some cases to replacement of gegenions by impurities of polyvalent salts is incorrect.

This suggestion of Reichenberg that traces of sulfate gegenion would replace monovalent gegenions had indicated that it might be possible to estimate the adsorption of a cationic agent (most commonly obtained as the chloride) by measuring the sulfate adsorption of a solution containing a little tagged sodium sulfate along with the cationic chloride. The experiments reported show that for the two cationic agents studied it is necessary to add more than a trace of sodium sulfate. In order to measure the long chain cation adsorption from the sulfate gegenion adsorption, it is necessary, in

general, either to prepare the cationic sulfate or to measure the sulfate adsorption as a function of sulfate concentration and establish that a maximum sulfate adsorption is reached.

Formation of Multilayers of Aerosol SE.—The adsorption of sulfate at the surface of solutions of A-SE sulfate is shown in Fig. 3. The data are shown by a log-log plot in order to cover a wide range of concentration and adsorption values. Above the critical concentration for micelle formation, the data plotted on a log-log scale appear to fit reasonably well to a straight line with a slope of approximately unity, indicating that the sulfate adsorption increases approximately linearly with the concentration of A-SE sulfate. However, there is a definite deviation from the linear relationship at low concentrations.

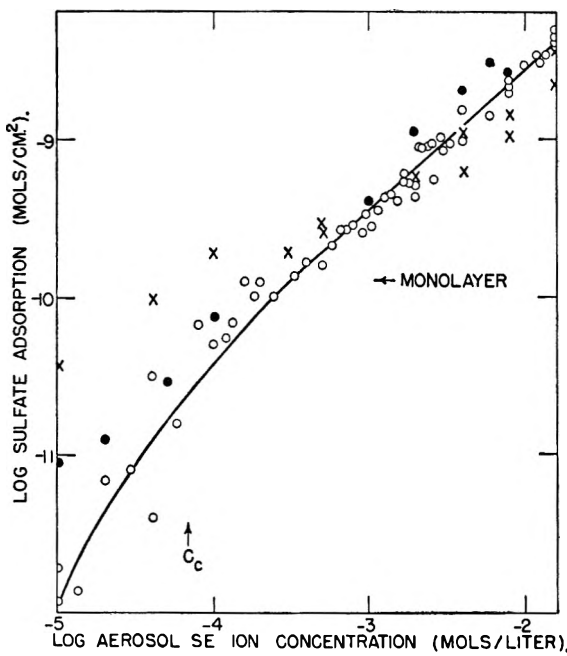

Fig. 3.—Adsorption of sulfate from A-SE solutions: ○, direct surface count for A-SE sulfate; ×, Hutchinson's method for A-SE sulfate; ●, direct surface count for equimolar mixtures of A-SE chloride and sodium sulfate. Critical concentration, 6.5×10^{-5} *M*. Adsorption in monolayer, 1.25×10^{-10} mole/cm.² sulfate ion; 2.5×10^{-10} mole/cm.² A-SE ion.

The adsorption of sulfate at the highest concentration measured is about 30 times the amount of sulfate adsorbed in a monolayer of A-SE sulfate as estimated from the surface tension *vs.* concentration data. The amount of long chain ion adsorbed in these solutions must be at least equal to the amount of gegenion adsorbed and may be larger if there is surface hydrolysis. However, the evidence presented below indicates that there is surface hydrolysis of A-SE sulfate only at low concentrations. It is therefore concluded that at the highest concentration measured a multilayer of A-SE sulfate is adsorbed which is equivalent to 30 monolayers of A-SE sulfate. Consideration of other evidence for multilayer adsorption may be found in a review by Henniker.[11]

(11) J. C. Henniker, *Rev. Mod. Phys.*, **21**, 322 (1949).

The multilayer as measured by the surface count method may be quite diffuse. The count for a layer 10,000 Å. below the surface would be experimentally indistinguishable from the count at zero depth, and any increase in the amount of S^{35} in the entire region of depth equal to the range of the S^{35} beta particle (about 0 2 mm.) would lead to an increase in the measured surface count.

Agreement was obtained between measurements of A-SE solutions prepared from A-SE chloride with silver sulfate and measurements with purified A-SE sulfate. Agreement was also obtained over a wide range of concentrations between measurements with a constant specific activity and measurements with a constant total activity.

Sulfate adsorption measurements for equimolar mixtures of A-SE chloride and sodium sulfate also agreed fairly well with measurements of A-SE sulfate solutions. The equimolar mixtures apparently contain sufficient excess sulfate so that the gegenion adsorbed is predominantly sulfate. This agrees with the results of the chloride–sulfate competition experiments which indicated that the chloride is substantially replaced by sulfate in solutions containing a moderate excess of sulfate.

Measurements of sulfate adsorption in A-SE sulfate solutions were made by Hutchinson's method as well as by the direct surface count method. The sulfate adsorption values obtained by Hutchinson's method are slightly lower than the direct surface count measurements at high concentrations and are slightly higher at low concentrations (Fig. 3). The lower values at high concentrations may be attributed to the much shorter time allowed for equilibrium in Hutchinson's method (a few seconds instead of a few minutes). The higher values by Hutchinson's method at low concentrations may also be due to the short time allowed for equilibrium. The direct surface count measurements at concentrations below 10^{-4} *M* showed a gradual decrease with time, requiring as much as one hour for equilibrium. Apparently at low concentrations where (as shown below) there is surface hydrolysis, some sulfate gegenions which are initially adsorbed are slowly replaced by hydroxyl gegenions. The sulfate adsorption measured by Hutchinson's method allowing a few seconds for equilibrium would therefore be too high. At concentrations above 10^{-4} *M* the direct surface count measurements were constant within a few minutes, the shortest period for which adsorption can be measured, but probably would show increases with time if very short intervals could be studied. (It was not found feasible to study the effect of varying time by Hutchinson's method.)

Similar data were obtained for equimolar mixtures of cetyl pyridinium chloride and sodium sulfate. Some 16 determinations by the direct surface count method and 6 determinations by Hutchinson's method gave an approximately linear adsorption with concentrations up to 30×10^{-10} mole/cm.² at 800×10^{-5} *M* (8 times the critical concentration).

It would appear that the adsorbed multilayers of cationic sulfate formed at high concentrations of

agent are made up mainly of micelles. The sulfate gegenions would then be partly bound in the micelles and partly unbound. The basis for believing that micelles are adsorbed is that above the critical concentration the single long chain ion concentration is approximately constant while the concentration of micelles increases continually with concentration. Since the adsorption of surface-active agent increases more or less linearly with concentration in this region, the adsorption depends on the micelle concentration and this suggests that the adsorbed layer is made up of micelles rather than single molecules.

Surface Hydrolysis of Aerosol SE.—The surface adsorption in solutions of A-SE sulfate may be calculated from Gibbs' equation[12,13]

$$-d\gamma = RT\Gamma_{SO_4^-}\, d \ln C_{SO_4^-} + RT\Gamma_{A\text{-}SE^+}\, d \ln C_{A\text{-}SE^+} \quad (1)$$

where γ is the surface tension, $C_{SO_4^-}$ and C_{A-SE^+} are the concentrations of sulfate and A-SE ions, respectively, and $\Gamma_{SO_4^-}$ and Γ_{A-SE^+} are the amounts adsorbed per cm.^{2}. Even though A-SE may be adsorbed as the hydroxide, the term due to Γ_{OH^-} in equation 1 is small and may be neglected because d ln C_{OH^-} is small. This agent is very little hydrolyzed in the bulk solution and the effect of adsorption on the bulk concentration of hydroxyl ion is also small. The concentration of hydroxyl ion does not change much either from hydrolysis or from adsorption as is shown by the constancy of the measured *p*H within 0.1 unit. That is $\Delta \log C_{OH^-}$ is less than 0.1 for the region 10^{-5} to 10^{-2} *M* A-SE sulfate in which $\Delta \log C_{A-SE^+}$ and $\Delta \log C_{SO_4^-}$ are equal to 3. The term due to Γ_{H^+} is also small. Finally the contribution of Γ_{Na^+} can be neglected because the amount of sodium sulfate used to tag the solution is negligible compared to the amount of A-SE sulfate present. The effect of activity coefficients can safely be neglected in these solutions which are dilute enough so that the activity is not affected either by micelle formation or by interionic attraction.

Since the concentrations of A-SE and sulfate are equal, the slope of the curve obtained for surface tension *vs.* concentration gives the sum of the adsorption of the A-SE ion and the adsorption of the sulfate ion. The value obtained is constant at about 25×10^{-10} mole/cm.^{2} for concentrations from 0.4×10^{-5} to 6×10^{-5} *M* (the critical concentration). This adsorption value calculated from the surface tension measurements is sufficiently larger than the sulfate adsorption at these concentrations as measured by the direct surface count method (lower curve in Fig. 4) as to indicate clearly that the surface layer at low concentrations contains predominantly hydroxyl gegenions rather than sulfate gegenions.

A-SE sulfate appears to be hydrolyzed at the surface even though quaternary ammonium salts are salts of strong bases and are not hydrolyzed in solution. The quaternary ammonium base must be considered as a weaker base in the surface than in the bulk of the solution. Data indicating surface hydrolysis for compounds which are not ordinarily considered to be hydrolyzed has been previously obtained by various methods for A-OTN,[3,7b] sodium lauryl sulfate[14] and thymolsulfonphthalein.[15]

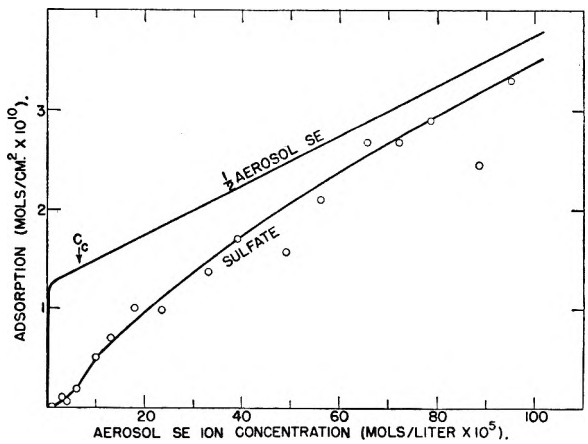

Fig. 4.—Adsorption of sulfate ion and A-SE ion from A-SE sulfate solutions: lower curve (points shown by circles), measured sulfate adsorption; upper curve, one-half of estimated A-SE ion adsorption (from Fig. 5). Critical concentration, 6.5×10^{-5} *M*.

The amount of surface hydrolysis apparently decreases with increasing concentration of A-SE sulfate because the ratio of sulfate to hydroxyl ions in solution becomes larger. At sufficiently high concentrations the amount of A-SE ion adsorbed should be equivalent to the amount of sulfate adsorbed.

Figure 5 shows the A-SE ion adsorption calculated from the sulfate ion adsorption for concentrations above 10^{-3} *M* A-SE ion. A reasonably good straight line can be drawn through these data which also passes through a point at 10^{-5} *M* representing the adsorption at the knee of the isotherm as calculated from the surface tension measurements. This line is therefore taken to represent the surface adsorption of A-SE ion at concentrations above 10^{-5} *M*. In Fig. 4 this estimated A-SE ion adsorption is compared with the measured sulfate ion adsorption for the region below 10^{-3} *M* in which the transition from adsorbed hydroxyl to adsorbed sulfate takes place.

It should be noted that the straight line drawn in Figs. 4 and 5 to represent the A-SE ion adsorption is not identifiable, except at high concentrations, with the straight line in the log-log plot of Fig. 3 which represents the sulfate adsorption. The A-SE ion adsorption line extrapolates to an adsorption of 1.25×10^{-10} mole/cm.^{2} at zero concentration and the log-log plot of this line would become horizontal at this value rather than continually decreasing to zero.

We can derive an expression for the variation in sulfate adsorption with concentration by using kinetic equations of the type used by Langmuir in

(12) E. A. Guggenheim, "Thermodynamics," Interscience Publishers, Inc., New York, N. Y., 1949, p. 326.

(13) It has been suggested recently by J. T. Davies, *Trans. Faraday Soc.*, **48**, 1052 (1952), that Gibbs' equation should be written with only a single term for the surface-active ion. While it is true that the gegenion term vanishes in the case considered by Davies in which an excess electrolyte is present, there seems to be no justification for omission of the gegenion term in the general case.

(14) M. A. Cook and E. L. Talbot, THIS JOURNAL, **56**, 412 (1952).

(15) D. Deutsch, *Z. physik. Chem.*, **136**, 353 (1928).

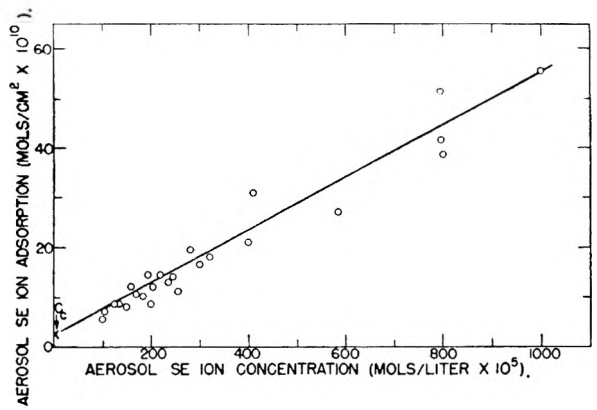

Fig. 5.—Adsorption of A-SE ion from A-SE sulfate solutions: ○, estimated from sulfate adsorption; ×, from surface tension measurements. Critical concentration, 6.5 × 10^{-5} M.

considering gas adsorption. Application of this kinetic treatment to adsorption from solutions is of limited value in the general case because there are no specific adsorption sites, but in special cases such as adsorption of electrolyte on an insoluble monolayer[16] and in this case involving adsorption of gegenions at sites already occupied by long-chain ions, the Langmuir treatment is of particular value. Adsorption of a sulfate ion requires two adjacent species so that the rate depends on the square of the number of vacant spaces[17]

$$k_1 \Gamma_{SO_4^-} = k_2 C_{SO_4^-} (\Gamma_{A\text{-}SE^+} - \Gamma_{OH^-} - 2\Gamma_{SO_4^-})^2 \quad (2)$$

and

$$k_3 \Gamma_{OH^-} = k_4 C_{OH^-} (\Gamma_{A\text{-}SE^+} - \Gamma_{OH^-} - 2\Gamma_{SO_4^-}) \quad (3)$$

where k_1 and k_3 are rate constants for desorption and k_2 and k_4 rate constants for absorption. On dividing this becomes

$$\Gamma_{SO_4^-}/\Gamma_{OH^-}^2 = K_1 C_{SO_4^-}/C_{OH^-}^2 \quad (4)$$

Assuming that the A-SE ion layer is to a sufficient approximation completely neutralized by hydroxyl and sulfate ions, then

$$\Gamma_{A-SE^+} = \Gamma_{OH^-} + 2\Gamma_{SO_4^-} \quad (5)$$

The term Γ_{OH^-} may be eliminated from equations 4 and 5 obtaining

$$\frac{\Gamma_{SO_4^-}}{(\Gamma_{A-SE^+} - 2\Gamma_{SO_4^-})^2} = \frac{K_1 C_{SO_4^-}}{C_{OH^-}^2} \quad (6)$$

If there is no hydrolysis in the bulk solution, which seems likely, the concentration of hydroxyl ion is a constant and then equation 6 can be written

$$\frac{\Gamma_{SO_4^-}/\Gamma_{A\text{-}SE^+}}{(1 - 2\Gamma_{SO_4^-}/\Gamma_{A\text{-}SE^+})^2} = K_2 C_{SO_4^-} \Gamma_{A-SE^+} \quad (7)$$

The experimental value of $\Gamma_{A\text{-}SE^+}$ read from Fig. 4 can be substituted in equation 7 in order to obtain $\Gamma_{SO_4^-}/\Gamma_{A\text{-}SE^+}$. The values of K_2 which fit the experimental data the best can then be determined by trial and error.

The calculated curves obtained using the values of $K_2 = 10^{12}$, 10^{13} and 10^{14} (moles/liter)$^{-1}$ (moles/cm.^{2})$^{-1}$ are shown in Fig. 6, along with the experimental curve. The experimental curve shows an inflection which occurs at a concentration considerably higher than the inflection found in the calculated curves. In fact the inflection in the calculated curves occurs at such a low concentration as to be hardly noticeable in Fig. 6. However, the qualitative agreement between the calculated and observed curves supports the postulated competition between sulfate and hydroxyl gegenions at the surface.

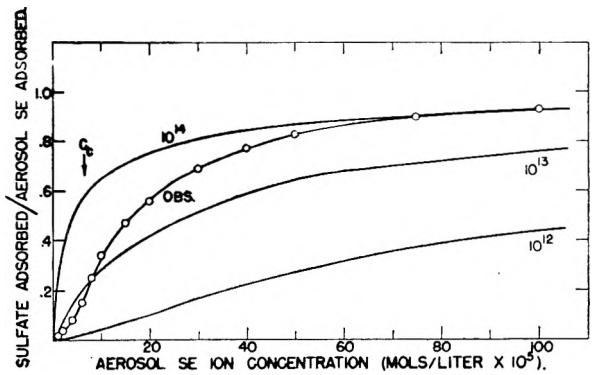

Fig. 6.—Observed and calculated values of ratio between sulfate ion adsorption and A-SE ion adsorption for solutions of A-SE sulfate. Calculated values for $K_2 = 10^{12}$ to 10^{14} compared to observed values from Fig. 4. Critical concentration, 6.5 × 10^{-5} M.

It is realized that the value obtained from surface tension for the A-SE ion adsorption below the critical concentration may be subject to considerable experimental error. However, within broad limits, a change in the value used for the adsorption below the critical concentration will not affect the qualitative picture of gegenion competition which has been developed.

The equilibrium constant K_1 for the competition between hydroxyl and sulfate gegenions may be estimated from the value 10^{13} taken for K_2 from Fig. 6 and the value 3 × 10^{-9} M for C_{OH^-} which is the measured value in water and in the A-SE solutions. The value obtained for K_1 is 10^{-4} mole/liter (moles/cm.^{2})$^{-1}$.

Qualitative mass action considerations would indicate that at sufficiently low concentrations of A-SE sulfate, some of the adsorbed sulfate ions would be replaced by adsorbed hydroxyl ions. It is possible to regard this qualitatively as a Donnan membrane effect, although application of the Donnan equations to this particular system necessarily involves arbitrary parameters. The quantitative treatment based on Langmuir type kinetic equations shows not only that some hydroxyl is adsorbed, but that adsorption of hydroxyl ions is favored over adsorption of sulfate ions. The explanation of why the adsorption of hydroxyl ions is favored seems to be that undissociated A-SE hydroxide is more strongly attracted from the polar bulk solution to the less polar surface because undissociated A-SE hydroxide molecules are less polar than dissociated A-SE sulfate molecules.

Sulfate Adsorption from Solutions of Anionic and Non-ionic Agents.—The adsorption of small ions of the same charge as the long chain ion has been studied by measurement of sulfate adsorption in solutions of A-OTN and A-OT. Data are shown in Figs. 7 and 8 for the adsorption of sulfate

(16) I. Langmuir and V. J. Schaefer, *J. Am. Chem. Soc.*, **59**, 2400 (1937).

(17) I. Langmuir, *ibid.*, **40**, 1361 (1918).

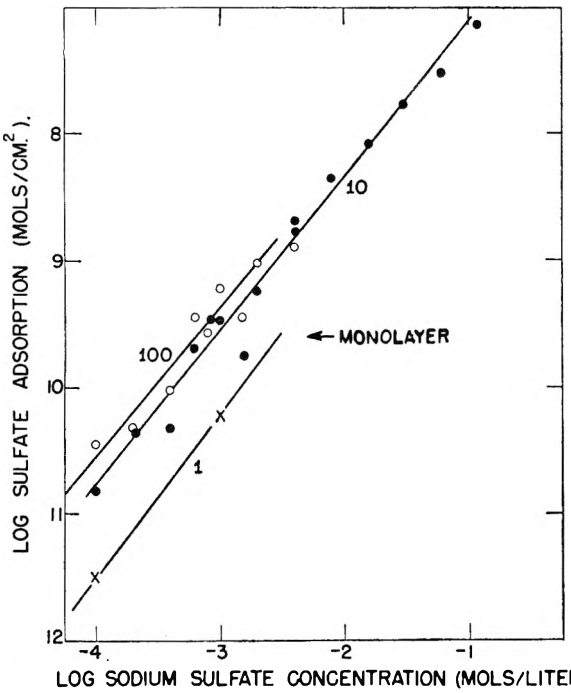

Fig. 7.—Adsorption of sulfate from solutions of A-OTN containing sodium sulfate; measured at constant A-OTN concentration: ○, 100×10^{-5} M; ●, 10×10^{-5} M; ×, 1×10^{-5} M. Critical concentration, 6.5×10^{-5} M. Adsorption in monolayer, 2.4×10^{-10} mole/cm.².

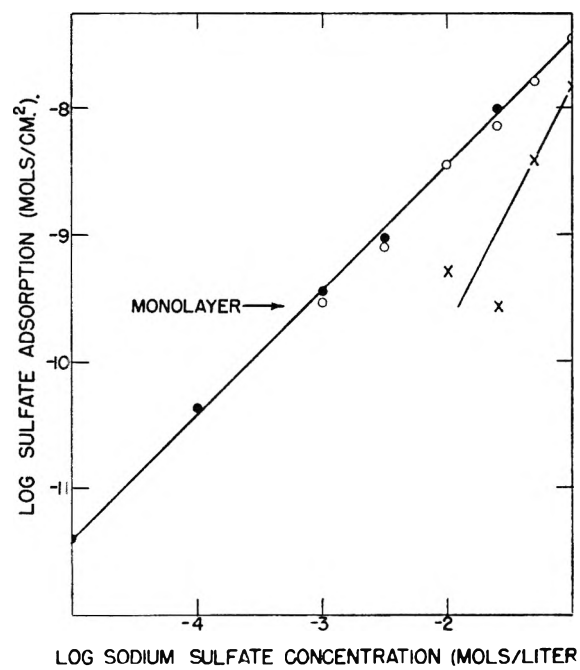

Fig. 8.—Adsorption of sulfate from solutions of A-OT containing sodium sulfate; measured at constant A-OT concentration: ●, 10^{-2} M; ○, 10^{-3} M; ×, 10^{-4} M. Critical concentration varies from 47×10^{-5} to 230×10^{-5} M as shown in Fig. 9. Adsorption in monolayer, 2.4×10^{-10} mole/cm.².

from solutions containing sodium sulfate and A-OT or A-OTN as a function of varying sulfate concentration. As in the case of A-SE sulfate adsorption, the log-log plot appears to be linear with a slope of approximately unity. Although the data obtained with 10^{-4} M A-OT solutions are not entirely consistent with the remaining data, it appears that the amount of sulfate adsorbed at any given concentration of agent is proportional to the concentration of sulfate.

The effect of varying the concentration of agent can best be seen from Fig. 9 in which adsorption is plotted against A-OT concentration. The sulfate adsorption increases with A-OT concentration up to a concentration about equal to the critical concentration at the sulfate concentration in question, and then remains approximately constant at higher concentrations of agent. The same effect can be seen in Fig. 8 where the sulfate adsorption is essentially equal for 10^{-2} and 10^{-3} M A-OT and in Fig. 9 where the increase in sulfate adsorption is much less between 10^{-3} and 10^{-4} M than between 10^{-4} and 10^{-5} M A-OTN. The critical concentration of A-OTN being 0.7×10^{-3} M, the adsorption in 10^{-3} M solution probably represents the maximum adsorption, although this has not been proven because no measurements were made at higher concentrations.

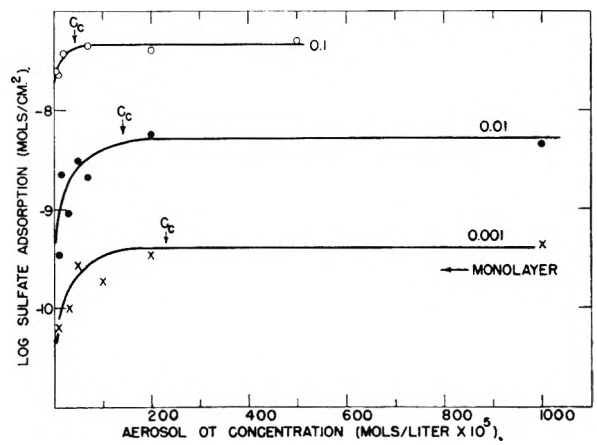

Fig. 9.—Adsorption of sulfate from solutions of A-OT containing sodium sulfate; measured at constant sodium sulfate concentration: ○, 0.1 M; ●, 0.01 M; ×, 0.001 M. Critical concentration varies from 47×10^{-5} to 230×10^{-5} M as shown. Adsorption in monolayer, 2.4×10^{-10} mole/cm.².

From measurements of surface tension with and without added sodium sulfate, it appears that in solutions of these agents at concentrations below the critical concentration the adsorption of the agent is approximately a monolayer. (It may be 2 monolayers as indicated from the surface adsorption measurements with A-OTN[2] but it cannot be much more than this.) The fact that addition of sodium sulfate does not appreciably affect the amount of agent adsorbed has been verified by measurements of the amount of tagged sulfosuccinate adsorbed in 2×10^{-5} M A-OTN with 0.1 M sodium sulfate added. The amount of sulfosuccinate adsorbed was essentially the same (within 15%) as in the absence of sodium sulfate.

In spite of the fact that the amount of long chain ion adsorbed from solutions below the critical concentration is only of the order of one monolayer, the amount of sulfate adsorbed when large amounts of sulfate are added may be very much greater. For example, with A-OT at 0.1 M Na_2SO_4 at the critical concentration the amount of sulfate ad-

sorbed is about 500×10^{-10} mole/cm.^{2}. This represents about 200 monolayers assuming that the adsorption in a monolayer of A-OT is about equal to the value 2.4×10^{-10} mole/cm.^{2} measured for the straight chain analog A-OTN.

These data indicate that in the region adjacent to a charged monolayer there is adsorption, not only of the gegenions of the surface active agent, but of ions of both charges. That is, any electrolyte present in the solution is apparently adsorbed in proportion to the concentration of the electrolyte. The mechanism of this adsorption is not at this time evident. However, from the fact that the amount of adsorption increases with concentration of agent up to the critical concentration and then becomes constant, it appears that the adsorption of electrolyte from solutions of anionic agents is due to the formation of a surface of single long chain ions and is not significantly affected by the accumulation of micelles at the surface which has been postulated to occur at higher concentrations.

Similar data for the adsorption of sulfate have been obtained in solutions of the non-ionic agent A-NL-10 as shown in Fig. 10. The same linear relationship in the log-log plot against sulfate concentration is shown. The critical concentration of this agent is about 10^{-4} M and is, in contrast with the situation for charged agents, independent of the salt concentration. The line for 10^{-5} M A-NL-10 in Fig. 10 represents adsorption due to a monolayer of non-ionic agent. The explanation of this adsorption of electrolyte due to a non-ionic monolayer probably depends on the possibility of forming a charged surface layer due to attachment of charged ions to the surface layer as a result of hydrogen bonding or dipole interaction. The surface thereby becomes charged and then acts in the same manner as a surface layer of cationic or anionic agent, attracting ions of both signs to the region adjacent to the surface layer.

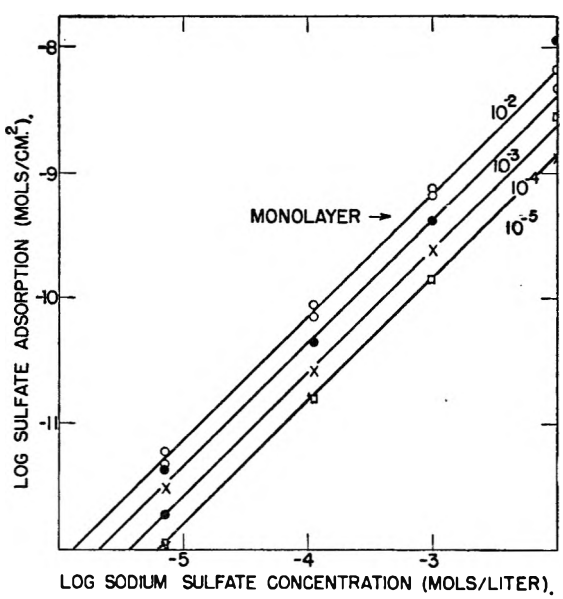

Fig. 10.—Adsorption of sulfate from solutions of A-NL-10 containing sodium sulfate: measured at constant A-NL-10 concentration: ○, 10^{-2} M; ●, 10^{-3} M; ×, 10^{-4} M; □, 10^{-5} M. Critical concentration, 1.5×10^{-4} M, independent of salt concentration. Adsorption in monolayer, 4.4×10^{-10} mole/cm.^{2}.

It should be noted that the adsorption of sulfate in solutions of the non-ionic agent A-NL-10 does not become constant at the critical concentration as it did with the anionic agents, but continues to increase with concentration of agent as far as the measurements were carried. This suggests that this non-ionic agent differs from the anionic agents studied in that the adsorption of micelles in the region of the surface contributes to the adsorption of electrolyte in the same region. Further investigation to establish whether this is a general difference between ionic and non-ionic agents would be of interest.

It is also worthy of note that the amount of sulfate adsorbed under comparable conditions is roughly the same for cationic, anionic and non-ionic agents. For example the adsorption of four different agents with equimolar amounts of sulfate is shown in Table I at 0.01 and 0.001 M concentration. Although it is not clear why the non-ionic agent A-NL-10 gives the highest sulfate adsorption in the 0.01 M solution, the qualitative agreement between the four different agents seems more significant than the differences between them. This qualitative agreement in the small ion adsorption by agents of different charge types suggests that small ions are adsorbed in the presence of a surface layer of long chain ions in a way which depends more on the concentrations than on the exact nature of the surface layer. Since there must be adsorbed sodium ions or adsorbed long chain cations equivalent to the amount of adsorbed sulfate ions in these solutions, it appears that the amount of cation adsorbed in the multilayer must also be approximately the same for the different agents, and does not depend very much on whether the cations are small ions such as sodium ions or long chain ions which are adsorbed (in the form of micelles) in A-SE sulfate solutions.

TABLE I

SULFATE ADSORPTION FROM SOLUTIONS CONTAINING EQUIMOLAR AMOUNTS OF SULFATE AND SURFACE-ACTIVE AGENT

Solution containing	Sulfate adsorbed (moles/cm.^{2} × 10^{10}) At 0.01 M	At 0.001 M
A-OT + Na_2SO_4	35	3.5
A-OTN + Na_2SO_4	45	2.8
A-NL-10 + Na_2SO_4	70	4.0
A-SE sulfate	40	5.0

The possibility should be considered that the sulfate adsorption observed with anionic and non-ionic agents was due to impurities of cationic agents. It does not appear that this is the case. The A-OT and A-NL-10 used may have contained traces of cationic impurities. However, the A-OTN used was a very pure sample as indicated by surface tension and other physical measurements and it seems unlikely that significant amounts of cationic impurity were present in this agent. At any rate the amount of cationic impurity which might have been present in any of these agents, while it might account for some sulfate adsorption, would hardly account for adsorption of sulfate of the same order

of magnitude as the sulfate adsorption with a pure sample of cationic sulfate. Therefore, it must be concluded that the sulfate adsorption is not due to cationic impurities but is due to inherent adsorption of electrolyte in the presence of a polar surface layer.

Acknowledgment.—Acknowledgment is made to Mr. R. B. Leavy, Dr. J. J. Carnes, Dr. W. T. Booth, Dr. A. J. Weith, Jr., and Miss R. Warner for assistance in the preparation and purification of the compounds used.

SURFACE CHEMISTRY OF FLUOROCARBONS AND THEIR DERIVATIVES[1]

BY H. M. SCHOLBERG, R. A. GUENTHNER AND R. I. COON

Contribution No. 63, Central Research Department, Minnesota Mining & Manufacturing Company, St. Paul, Minnesota

Received April 9, 1953

Data are given for the free surface energy of a number of fluorocarbons. These data show that fluorocarbons as a class have lower surface energies than all other compounds. Curves for the lowering of surface tension as a function of concentration are given for a series of completely fluorinated acids. These surface active compounds cause a greater lowering of the surface tension of water than has ever been found before. Fluorocarbon surface active compounds are shown to lower the surface tension of organic substances very materially. Some measurements of interfacial tensions between fluorocarbons and water and between fluorocarbons and organic solvents are presented. An attempt is made to show some correlation between the above effects in the formation of emulsions and in the wetting of fluorocarbon surfaces.

The fluorocarbons have unique surface properties. As a class they have the lowest free surface energy of any known compounds. This is illustrated by the data in Table I.

TABLE I

	γ, 20°	Ref.	K, 20°		γ, 20°	Ref.	K, 20°
n-C_6F_{12}	9.87	4	2.0	C_8F_{18}	13.6	5	2.0
iso-C_6F_{12}	10.48	4	2.1	$(C_2F_5)_3N$	13.6	5	2.3
cyclo-C_6F_{12}	11.09	4	2.2	$C_2F_5(C_3F_7)_2N$	14.0	5	2.1
n-C_7F_{16}	12.06	4	1.9	$(C_3F_7)_3N$	15.0	5	2.1
$(C_4F_9)_2O$	12.2	5	2.4	$(C_4F_9)_3N$	16.8	5	2.2

The values measured in our laboratory are not precision measurements and it is believed that they are a little too high. Simons and Pearlson,[2] Fowler[3a] and Haszeldine and Smith[3b] have measured the free surface energies of a number of fluorocarbons. Their values tend to be somewhat higher than the more precise measurements of Rohrback and Cady.[4]

Although the free surface energies of these compounds are generally the lowest known, they are not unique from the standpoint of the Eötvös equation

$$\gamma(M/\rho)^{2/3} = K(T_c - T - 6)$$

which predicts their surface tension fairly well from molecular weight, density and critical temperature. The values for K are given in Table I and it will be observed that they do not vary greatly from the accepted value for K, 2.2.

The low values observed for these fluorocarbons make it very interesting to examine the effect of surface active fluorocarbon derivatives. One would expect that these derivatives would show pronounced surface active properties. This was found to be true for aqueous and non-aqueous solutions. Curves for the surface tension of solutions of various derivatives are given in Figs. 1, 2 and 3 which show the surface tension as a function of concentration. For these determinations the experimental values were within ±1 dyne of the average curve values in the concentration below micelle formation.

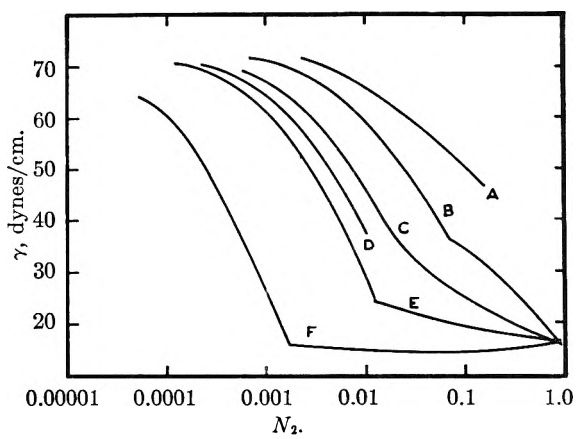

Fig. 1.—Surface tensions of aqueous solutions at 25°: A, perfluorosuccinic acid; B, perfluoroacetic acid; C, perfluoropropionic acid; D, perfluoroadipic acid; E, perfluorobutyric acid; F, perfluorocaproic acid.

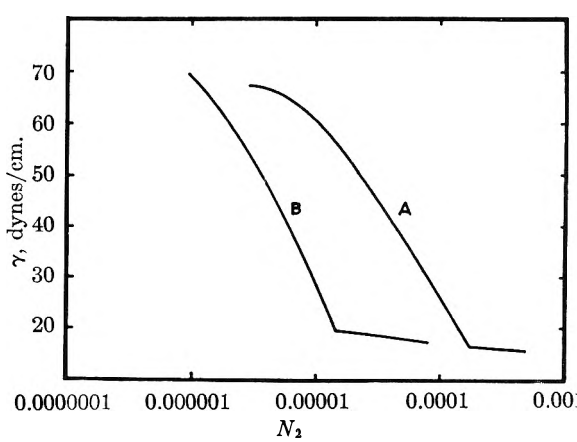

Fig. 2.—Surface tensions of aqueous solutions at 25°: A, perfluorocaprylic acid; B, perfluorocaproic acid.

(1) Presented at the 116th Meeting of the American Chemical Society, Atlantic City, September, 1949.

(2) J. H. Simons and W. H. Pearlson, presented before the Division of Industrial and Engineering Chemistry of the American Chemical Society, 112th Meeting, New York, September, 1947.

(3) (a) R. D. Fowler, *Ind. Eng. Chem.*, **39**, 375 (1947); (b) R. N. Haszeldine and F. Smith, *J. Chem. Soc.*, 603 (1951).

(4) G. H. Rohrback and G. H. Cady, *J. Am. Chem. Soc.*, **71**, 1938 (1949).

(5) Values measured in our laboratory.

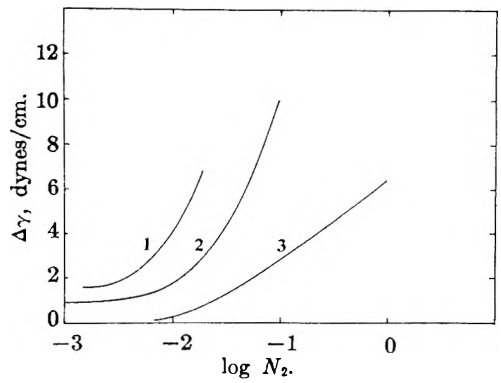

Fig. 3.—Surface pressure–log mole fraction curves: 1, $C_5F_{11}COOH$ in benzene; 2, C_3F_7COOH in benzene; 3, $C_3F_7CH_2OH$ in butanol.

In the dilute region Gibbs' law may be applied and FA/kT may be calculated by the method of Schofield and Rideal[6] where F is the surface pressure of the adsorbed film, A the area per molecule, k the gas constant per molecule, and T the absolute temperature. This has been done for trifluoroacetic acid, and the result plotted against F. Since trifluoroacetic acid is one of the strongest acids known and since no activity data are available, concentrations instead of activities were used in the calculation. The results are shown in Fig. 4. Since the surface tension curves of all of the normal acids are substantially parallel, the curve calculated for trifluoroacetic acid fits all the others. This may be interpreted as meaning that the fluorocarbon radicals have very little attraction for each other. That is, the surface films, despite the slight lowering of surface tensions, are gaseous. This means that completely fluorinated surface active compounds will not be so suitable for those purposes where a rigid solid type film is required such as in an emulsion. Fluorocarbon wetting agents give low interfacial surface energies between fluorocarbons and water. Emulsions of these materials break very quickly, presumably because the film will not resume deformation. Table II shows the results of the measurements made on the interfacial tensions of various systems of fluorocarbons and other materials. It should be noticed that the interfacial tensions of a fluorocarbon with benzene and with heptane are in the same order as their solubilities. From this, one would expect that ordinary emulsifying resins would not be effective for dispersing fluorocarbons in water. This is found to be so and, therefore, it is not surprising to see the results shown for "Octab" and "Aresklene 400."

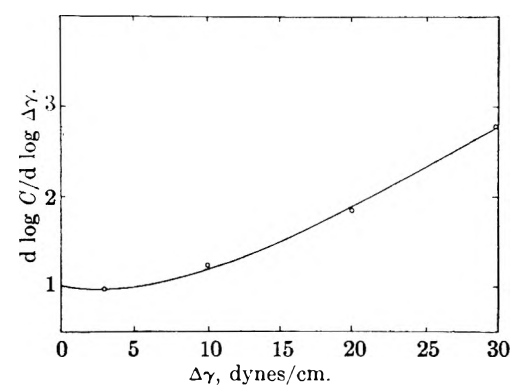

Fig. 4.—Curve of $\Delta\gamma A/kT$ *vs.* $\Delta\gamma$ for CF_3COOH.

(6) R. K. Schofield and E. K. Rideal, *Proc. Roy. Soc.* (*London*), **A109**, 58 (1925).

TABLE II

INTERFACIAL TENSION OF FLUOROCARBONS

Interface	γ dynes/cm.	Temp., °C.
$(C_4F_9)_2O$–Water	51.9	22
$(C_4F_9)_2O$–Benzene	5.7	22
$(C_4F_9)_2O$–*n*-Heptane	3.6	22
$(C_4F_9)_3N$–Water	25.6	23
$(C_4F_9)_3N$–Benzene	6.4	25
$(C_4F_9)_3N$–*n*-Heptane	1.6	25
$(C_4F_9)_3N$–Satd. water soln. of $C_9F_{19}COOH$	23.4	28
$(C_4F_9)_3N$–Satd. benzene soln. of $C_9F_{19}COOH$	5.2	28
$(C_4F_9)_3N$–0.5% water soln. of "Octab"[a]	5.3	28
$(C_4F_9)_3N$–0.5% water soln. of "Aresklene 400"[b]	5.2	28

[a] Octadecyldimethylammonium chloride. [b] Dibutylphenol sodium disulfonate.

Very dilute solutions of the fluorocarbon acids in toluene, about 0.1%, cause the angle of contact with glass to be finite. This is not a new phenomenon since long chain amines will do the same thing. This observation has been made on all the acids with the exception of CF_3COOH. Evidently a very small adsorption is enough to lower the air and toluene interfaces of the glass to nearly the identical low value. This could mean that when a well oriented, close-packed fluorocarbon interface can be made, it will be found to be repellent to almost all substances. Although angles of contact to Teflon are not reliable because of the roughness of the Teflon surface and the presence of impurities, qualitatively the evidence seems to support these ideas. Aromatic compounds show a rather large angle of contact, as do water and carbon tetrachloride, while aliphatic compounds, such as heptane, show almost zero angles.

Experimental

All of the surface tension and interfacial tension data reported here were measured by means of the maximum bubble pressure method. Interfacial tensions can be measured by a slight modification of the usual apparatus. In making a measurement the cell containing the liquid to be measured is raised slowly until the end of the capillary just contacts the liquid surface. Pressure is applied to the capillary tube and attached manometer by means of slowly displacing air in a flask by dropping water in from a buret. A surface active solution is useful in the buret, since it allows the formation of smaller droplets. By carefully adjusting the rate of air displacement, an equilibrium will be reached, at which a bubble is formed every few seconds. At the moment the bubble forms a marked drop in pressure will be noted. The maximum pressure is attained just prior to bubble formation, and this value is recorded.

This method can be used to measure absolute values of surface tension or the apparatus can be calibrated against a number of standard liquids. Water is the calibration liquid used for aqueous solutions. The relationship is

$$k = \frac{\gamma_t^{H_2O}}{h_{cm}}$$

and for aqueous solutions at the same temperature

$$\gamma_t = h_{cm} \times k_t$$

For other systems, the solvent may be used for calibration. A new k value must be determined periodically, since it is affected by the room temperature and atmospheric pres-

sure. This method provides quick and reasonably precise surface tension values. It was used in these investigations because the method is independent of the angle of contact and density of the liquid being measured. This is particularly important when measuring interfacial tensions between two liquids.

Because spreading is a function not only of the air–liquid interfacial energy but also of the solid–air and solid–liquid interfaces, it is too early to generalize as to the wetting and penetrating effects of fluorochemicals. However, it is safe to say that fluorochemicals will contribute to the pure and applied science of surface chemistry.

KINETICS OF THE REACTIONS BETWEEN IRON(II) AND SOME HYDROPEROXIDES BASED UPON CUMENE AND CYCLOHEXANE

By R. J. Orr and H. Leverne Williams

Research and Development Divison, Polymer Corporation Limited, Sarnia, Ontario, Canada

Received April 9, 1953

An investigation of the rates of reduction of phenylcyclohexane, *p*-menthane and *p*-nitrocumene hydroperoxides by iron(II) has been made. The Arrhenius equation was: $k = 8 \times 10^{10} e^{-13,100/RT}$ l. mole^{-1} sec.$^{-1}$ for *p*-nitrocumene hydroperoxide; $k = 6.3 \times 10^{9} e^{-11,100/RT}$ l. mole^{-1} sec.$^{-1}$ for *p*-menthane hydroperoxide; and $k = 2.4 \times 10^{9} e^{-10,600/RT}$ l. mole^{-1} sec.$^{-1}$ for phenylcyclohexane hydroperoxide. From the change of frequency factor and activation energy with structure of the hydroperoxide for these and other reactions investigated earlier, it was concluded that complex formation must take place between the iron(II) and hydroperoxide, with subsequent decomposition to the final products. There is a relationship between the frequency factor and energy of activation. The mechanism of the electron transfer is explained in terms of Rollefson's concept of frequency factors. The behavior of the different hydroperoxides in emulsion polymerization is described and an attempt is made to correlate this behavior with the characteristics of the reactions studied.

Introduction

General purpose chemical rubbers are made in an aqueous emulsion of butadiene and styrene or acrylonitrile. For many years these copolymers have been prepared at 30 to 50°. It was found that better copolymers could be prepared at lower polymerization temperatures. A large number of publications have described methods of preparing polymers at low temperatures, particularly 5°, and the properties of the copolymers so prepared.

Of great importance in the development of processes for use at such temperatures was the discovery of cumene hydroperoxide[1] as catalyst. This hydroperoxide has been used with various reducing substances, in particular iron(II),[1] ethylene dinitrilotetraacetic acid salts[2] and polyethylene polyamines.[3–5] Lists[6–8] of alternative hydroperoxides have now been described, some of which are considered superior to cumene hydroperoxide. It is of importance to show in what ways they are superior and to understand the reason for the improved performance.

Davidson in this Laboratory compared hydroperoxides as catalysts in a low temperature recipe similar to that described earlier.[2] The order of decreasing effectiveness, measured by yield of polymer and rate of polymer formation, was found to be *t*-butylcumene hydroperoxide, isopropylcumene hydroperoxide, *p*-menthane hydroperoxide, *p*-cymene hydroperoxide and cumene hydroperoxide. The data showed that less reducer was required and the reaction mixture could tolerate inhibitors introduced with the monomers, the emulsifier, or other recipe ingredients. Smaller amounts of catalyst with other recipe ingredients constant, resulted in little change in the initial rate of polymerization but subsequent cessation of the polymerization reaction at lower conversion of monomers to polymer. This fault could be overcome by bringing the amount of reducer more nearly into molar balance with the catalyst.

Embree in this Laboratory has studied peroxides as catalysts in the butadiene–acrylonitrile recipe.[3] Similar results were obtained except that an optimal concentration of hydroperoxide for maximal yield of polymer was observed which varied with the amount of other recipe ingredients present. From the conversion of monomers to polymer achieved in three hours, the relative effectiveness of the hydroperoxides in promoting polymerization was, in decreasing order of effectiveness, *t*-butylcumene hydroperoxide, oxidized dipentene hydroperoxide, nitrocumene hydroperoxide, *p*-cymene hydroperoxide, cumene hydroperoxide and *s*-butylbenzene hydroperoxide. Ineffective were *t*-butyl hydroperoxide, benzoyl peroxide, dicumyl peroxide and tetralin hydroperoxide. The rate of conversion was found to be more dependent upon the concentration of hydroperoxide than for the butadiene–styrene system.

The relative effectiveness of peroxides as initiators of polymerization has been studied by others. The most recent and comprehensive works are those of Cooper[9,10] and Swain, *et al.*,[11] who studied substituted benzoyl peroxides and concluded that the substituent groups affected the rate of polymer-

(1) E. J. Vandenberg and G. E. Hulse, *Ind. Eng. Chem.*, **40**, 932 (1948).

(2) J. M. Mitchell, R. Spolsky and H. L. Williams, *ibid.*, **41**, 1592 (1949).

(3) W. H. Embree, R. Spolsky and H. L. Williams, *ibid.*, **43**, 2553 (1951).

(4) R. Spolsky and H. L. Williams, *ibid.*, **42**, 1847 (1950).

(5) G. S. Whitby, N. Wellman, V. W. Floutz and H. L. Stephens, *ibid.*, **42**, 445 (1950).

(6) G. S. Fisher, L. A. Goldblatt, I. Kniel and A. D. Snyder, *ibid.*, **43**, 671 (1951).

(7) C. F. Fryling and A. E. Follet, *J. Polymer Sci.*, **6**, 59 (1951).

(8) J. E. Wicklatz, T. J. Kennedy and W. B. Reynolds, *ibid.*, **6**, 45 (1951).

(9) W. Cooper, *Nature*, **162**, 897, 927 (1948).

(10) W. Cooper, *J. Chem. Soc.*, 3106 (1951).

(11) C. G. Swain, W. H. Stockmayer and J. J. Clarke, *J. Am. Chem. Soc.*, **72**, 5426 (1950).

ization through steric and resonance factors associated with the individual structures. It was suspected that resonance and conjugation would also be factors in the effectiveness of hydroperoxides as initiators of cold rubber polymerization through affecting the rate of decomposition of the hydroperoxide. In addition, the rate of initiation of polymerization might be affected by the reactivity of the free radical formed, a property which might be expressed in a manner described by Herbst.[12] It was also suggested[7] that there was an optimal water solubility of the hydroperoxide but this did not hold rigidly for all hydroperoxides.[13] Earlier papers[14–18] and the following results are part of a series intended to elucidate the various factors. The work of Kolthoff is also relevant.[19]

A study of the kinetics of reduction of these hydroperoxides by iron(II) must be made before it is possible to find the reason for the varying effectiveness of these hydroperoxides in emulsion polymerization recipes. Such a study should also indicate the mechanism of electron transfer taking place in reactions of this nature.

Results

The reaction of a hydroperoxide with iron(II) consists of several steps. The primary radical-producing step is followed by several radical-induced reactions. Some of these cause oxidation of iron(II) so that in the study of this reaction by measuring the rate of iron(II) disappearance, it is necessary to eliminate the side reactions. This is done by conducting the reaction in a solution of some water-soluble monomer such as acrylonitrile. When this is done, iron(II) disappears according to a second order reaction for which the integrated equation can be shown to be

$$-\ln (1 - [\mathrm{Fe(II)}]_\infty/[\mathrm{Fe(II)}]) = [\mathrm{Fe(II)}]_\infty kt + C$$

where $[\mathrm{Fe(II)}]_\infty$ is the residual iron(II) concentration, and [Fe(II)] is the iron(II) concentration at time t. This equation is such as to eliminate any effect from residual traces of oxygen which reacts rapidly during the initial part of the experiment.

p-Menthane Hydroperoxide–Iron(II) Reaction.—Preliminary experiments were done using samples of hydroperoxide which had been concentrated and purified in the form of the sodium salt. The results were quite irreproducible and differed when various samples of hydroperoxide were used. This was ascribed to the sodium salt being unstable and decomposing into less active peroxides or hydroperoxides. Since some of these impurities were believed to be isomers, physical and chemical methods of separation did not show promise. Attention was directed to methods of studying the kinetics of the oxidation–reduction reaction in the presence of impurities which also reacted with iron(II). The over-all reactions would correspond to two simultaneous primary reactions

$$\mathrm{Fe(II)} + \mathrm{PMHP} \longrightarrow \mathrm{Products} \quad (1)$$

$$\mathrm{Fe(II)} + \mathrm{Impurities} \longrightarrow \mathrm{Products} \quad (2)$$

The initial assumption that $-|\mathrm{d}[\mathrm{Fe(II)}]/\mathrm{d}t|_1 >> -|\mathrm{d}[\mathrm{Fe(II)}]/\mathrm{d}t|_2$ was made. The errors introduced into a measurement of k_1 by assuming $-|\mathrm{d}[\mathrm{Fe(II)}]/\mathrm{d}t|_2 = 0$, are due to the erroneous $[\mathrm{Fe(II)}]_\infty$ value. It is necessary to have a measure of the Fe(II) consumed by reaction 1 going to completion from which could be obtained an $[\mathrm{Fe(II)}]_\infty$ value valid for reaction 1.

After the elapse of a certain time interval, the [Fe(II)] time plot became nearly linear, as would be expected if the previous assumption as to the rate of $-|\mathrm{d}[\mathrm{Fe(II)}]/\mathrm{d}t|_2$ were true. Thus extrapolation of this linear portion of the [Fe(II)]–time curve to zero time at least partially compensates for the Fe(II) consumed in reaction 2 and yields a true value of the $[\mathrm{Fe(II)}]_\infty$ for reaction 1. This method would then be applicable to partially decomposed samples from the sodium salt as well as to unpurified hydroperoxides. For each experiment a value of $[\mathrm{Fe(II)}]_\infty$ for reaction 1 was calculated. This was the value substituted in the rate equation for the calculation of the rate constant. Hydroperoxide samples for which purification had been attempted but which gave different results from sample to sample, as well as hydroperoxide samples for which no purification had been attempted, were studied. Some typical plots are in Fig. 1 and the rate constants determined for this hydroperoxide are in Table I.

TABLE I

CORRECTED RATE CONSTANTS FOR p-MENTHANE HYDROPEROXIDE–FE(II) REACTION

T, °C.	$[\mathrm{Fe(II)}]_\infty \times 10^5$	k, l. mole^{-1} sec.$^{-1}$	$k_{av.}$, l. mole^{-1} sec.$^{-1}$
0	3.45	12.0	11.3 ± 0.2
	3.50[a]	11.8	
	3.50[a]	10.5	
	4.76	10.5	
	5.05[a]	10.0	
	6.10[a]	11.1	
	6.24	12.4	
9	2.36	23.1	24.1 ± 1.9
	4.74	22.1	
	4.90	26.9	
	5.85	22.6	
	6.00	25.5	
16	1.34	38.3	33.5 ± 3.8
	3.15	34.3	
	3.50	40.0	
	4.30	27.5	
	5.02	32.0	
	6.10	30.1	
	7.10	32.6	

[a] Determined on unpurified p-menthane hydroperoxide samples.

The changes in the observed rate constants brought about by substitution of an $[\mathrm{Fe(II)}]_\infty$ value determined by extrapolation for a value which was observed directly differed from sample to sample according to the purity of the sample.

(12) R. L. Herbst, Jr., *J. Polymer Sci.*, **7**, 587 (1951).

(13) Hercules Powder Company, private communication.

(14) J. W. L. Fordham and H. L. Williams, *J. Am. Chem. Soc.*, **72**, 4465 (1950).

(15) J. W. L. Fordham and H. L. Williams, *ibid.*, **73**, 1634 (1951).

(16) J. W. L. Fordham and H. L. Williams, *Can. J. Research*, **27B**, 943 (1949).

(17) J. W. L. Fordham and H. L. Williams, *ibid.*, **28B**, 551 (1950).

(18) R. J. Orr and H. L. Williams, *Can. J. Chem.*, **30**, 985 (1952).

(19) I. M. Kolthoff and A. I. Medalia, *J. Am. Chem. Soc.*, **71**, 3789 (1949).

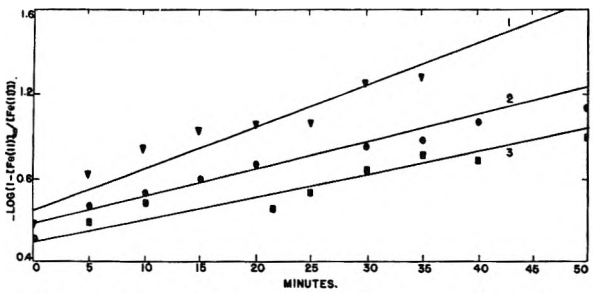

Fig. 1.—Disappearance of iron(II) by reaction with *p*-menthane hydroperoxide at 0°. Final $[Fe(II)]_\infty$: curve 1, 6.24×10^{-5} *M*; curve 2, 4.76×10^{-5} *M*; curve 3, 3.45×10^{-5} *M*.

The above data are only as reliable as the initial assumption that $-|d(Fe(II))/dt|_2 << -|d(Fe(II)/dt|_1$. There are four reasons why this assumption may be valid.

(1) Variations in the rate constant were random, showing no trend with $[Fe(II)]_\infty$ values. If the revised value of $[Fe(II)]_\infty$ for reaction 1 were consistently either too low or too high, then the rate constants would either increase or decrease with an increasing $[Fe(II)]_\infty$ value.

(2) The values obtained on peroxide samples possessing different purification histories agree (such as at 0°). If the values of $[Fe(II)]_\infty$ for reaction 1 were erroneous, then they should depend on the amount of impurity in the system, which would necessarily vary with varying purification history.

(3) The plot of rate equation *versus* time is linear over the initial stages of the reaction when the revised value of $[Fe(II)]_\infty$ is used for reaction 1, as long as the impurities are less reactive than the compound under study, as there is reason to believe they are. If, for instance $[Fe(II)]_\infty$ were too low, then, as time progressed, the curve would become progressively further below linearity.

(4) The plot of log *k vs.* $1/T$ was linear. The Arrhenius plots fit these data quite well. If the method used in the calculation of *k* were invalid, this good fit would only be the case if the activation energies of the different reactions proceeding simultaneously were equal. It should be stressed that not as much weight may be assigned to this reason as the others, since the temperature range over which studies may be made is relatively narrow.

The Arrhenius equation was calculated and it was found that $k = 6.3 \times 10^9\ e^{-11,000/RT}$, with a standard deviation of 0.557 for $\log_{10} A$ and 458 cal./mole for *E*.

Phenylcyclohexane Hydroperoxide–Iron(II) Reaction.—Since this was used without further purification, the first requisite of the investigation was to ascertain if any other compound capable of reacting with the ferrous iron was present in sufficient quantity to necessitate consideration when calculating rate constants. If such be the case, it would be indicated by the presence of the four conditions: (1) non-linearity of rate equation plots; (2) trends of the apparent rate constant with $[Fe(II)]_\infty$; (3) [Fe(II)]-time curves showing a slow linear decrease of [Fe(II)] with time after prolonged periods of time had elapsed; and (4) non-linearity of the Arrhenius plot of the rate constants. Rate constants were determined at three temperatures. Typical plots of data are in Fig. 2 and the rate

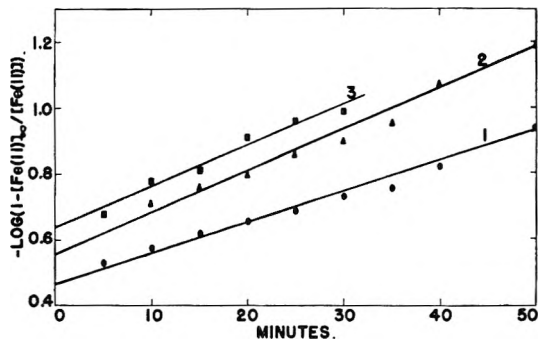

Fig. 2.—Disappearance of iron(II) by reaction with phenylcyclohexane hydroperoxide at 0°. Final $[Fe(II)]_\infty$: curve 1, 4.84×10^{-5} *M*; curve 2, 5.87×10^{-5} *M*; curve 3, 6.75×10^{-5} *M*.

constants are listed in Table II. Conditions (1) and (2) for the absence of impurity have been satisfied. Rate equation plots were linear in that distribution of points about the best straight line was random and there was no trend in the value of

TABLE II

RATE CONSTANTS FOR PHENYLCYCLOHEXANE HYDROPEROXIDE–FE(II) REACTION

T, °C.	$[Fe(II)] \times 10^5$	*k*, l. mole^{-1} sec.$^{-1}$	$k_{av.}$, l. mole^{-1} sec.$^{-1}$
0	4.84	7.95	7.66 ± 0.39
	5.87	8.00	
	6.75	7.15	
18.0	4.56	21.0	22.7 ± 1.2
	4.64	22.2	
	5.05	24.2	
	7.00	23.5	
25.5	2.95	40.2	41.3 ± 1.7
	4.05	39.0	
	4.28	42.8	
	5.44	40.4	
	5.45	43.9	

rate constant with $[Fe(II)]_\infty$ (see Fig. 2). The Fe(II) *versus* time curves indicated that no appreciable amount of impurity was present in the sample thus satisfying the third condition. The fourth condition was also fulfilled; the Arrhenius plot was linear. From this the Arrhenius equation for the phenylcyclohexane hydroperoxide reaction was calculated to be

$$k = 2.4 \times 10^9 e^{-10,600/RT}\ \text{l. mole}^{-1}\ \text{sec.}^{-1}$$

with a standard deviation of 0.307 for $\log_{10} A$ and 403 cal./mole for *E*.

***p*-Nitrocumene Hydroperoxide–Iron(II) Reaction.**—The disappearance of the iron(II) is accelerated by radical-induced oxidation. To suppress this and render the iron(II) disappearance bimolecular, excess acrylonitrile is added to the reaction mixture. In all previous investigations[18] a standard concentration of 3.0×10^{-1} *M* had been adopted as satisfactory in all cases but one, since at this monomer concentration, rate constants were reproducible and showed no dependence on [Fe-

$(II)]_\infty$ as they would have had not the steady state free radical concentration been zero. The one exception, isopropylcumene hydroperoxide reduction at 0°, was found to show considerable resistance to the suppression of these secondary processes. With the nitro analog, the difficulty was evident at all temperatures under investigation. It was finally traced to the age of the acrylonitrile solution. At lower temperatures it was necessary to use freshly prepared acrylonitrile solution, although as the temperature at which the reaction occurred was raised, the age of the monomer solution became less critical. The reason for the loss in activity of the monomer solution with age was not elucidated but may be connected with oxygen sensitized polymerization of the acrylonitrile to a low molecular weight product. That age rather than the monomer concentration was the agent responsible for the inability to suppress radical-induced oxidation was shown when rate constants at 0° were determined with fresh acrylonitrile solution of varying concentration (see Table III). These proved to be independent of monomer concentration.

In previous studies[18] it was not found possible to store stock solutions of hydroperoxides for extended periods of time, since they decomposed giving erroneous rate constants. This decomposition may be thermal but is probably catalyzed by the acetic acid present in the stock solution. This acetic acid had been added to regenerate the hydroperoxide from its sodium salt. This procedure was not necessary in this case since the sodium salt was quite soluble in water. It was felt advisable to check the stability of the compound. In Table III the results were obtained with hydroperoxide solutions of various ages. The replacement of an aged solution by a fresh solution caused no significant difference in the observed rate constants, nor did the constants show any irreproducibility due to the age of the monomer stock solution. It was therefore concluded that no thermal decomposition had occurred in the hydroperoxide solution on storage. Standard deviations shown by the results in Table III are not considered unreasonable for this type of measurement. Some typical plots of data are in Fig. 3. The Arrhenius plot was made and the Arrhenius equation was found to be

$$k = 8 \times 10^{10} e^{-13,000/RT} \text{ l. mole}^{-1} \text{ sec.}^{-1}$$

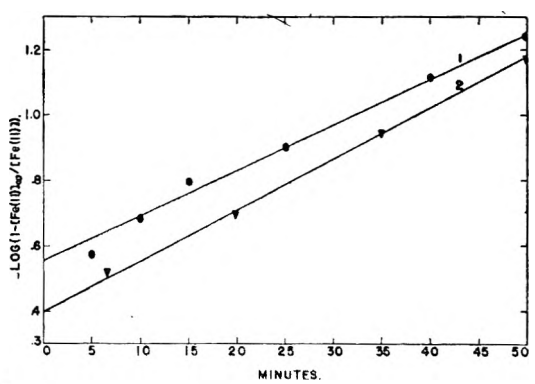

Fig. 3.—Disappearance of iron(II) by reaction with nitrocumene hydroperoxide. Final $[Fe(II)]_\infty$: curve 1, 4.29×10^{-5} M at 16°; curve 2, 1.87×10^{-5} M at 25.5°.

with a standard deviation of 0.280 for $\log_{10} A$ and 365 cal./mole for E.

Table III

Rate Constants for *p*-Nitrocumene Hydroperoxide–Iron(II) Reaction

T, °C.	$[Fe(II)]_\infty \times 10^5$	$[AcN]_0$	k, l. mole^{-1} sec.$^{-1}$	$k_{av.}$, l. mole^{-1} sec.$^{-1}$
0	4.60	1.2	3.7	3.8 ± 0.2
	2.50	1.2	3.9	
	4.96	1.2	3.6	
	5.70	1.2	3.4	
	7.55	1.2	3.8	
	4.10	0.3	4.1	
16	7.90	.3	12.9	12.9 ± 0.9
	2.14	.3	12.2	
	4.85	.3	12.6	
	4.79	.3	12.2	
	7.90	.3	14.6	
25.5	1.87	.3	31.5	32.9 ± 1.3
	2.95	.3	31.7	
	3.20	.3	35.3	
	5.20	.3	32.2	
	3.75	.3	32.0	
	2.36	.3	33.7	

Discussion

There is a correlation between the ease of reduction of the hydroperoxide and its effectiveness in emulsion polymerization. It seems doubtful if the increased rate of decomposition of the hydroperoxide is totally responsible for the improved performance in initiation of polymerization, since it should be possible to bring about identical rates of conversion of monomer by adjusting the concentration of hydroperoxide and hence of free radicals formed. This is not the case, especially at low temperatures. The rate of attack of the free radical on the monomer must be considered. The water solubility or solubilization of these compounds cannot be neglected since this may determine the availability of initiating free radical to the monomer molecule. The behavior of peroxides in initiating emulsion polymerization is governed by the factors outlined with a probability that a structural change in the peroxide to change one of the factors brings about changes in the others which mutually enhance the result.

Mechanism of Electron Transfer.—A comparison of frequency factors, activation energies and entropies of activation calculated at 300°K.[20] for the hydroperoxide–iron(II) reactions is in Table IV.

Table IV

Comparison of Hydroperoxide–Iron(II) Reaction

Hydroperoxide	A	Std. dev. $\log_{10} A$	ΔS, e.u.	E, kcal./mole	Std. dev., E
Nitrocumene	8×10^{10}	0.28	−10.77	13.1	0.365
Cumene	1×10^{10}	.27	−14.93	12.0[16]	.352
p-Menthane	6.3×10^{9}	.56	−15.91	11.0	.458
p-Isopropylcumene	4.0×10^{9}	.46	−16.49	10.8[18]	.600
Phenylcyclohexane	2.4×10^{9}	.31	−17.81	10.6	.403
p-*t*-butylcumene	1.8×10^{9}	.40	−18.31	9.9[18]	.516

In the cumene hydroperoxide series, the variation of activation energy observed between nitrocumene

(20) S. Glasstone, K. J. Laidler and H. Eyring, "Theory of Rate Processes," McGraw-Hill Book Co., Inc., 1941, p. 21.

hydroperoxide and cumene hydroperoxide is quite normal. When an electropositive group was added to the *p*-position on the benzene nucleus, the activation energy of the reaction decreased. It is not surprising that addition of an electronegative group caused it to increase. The magnitude of the changes is interesting since it may be a quantitative measure of electrostatic potential. Comparison of the activation energies with the Hammett value of σ[21] for the substituent groups proved fruitful. The greater the activation energy the more positive is the value of the corresponding σ, as may be seen in one comparison of and activation energy below.

Group on cumene hydroperoxide	σ	E, kcal./mole
p-NO_2	0.778	13.1
H	0	12.0
p-*i*-C_3H_7	− .151	10.8
p-*t*-C_4H_9	− .197	9.9

An empirical relation was found between σ and E such that log $(\sigma + k)$ is proportional to E, where k is approximately 0.22. This should prove useful for making an estimate of the reactivity of any hydroperoxide in the cumene series possessing substituents with a known σ. For example, the reaction of *p*-chlorocumene hydroperoxide with Fe(II) should have an approximate Arrhenius equation of $k = 2.6 \times 10^{10}\, e^{-12.4/RT}$ l. mole^{-1} sec.$^{-1}$ since the *p*-Cl group has a σ-value of +0.227. However, this is only an estimate and it might be dangerous to attempt to predict when groups with σ-values lying outside the range investigated, such as *p*-NH_2 with a σ-value of +0.660, are present, or when more than one group is present.

The explanation in the variation in the frequency factor is not clear. If A depended only on steric considerations, then for the nitrocumene hydroperoxide this factor should have decreased from that shown by cumene hydroperoxide in a manner similar to the *p*-alkyl cumene hydroperoxides. This it did not do. The frequency factor is dependent on the same things that cause change in the activation energy, *i.e.*, electrostatic influences.

There is some justification for this view. Moelwyn-Hughes[22] discusses behavior of this nature. Normal values of $A(2.77 \times 10^{11})$ result from a reaction between an ion and a molecule, while reaction between either two polar molecules or two ions gives rise to an abnormally high or low frequency factor. It would appear that the presence of an electrostatic field has a great effect on frequency factors. This may be due to existence of repulsive forces, deactivation by solvent molecules, or variation in orientation restrictions necessary for reaction.

In a recent paper, Rollefson[23] considers that a frequency factor of about 10^{12}–10^{13} (l./mole/sec.) corresponds to reaction every time the molecules come within a molecular diameter of each other and 10^{8}–10^{9} corresponds to the necessity of formation of an activated complex in which the molecules are bonded to each other. All of the frequency factors found in the present study are very close to this latter range. To account for the changes in activation energy with structure in a previous paper on this topic,[18] it was necessary to postulate that the iron(II) coördinated with the hydroperoxide and the resultant complex decomposed thermally. The fact that the reduction of nitrocumene hydroperoxide had a higher energy of activation than did the reduction of cumene hydroperoxide reinforced this argument considerably. This order in the reactivity of the hydroperoxides with iron(II) is dependent on the availability of a coördination space on the iron(II). If conditions were such that this coördination space were not available to one hydroperoxide, then there would be either no reaction, or the order of reactivity of the peroxides would be reversed from that recorded here.

There exists a statistically significant correlation between E and A. This is not a new observation but has been recorded by other workers. Evans and Polanyi[24] have shown that with regard to heats and entropies of solution, the relation $T\,\Delta S = \Delta H + \beta$ holds. Laidler and Eyring[25] reasoned that this should also apply to energies and entropies of activation. Fairclough and Hinshelwood[26] believe that log A is linear with the reciprocal of the square root of the energy of activation. While the spread of the Arrhenius constants for the system described here is much too small, in view of the standard deviation which these constants possessed, to differentiate between these two latter relations, the excellent fit of the data to the linear relation of Laidler and Eyring (Fig. 4) suggested (but by no means proved) that this was a satisfactory manner in which to treat the data. It is possible to describe the data shown in Fig. 4 by the equation

$$\log_{10} A = 1.1E - 3.6$$

and to describe the hydroperoxide–Fe(II) reaction in terms of a generalized Arrhenius equation

$$k = 2.5 \times 10^{-4} e^{(E(2.56RT-1)/RT)}$$

The values of A and E obtained for the hydrogen peroxide–iron(II) reaction by Barb, Baxendale,

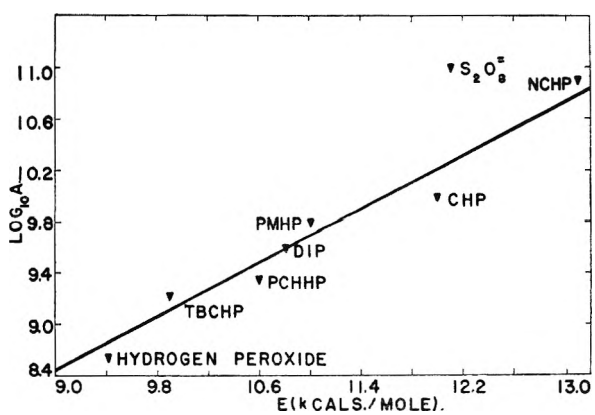

Fig. 4.—Log A *versus* E: the reactions of iron(II) with hydrogen peroxide and organic hydroperoxides.

(21) L. P. Hammett, "Physical Organic Chemistry," McGraw-Hill Book Co., Inc., New York, N. Y., 1940, p. 188.

(22) E. A. Moelwyn-Hughes, "Kinetics of Reactions in Solutions," II Edition, Oxford Press, 1947, pp. 68-81.

(23) G. K. Rollefson, THIS JOURNAL, **66**, 976 (1952).

(24) M. G. Evans and M. Polanyi, *Trans. Faraday Soc.*, **32**, 1333 (1936).

(25) K. J. Laidler and H. Eyring, *Ann. N. Y. Acad. Sci.*, **39**, 303 (1940).

(26) R. A. Fairclough and C. N. Hinshelwood, *J. Chem. Soc.*, 538 (1937).

George and Hargrave[27] ($k = 4.45 \times 10^8\ C^{-9,400/RT}$ l. mole^{-1} sec.$^{-1}$) fit this relation admirably (see Fig. 4). A slightly different method of treating the above is to consider the relation between ΔS of activation and E. This too is linear showing the relationship

$$E = 0.455\Delta S + 17.3$$

This is an arithmetical conversion of the previous relation between $\log_{10} A$ and E. For all hydroperoxide–iron(II) reactions investigated the rates may be described in terms of one adjustable parameter (the activation energy) and two constants α and β by a generalized Arrhenius equation.

Some deductions may be made from the paper by Rollefson regarding the probability of formation of the activated complex by coördination of the iron(II) and hydroperoxide. As the complex becomes more stable (*i.e.*, the hydroperoxide reduction shows a higher energy of activation), the entropy of activation increases from about -18 to about -10. Rollefson[23] considers that the entropy of activation is a measure of the entropy change on formation of the activated complex, and represents the loss in translational entropy on formation of the activated complex. If the formation of this complex is analogous to an addition reaction in which the bonds formed are of normal strength, a ΔS of -30 results, corresponding to the loss by one of the reactants of three degrees of translational freedom. If there is only a simple collision process with no bond formation, then ΔS is -10, *i.e.*, the loss of only one degree of translational freedom. There is a range between -10 and -30 corresponding to pseudo bonds of varying strength. This could be compared to the "rigidity" of the complex. A consideration of two of the peroxides which have been studied will illustrate the point.

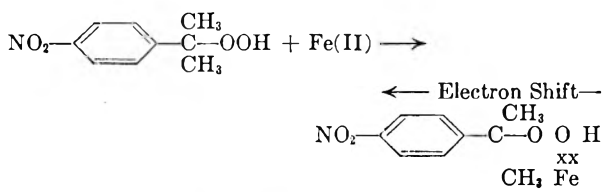

p-Nitrocumene hydroperoxide

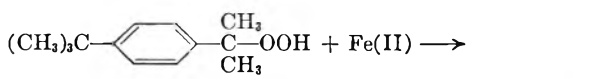

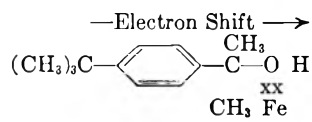

p-t-Butylcumene hydroperoxide

The factors contributing to a low activation energy, *i.e.*, the repulsion of an electron excess into the O–O bond should also increase the availability of the coördinating electrons to which the iron bonds. This in turn yields a stronger bond, a more rigid complex, and hence a lower value of ΔS.

Conversely, in the case of *p*-nitrocumene hydroperoxide, the withdrawal of electrons from the O–O bond not only increases the energy of activation of the reduction but also weakens the O–Fe(II) bond by decreasing the availability of the coördinating electrons and bringing about a higher value of $+\Delta S$. The frequency factor and activation energy should show a significant correlation. The similarity between these conclusions and those of Moelwyn-Hughes[22] is striking. Since these different effects arise from a common cause, the changes always brought about are directly proportional to each other, giving rise to a linear *E versus S* relation.

The question arises whether an oxidation–reduction reaction between two ions, conforming to the general chemical picture may also be described by the linear relationship. Such a reaction is the reducing of the persulfate ion by iron(II)

$$\text{Fe(II)} + S_2O_8 \longrightarrow \text{Fe(III)} + SO_4^- + SO_4^=$$

This has been investigated[28,29] and it has been shown that for this reaction

$$k_\theta = 1.0 \times 10^{11} e^{-12,100/RT}\ \text{l. mole}^{-1}\ \text{sec.}^{-1}$$

Plots of these data on Fig. 4 yield a point which is an abnormal distance from the best straight line for the other data. It may be assumed that this reaction is governed by factors other than those entering into reaction between an un-ionized hydroperoxide and iron(II). Possibly the added electrical attraction due to the negative charged persulfate ion increases the frequency factor with respect to the energy of activation.

An attempt was made to find reported in the literature a series of reactions which might also show a linear log *A versus E* relation. A review on the thermal decomposition of paraffins[30] was used as a source of data. $\text{Log}_{10} A$ *versus* E was plotted and a linear relationship was found which embraced all studied paraffins except the two members of the series, methane and ethane. Methane and ethane probably fall off the line due to scission at a C–H rather than a C–C bond. It might be further noted that the values for E and A of *n*-butane are taken from data of four different experimenters and differ by 25%, but all values nevertheless fit the curve. No attempt is being made to compare this series of reactions with those reported here but only that the linear relationship suggested by Laidler and Eyring between log A and E is quite probably the proper one for such reactions involving formation of free radicals. The generalized Arrhenius equation was calculated for this series as $k = 0.72\ e^{E(0.5RT-1)/RT}$ l. mole^{-1} sec.$^{-1}$ This does not mean that all reactions follow the same pattern but the similarity between two such unrelated families is interesting.

Experimental

The hydroperoxides of the following purity were supplied by Hercules Powder Company, Experiment Station, and used in the polymerization experiments cited; cumene hydroperoxide 68%, *p*-cymene hydroperoxide 29%, *p*-menthane hydroperoxide 50%, *t*-butylcumene hydroperoxide 23.6%, tetralin hydroperoxide 81.9%, oxidized dipentene 18.5%, nitrocumene hydroperoxide 29.6%, dicumene peroxide 46.5%, isopropylcumene hydroperoxide 62% and *s*-butylbenzene hydroperoxide 23.6%. *t*-Butyl hydroperoxide 62% (Shell), benzoyl peroxide 100% (B.D.H.), and

(27) W. G. Barb, J. H. Baxendale, P. George and K. R. Hargrave, *Trans. Faraday Soc.*, **47**, 462 (1951).

(28) J. W. L. Fordham and H. L. Williams, *J. Am. Chem. Soc.*, **73**, 4855 (1951).

(29) J. H. Merz and W. A. Waters, *Faraday Soc. Disc.*, **2**, 179 (1947).

(30) E. W. R. Steacie, *Chem. Revs.*, **22**, 311 (1938).

t-butylcumene hydroperoxide 54.2% (Phillips Petroleum Co.) were also used.

Those used in the present study were purified. Concentration and purification of the nitrocumene hydroperoxide was accomplished by formation of the sodium salt. The crude material was poured directly into 25% sodium hydroxide at 0°. Three layers were formed. A nearly colorless top layer which was benzene soluble separated from a middle brown layer. This middle layer appeared initially as a rather viscous layer which was water soluble and benzene insoluble. This layer overlay a bottom portion which was colored and was obviously the residual sodium hydroxide solution.

The middle layer liberated iodine from an acidic potassium iodide solution, which the top layer did not do and the bottom layer did to only a slight degree. This middle layer contained the sodium salt. Separation from the alkali and oil layers was done in a separatory funnel, and the sodium salt was then washed twice with benzene. Prolonged drying under high vacuum converted the brown viscous liquid layer to a solid, through removal of water in the initially prepared salt. This salt was soluble in water and stock solutions for experimental work were prepared by dissolving the sodium salt directly.

Phenylcyclohexane hydroperoxide was added to a saturated sodium hydroxide solution at 0° in an attempt to purify the hydroperoxide. A voluminous white precipitate was formed which did not contain the sodium salt but was sodium hydroxide.

p-Menthane hydroperoxide sodium salt was prepared but the salt proved unstable and it was impossible to get consistent results over a period of time. Difficulties with the stability of the sodium salts of hydroperoxides have not been confined to this Laboratory. Cooper[31] reports deterioration of the sodium salt of cumene hydroperoxide due to absorption of carbon dioxide.

p-Nitrocumene hydroperoxide was supplied as all para[13] with no meta present. The ortho form could not exist due to the steric hindrance exerted by the CH_3 groups. *p*-Menthane hydroperoxide was supplied as consisting almost totally of the 1-hydroperoxy isomer.[13] Small amounts of the 4 and 8 isomers may be present. Phenylcyclohexane hydroperoxide was supplied as having no measurable quantity of any isomers present.[13]

Other reagents were: acetic acid, C.P.; sodium acetate, C.P.; iron(II) sulfate, C.P.; acrylonitrile, middle fraction from distillation of technical grade; water, once distilled, redistilled from a sodium hydroxide-potassium permanganate solution; nitrogen, technical grade, scrubbed three times with alkaline pyrogallol and then passed over hot copper filings at 400°; and α,α'-bipyridyl, C.P.

Oxygen-free nitrogen was bubbled through the reaction mixture containing all reagents except the iron(II) sulfate for 45 minutes. The iron(II) sulfate was in water which had had the oxygen removed by bubbling nitrogen through for 15 minutes. The time of addition of iron(II) sulfate solution was the starting time of reaction. The solution was buffered at a *p*H of 4.2 by a sodium acetate–acetic acid buffer solution. Methanol was added to the hydroperoxide solution to solubilize the hydroperoxide so that the final solution in which reaction occurred contained 0.90% methanol. Aliquots were withdrawn from the reaction cell at specified times and analyzed for iron(II) by a colorimetric procedure with α,α'-bipyridyl.[32] The sample was centrifuged before analysis to remove polyacrylonitrile.

The analysis for Fe(II) was done with α,α'-bipyridyl complex since the reaction between Fe(II) and hydroperoxide was stopped by the addition of α,α'-bipyridyl, and the color of the Fe(III)–bipyridyl complex could be eliminated.

At low *p*H the Fe(III) might remain in solution and contribute to the reaction. Since Fe(III) would remove hydroperoxide, this would slow the removal of iron(II) and give an erronously low value for the rate constant. Since the [Fe(II)]/[hydroperoxide] ratio was always large and the initial hydroperoxide concentration was quite small, the rate of removal of hydroperoxide by Fe(III) would be very small relative to the rate of peroxide removal by Fe(II). Fe(III) in high concentration may be expected only in the later stages of the reaction and may approach the hydroperoxide concentration. As [Fe(III)] increases, the [Fe(II)]/[hydroperoxide] ratio also increased. Any contribution of the Fe(III) would show as a trend in the rate constant values so that these would appear to increase with increasing $[Fe(II)]_\infty$ values. This was not the case. This difficulty would have been avoided by carrying out the reaction at a higher *p*H (7) so that as Fe(III) was formed, it precipitated as $Fe(OH)_3$. At these *p*H values a possibility existed that there would be hydroxyl ion catalysis of the primary reaction. Since it is desirable to identify the measured rate constant with the k_0 of the reaction, regardless of what mechanism is ascribed to the *p*H catalysis, it is necessary to conduct the experiment at low *p*H values, where it was assumed that the OH ion catalysis would be negligible.

Any effect of inhomogeneity in the reaction mixture would appear only at the initial portion of the reaction. The method of calculation involved only analyses obtained after the reaction was in progress. The readings at zero time from analyses in the iron(II) stock solution had to be ignored, the [Fe(II)] value being too high. This would be explained by a local excess of iron(II) developing at the point of addition and radical induced oxidations of iron(II) taking place. Part of this discrepancy would arise from the presence of trace amounts of oxygen in the solution. Since the amount of this discrepancy was irreproducible, it was not all due to oxygen, for the removal of oxygen was carefully standardized and the initial oxygen content should have been constant. This method of oxygen removal has been shown[33] to reduce the oxygen level below 0.005%.

Acrylonitrile stock solution was made daily by saturating water with acrylonitrile at room temperatures. The concentration of acrylonitrile in the reaction cell was 3.0×10^{-1} *M* at zero time, unless otherwise specified.

In previous studies[18] the stock solution of hydroperoxide deteriorated by decomposition of the hydroperoxide. Measurement of rate constants using these solutions gave erroneous values. To anticipate this difficulty the aqueous stock solution was prepared daily from the *p*-menthane and phenylcyclohexane hydroperoxides. For nitrocumene hydroperoxide, this was not necessary since the sodium salt was used.

Acknowledgments.—The authors appreciate the permission to publish this paper extended by Polymer Corporation, Limited. Mr. S. Butler assisted with this study. A discussion of these data was presented before the International Congress of Pure and Applied Chemistry, Stockholm, 1953.

(31) W. Cooper, Dunlop Research Centre, Birmingham, England. Private communication.

(32) S. H. Jackson, *Ind. Eng. Chem., Anal. Ed.*, **10**, 302 (1938).

(33) H. A. Laitinen, T. Higuchi and M. Czuha, *J. Am. Chem. Soc.*, **70**, 561 (1948).

DETERMINATION OF PARTICLE SIZES IN COLLOIDAL SILICA

BY G. B. ALEXANDER AND R. K. ILER

A Contribution from the Grasselli Chemicals Department, Experimental Station, E. I. du Pont de Nemours and Company, Inc.

Received April 10, 1953

A series of alkali stabilized solutions of colloidal silica consisting of relatively uniform discrete non-porous particles ranging in diameter from about 16 to 60 millimicrons has been prepared and characterized in regard to (a) particle weight by light scattering, (b) particle size as determined from electron micrographs, and (c) specific surface area of the dried silica, measured by nitrogen adsorption. The particles appear to consist of dense amorphous silica, since the "weight average" particle diameter, estimated from electron micrographs, agreed reasonably well with the "weight average" particle diameter calculated from the particle weight determined by light scattering, assuming a density of 2.2 for the silica; the ratio of the two figures ranged from 0.83 to 1.26. The particle diameter calculated from the specific surface area of the dried silica, in five out of six sols also was fairly close to the "surface average" particle size estimated from electron micrographs; the ratio of the two values ranged from 0.75 to 0.89. The uniformity of particle size in the sols is indicated by the fact that the "weight average" particle size, determined from electron micrographs, averaged only 26% greater than the "number average" size; this corresponds to a "weight average" particle weight about twice the "number average."

Introduction

The process developed by Bechtold and Snyder[1] has made it possible to prepare silica sols of relatively uniform particle size within the range from about 15 to 130 millimicrons in particle diameter. Colloidal solutions of silica of this type offer an opportunity to compare various techniques for measuring particle diameter or weight, including direct observation of diameter from electron micrographs and calculation from specific surface area and, alternatively, from the particle weight determined by light scattering.

For such comparison, a series of six sols, ranging in particle diameter from about 16 to 60 millimicrons, has been prepared, the particle size distribution observed from the electron micrographs, the specific surface area found by the nitrogen adsorption method, and the particle weight determined by light scattering.

Experimental

Preparation of Sols.—As a starting material for the preparation of silica particles of desired size, a commercially available silica sol, "Ludox" Colloidal Silica[2] was employed.

A steel, submerged tube evaporator was charged with 12.5 gallons of the starting sol which contained 30% SiO_2, consisting of particles averaging about 15 millimicrons in diameter, and stabilized with sufficient alkali to give a molecular ratio of SiO_2:Na_2O of 85:1. The particles were then grown by the process of Bechtold and Snyder,[1] using a freshly made silica sol prepared by ion-exchange in accordance with example 3 of their patent. In this step a solution of sodium silicate having a weight ratio of SiO_2:Na_2O of 3.25:1.00 was diluted to give a solution containing 2.4% SiO_2, which was then passed through a column of the hydrogen form of an ion exchange resin ("Nalcite" HCR). The effluent solution of polysilicic acid was alkalized by the addition of a sufficient amount of the dilute solution of sodium silicate to give a mole ratio of SiO_2:Na_2O of 85:1. The dilute solution was added to the evaporator at the rate of 21 gallons per hour. Evaporation was controlled so as to maintain 12.5 gallons of sol in the evaporator, while at the same time continuously withdrawing product at the rate of 1.4 gallons per hour from the evaporator. With minor variations, this rate of withdrawal served to maintain the concentration of SiO_2 in the evaporator very close to 30% by weight, which was followed by noting the specific gravity of the sol.

The product sol was collected in fifty-five consecutive one-gallon fractions. The turbidity of the product increased gradually and continuously from the first fraction, which was almost clear, to the last, which was extremely white and opaque, though in a thin layer, or when diluted, was transparent but red in transmitted light. Fractions 1, 9, 18, 27, 35 and 50 were selected for characterization.

(1) M. F. Bechtold and O. E. Snyder, U. S. Patent 2,574,902.

(2) M. Sveda, Soap and Sanit. Chemicals (1949).

The growth of silica particles during the process has been calculated, based on the theory that all of the active, low molecular weight silicic acid fed into the evaporator is deposited on the colloidal particles which are present.

Consider 1 unit volume of sol initially in the evaporator, *e.g.*, 1 liter of sol containing G grams of SiO_2. Let this contain N particles at time, t, and N_0 particles at $t = 0$. Let the particle weight of the particles be M and M_0 and diameter of the particles be D and D_0 millimicrons at time t and $t = 0$, respectively.

Let there be X volume of product containing G grams of SiO_2 per liter withdrawn at time, t; X is proportional to the weight of active SiO_2 which has been added to the evaporator in time, t. Then

$$N = 6 \times 10^{23} (G/M) \tag{1}$$

The rate of addition of active silica to the system in grams per liter per unit time is $(dX/dt)G$.

The rate of increase in weight (W grams) of a single silica particle in grams is

$$\frac{dW}{dt} = \frac{dX}{dt} \times \frac{G}{N} \tag{2}$$

Since

$$W = M/6 \times 10^{23}$$

$$\frac{dW}{dt} = \frac{1}{6 \times 10^{23}} \times \frac{dM}{dt} \tag{3}$$

Then

$$\frac{1}{6 \times 10^{23}} \times \frac{dM}{dt} = \frac{dX}{dt} \times \frac{G}{6 \times 10^{23}} \times \frac{M}{G}$$

whence

$$dM/dt = M(dX/dt) \tag{4}$$

$$\ln (M/M_0) = X \tag{5}$$

Since $M = 692D^3$ (assuming the particle has a density of 2.2)

$$\ln (D_3/D_0^3) = X$$

$$3(2.30) \log_{10} \frac{D}{D_0} = X$$

$$\log_{10} \frac{D}{D_0} = 0.145X \tag{6}$$

The slope of log particle size *versus* X according to the above equation is shown in Fig. 1, in comparison with the general slopes of the curves based on particle size data.

Characterization of Sols. Particle Weight by Light Scattering.—The method of Stein and Doty[3] was employed using the light scattering photometer such as that described by Debye[4] supplied by the Phoenix Precision Instrument Co., and originally described by Speiser and Brice.[5]

According to the theory of Stein and Doty, the weight average particle weight, M_w, is a function of the turbidity,

(3) R. Stein and P. Doty, *J. Am. Chem. Soc.*, **68**, 159 (1946).

(4) P. Debye, *J. Applied Phys.*, **17**, 392 (1946).

(5) Speiser and Brice, *J. Opt. Soc. Am.*, **36**, 346 (1946).

TABLE I

PARTICLE SIZE DISTRIBUTION FROM ELECTRON MICROGRAPHS

Fraction no.	Percentage of particles within ±2.5 millimicrons of given size																	Total particles counted
	10[a]	15	20	25	30	35	40	45	50	55	60	65	70	75	80	85	90	
1	27.1	28.6	30.5	13.8														269
9	16.8	30.3	24.8	17.5	10.2	0.4												274
18	8.7	22.2	26.9	23.2	17.4	1.5	0	0.4										275
27	0.7	6.0	15.2	23.6	24.0	19.4	9.5	1.4										283
35	8.8	1.0	3.3	8.8	12.7	19.6	20.3	11.4	7.9	6.2								306
50	..	..	..	..	0.7	2.4	2.4	2.7	23.2	19.8	12.3	9.6	14.3	6.8	4.8	0.3	0.7	293

[a] Includes all visible particles smaller than 12.5 millimicrons in diameter.

τ, and the concentration, C, of a polymeric dispersion or solution, according to the equation

$$HC/\tau = 1/M_w + 2BC/RT \quad (1)$$

where

C = concn. of solute in g. solute per cc. of soln.
M_w is wt. average particle wt. of the solute in g. per mole
B is a constant, characteristic of the system, which may be determined by osmotic pressure measurement, in ergs × cc./g.^{2} of solute.
R = gas constant in ergs/mole of solute per degree of temp.
T = absolute temperature in degrees
τ = turbidity (extinction coefficient for scattering at right angles in reciprocal centimeters)

$$H = \frac{32\pi^3 n_0^2 (dn/dC)^2}{2\gamma_4 N_0} \quad (3)$$

n_0 = refractive index of the solvent
dn/dC is equal to the index of refraction gradient between solvent and solution in terms of cc. per g.
γ = the wave length in air of light used in centimeters.
$N_0 = 6.02 \times 10^{23}$ particles per mole (Avogadro's number).

The calibration of the photometer was based on opal glass standard. Then turbidity measurements were made on polymer solutions at several concentrations. The particle weight was determined by plotting HC/τ *vs.* C for the readings taken, and extrapolating to zero concentration; the values used for n_0 and dn/dC were 1.3338 (at 27° and a wave length of 547 millimicrons) and 0.076, respectively. The particle weight was determined by the reciprocal of the intercept (see equation 1).

Particle Size from Electron Micrographs.—Samples of sols were diluted to 0.1% SiO_2 or less before application to the supporting screen; negatives were obtained at 5000 × magnification, and these projected on a screen at an over-all magnification of about 100,000 for measurement. All particles in randomly selected areas were classified as being 10, 15, 20, etc., millimicrons in diameter and the distribution of particle sizes (based, in each case, on measurement of about 300 particles) is shown in Table I.

As described by Cohan and Watson,[6] the number average (D_n), surface average (D_s) and the weight average (D_w) diameters were calculated, D_n representing the arithmetic average diameter, and D_s representing the diameter of a particle having a specific surface area equal to that calculated from the distribution of diameters observed in the electron micrographs, and D_w being the diameter of a particle having a weight equal to that calculated from the average particle weight estimated for each particle measured in the micrographs.

Specific Surface Area.—Samples of the sols were converted to powders by adding concentrated HCl to lower the *p*H to 8.0, then adding an equal volume of *t*-butyl alcohol, which brought about incipient gelling. The mass was then dried in air at 110° and the specific surface area determined[7] by nitrogen adsorption by the method described by Emmett.

TABLE II

Fraction no.	Vol. of product, X	Particle diameter D_n	D_s	D_w	Nitrogen adsorp. Spec. surf., m.^{2}/g.	Calcd. diam., D_a[a]	Light scattering Particle wt., millions[b]	Calcd. diam., D_m
1	0.08	16.5	19.5	21.2	185	14.7	3.8	17.5
9	0.73	18.8	22.6	25.3	144	18.9	8.3	23
18	1.45	21.1	24.6	27.6	125	21.8	19.5	30
27	2.17	28.4	31.8	34	97	28.1	54.0	43
35	2.80	35.2	41.6	45	84	32.5	100.0	53
50	4.0	59.2	63.3	67	68	40.0	210.0	66

[a] Assuming density of amorphous silica is 2.2, the specific surface area of a silica sphere D_a millimicrons in diameter is calculated to be $(2700 D_a^{-1})$ square meters per gram. [b] Assuming density of amorphous silica is 2.2, the particle weight of a particle D_m millimicrons in diameter is $(690 D^3)$.

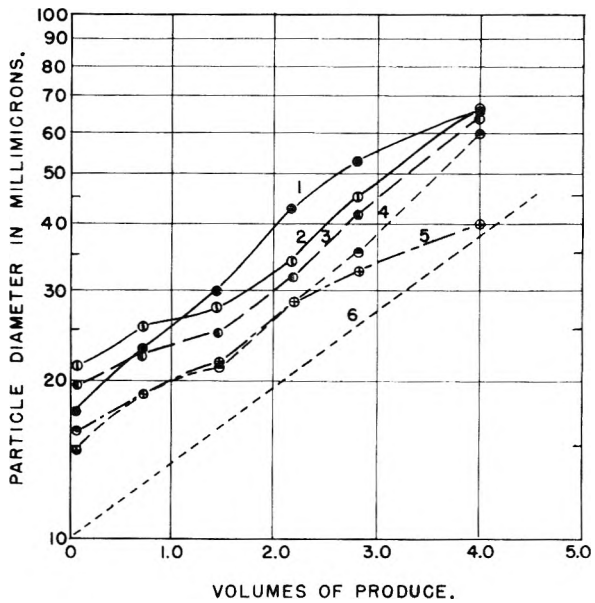

Fig. 1.—1, D_m (light scattering); 2, D_w (electron micrograph); 3, D_s (electron micrograph); 4, D_n (electron micrograph); 5, D_a (nitrogen adsorption); 6, theoretical slope according to equation 6.

Conclusions

1. As shown in Fig. 1, the diameter D_m calculated from the particle weight determined by light scattering was generally somewhat greater than D_w, the "weight-average" particle diameter estimated from electron micrographs, except in the case of sols containing an appreciable proportion of particles smaller than 19 millimicrons, which were difficult to measure in the micrographs.

2. The particle diameter D_s, in five out of six sols, calculated from the specific surface area of the silica obtained by drying the sol, averaged 17% smaller than D_s, the "surface-average" particle size estimated from electron micrographs. The sol of largest average particle size, which contained an appreciable fraction of small particles, along with a

(6) L. H. Cohan and J. H. L. Watson, *Rubber Age*, 68, 687 (1951).

(7) P. H. Emmett, "Symposium on New Methods for Particle Size Determination," p. 95, published by the American Society for Testing Materials, Mar. 4, 1941.

majority of larger ones, was not included because it was difficult to measure all the smaller particles. The specific surface area of the silica agreed more closely with D_n, the "number average" particle size estimated from electron micrographs.

3. The "weight average" particle diameter, D_w, measured on micrographs, averaged 26% greater than D_n, the "number average" diameter; this corresponds to a "weight average" particle weight about twice the "number average" particle weight.

The authors wish to acknowledge the work of L. A. Dirnberger in conducting the engineering studies and making mathematical calculations, W. M. Heston, Jr., in preparing samples for characterization, R. E. Lawrence in carrying out the analyses, and Dr. C. E. Willoughby of the Chemical Department in preparing the electron micrographs.

THE MAXWELL–WAGNER DISPERSION IN A SUSPENSION OF ELLIPSOIDS[1]

BY HUGO FRICKE

Walter B. James Laboratory of Biophysics, Biological Laboratory, Cold Spring Harbor, N. Y.

Received April 14, 1953

The dispersion equations are first derived for the conductivity and permittivity of a suspension of ellipsoids of vanishing volume concentration, in which the components are characterized by both conductivity and permittivity, by extending to complex admittances an earlier treatment[2] of this system for the case of pure conductors. The expressions contain a "form factor" which is expressed in terms of elliptic integrals. Its numerical values are tabulated. For random orientation of the ellipsoidal axis, the suspension is shown to be electrically equivalent to a simple resistance–capacity network and to be characterized by three dispersion regions inside each of which, it behaves quantitatively like a Debye dipole system. This treatment is subsequently extended to more concentrated suspensions on basis of the semitheoretical general conductivity equation given in ref. 2.

A heterogeneous system of conducting dielectrics, in which the ratio of permittivity to conductivity is different in the different phases, exhibits Maxwell–Wagner (M–W)[3,4] dispersion in the frequency zone where the field shifts over from its low to high frequency course. Below the dispersion region, where the field is determined by the conductivities of the constituent phases, the conductivity of the system has its minimal value, referred to in the usual kind of mixture formula, while the permittivity is greater than the (minimal) value obtained when the field is determined by the permittivities. The opposite condition, minimal permittivity, increased conductivity, is found at frequencies above the dispersion region.

Although the M–W effect is of considerable practical interest, its theoretical treatment does not appear to have been extended beyond the two simple systems considered by Wagner,[4] *viz.*, a stratified body and a dilute suspension of spheres. The behavior of fibrous systems has been discussed qualitatively by different authors,[5–7] by using supposedly equivalent electric circuits. A more general treatment of suspensions which takes into account both the effect of particle form and higher volume concentrations, has recently become of interest in studies of biological materials in the ultra high frequency zone.[8–10]

(1) Supported by the U. S. Office of Naval Research.

(2) H. Fricke, *Phys. Rev.*, **24**, 575 (1924).

(3) J. C. Maxwell, "A Treatise on Electricity and Magnetism," 2nd Ed., Clarendon Press, Oxford, 1881, p. 398.

(4) K. W. Wagner, *Arch. Elektrotech.* **2**, 371 (1914).

(5) S. Setch and Y. Toriyama, *Inst. Phys. Chem. Research, Tokyo Sci. Papers*, 3, 283 (1926).

(6) D. DuBois, *A. I. E. E.*, 41, 689 (1922).

(7) E. J. Murphy, THIS JOURNAL, **33**, 200 (1929).

(8) B. Rajewsky and H. Schwan, *Naturwissenschaften*, **35**, 315 (1948).

(9) H. F. Cook, *Nature*, 168, 247 (1951).

(10) H. F. Cook, *Brit. J. Appl. Phys.*, **2**, 295 (1951).

The problem can be dealt with in a simple manner by making use of the theoretical information already available on the electric behavior of heterogeneous systems composed of pure conductors. By introducing complex variables, the conductivity equation for such a system is transformed to the complex conductivity equation for the same geometrical system of conducting dielectrics, from which equation the dispersion equations for conductivity and permittivity are thereafter obtained by separating real and imaginary terms. By using this method, Wagner's treatment of a suspension of spheres could have been simplified since the conductivity equation for this system was already given by Maxwell.

The object of the present paper is to extend this treatment to a suspension of ellipsoids. The conductivity equation for this system was dealt with by Fricke,[2] where references to the earlier literature will be found. The equation can be derived rigorously only when the volume concentration is low, but reference 2 describes also the derivation of a general conductivity equation, which has been found to agree well with the experimental evidence. In dealing with the dispersion problem, we shall therefore first consider the case of low volume concentrations and thereafter extend this treatment to higher concentrations by using the general conductivity equation of this earlier work.

Theory.—We shall consider a suspension of homogeneous ellipsoids (axis $2a \geqq 2b \geqq 2c$) distributed at random in a homogeneous medium. When the components are pure conductors, the conductivities of suspension, suspending and suspended phases are called k, k_1 and k_2, respectively, expressed in $(9 \times 10^{11})^{-1}$ ohm^{-1} cm.$^{-1}$. In the complex system, the corresponding quantities are written $\sigma + j\epsilon/2\pi n$, etc., where σ and ϵ represent conductivity

and permittivity, respectively, and n is the frequency in c.p.s.

(1) **Low Concentration Suspensions.**—The suspended ellipsoids are assumed to be so far apart that the local field can be taken to be equal to the external field. Consider first a suspension in which the ellipsoids are arranged with axis $2\alpha(\alpha = a, b$ or c) parallel with the field. When higher powers of ρ are neglected, the conductivity equation can then be written[2]

$$k = k_1 + \rho(k_2 - k_1)\frac{1 + x_\alpha}{x_\alpha + k_2/k_1} \qquad (1)$$

where ρ is the fractional volume of the suspended ellipsoids and

$$x_\alpha = \frac{2 - abcL_\alpha}{abcL_\alpha} \qquad (2)$$

$$L_\alpha = \int_0^\infty \frac{d\lambda}{(\alpha^2 + \lambda)\sqrt{(a^2 + \lambda)(b^2 + \lambda)(c^2 + \lambda)}} \qquad (3)$$

For random orientation of the ellipsoidal axis

$$k = k_1 + \frac{1}{3}\rho(k_2 - k_1)\sum_{\alpha=a,b,c}\frac{1 + x_\alpha}{x_\alpha + k_2/k_1} \qquad (4)$$

The k's are now replaced by their complex correspondents and real and imaginary terms are separated. For random orientation of the ellipsoidal axis, we obtain

$$\sigma = \sigma_1 + \frac{\sigma_1}{3}\rho\sum_{(\alpha)}'(1 + x_\alpha)\frac{(\sigma_2 - \sigma_1)(\sigma_2 + x_\alpha\sigma_1) + \frac{n^2}{4}(\epsilon_2 - \epsilon_1)(\epsilon_2 + x_\alpha\epsilon_1) + \frac{n^2}{4}(1 + x_\alpha)\epsilon_1^2\left(\frac{\sigma_2}{\sigma_1} - \frac{\epsilon_2}{\epsilon_1}\right)}{(\sigma_2 + x_\alpha\sigma_1)^2 + \frac{n^2}{4}(\epsilon_2 + x_\alpha\epsilon_1)^2} \qquad (5)$$

$$\epsilon = \epsilon_1 + \frac{\epsilon_1}{3}\rho\sum_{(\alpha)}(1 + x_\alpha)\frac{(\sigma_2 - \sigma_1)(\sigma_2 + x_\alpha\sigma_1) + \frac{n^2}{4}(\epsilon_2 - \epsilon_1)(\epsilon_2 + x_\alpha\epsilon_1) + (1 + x_\alpha)\sigma_1^2\left(\frac{\epsilon_2}{\epsilon_1} - \frac{\sigma_2}{\sigma_1}\right)}{(\sigma_2 + x_\alpha\sigma_1)^2 + \frac{n^2}{4}(\epsilon_2 + x_\alpha\epsilon_1)^2} \qquad (6)$$

By removing the summation sign and replacing $\rho/3$ by ρ, we obtain the dispersion equations (5a and 6a) for a suspension of ellipsoids having axis 2α parallel with the external field. For spheres $x = 2$ and the expressions are then the same as those given by Wagner.

The values of L_α were calculated before[2] only for ellipsoids of rotation. The general solution is obtained by substituting $\lambda = (a^2 - c^2)/z^2 - a^2$ and $\lambda = (b^2z^2 - c^2)/(1 - z^2)$ in L_a and L_c, respectively, whereby these integrals are reduced to elliptic integrals of first and second kind

$$abcL_a = \frac{2abc}{(a^2 - b^2)\sqrt{a^2 - c^2}}\left(F\left(\arccos\frac{c}{a}, k\right) - E\left(\arccos\frac{c}{a}, k\right)\right) \qquad (7)$$

$$abcL_b = 2 - abcL_a - abcL_c \qquad (8)$$

$$abcL_c = \frac{2a^2}{a^2 - c^2} - \frac{2abc}{(b^2 - c^2)\sqrt{a^2 - c^2}}\left(E\left(\frac{\pi}{2}, k\right) - E\left(\arcsin\frac{c}{b}, k\right)\right) \qquad (9)$$

$$\text{Modulus } k = \sqrt{\frac{a^2 - b^2}{a^2 - c^2}}$$

The values of x_α for different axial ratios are recorded in Table I and Fig. 1. For cylinders arranged with their axis at right angle to the electric field, $x = 1$.

TABLE I

FORM FACTORS x FOR DIFFERENT ELLIPSOIDAL AXIAL RATIOS

a/b	b/c	x_a	x_b	x_c	a/b	b/c	x_a	x_b	x_c
1	1	2	2	2	3	1	8.2	1.24	1.24
1	1.5	2.61	2.61	1.23	3	1.5	11.1	1.77	0.80
1	2	3.23	3.23	0.90	3	2	13.7	2.29	0.59
1	3	4.49	4.49	0.57	3	3	19.5	3.35	0.389
1	4	5.8	5.8	0.417	3	4	25.1	4.45	0.285
1	6	8.30	8.30	0.274	3	6	36.6	6.5	0.190
1.5	1	3.29	1.61	1.61	4	1	12.1	1.16	1.16
1.5	1.5	4.33	2.17	1.01	4	1.5	16.5	1.69	0.74
1.5	2	5.3	2.74	0.73	4	2	20.8	2.19	0.56
1.5	3	7.5	3.88	0.478	4	3	29.6	3.22	0.366
1.5	4	9.6	5.1	0.348	4	4	38.4	4.29	0.273
1.5	6	13.9	7.3	0.230	4	6	56	6.4	0.181
2	1	4.79	1.42	1.42	6	1	21.6	1.09	1.09
2	1.5	6.3	1.96	0.90	6	1.5	30.1	1.61	0.71
2	2	7.9	2.50	0.66	6	2	38.8	2.10	0.53
2	3	11.0	3.63	0.432	6	3	55	3.10	0.355
2	4	14.2	4.76	0.314	6	4	70	4.22	0.259
2	6	20.7	6.9	0.209	6	6	103	6.2	0.174

The equations obtained for σ and ϵ show that a suspension of ellipsoids having one of the principal axes parallel with the field, is characterized by a single Debye type dispersion zone. When the axes are oriented at random, there are three such dispersion zones, the electric behavior of the suspension being the same as that of an even mixture of the three principal orientations of the ellipsoids.

It will readily be verified also, that a suspension of randomly oriented ellipsoids is electrically equivalent to the diagram in Fig. 2 where

$$R_1^{-1} = \sigma(0) \qquad (10)$$

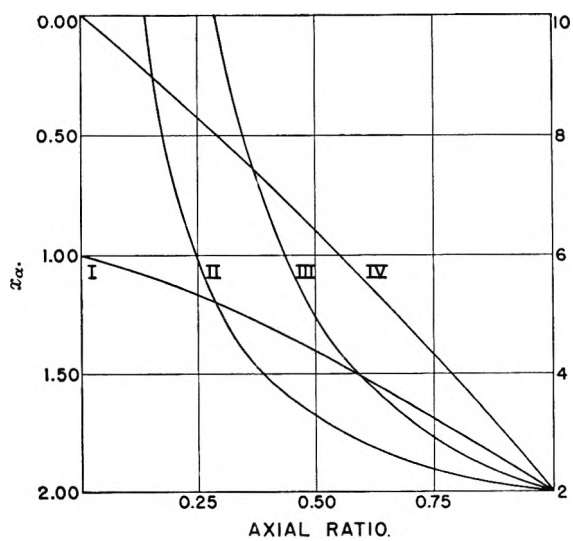

Fig. 1.—Form factors x_α for ellipsoids of rotation, half axis $a \geqq b \geqq c$.

$a = b$ { $x_a = x_b$, graph II, right scale.
x_c, graph IV, left scale.

$b = c$ { x_a, graph III, right scale.
$x_b = x_c$, graph I, left scale.

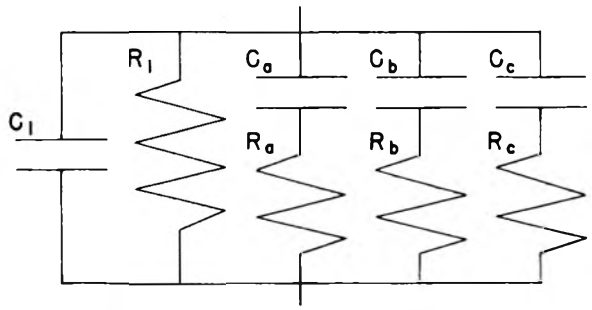

Fig. 2.—Electrical diagram of suspension of ellipsoids.

$$C_1 = \frac{\epsilon(\infty)}{4\pi} \tag{11}$$

$$R_\alpha^{-1} = \frac{1}{3}\rho(1 + x_\alpha)^2 \frac{(\sigma_2\epsilon_1 - \sigma_1\epsilon_2)^2}{(\sigma_2 + x_\alpha\sigma_1)(\epsilon_2 + x_\alpha\epsilon_1)^2} \tag{12}$$

$$C_\alpha = \frac{1}{12\pi}\rho(1 + x_\alpha)^2 \frac{(\sigma_2\epsilon_1 - \sigma_1\epsilon_2)^2}{(\sigma_2 + x_\alpha\sigma_1)^2(\epsilon_2 + x_\alpha\epsilon_1)} \tag{13}$$

The quantities $\sigma(0)$, $\epsilon(0)$ and $\sigma(\infty)$, $\epsilon(\infty)$ are the values of σ and ϵ at frequencies below and above all dispersion regions, respectively.

The spectral position of the dispersion region, which is associated with ellipsoids having axis 2α parallel with the field, can be defined by frequency

$$n_\alpha = 2\frac{\sigma_2 + x_\alpha\sigma_1}{\epsilon_2 + x_\alpha\epsilon_1} \tag{14}$$

which is the frequency at which σ and ϵ are the arithmetical means of their respective values above and below the region. When $\sigma_2/\sigma_1 > \epsilon_2/\epsilon_1$, the value of n_α decreases when x_α increases. The opposite is the case when $\sigma_2/\sigma_1 < \epsilon_2/\epsilon_1$.

Since $x_a \geqq x_b \geqq x_c$, the dispersion regions are therefore placed in the spectrum as follows. When

$$\sigma_2/\sigma_1 > \epsilon_2/\epsilon_1 : n_a \leqq n_b \leqq n_c \tag{15}$$

$$\sigma_2/\sigma_1 < \epsilon_2/\epsilon_1 : n_a \geqq n_b \geqq n_c \tag{16}$$

If the electrical characteristics of the phases are the same in a suspension of parallel ellipsoids of rotation and in a suspension of spheres, it will also be seen that, when $\sigma_2/\sigma_1 > \epsilon_2/\epsilon_1$, the dispersion region in the former system always lies below that in the latter, when the field is parallel with a major axis and above it when the field is parallel with a minor axis, while the opposite is the case when $\sigma_2/\sigma_1 < \epsilon_2/\epsilon_1$.

If n_l and n_h are frequencies below and above a dispersion region, respectively, the apparent dielectric loss factor, associated with this region and measured at the frequency n, may be defined by

$$\tan\delta = \frac{\sigma(n) - \sigma(n_l)}{(n/2)\epsilon(n)} \tag{17}$$

It will be verified easily, then, that

$$\tan\delta = \frac{\epsilon(n_l) - \epsilon(n_h)}{\epsilon(n_l) + \epsilon(n_h)\,(n/n_\alpha)^2} \times \frac{n}{n_\alpha} \tag{18}$$

which is the relation characteristic of a Debye system.[11] Inside a dispersion region, an ellipsoidal suspension behaves therefore dielectrically as a Debye system with the relaxation time

$$\tau = \frac{1}{2\pi n_\alpha}\frac{\epsilon(n_h) + 2}{\epsilon(n_l) + 2} \tag{19}$$

(11) P. Debye, "Polar Molecules," Chemical Catalog Company, New York, N. Y., 1929, pp. 92-94.

A suspension of randomly oriented ellipsoids behaves as an even mixture of three different Debye dipole species.

Below and above all dispersion regions, the conductivities and permittivities of a suspension are

$$\sigma(0) = \sigma_1 + \frac{1}{3}\rho(\sigma_2 - \sigma_1)\sigma_1 \sum_{(\alpha)} \frac{1 + x_\alpha}{\sigma_2 + x_\alpha\sigma_1} \tag{20}$$

$$\epsilon(0) = \epsilon_1 + \frac{1}{3}\rho(\sigma_2 - \sigma_1)\epsilon_1 \sum_{(\alpha)} \frac{1 + x_\alpha}{\sigma_2 + x_\alpha\sigma_1} + \frac{1}{3}\rho(\epsilon_2\sigma_1 - \epsilon_1\sigma_2)\sigma_1 \sum_{(\alpha)} \frac{(1 + x_\alpha)^2}{(\sigma_2 + x_\alpha\sigma_1)^2} \tag{21}$$

$$\sigma(\infty) = \sigma_1 + \frac{1}{3}\rho(\epsilon_2 - \epsilon_1)\sigma_1 \sum_{(\alpha)} \frac{1 + x_\alpha}{\epsilon_2 + x_\alpha\epsilon_1} + \frac{1}{3}\rho(\sigma_2\epsilon_1 - \sigma_1\epsilon_2)\epsilon_1 \sum_{(\alpha)} \frac{(1 + x_\alpha)^2}{(\epsilon_2 + x_\alpha\epsilon_1)^2} \tag{22}$$

$$\epsilon(\infty) = \epsilon_1 + \frac{1}{3}\rho(\epsilon_2 - \epsilon_1)\epsilon_1 \sum_{(\alpha)} \frac{1 + x_\alpha}{\epsilon_2 + x_\alpha\epsilon_1} \tag{23}$$

From equation 21, we obtain the permittivity of the suspension when the frequency is so low that the field is determined by the conductivities of the phases. From equation 22 we obtain the conductivity when the frequency is so high that the field is determined by the permittivities.

The dispersion in conductivity $\sigma(\infty) - \sigma(0)$ and permittivity $\epsilon(0) - \epsilon(\infty)$ over the whole dispersion region is given by $\sum_{(\alpha)} R_\alpha^{-1}$ and $\sum_{(\alpha)} 4\pi C_\alpha$ of equations 12 and 13. Both quantities are always positive and exhibit, when plotted against σ_2/ϵ_2, a minimum at $\sigma_2/\epsilon_2 = \sigma_1/\epsilon_1$, as could be predicted since the lines of electric force through a heterogeneous system composed of pure conductors or pure dielectrics are distributed in such a manner that the energy consumed or stored is minimum. When the difference between σ_2/ϵ_2 and σ_1/ϵ_1 is only moderate, the dispersion in conductivity and permittivity of a suspension is therefore relatively small.

The dispersion equations give us the means of calculating the electric characteristics of the suspended phase, when the other quantities have been measured. When the ellipsoids are parallel (including sphere and cylinder) solution of equations 5a and 6a with respect to σ_2 and ϵ_2 leads to equations 29 and 30 of the following section. When the axes are distributed at random, the calculation is generally best carried out by trial and error, except when the frequency is so high or so low that equations 22 and 23 or 20 and 21, respectively, are valid. When the frequency is very high, for example, the value of ϵ_2 can be obtained, from equation 23, by solving a cubic (quadratic in the case of ellipsoids of rotation) algebraic equation and σ_2 can thereafter be obtained from equation 22.

Higher Volume Concentrations.—The following treatment deals with suspensions in which the suspended particles are all alike and distributed at random in space. Under these conditions, the conductivity equation for the suspension was derived in ref. 2 on the assumption that the effective internal field acting upon a suspended particle is equal to the average field in the suspending

fluid. This conductivity equation has been found in good agreement with the experimental evidence, which covers a broad variety of conditions.[12–16] It appears of interest therefore, to derive the corresponding dispersion equations. The cases are treated separately when the ellipsoidal axes are (a) parallel with the external field and (b) oriented at random.

(a) Parallel Ellipsoids.—When axis 2α is parallel with the external field, the conductivity equation is[2]

$$k = k_1 \frac{k_2 + x_\alpha k_1 + x_\alpha \rho(k_2 - k_1)}{k_2 + x_\alpha k_1 - \rho(k_2 - k_1)} = k_1 \frac{A(k_2 k_1)}{B(k_2 k_1)} \quad (24)$$

The introduction of complex variables gives

$$\sigma = \sigma_1 \frac{A(\sigma_2\sigma_1)B(\sigma_2\sigma_1) + \frac{n^2}{4} A(\epsilon_2\epsilon_1)B(\epsilon_2\epsilon_1) + \frac{n^2}{4}(x_\alpha + 1)^2 \rho\epsilon_1^2 \left(\frac{\sigma_2}{\sigma_1} - \frac{\epsilon_2}{\epsilon_1}\right)}{[B(\sigma_2\sigma_1)]^2 + \frac{n^2}{4}[B(\epsilon_2\epsilon_1)]^2} \quad (25)$$

$$\epsilon = \epsilon_1 \frac{A(\sigma_2\sigma_1)B(\sigma_2\sigma_1) + \frac{n^2}{4} A(\epsilon_2\epsilon_1)B(\epsilon_2\epsilon_1) + (x_\alpha + 1)^2\rho\sigma_1^2 \left(\frac{\epsilon_2}{\epsilon_1} - \frac{\sigma_2}{\sigma_1}\right)}{[B(\sigma_2\sigma_1)]^2 + \frac{n^2}{4}[B(\epsilon_2\epsilon_1)]^2} \quad (26)$$

A closer examination of these equations will show that they represent the electric behavior of the same two model systems—an electrical circuit of the form shown in Fig. 2 (with one $C_\alpha R_\alpha$ branch) and a Debye dipole system—which were found to represent the behavior of a low concentration suspension. The dispersion in conductivity and permittivity can be written in the forms

$$\sigma(\infty) - \sigma(0) = \frac{\rho(1-\rho)(1+x_\alpha)^2(\sigma_2\epsilon_1 - \epsilon_2\sigma_1)^2}{B(\sigma_2\sigma_1)[B(\epsilon_2\epsilon_1)]^2} \quad (27)$$

$$\epsilon(0) - \epsilon(\infty) = \frac{\rho(1-\rho)(1+x_\alpha)^2(\sigma_2\epsilon_1 - \epsilon_2\sigma_1)^2}{[B(\sigma_2\sigma_1)]^2 B(\epsilon_2\epsilon_1)} \quad (28)$$

As in the case of the low concentration suspension, the expressions contain the difference between σ_2/σ_1 and ϵ_2/ϵ_1 in its squared form, showing again that the dispersion is relatively small, when the difference between σ_2/σ_1 and ϵ_2/ϵ_1 is not very large.

Solution of equations 25 and 26 with respect to σ_2 and ϵ_2 gives

$$\sigma_2 = \sigma_1 \frac{C(\sigma\sigma_1)D(\sigma\sigma_1) + \frac{n^2}{4} C(\epsilon\epsilon_1)D(\epsilon\epsilon_1) + \frac{n^2}{4}(x_\alpha + 1)^2 \rho\epsilon_1^2 \left(\frac{\sigma}{\sigma_1} - \frac{\epsilon}{\epsilon_1}\right)}{[D(\sigma\sigma_1)]^2 + \frac{n^2}{4}[D(\epsilon\epsilon_1)]^2} \quad (29)$$

$$\epsilon_2 = \epsilon_1 \frac{C(\sigma\sigma_1)D\sigma\sigma_1) + \frac{n^2}{4} C(\epsilon\epsilon_1)D(\epsilon\epsilon_1) + (x_\alpha - 1)^2\rho\sigma_1^2 \left(\frac{\epsilon}{\epsilon_1} - \frac{\sigma}{\sigma_1}\right)}{[D(\sigma\sigma_1)]^2 + \frac{n^2}{4}[D(\epsilon\epsilon_1)]^2} \quad (30)$$

$$C(kk_1) = x_\alpha(k - k_1) + \rho(k + x_\alpha k_1)$$

$$D(kk_1) = -(k - k_1) + \rho(k + x_\alpha k_1)$$

(b) Random Orientation of Ellipsoidal Axis.—The conductivity equation can be written[2]

$$k = k_2 + \frac{(k_1 - k_2)(1-\rho)}{1 + \frac{\rho}{3}\sum_{(\alpha)} \frac{k_1 - k_2}{k_2 + x_\alpha k_1}} \quad (31)$$

Since the complete dispersion equations are rather complicated, we shall set down only the expressions for σ and ϵ at frequencies above all dispersion regions. Analogous expressions are obtained at frequencies below the dispersion regions.

$$\sigma(\infty) = \sigma_2 + \frac{(\sigma_1 - \sigma_2)(1-\rho)}{1 + \frac{\rho}{3}\sum_{(\alpha)} \frac{\epsilon_1 - \epsilon_2}{\epsilon_2 + x_\alpha\epsilon_1}} + \frac{\frac{\rho}{3}(1-\rho)(\sigma_2\epsilon_1 - \sigma_1\epsilon_2)(\epsilon_1 - \epsilon_2)\sum \frac{x_\alpha + 1}{(\epsilon_2 + x_\alpha\epsilon_1)^2}}{\left(1 + \frac{\rho}{3}\sum_{(\alpha)} \frac{\epsilon_1 - \epsilon_2}{\epsilon_2 + x_\alpha\epsilon_1}\right)^2} \quad (32)$$

$$\epsilon(\infty) = \epsilon_2 + \frac{(\epsilon_1 - \epsilon_2)(1-\rho)}{1 + \frac{\rho}{3}\sum_{(\alpha)} \frac{\epsilon_1 - \epsilon_2}{\epsilon_2 + x_\alpha\epsilon_1}} \quad (33)$$

The calculation of σ_2 and ϵ_2 from these equations can be carried out in a manner similar to that in the low concentration case.

(12) H. Fricke and S. Morse, *Phys. Rev.*, **25**, 361 (1925).
(13) H. Fricke, *Physics*, **1**, 106 (1931).
(14) E. Ponder, *J. Physiol.*, **85**, 439 (1935).
(15) E. F. Burton and L. G. Turnbull, *Proc. Roy. Soc. (London)*, **A158**, 182 (1937).
(16) S. Velick and M. Gorin, *J. Gen. Physiol.*, **23**, 753 (1940).

THE REFRACTIVE INDEX OF GERMANE[1]

BY MINO GREEN[2] AND PAUL H. ROBINSON[2,3]

Lincoln Laboratory, Massachusetts Institute of Technology, Cambridge, Mass., and Department of Chemistry of the Polytechnic Institute of Brooklyn, Brooklyn, N. Y.

Received April 15, 1953

The refractive index of germane has been determined. The values obtained are 1.0009095 at 5484 Å. and 1.0008940 in the 5893 Å. region. The atomic refraction of germanium is given as 8.95 cm.^{3}

The difference in refractive index between hydrogen and germane has been used as the basis of a method for assaying GeH_4–H_2 ratios. The calibration of the apparatus entailed the preparation of a quantity of pure GeH_4 for making up known GeH_4–H_2 mixtures. In the course of this work it became a relatively simple matter to determine the refractive index of GeH_4, no measured value for which has been reported in the literature.

The GeH_4 obtained[4] was purified by trap-to-trap distillation under high vacuum until it gave vapor pressures agreeing with Paneth's values[5] at two different temperatures. Measurements of refractive index were made using a Rayleigh–Zeiss interferometer the detailed construction and use of which is described elsewhere.[6,7] The body of the instrument was carefully insulated in order to avoid any effect due to rapid room temperature changes. A double cell 500 mm. in length was used; one chamber of the double cell was evacuated and the other chamber was filled with GeH_4 at a known temperature and pressure. A mercury filled U-tube absolute manometer, with 20 mm. diameter limbs, was used for measuring pressure. The meniscuses were illuminated according to the method of Beattie and co-workers[8] in order to avoid errors due to parallax. The distance between the mercury levels was measured using a precision cathetometer. Light of two different wave lengths was employed. One source was a sodium arc lamp with most of the light intensity in the 5893 Å. region (lines D_1 and D_2), and the other was a mercury arc used in conjunction with a multilayer narrow band filter which isolated the 5484 Å. line.

The refractive index of GeH_4, at two different wave lengths, was measured over the pressure range 2 to 10 cm. of mercury and no perceptible deviation from linearity between pressure and refractive index was observed. The data in Table I are in each case the average of ten determinations, corrected to 0° C. and 1 atm., the deviation quoted being the standard deviation.

TABLE I

REFRACTIVE INDEX OF GeH_4 AT 0° C. AND 1 ATM.

Wave length, Å.	Refractive index
5484	$1.0009095 \pm 2.3 \times 10^{-6}$
5893	$1.0008940 \pm 1.6 \times 10^{-6}$

The mole refraction of GeH_4 for the D-line is 13.35 ± 0.04 cm.^{3}. Taking 1.100 as the atomic refraction of H, the atomic refraction of Ge is found to be 8.95 ± 0.04 cm.^{3}. Calculations from refractive index data[9] for tetraethylgermanium gives 8.97 cm.^{3}, and for germanium tetrachloride 7.60 cm.^{3}.[10]

(1) The research in this document was supported jointly by the Army, Navy and Air Force under contract with the Massachusetts Institute of Technology.

(2) Staff member, Lincoln Laboratory, Massachusetts Institute of Technology.

(3) This work has been done as part of a thesis submitted in partial fulfillment for the requirements for the degree of Master of Science.

(4) Metal Hydrides, Beverly, Massachusetts.

(5) F. A. Paneth and E. Rabinowitsch, *Ber.*, 58B, 1138 (1924)

(6) C. Candler, "Modern Interferometers," Hilger and Watts, London, 1951.

(7) L. H. Adams, *J. Wash. Acad. Sci.*, 5, 265 (1915).

(8) J. A. Beattie, *et al.*, *Proc. Am. Acad. Arts and Sci.*, 74, 327 (1941).

(9) D. L. Tabern, W. R. Orndorff and L. M. Dennis, *J. Am. Chem. Soc.*, 47, 2039 (1925).

(10) A. W. Laubengayer and D. L. Tabern, THIS JOURNAL, 30, 1047 (1926).

THE VIBRATIONAL SPECTRA OF SOME TIN AND GERMANIUM HALOGEN METALORGANIC COMPOUNDS

BY ELLIS R. LIPPINCOTT

Department of Chemistry, Kansas State College, Manhattan, Kansas

PHILIP MERCIER AND MARVIN C. TOBIN

Department of Chemistry, University of Connecticut, Storrs, Connecticut

Received April 15, 1953

The Raman spectra of tin trimethyl iodide, tin dimethyl diiodide, germanium ethyl trichloride and germanium diethyl dichloride are reported along with the infrared spectra of tin trimethyl iodide and tin dimethyl diiodide in the region from 3 to 15 microns. Tentative assignments of frequencies to normal modes of vibration are given for tin trimethyl iodide and tin dimethyl diiodide, along with assignments of the low frequencies for germanium ethyl trichloride and germanium diethyl dichloride.

Introduction

The halogen metalorganic compounds represent "hybrids" of purely inorganic compounds and metalorganic compounds. In favorable cases, such as the compounds of the group IV elements, it is possible to make the transition stepwise. One is thus able to follow the change in properties of a series of compounds as one substitutes halogen atoms for organic radicals on the nucleus.

The type of series thus formed is of particular interest from the point of view of vibrational spectroscopy. The set $MX_4 \rightarrow MY_4$ contains five distinct compounds of three different symmetries. Since it is to be expected (an expectation borne out by experience) that the vibrational force constants will not vary much from one compound to another, normal coördinate analyses using quite general potential functions may be made for the series.

The interpretation of vibrational spectra for these compounds is, of course, simplest for methyl compounds. There is an enormous increase in the complexity of the observed spectra in passing from the methyl to the ethyl compounds. Crawford and Wilson[1] have shown that, under the assumption of zero torsional force constants, molecules consisting of spinning tops on a rigid frame can be treated as having the symmetry of the frame, in making interpretations and normal coördinate analyses. Thus, interpretation of the observed spectra of, say, ethyl germanium trichloride might give some indication of the nature and extent of interaction between the $-GeCl_3$ frame and the ethyl group.

The halogen metalorganics of group IV have come in for little study by physical methods. Skinner and Sutton,[2] using electron diffraction techniques, have reported bond distances and angles for all of the methyl tin chlorides, bromides and iodides. Shimanouchi and others[3] have reported Raman spectra for the methyl silicon chloride series. Murata and co-workers[4] have reported Raman spectra for the ethyl silicon chloride and methyl silicon bromide series.

To date, no spectroscopic studies of germanium, tin, or lead halogen–metalorganics have been reported.

(1) B. Crawford and E. B. Wilson, *J. Chem. Phys.*, **9**, 323 (1941).

(2) H. A. Skinner and L. E. Sutton, *Trans. Faraday Soc.*, **40**, 164 (1944).

(3) T. Shimanouchi, I. Tsuchiya and Y. Mikawa, *J. Chem. Phys.*, **18**, 1306 (1950); **17**, 245 (1949); **17**, 848 (1949).

(4) H. Murata, R. Okawasa and T. Watase, *ibid.*, **18**, 1308 (1950).

Compounds.—Samples of ethyl germanium trichloride and diethyl germanium dichloride were kindly provided by Professor Eugene Rochow of Harvard University. Stannic iodide was prepared by reaction of the elements in the presence of a small amount of carbon disulfide. The product was recrystallized three times from benzene freshly distilled from a clean, all glass still.

Tin trimethyl iodide and tin dimethyl diiodide were prepared by slowly adding three moles of methylmagnesium iodide to one mole of stannic iodide in an ether slurry. The mixture was refluxed for two hours, then all volatile products were rapidly distilled off and collected. The residue in the flask was hydrolyzed with a minimum of water and repeatedly extracted with ether. The distillate and extractate were fractionally distilled, the ether coming off at atmospheric pressure, and the products coming off under vacuum. The Me_3SnI came over first as a liquid; then the Me_2SnI_2 crystallized in the still. It was removed by gently warming the various parts of the still with a Bunsen burner, so as to liquefy it. The Me_2SnI_2 was purified by recrystallization from *n*-hexane. A red-colored impurity which came over with the Me_3SnI, in one run, was discharged by shaking with mercury, followed by distillation. The Me_3SnI was a colorless liquid with a pungent odor, b.p. 170° at 735 mm., n^{25} 1.5728. The Me_2SnI_2 formed colorless crystals having a faint odor of chestnuts, m.p. 41.5–42.5°. No $SnMe_4$ or $MeSnI_3$ was found in an appreciable quantity.

The sample of $MeSnI_3$ was obtained from the Delta Chemical Company, New York. It was purified by recrystallization from absolute ethanol.

Raman Spectra.—The spectra were obtained with a Hilger E 612 glass spectrograph.[5,6] The spectra of $EtGeCl_3$, Et_2GeCl_2, Me_3SnI and Me_2SnI_2 were taken on Kodak 103-J plates, using the Hg 4358 Å. line for excitation, and a $NaNO_2$ filter. The spectra of SnI_4 and $MeSnI_3$ were taken on Kodak 103-E plates using a $NdCl_3$ filter, and the Hg 5461 Å. line for excitation.

The techniques used in obtaining the spectra of Me_2SnI_2, SnI_4 and $MeSnI_3$ require some comment. Me_2SnI_2 which is a solid at room temperature, was kept liquid by circulating water at 60° through the water jacket holding the Raman tube. It was found impossible to get optically blank melts, since the material slowly decomposed even at 60°. However, one plate which showed six skeletal lines, and one extra-skeletal line, was obtained.

The spectra of SnI_4 and $MeSnI_3$ were taken in solution. The sample of SnI_4 was recrystallized from benzene, and the sample of $MeSnI_3$ from absolute ethanol, and solutions prepared by the technique recently described.[6]

While optically blank solutions of SnI_4 in benzene or carbon disulfide were easily obtained, the SnI_4 decomposed so rapidly upon exposure to the exciting light, that no spectra could be obtained. Using a K_2CrO_4 filter to cut out light of shorter wave length than 5300 Å. was of no avail. That photochemical decomposition was involved was shown by exposing a sample of SnI_4 to ultraviolet light, part of the sample being shielded. After 12 hours, the color of the unshielded portion had changed visibly.

(5) E. R. Lippincott and M. C. Tobin, "The Thermodynamic Functions of Tin Tetramethyl and Germanium Tetramethyl," ONR Report No. 2, University of Connecticut, 1951.

(6) E. R. Lippincott and M. C. Tobin, *J. Chem. Phys.*, **21**, 1559 (1953).

Likewise, with solutions of $MeSnI_3$ in alcohol, no success was attained. No evidence of photosensitivity was visible, but background on the plate was so heavy as to completely obscure any Raman lines. It is believed that this background was due either to fluorescence of the compound, or to some fluorescent impurity.

Infrared Spectra.—Infrared spectra of Me_3SnI and Me_2SnI_2 were taken in the region 670–3700 cm.$^{-1}$ on a Beckman IR-2 recording infrared spectrometer.

Spectra of Me_3SnI were obtained in a 0.23-mm. cell. Strong bands were observed on a capillary film sandwiched between two rock salt plates.

Spectra of Me_2SnI_2 were taken of a sample melted on a rock salt plate and allowed to solidify. Spectra in the region 670–750 cm.$^{-1}$ were taken of a Nujol mull, due to the intensity of the band found in this region.

Me_3SnI and Me_2SnI_2.—The experimental results for these compounds are shown in Tables I and II. While only the skeletal frequencies show up clearly in the Raman spectrum for Me_2SnI_2, some extra-skeletal frequencies can be obtained from the infrared spectrum. As may be seen from Table III, making a complete assignment of frequencies is a matter of some difficulty, due to the large number of fundamentals in any one species. However, the skeletal frequencies of these compounds may be assigned quite readily, by analogy with the chloromethanes, etc.

TABLE I

OBSERVED RAMAN FREQUENCIES OF Me_3SnI AND Me_2SnI_2 IN CM.$^{-1}$

Me_3SnI		Me_2SnI_2
117(10)	1195(8)	65(3)
149(10)	1328(1)	145(3)
177(10)	1402(1)	182(10)
511(9)	2917(8)	197(5)
538(4)	2992(8)	513(10)
704(1)		544(8)
795(1)		1191(7)

TABLE II

OBSERVED INFRARED FREQUENCIES OF Me_3SnI AND Me_2SnI_2 IN CM.$^{-1}$

vs, very strong; s, strong; m, medium; w, weak; sh, shoulder.

Me_3SnI			Me_2SnI_2	
704 m	1310 sh w	1980 w	700 m	1051 w
714 m	1335 sh w	2770 w	715 s	1187 s
770 vs	1380 vs	2905 s	770 vs	1385 s
778 vs	1445 sh m	3000 s	775 vs	1691 s
785 vs	1600 vw	4100 m	787 vs	1738 s
1012 w	1700 s	4350 s	800 vs	2745 m
1075 vw	1740 s		1015 w	2900 s
1190 vs	1775 s		1042 w	3000 m

TABLE III

SELECTION RULES FOR Me_3SnI AND Me_2SnI_2

	Fundamentals Total	Skeletal		Fundamentals Total	Skeletal
	Me_3SnI			Me_2SnI_2	
A_1	8	3	A_1	9	4
A_2	4	0	A_2	5	2
E	12	3	B_1	7	1
			B_2	6	2

The skeletal modes of Me_3SnI, on the basis of a C_{3v} symmetry, should have three vibrations of species A_1, and three of species E. The A_1 frequencies should correspond to Sn–C stretching, Sn–I stretching and C–Sn–C bending. The E modes should correspond to Sn–C stretching, C–Sn–C bending and C–Sn–I bending. By analogy with $SnMe_4$ and assuming both C–Sn–C vibrations to be piled up at 149 cm.$^{-1}$, we can assign 538 cm.$^{-1}$ to E, 511 cm.$^{-1}$ to A_1 and 149 cm.$^{-1}$ to A_1 and E. This leaves 177 cm.$^{-1}$ to be assigned to the A_1 Sn–I stretching, and 117 cm.$^{-1}$ to the E C–Sn–I bending.

The interpretation of the skeletal frequencies of Me_2SnI_2 is somewhat more difficult, as only six of the nine expected lines are observed. While a line could easily have been missed, the spectrum will be interpreted on the assumption that it is complete, and that the small number of lines is due to piling up of frequencies. This assumption could be checked either by a normal coördinate analysis, using force constants obtained from Me_4Sn and Me_3SnI, or by a comparison with the spectra of Me_2SnBr_2, when such becomes available.

By analogy with dichloromethane, there should be two Sn–C stretchings, one of species A_1, and one of species B_1, and two Sn–I stretchings, of species A_2 and B_2. These are easily assigned as shown in Table IV.

TABLE IV

ASSIGNMENT OF FREQUENCIES FOR Me_2SnI_2

	Frequency, cm.$^{-1}$	Assignment	Type of vibration
1	3000	A_1	ν (CH_3)
2	2900	A_1	ν (CH_3)
3	1385	A_1	δ (CH_3)
4	1187	A_1	δ (CH_3)
5	715	A_1	CH_3 rocking
6	513	A_1	ν (SnC)
7	182	A_1	ν (SnI)
8	145	A_1	δ (Sn–C_2)
9	65	A_1	δ (Sn–I_2)
10	3000	A_2	ν (CH_3)
11	1385	A_2	δ (CH_3)
12	800	A_2	CH_3 rocking
13	65	A_2	Twist
14	..	A_2	CH_3 torsion
15	3000	B_1	ν (CH_3)
16	2900	B_1	ν (CH_3)
17	1385	B_1	δ (CH_3)
18	1187	B_1	δ (CH_3)
19	800	B_1	CH_3 rocking
20	544	B_1	ν (Sn–C)
21	145	B_1	Rocking
22	2900	B_2	ν (CH_3)
23	1187	B_2	δ (CH_3)
24	715	B_2	CH_3 rocking
25	197	B_2	(Sn–I)
26	145	B_2	Rocking
27	..	B_2	CH_3 torsion

This leaves five vibrational modes to be assigned to two observed frequencies, at 65 and 145 cm.$^{-1}$. The A_1 I–Sn–I bending may be assigned to 65 cm.$^{-1}$, and the A_1 C–Sn–C bending to 145 cm.$^{-1}$. This leaves three I–Sn–C bending modes, of species B_1, B_2 and A_2 to be assigned. While the assignment of these is somewhat uncertain, the A_2 frequency, corresponding to torsion of the C–Sn–C and I–Sn–I planes with respect to each other, may be

assigned to 65 cm.$^{-1}$, and the two rocking frequencies of species B_1 and B_2, to 145 cm.$^{-1}$.

The assumption of this distribution of piling up is supported by the spectra of CCl_2Br_2 and $SiCl_2Br_2$.[7] In these compounds, the two lowest frequencies are quite close together, while the next three highest, while far from the two lowest, are quite close to each other. The separation of the two groups, however, is not quite so sharp in $SiCl_2I_2$.

The assignment of the extra-skeletal frequencies is more ambiguous than that of the skeletal frequencies, but is needed for such purposes as the calculation of thermodynamic functions. For such calculations we have given a tentative assignment of frequencies for both tin trimethyl iodide and tin dimethyl diiodide in Tables IV and V, respectively.[8]

TABLE V

ASSIGNMENT OF FREQUENCIES FOR Me_3SnI

	Frequency, cm.$^{-1}$	Assignment	Type of vibration
1	2992	A_1	ν (CH_3)
2	2917	A_1	ν (CH_3)
3	1328	A_1	δ (CH_3)
4	1195	A_1	δ (CH_3)
5	704	A_1	CH_3 rocking
6	511	A_1	ν (Sn–C)
7	177	A_1	ν (Sn–I)
8	149	A_1	δ (SnC_3)
9	(2992)	A_2	ν (CH_3)
10	(1402)	A_2	δ (CH_3)
11	(795)	A_2	CH_3 rocking
12	..	A_2	CH_3 torsion
13	2992	E	ν (CH_3)
14	2992	E	ν (CH_3)
15	2917	E	ν (CH_3)
16	1402	E	δ (CH_3)
17	1328	E	δ (CH_3)
18	1195	E	δ (CH_3)
19	795	E	CH_3 rocking
20	704	E	CH_3 rocking
21	538	E	ν (Sn–C)
22	149	E	δ (SnC_3)
23	117	E	Rocking
24	..	E	CH_3 torsion

Et_2GeCl_2 and $EtGeCl_3$.—As was stated above, the spectra of the ethyl germanium chlorides will be complicated by several phenomena. As a first-order approximation, these compounds may be considered as freely rotating ethyl tops[9] attached to a rigid frame.[1] To this approximation, $EtGeCl_3$ may be considered as having C_{3v}, and Et_2GeCl_2 may be considered as having C_{2v} symmetry. The degenerate modes of vibration characteristic of ethane will, of course, be split even in this approximation, although the splitting may not always be experimentally observable.

A further complication arises from the fact that some of the low-lying extra-skeletal modes will lie in the region in which the skeletal modes lie, and must be sorted from these.

(7) M. Delwaulle, THIS JOURNAL, **56**, 355 (1952).

(8) M. C. Tobin, *J. Am. Chem. Soc.*, **75**, 1788 (1953).

(9) The situation is further complicated, of course, by the fact that in the ethyl residue, the end methyl group can be considered as a top rotating with respect to the remainder of the molecule.

The observed Raman spectra of $EtGeCl_3$ are given in Table VI. For comparison the observed skeletal frequencies of $GeMe_4$[6] and $GeCl_4$ are given in Table VII.[5]

TABLE VI

OBSERVED RAMAN SPECTRA OF $EtGeCl_3$ AND Et_2GeCl_2

$EtGeCl_3$		Et_2GeCl_2	
112 (0)	986 (1)	155 (5)	985 (1)
136 } (2)	1022 (1)	165 (1) shoulder	1024 (3)
150 } (3)	1160 } (4)	275 } (3)	1134 (0)
174 (4)	1168 } (4)	288 } (3)	1148 (0)
295 (6)	1228 (5)	320 (2)	1229 (10)
333 (2)	1400 (1)	370–406 (8)	1385 (0)
397 (10)	1458 (3)	Max. at 376	1459 (6)
425 (5) br	2925 } (5)	561 (6)	2924 (8)
596 (8)	2935 } (5)	605 (4)	2942 (4)
970 (1)	2968 (4)	965 (1)	2972 (7)

TABLE VII

ASSIGNMENT OF SKELETAL FREQUENCIES OF $GeCl_4$ AND $GeMe_4$

	$GeCl_4$	$GeMe_4$
E	132	175
F_2	171	195
A_1	397	558
F_2	451	595

The line at 596 cm.$^{-1}$ may reasonably be assigned to the A_1 C–Ge stretching corresponding to the 595 cm.$^{-1}$ line in Me_4Ge.

By analogy with $GeCl_4$ we may assign 425 cm.$^{-1}$ to the E Ge–Cl stretching, and 397 cm.$^{-1}$ to the A_1 Ge–Cl stretching. We may likewise assign 174 cm.$^{-1}$ to the A_1 Cl–Ge–Cl bending, 136 cm.$^{-1}$ to the E Cl–Ge–Cl bending, and 150 cm.$^{-1}$, since it is intermediate between Cl–Ge–Cl bending and C–Ge–C bending to the E C–Ge–Cl bending.

This completes the assignment of the expected skeletal frequencies, but fails to account for the observed frequencies at 112, 295 and 333 cm.$^{-1}$. The assignment of these frequencies can be at best an enlightened guess.

It seems reasonable to assign 333 cm.$^{-1}$ to C–C–Ge bending, by analogy with the 375 cm.$^{-1}$ frequency in propane. 295 cm.$^{-1}$ may well be assigned to the H–C–C–H torsion, estimated to lie at 275 cm.$^{-1}$ in ethane, while 112 cm.$^{-1}$ may be a C–C–Ge–Cl torsion.

The observed spectra of Et_2GeCl_2 are given in Table VI. The lines at 605 and 561 cm.$^{-1}$ are readily assigned to the B_1 and A_1 C–Ge stretching frequencies, respectively. The broad line from 370–406 cm.$^{-1}$ is definitely asymmetric, with maximum density at 376 cm.$^{-1}$. We may therefore assign the A_1 Ge–Cl stretching to 376 cm.$^{-1}$, and the B_2 Ge–Cl stretching to 395 cm.$^{-1}$. The broad band at 155 cm.$^{-1}$ has a weak shoulder on the long wave length side at 165 cm.$^{-1}$. To these two bands must be assigned the A_1 Cl–Ge–Cl and C–Ge–C bendings, and the A_2, B_1 and B_2 C–Ge–Cl bendings. Although the assignment must of necessity be uncertain, we may tentatively assign the Cl–Ge–Cl bending and the A_2 torsion to 155 cm.$^{-1}$, and the C–Ge–C bending and the B_1 and B_2 rockings to 165 cm.$^{-1}$. This radical piling up is not unexpected, in view of the fact that, by analogy with Me_4Ge, $GeCl_4$

and $EtGeCl_3$, the expected range for the skeletal bendings of all types is 150–175 cm.$^{-1}$. Again, a Raman line could be too weak to show up.

The line at 320 cm.$^{-1}$ may, as was 333 cm.$^{-1}$ in $EtGeCl_3$, be ascribed to C–C–Ge bending. However, instead of having a single line at 295 cm.$^{-1}$, as in $EtGeCl_3$, we now have two lines, at 275 and 288 cm.$^{-1}$. These may tentatively be ascribed to symmetric and asymmetric torsions of the H–C–C–H angles in the two ethyl groups. The non-appearance of the 112 cm.$^{-1}$ line in Et_2GeCl_2 may be ascribed to the hindrance of this mode by steric effects, if it indeed corresponds to the C–C–GeCl torsion.

The extra-skeletal frequencies for both compounds are closely similar. They fall roughly into three classes: C–C stretching and H–C–C bending, 900–1100 cm.$^{-1}$, H–C–H bending, 1100–1500 cm.$^{-1}$ and C–H stretching, 2900–3000 cm.$^{-1}$. These assignments are tabulated in Table VIII.

It seems worth while to make some comments on the interaction of the ethyl groups with the frame of the molecules. As is apparent from the discussion above, the ethyl groups have little effect on the frame vibrations, and the skeletal spectra are readily interpreted in terms of the $CGeCl_3$ and C_2GeCl_2 frames. The symmetry of the ethyl groups, however, is reduced from the D_{3d} symmetry of free ethane, to C_s. In consequence, the A_{1u} species is activated, and the degenerate modes are split. This accounts for the appearance of the line at 295 cm.$^{-1}$ in $EtGeCl_3$.

If the assignments proposed for the lines at 112 and 295 cm.$^{-1}$ in $EtGeCl_3$ are correct, we may assume that there is a small interaction between the ethyl group and the frame, on one hand and, in Et_2GeCl_2, between the two ethyl groups on the other hand.

Table VIII

Assignment of Low Frequencies for Et_2GeCl_2 and $EtGeCl_3$

	Frequency, cm.$^{-1}$	Assignment	Type of vibration
		$EtGeCl_3$	
	112		τ (C–C–Ge–Cl)
ν_6	136	E	δ (Cl–Ge–Cl)
ν_5	150	E	δ (C–Ge–Cl)
ν_3	174	A_1	δ (Cl–GeCl)
	295		τ (H–C–C–H)
	333		δ (C–C–Ge)
ν_2	397	A_1	ν (Ge–Cl)
ν_4	425	E	ν (Ge–Cl)
ν_1	596	A_1	ν (Ge–C)
		Et_2GeCl_2	
ν_5	155	A_2	Twist
ν_4	155	A_1	δ (Cl–GeCl)
ν_7	165	B_1	Rocking
ν_3	165	A_1	δ (C–Ge–C)
ν_9	165	B_2	Rocking
	275		τ (H–C–C–H)
	288		τ (H–C–C–H)
	320		δ (C–C–Ge)
ν_2	376	A_1	ν (Ge–Cl)
ν_8	395	B_2	ν (Ge–Cl)
ν_1	561	A_1	ν (C–Ge)
ν_6	605	B_1	ν (C–Ge)

If this is the case, the skeletal lines in $EtGeCl_3$ corresponding to the E vibrations are in reality unresolved doublets. The breadth of the line at 425 cm.$^{-1}$ suggests that this might be the case. Any definite conclusion, however, must await further study with high dispersion spectrographs.

The authors wish to acknowledge financial support from the office of Naval Research Contract M 8 onr-72700.

AN APPLICATION OF THE ABSOLUTE RATE THEORY TO PHASE CHANGES IN SOLIDS[1]

By F. Wm. Cagle, Jr., and Henry Eyring

Department of Chemistry and Institute for Rate Processes, University of Utah, Salt Lake City 1, Utah

Received April 16, 1953

A theory for phase transitions in solids, based on the absolute reaction rate theory, has been developed. It has been applied quantitatively to the transition of white to gray tin. This theory leads to the interpretation that only where growth lines for white tin cross those for grey tin can the transition occur. As might be expected, such crossing points are exceptionally rare and account for most of the slowness of the transition. The transformation of monoclinic to orthorhombic sulfur has also been discussed in terms of the theory. The effect of external constraints, especially pressure, has been considered both upon the thermodynamics and upon the kinetics of such transformations.

Introduction

Quite aside from the enormous practical interest attached to phase changes in solids, one readily observes that at least in the case of pure solids, these changes permit a study of a one-component reaction which occurs at an interface between phases. It is, of course, of primary importance to examine carefully such systems, which on account of their relative simplicity, are able to provide information concerning the nature of the activated complex.

We consider first the β- to α-tin transition. This system undergoes transition at a convenient temperature and therefore has been the subject of numerous investigations. While most of these investigations were undertaken to elucidate the thermodynamic relationship of the system, some are concerned with the kinetics of the reaction.

(1) This paper was presented on July 14 at the 1952 Gordon Conference on Physics and Chemistry of Metals, New Hampton, New Hampshire.

The enantiotropic transformation of tin occurs slightly under room temperature. White tin is the β-form and crystallizes in the tetragonal system (a_0 = 5.822 Å., c_0 = 3.165 Å.).[2] The α- or grey form is stable at lower temperatures and has the diamond structure (a_0 = 6.46 Å.).[3,4] The exact temperature of transformation is uncertian but is given as 18° by Cohen and Van Eijk[5] or 13.2° by Cohen and van Lieshout.[6]

The great disparity between the densities of α-tin (5.75 g./cc.) and β-tin (7.30 g./cc.) indicates that the transformation would cause the failure of any item made of tin. In fact, the name of the transformation β-tin → α-tin (tin disease) is derived from the pustules of grey tin which spread over the surface of the metal undergoing this phase change. Since tin alloys are much used as solder and are observed to undergo phase change in very cold climates, a study of this phenomenon is of practical value.

Theoretical

Experimental studies of the kinetics of the transformation

$$\mathrm{Sn(w)} \underset{k_2'}{\overset{k_1'}{\rightleftharpoons}} \mathrm{Sn(g)} \qquad (1)$$

have been made by Cohen and Van Eijk,[5] Cohen and van Lieshout,[6] Jänecke[7] and Tammann and Dreyer.[8] An equation for the rate of transformation of grey and white tin was proposed by Stepanoff.[9] While the equation developed gives calculated rates in good agreement with experimental values, it does not seem possible to interpret it in terms of the molecular processes which occur. It was, therefore, decided to investigate this transformation with a view toward the application of the theory of absolute reaction rates. This treatment has the advantage of being interpretable in terms of molecular processes.

Tammann and Dreyer[8] investigated the growth of pustules of grey tin on a white tin matrix at various temperatures. These studies were made on a tin surface in contact with the atmosphere and on a surface immersed in a solution of ammonium chlorostannate. They observed that the rate of increase of the radius of the pustule was constant at a fixed temperature, and that when inoculated at a point with a small crystal of grey tin, the growth occurred from the point of inoculation. In view of this and equation 1, we may write the rate of increase of radius as

$$\frac{dr}{dt} = \bar{X}\lambda(k_1' - k_2') \qquad (2)$$

In this expression, λ is the average distance from one white tin atom to its neighbor and $\bar{X}$ represents the mole fraction of white tin atoms at an interface which are so located that they may react. The rate constants may now be written in terms of the absolute reaction rate theory

$$k' = \frac{\mathfrak{K}kT}{h}\frac{f^{\ddagger}}{f_i}\exp(-E^{\circ}/RT) \qquad (3)$$

The absolute rate constant is given by k', while $\mathfrak{K}$ is the transmission coefficient; k, Boltzmann's constant; T, the absolute temperature; h, Planck's constant; $f^{\ddagger}$, the partition function for the activated state; f_i the partition function for the initial state; E^0, the energy to go from the ground state to the activated state at the absolute zero; and R, the gas constant. There is one less degree of freedom in $f^{\ddagger}$ than in f_i since that degree has gone into the translation in the direction of the reaction coördinate and is included in $\mathfrak{K}kT/h$. Rigorously, the tin sample should be treated as a single giant molecule when writing $f^{\ddagger}/f_i$ for the transition process. However, degrees of freedom, remote from the reaction site, are the same in the initial and activated state and so their partition functions cancel. The practical question of how many degrees of freedom need be retained, remains.

For a crystalline solid, the degrees of freedom of each atom are given in the partition function as the product of the vibrational contributions, so that we may write these in the form

$$f_{\mathrm{ivib}} = [1 - \exp(-\theta/T)]^{-1} \qquad (4)$$

Where θ is the Einstein temperature for the material in question, all of the quoted characteristic temperatures in this paper are for Einstein partition functions. The Einstein temperatures are appropriate for temperatures not too far removed from the melting point. In the range with which we are interested, the use of Einstein temperatures should not give rise to serious error. This has been discussed by Guggenheim.[10]

It is possible to write equation 2 as

$$\frac{dr}{dt} = \bar{X}\lambda\frac{\mathfrak{K}kT}{k}\left\{\frac{f^{\ddagger 3n-1}}{f_w^{3p} f_G^{3(n-p)}}\exp(-E_w^0/RT) - \frac{f^{\ddagger 3n-1}}{f_w^{3(p-1)} f_G^{3(n-p+1)}}\exp(-E_G^0/RT)\right\} \qquad (5)$$

or

$$\frac{dr}{dt} = \bar{X}\lambda\frac{\mathfrak{K}kT}{h}\frac{f^{\ddagger 3n-1}}{f_w^{3p} f_G^{3(n-p)}}\exp(-E_w^0/RT)\{1 - K^{-1}\} \qquad (6)$$

where

$$K^{-1} = \frac{f_w^3}{f_G^3}\exp(E_w^0 - E_G^0/RT) \qquad (7)$$

In the case at hand, the activated complex consists of n atoms and of these p, in the initial state, were white tin. The Debye temperatures (from which Einstein temperatures can be determined since $\theta_E = {}^3/_4\,\theta_D$) have been calculated for white and grey tin by Brönsted[11] from specific heat data. For white tin, one obtains θ = 148, and for grey tin, the value of θ is 190. Since the reaction proceeds at the

(2) A. J. Bijl and N. H. Kolkmeyer, *Chem. Weekblad*, 18, 1077, 1264 (1918).

(3) W. C. Phebus and F. C. Blake, *Phys. Rev.*, 25, 107 (1925).

(4) P. P. Ewald and C. Hermann, *Strukturbericht.*, 1, 54 (1913-1928).

(5) E. Cohen and C. Van Eijk, *Z. physik. Chem.*, 30, 601 (1899).

(6) E. Cohen and A. K. W. A. van Lieshout, *Z. physik. Chem.*, [A] 173, 23 (1935).

(7) E. Jänecke, *ibid.*, 90, 257, 313 (1915).

(8) G. Tammann and K. L. Dreyer, *Z. anorg. allgem. Chem.*, 199, 97 (1931).

(9) N. I. Stepanoff, *Ann. Inst. Phys. Chem. (Leningrad)*, 2, 500 (1924).

(10) E. A. Guggenheim, "Thermodynamics," Interscience Publishers, Inc., New York, N. Y., 1949, p. 118, *et seq.*

(11) J. N. Brönsted, *Z. physik. Chem.*, 88, 479 (1914).

surface, it might be supposed that the Einstein temperatures should be for a surface atom and that this is the true initial state. However, the transformation of a surface atom must make another surface atom of one which was in the bulk of the metal. Thus, the initial state consists of normal atoms and the usual Einstein temperature should be used. From heat capacity data and an observed value of the heat of transformation of tin, Brönsted gave the value of $E_w^0 - E_g^0$ (the energy of transformation at the absolute zero) as 371 cal./g. mole. The possible error in this datum cannot be easily stated since it depends upon a measured heat of transformation whose value is only approximately known.

Figure 1 represents diagrammatically the situation prevailing for opposing reactions. The rate of both is, of course, nil at the absolute zero, and the difference between the two rates reaches a maximum at temperature T_1. The difference in rates becomes zero at the transition temperature where the two rate *vs.* temperature curves cross.

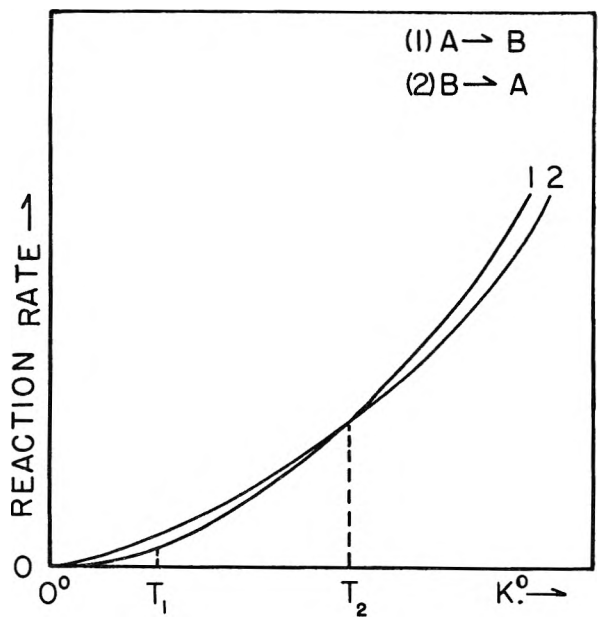

Fig. 1.—Reaction rate *vs.* Kelvin temperature for the reaction A ⇆ B.

From the transition temperature and equation 6, one may calculate a value of $E_w^0 - E_g^0$, the necessary characteristic temperatures being known. At this temperature $dr/dt = 0$. The values obtained are 312 cal./g. mole for a transition temperature of 13.2° and 323 for a transition temperature of 18°. The latter value has been used in the numerical calculations for this work.

A comparison of the experimental values for the rate of formation of grey tin by Cohen and Van Eijk[5] and those of Tammann and Dreyer[8] indicates considerable dependence upon the actual sample of tin used. For example, the temperature at which the conversion proceeds at a maximum rate is given as −50° by Cohen and as −30° by Tammann.

In Fig. 2, the calculations for one atom (curve 1) and three atom (curve 2) activated complexes are

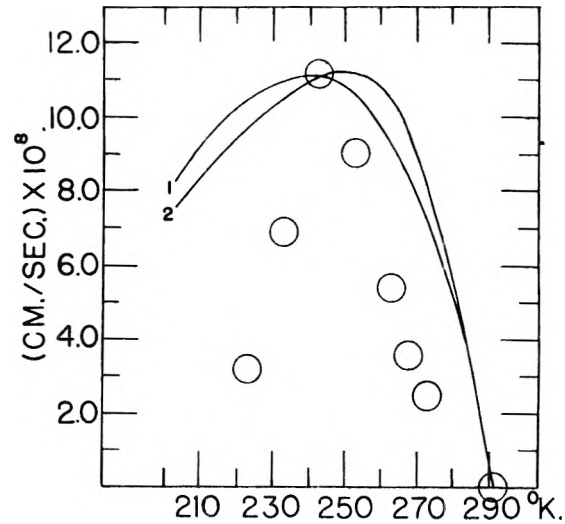

Fig. 2.—Comparison of the experimental data of Tammann with the theoretical curve calculated from equation 6. Curve 1 is for a one atom activated complex and curve 2 is for a three atom complex.

compared with the experimental data of Tammann and Dreyer.[8] The value of the characteristic temperature for the tin atoms in the activated state was taken to be 100. This is in accord with the expected lower vibrational frequency than for either white or grey tin. In any event, this parameter can be varied considerably without great effect on the calculated value of dr/dt. For curve 1, the value of E_w^0 is 2,000 cal./g. mole and the value of $\bar{X}$ is 3.98×10^{-10}. For curve 2, the value of E_w^0 is 2,000 cal./g. mole and $\bar{X}$ is 4.16×10^{-11}.

Figure 3 shows a comparison of some five atom complexes with the experimental data. Curve 1 represents the complex of four white tin atoms and one grey tin atom going to two grey tin atoms and three white tin atoms. The value of E_w^0 is 2,000 cal./g. mole and $\bar{X} = 6.87 \times 10^{-12}$. The curve for the three–two complex is not distinguishable from

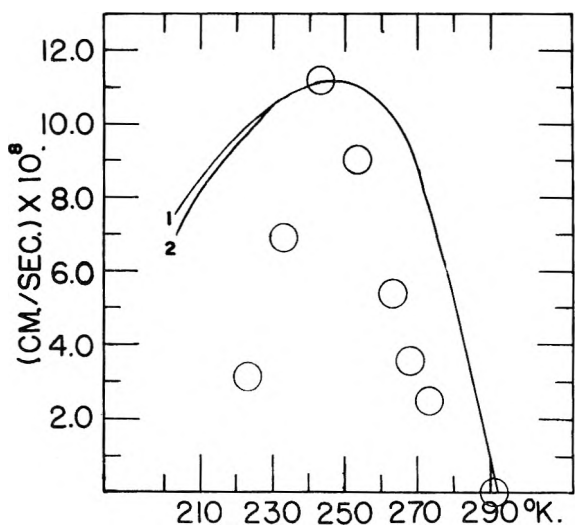

Fig. 3.—Comparison of the experimental data of Tammann with the theoretical curve calculated from equation 6. Curve 1 is for a five atom activated complex. Curve 2 was calculated with two very weak vibrational frequencies for the atom which transitions (θ = 25).

1 when plotted on this scale. In the case of curve 2 of this figure, the atom making the transition was presumed to have two weak vibrations and these were taken to correspond to $\theta = 25$. It will be noted that this depressed the low temperature end of the curve only slightly.

The three curves of Fig. 4 result from assuming an eight-atom activated complex (five white tin and three grey tin atoms changing over to four white tin and four grey tin atoms). The value of E_w^0 is 2,000 cal./g. mole and the values of $\bar{X}$ are 1.55×10^{-13}, 1.24×10^{-13} and 0.93×10^{-13} for curves 1, 2 and 3, respectively.

In estimating the degree of agreement between theory and experiment, it should be observed that the graphs are very sensitive tests since the rates are plotted rather than the logarithms of the rate constants as is often done.

It is interesting to consider the probable physical significance of these small values for the mole fraction of tin atoms which are in a position to undergo this transition. It is not to be expected that the average atom in the center of a completed face can undergo transition across the interface to the other phase. The hole left by its departure would be unstable and would immediately be refilled by a return of the wandering atom. Only the last atom added to a line advancing across the face of a growing crystal is a likely candidate for migration. Such an atom migrates along this line to a point where it is opposite an analogous line on the face of the other phase. At this point the atom crosses the interface and identifies itself with the new phase. Such crossing points where the advancing lines on each of the two phases pass by each other will at best provide only a very few transition points per square centimeter. It will equal the product of the number of lines per centimeter in each phase at the interface which make contact. Thus, a value of $\bar{X}$ of 1.24×10^{-13} when multiplied by 10^{15}, the approximate number of atoms per square centimeter yields 124 such crossing points per square centimeter and suggests that on the average the growth lines, making successful contacts, average about a millimeter apart on each phase.

One may now equally well write equation 6 in the form

$$\frac{dr}{dt} = \bar{X}\lambda k'_1(1 - K^{-1}) \qquad (6a)$$

From the previous calculations, one may evaluate $\Delta H^{\pm}$ for the rate at which white tin goes to grey tin and one obtains 2,600 cal./g. mole. Fensham has measured the Arrhenius activation energy for self-diffusion in tin crystals.[12] He found, for self-diffusion along the a-axis, a value of $E = 5{,}900$ cal./g. mole. This would correspond to a $\Delta H^{\pm}$ of 5,000 cal./g. mole. One would expect, since the processes are similar, that the $\Delta H^{\pm}$ values would not be very different and in the observed direction. Fensham also comments that generally the diffusion at grain boundaries is more rapid than bulk diffusion, though no numerical data are given by him on this point.[13]

(12) P. J. Fensham, *Australian J. Sci. Research*, **A3**, 91 (1950).
(13) P. J. Fensham, *ibid.*, **A3**, 105 (1950).

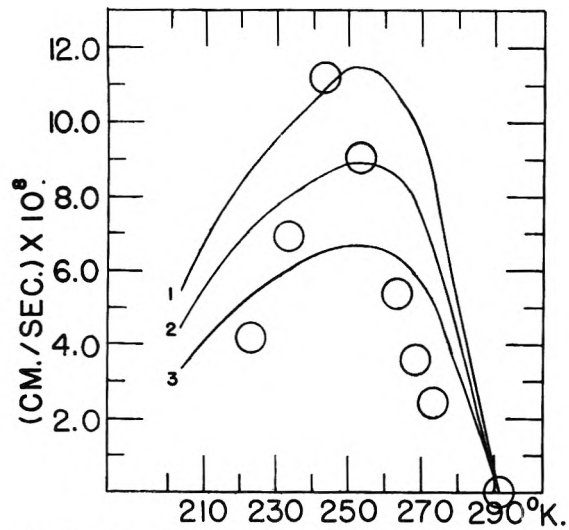

Fig. 4.—Comparison of the experimental data of Tammann with the theoretical curve calculated from equation 6. Curves 1, 2 and 3 are for an eight atom activated complex. For curves 1, 2 and 3 $\bar{X}$ is equal to 1.55×10^{-13}, 1.24×10^{-13} and 0.93×10^{-13}, respectively.

Frye, Stansbury and McElroy[14] have given a very interesting treatment of the rate of growth of pearlite in high purity Fe–C alloys which parallels, in part, the above treatment.

The transition of rhombic (α) to monoclinic (β) sulfur occurs at 368.6°K. It has been frequently studied and several measurements of the rate are reported.[15–18]

From the specific heat data of Eastman and and McGavock,[19] one may calculate the Einstein temperature of 298 for the orthorhombic modification and 294 for the monoclinic modification of sulfur. These data, together with the transition temperature permit the evaluation of the term $(1 - K^{-1})$ in equation 6. The actual rate of transition, however, is quite dependent upon previous treatment of the sample.

Elias, Hartshorne and James[18] have reported a value of E_{exp} for the transition of β- to α-sulfur with observations at 293, 303 and 313°K. This gives a value for $\Delta H^{\pm}$ of 14,400 cal./g. mole. In view of the dependence of rate on previous thermal history, it does not seem that sufficient data are available to evaluate the constants of equation 6. It should be noted, however, that the effect of temperature on rate is known qualitatively to be of the form expected from this relation. This dependence of observed rate on thermal history suggests that previously formed nuclei probably persist and much affect the observed rate.

The work of Hartshorne, Walters and Williams[20]

(14) The article, "Absolute Rate Theory Applied to Rate of Growth of Pearlite," by J. J. Frye, Jr., E. E. Stansbury and D. L. McElroy will be published in *Trans. A.I.M.E.*, **197** (1953), and has been preprinted in *J. of Metals* (February, 1953, p. 219).
(15) D. Gernez, *Compt. rend.*, 100, 1343, 1382 (1885).
(16) D. Lehmann, "Molecularphysik," Vol. 1, 1888, p. 179.
(17) W. Fraenkel and W. Goez, *Z. anorg. Chem.*, 144, 45 (1925).
(18) P. G. Elias, N. H. Hartshorne and J. E. D. James, *J. Chem. Soc.*, 588 (1940).
(19) E. D. Eastman and W. C. McGavock, *J. Am. Chem. Soc.*, **59**, 145 (1937).
(20) N. H. Hartshorne, G. S. Walters and W. O. M. Williams, *J. Chem. Soc.*, 1860 (1935).

on the transformation of α- into β-*o*-nitroaniline provides a study of a monotropic system. They studied this conversion in the temperature range 273 to 313°K. They observed an experimental energy (Arrhenius) of activation which is 17,300 cal./g. mole. and corresponds to $\Delta H^{\ddagger} = 16{,}700$ cal./g. mole. As they point out, this is very close to the measured heat of sublimation (19,000 cal./g. mole for the β-form) and the transformation proceeds essentially through the vapor phase. Their work also includes an instructive theoretical consideration of this process.

It is instructive to examine equation 6a for the case of applied stresses. The case we shall consider is that of a pV term. This equation should then be written

$$\frac{dr}{dt} = \bar{X}\lambda k'_1 \exp\left[-(p-1)\Delta V^{\ddagger}/RT\right] \{1 - K^{-1}\exp\left[(p-1)\Delta V/RT\right]\} \quad (8)$$

The term $\Delta V^{\ddagger}$ is the change in volume in going to the activated state and the term ΔV is the change in volume per mole of the products less the reactants. It should be noted that these terms may oppose each other. An example is the graphite → diamond transition. In this case the equilibrium is displaced in favor of diamond by high pressures but the term $\Delta V^{\ddagger}$ is large and positive so that the rate of the transition is reduced by increasing pressure.[21-23]

Another case similar to the above may be formulated about the well-known recrystallization often observed in metals. In this case, the larger grains of the metal grow at the expense of smaller ones. The driving energy is the high surface energy of the grains and the reaction goes in such a way as to yield large grains, thus minimizing the number of surface atoms and so the surface energy of the grains.

Acknowledgment.—This research was supported by the Office of Naval Research under Contract N7-onr-45101, Project Number NR-032-168 with the University of Utah. We wish to express our thanks for this support.

(21) P. W. Bridgman, *J. Chem. Phys.*, 15, 92 (1947).
(22) D. P. Mellor, *Research*, 2, 314 (1949).
(23) H. Eyring and F. Wm. Cagle, Jr., *Z. Elektrochem.*, 56, 480 (1952).

THE THERMAL TRANSFORMATIONS OF THE ALUMINAS AND THEIR HYDRATES

By M. K. B. Day and V. J. Hill

Research Laboratories, The British Aluminum Co., Ltd., Chalfont Park, Gerrards Cross, Bucks, England

Received April 18, 1953

It has been concluded that the monohydrate böhmite, encountered in the dehydration of both gibbsite and bayerite, is produced by secondary reactions between the original dehydration products, which are virtually anhydrous aluminas, and the water which is released during the dehydration. Bayerite and böhmite yield on calcination γ-Al_2O_3 which gives rise to the δ-, θ-, α-forms of anhydrous alumina. Gibbsite dehydrates primarily to χ-Al_2O_3 which on further calcination passes through κ-Al_2O_3 to the stable α-form. In practice, however, the occurrence of a secondary reaction between χ-Al_2O_3 and water leads to the formation of some böhmite so that on subsequent calcination mixtures of the two series of anhydrous aluminas are obtained.

Although considerable attention has been devoted in recent years to the study of the different forms of alumina and its hydrates, the literature is still confused, particularly in the interpretations made of the relationships existing between the hydrated and anhydrous forms.

In a previous note[1] we concluded that the initial product of the dehydration of either trihydrate is an anhydrous oxide, χ in the case of gibbsite and γ in that of bayerite, both oxides being capable of undergoing rehydration. Our conclusions were embodied in the diagram reproduced below showing an idealized alumina–water system. It will be seen from the diagram that the apparent complications associated with the calcination of gibbsite result from the formation of böhmite, by a secondary reaction, which gives rise to a separate and distinct series of anhydrous products.

Brown, Clark and Elliott[2] have since come to a somewhat similar conclusion relating to the origin of the two series of anhydrous products. They postulate, however, that gibbsite decomposes through two routes, either *via* böhmite or χ-alumina, without there being a full understanding of the factors controlling such a decomposition.

The purpose of this paper is to amplify the information given in our previous publication, and to demonstrate that the dehydration processes are, in themselves, fundamentally simple, confusion only arising through the occurrence of secondary reactions. It is, incidentally, shown that the hypothesis of two routes for the initial decomposition of gibbsite or of böhmite is unnecessary.

A convenient and informative approach to the study of the interrelationships existing between true hydrates and their corresponding oxides is to investigate the pressure–temperature relationship during the dehydration of the hydrates. Thus Milligan[3] obtained a dehydration isobar for a gibbsite, prepared by the Bayer process, which indicated marked instability of the trihydrate phase at about 145° at ordinary atmospheric pressure and humidity. Dehydration proceeded smoothly until the system approached the composition of a hemihy-

(1) M. K. B. Day and V. J. Hill, *Nature*, 170, 539 (1952).
(2) J. F. Brown, D. Clark and W. W. Elliott, *J. Chem. Soc.*, 84 (1953).
(3) L. H. Milligan, This Journal, 26, 247 (1929).

drate. Weiser and Milligan[4] reported a similar curve for a synthetic gibbsite, the dehydration continuing smoothly to a composition of $Al_2O_3 \cdot 0.35\text{-}H_2O$. In neither case did an inflection reveal the presence of a monohydrate. The product gave, however, an X-ray diffraction pattern characteristic of the monohydrate böhmite which persisted until the dehydration had been carried to 400°. The isomer, bayerite, gave a similar dehydration isobar, the temperature at which decomposition occurred being somewhat lower than that for gibbsite. The present authors have carried out dehydrations of these hydrates in a vacuum and have confirmed the observations of Weiser and Milligan.

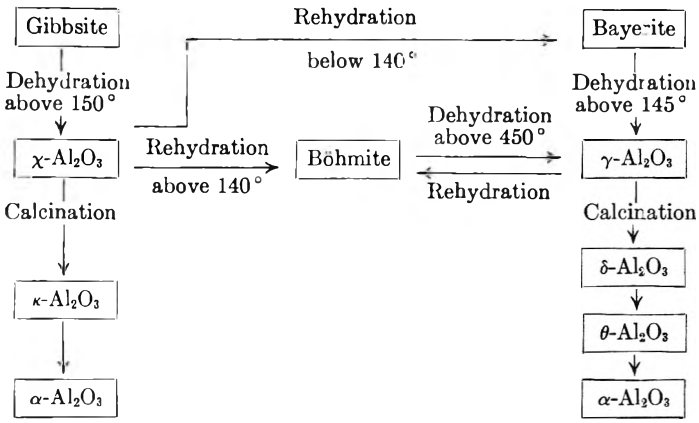

Fig. 1.—Idealized alumina–water system.

The presence of böhmite in the dehydration product, and the absence of an inflection in the dehydration isobar at the böhmite composition may be explained in a number of ways.

Weiser and Milligan attributed the absence of an inflection in the isobar to the formation of an intermediate colloidal phase of böhmite which is able to lose water below the true decomposition temperature of the mass of the hydrate. A second explanation of the absence of the inflection at the monohydrate stage and the incompleteness of dehydration, is that the trihydrate dehydrates directly to an anhydrous alumina, which adsorbs water and subsequently partially rehydrates to böhmite. Some support for this argument is available from the work of Bentley and Feachem[5] who demonstrated that an anhydrous alumina was capable of rehydration in steam to böhmite. If this is the mechanism of the dehydration, then the proportion of böhmite in the product would be influenced by the conditions of the dehydration, *i.e.*, those favoring adsorption would lead to a higher concentration of böhmite in the dehydration product. Certainly the dehydration of gibbsite in a closed system leads to a greater yield of böhmite than is obtained under vacuum conditions. The results of X-ray crystallographic examination of the products of the dehydrations and subsequent calcinations allow a discrimination between the two dehydration mechanisms just discussed.

Recent investigations of the phase transformations occurring during the thermal decomposition of alumina hydrates have shown that a series of distinct changes in crystal structure are associated with the crystal growth which takes place prior to the formation of the stable α-Al_2O_3 or corundum. Rooksby[6] identified several anhydrous forms and reported that the initial products of the dehydration of either gibbsite or bayerite, *i.e.*, böhmite and γ-Al_2O_3, were converted entirely to γ-Al_2O_3 on subsequent calcination, and this then passed through crystal forms designated δ-Al_2O_3 and θ-Al_2O_3 before ultimately yielding α-Al_2O_3. Stumpf, Russell, *et al.*,[7] although employing a different nomenclature, confirmed that these transformations occurred in the calcinations of bayerite and of böhmite, whether the latter was prepared by precipitation or as a product of the low temperature dehydration of bayerite. They reported, however, that gibbsite on dehydration yielded a form of böhmite which on subsequent calcination gave rise to a new anhydrous form which they called χ-Al_2O_3; χ-Al_2O_3 was characterized by the presence of extra lines on the pattern previously attributed to γ-Al_2O_3. On further heating χ-Al_2O_3 yielded another polymorph, designated κ-Al_2O_3, before final conversion to α-Al_2O_3. Rooksby also confirmed that some samples of gibbsite have yielded χ- and κ-Al_2O_3 on calcination, but has drawn attention to the fact that the American κ-form is really a mixture of the true κ-form with θ-Al_2O_3.

The confusing feature of this work lies in the fact that böhmite can apparently give rise to two series of transformations in the anhydrous alumina region, depending on its origin.

Experimental

Gibbsite used in these investigations was a commercial Bayer product having a loss of 34.6% on ignition and containing 0.28% Na_2O. Bayerite was produced by the method of Fricke and Severins[8] in which the rapid decomposition of a sodium aluminate solution was initiated by carbon dioxide. The product was filtered and washed until as free as possible from soda; it showed, after drying at 110°, a loss of 34.6% on ignition. The böhmite used as a starting material was produced by the autoclaving of commercial gibbsite with dilute caustic soda at a temperature of 190°, and showed a high loss on ignition, *i.e.*, 16.7% against 15.0% theoretical.

Small quantities of materials were used for calcination. Powder was spread thinly on a silica dish and calcined in a muffle furnace controlled potentiometrically. Rehydrations were carried out in sealed glass tubes which were heated in a thermostatically controlled air oven.

X-Ray diffraction photographs were taken in either a 9.0 or 19.0 cm. diameter Debye–Scherrer powder camera of the Bradley type using Copper Kα filtered radiation.

Results

The various heat treatments employed and the products obtained are shown in Table I. The corresponding X-ray diffraction patterns are reproduced in Fig. 2 and the X-ray diffraction data for the anhydrous forms are given in Table II.

(4) H. B. Weiser and W. O. Milligan, *ibid.*, 36, 3010 (1932); *ibid.*, 38, 1175 (1934).

(5) F. J. L. Bentley and C. G. P. Feachem, *J. Soc. Chem. Ind.*, 64, 148 (1945).

(6) H. D. Rooksby, "X-Ray Identification and Crystal Structures of Clay Minerals," Mineralogical Society, 1951, p. 244.

(7) H. C. Stumpf, A. S. Russell, J. W. Newsome and C. M. Tucker, *Ind. Eng. Chem.*, 42, 1398 (1950).

(8) R. Fricke and H. Severins, *Z. anorg. Chem.*, 175, 249 (1928); *ibid.*, 179, 287 (1929).

Table I

Series of Anhydrous Aluminas Obtained from Calcination of Aluminium Hydrates

	Heat treatment	Böhmite	Gibbsite	Bayerite
1	5 hr. at 300°	Böhmite	Böhmite + major χ lines	Böhmite + γ
2	3 hr. at 500°	γ with 400 line split	$\gamma + \chi^a$	γ
3	Treatment 2 plus 1 hr. at 600°	γ with 400 line split	$\gamma + \chi^a$	γ
4	Treatment 3 plus 1 hr. at 700°	γ with 400 line split	$\gamma + \chi^a$	γ with 400 line split
5	Treatment 4 plus 1 hr. at 800°	$\gamma \longrightarrow \delta$	$\gamma + \chi^a$	$\gamma \longrightarrow \delta$
6	Treatment 5 plus 1 hr. at 900°	δ	$\gamma + \chi^a$	δ
7	Treatment 6 plus ½ hr. at 1,000°	δ	$(\delta \longrightarrow \theta) + (\chi \longrightarrow \kappa)$	
8	Treatment 6 plus 1 hr. at 1,000°	$\delta \longrightarrow \theta$	$\kappa + \theta$	$\delta \longrightarrow \theta$
9	Treatment 8 plus 1 hr. at 1,100°	α + little θ	$\kappa + \theta + \alpha$	θ + trace α
10	Treatment 9 plus 1 hr. at 1,200°	α	α	θ + little α
11	Treatment 10 plus 1 hr. at 1,300°			α + trace θ
12	Treatment 11 plus 2 hr. at 1,300°			α

[a] 400 line is split, and the 440 line is beginning to split and give an extra line at higher d-value—in other words the γ present in the mixture is gradually being transformed into δ.

Table II

X-Ray Diffraction Data for Anhydrous Aluminas

γ			δ			θ		$\gamma + \chi$		$\kappa + \theta$[b]		α		
d	I	hkl	d	I	hkl	d	I	d	I	d	I	d	I	hkl
4.54	3	111	4.49	3	111	5.44	2	4.50	1	6.11	3	3.47	8	102
2.79	2	220	2.85	3		4.51	3	2.82	2	5.42	1	2.55	9	104
2.388	7	311	2.72	5		3.46	1	2.394	6	4.47	4	2.371	8	110
2.277	5	222	2.61	1		2.83	7	2.271	6	4.19	1	2.14	1	006
1.982	9	400	2.43	7	311	2.718	10	2.11	4	3.17	1	2.078	10	113
1.518	2	511	2.275	6	222	2.62	2	1.983	7	3.04	6	1.95	1	202
1.394	10	440	1.985	8	400	2.436	9	1.965[a]	3	2.84	2	1.735	8	204
1.22	1	533	1.946	5	004	2.305	8	1.88	1	2.79	7	1.596	10	116
1.139	3	444	1.79	1	240	2.250	7	1.52	2	2.73	6	1.540	2	121
1.02	1	731	1.521	3	333	2.016	8	1.44	1	2.57	9	1.508	4	108
0.989	2	800	1.398	3	440	1.948	2	1.393	10	2.42	6	1.400	7	214
.910	?		1.388	10	404	1.902	6	1.136	1	2.31	6	1.369	10	300
.884	1	840	1.138	2	444	1.794	4	0.992	2	2.26	2	1.335	2	125
.832	?		0.993	2	800	1.756	2	.883	1	2.16	1	1.273	3	208
.807	4	844				1.728	3	.806	4	2.12	8	1.237	5	10 (10)
						1.614	1			2.06	3	1.235	4	119
						1.561	2			2.00	5	1.186	4	220
						1.536	5			1.94	2	1.16	1	306
						1.509	1			1.90	1	1.144	3	223
						1.482	4			1.868	5	1.123	3	312
						1.450	5			1.825	2	1.096	4	20 (10)
						1.425	2			1.790	1	1.08	1	00 (12)
						1.399	5			1.747	2	1.075	4	314
						1.382	10			1.70	1	1.040	6	226
						1.293	1			1.632	6	1.014	3	402
						1.279	2			1.60	1	0.995	5	21 (10)
						1.254	2			1.574	1			
						1.234	1			1.537	3			
						1.190	?			1.483	3			
						1.155	1			1.447	4			
						1.107	1			1.430	7			
						1.064	1			1.400	1			
						1.041	1			1.386	10			
						1.028	1			1.337	3			
						1.007	3			1.306	3			
						0.997	3			1.284	1			
										1.262	3			
										1.241	1			
										1.217	2			

[a] γ-Component beginning to transform into δ.
[b] d-Values of principal θ lines are underlined.

Since confusion can arise when reference is made to the published work on alumina and its hydrates owing to the fact that workers in this country and America have adopted different systems of nomen-

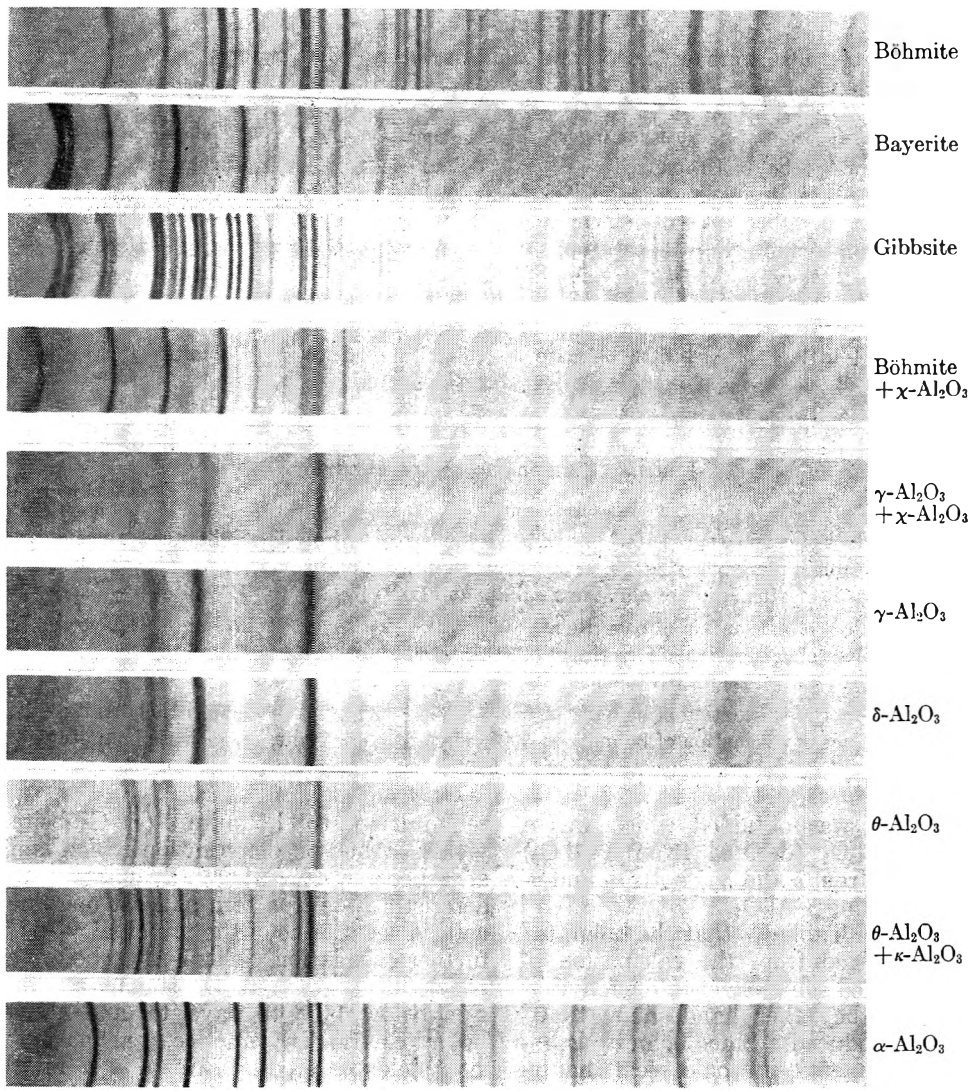

Fig. 2.

clature, and, in our opinion, some of the anhydrous aluminas identified by Stumpf and Russell are in fact mixtures of two different forms, the relationships between the two nomenclatures are shown in Table III.

TABLE III

SYSTEMS OF NOMENCLATURE

Mineral	Alumina hydrates		Anhydrous aluminas	
	American system	British system	American system	British system
Böhmite	α-Monohydrate	γ-Monohydrate	η	γ
Diaspore	β-Monohydrate	α-Monohydrate	γ	δ
Gibbsite	α-Trihydrate	γ-Trihydrate	δ	δ + θ
Bayerite	β-Trihydrate	α-Trihydrate	θ	θ
			α	α
			χ	χ + γ
			κ	κ + θ

The results of the rehydration experiments are recorded in Tables IV and V.

Discussion

It will be seen that bayerite and böhmite gave rise to the same series of aluminas as described by Rooksby and Stumpf, Russell, *et al.*, *i.e.*, γ-Al_2O_3 was first observed and this passed through the δ- and θ-forms to α-Al_2O_3. The calcination of gibbsite at 300°, however, gave a product whose X-ray diffraction pattern showed, in addition to the characteristic lines of böhmite, extra haloes at *d*-values of 2.11 and 1.39. As illustrated in Fig. 2, the former is in the same position as the main characteristic χ line, whereas the latter coincides with one of the two most intense lines of the γ-Al_2O_3 pattern. The fact that the other principal γ-Al_2O_3 line was absent led us to conclude that the two haloes observed were the principal ones of true χ-Al_2O_3. At 500° all traces of böhmite had disappeared and a pattern, previously designated χ-Al_2O_3 by Stumpf and Russell, was obtained. It will be seen that this pattern corresponds to the accepted γ-Al_2O_3 pattern with extra lines at *d*-values of 2.11, 1.88 and 1.44. This suggested to us that the previously reported χ-Al_2O_3 was in fact a mixture of two oxides, *i.e.*, true χ-Al_2O_3 and γ-Al_2O_3, the former having its own characteristic X-ray pattern at least one line of which coincides with one of the principal lines of the γ-Al_2O_3 pattern. We interpreted the diffraction patterns of the products of subsequent calcinations in the light of this conclusion. On further calcination the γ-component of the (γ + χ) mixture began to be transformed into δ-Al_2O_3; sub-

Table IV

Products of Calcination and Rehydration Treatments

Rehydration treatment	γ-Alumina (with 400 line split) Product of calcination of bayerite at 500°	Product of calcination of böhmite at 500°	(γ + χ) Aluminas Products of calcination of gibbsite at 500°	Böhmite + χ-alumina Products of calcination of gibbsite at 300°	Böhmite
5 hr. at 120°	γ + böhmite + bayerite	Unchanged	Böhmite + γ + χ	Unchanged	Unchanged
70 hr. at 120°	As above, but rather less γ	γ + little böhmite + little bayerite	Böhmite + bayerite + some (γ + χ)	Böhmite + little bayerite + trace χ	Unchanged
24 hr. at 140°	Böhmite + little γ + trace bayerite	γ + little böhmite	Böhmite + little (γ + χ) + trace bayerite	Böhmite	Unchanged
5 hr. at 170°	Böhmite + little γ	γ + little böhmite	Böhmite + trace (γ + χ)	Böhmite	Unchanged

Table V

Further Rehydration Experiments

Material	Previous treatment	Result of rehydration 24 hr. at 130°
Pure γ-alumina	Product of calcination at 700° of hydrate obtained by hydrolysis of aluminum *s*-butoxide	Böhmite + trace γ
	Product of calcination of aluminum sulfate at 1,000°	Böhmite + γ
γ-Alumina derived from bayerite	Product of calcination of bayerite at 500°	Böhmite + bayerite + little γ
	Product of calcination of bayerite at 500° rehydrated for 5 hr. at 170°, and subsequently calcined at 500°	Böhmite + γ
γ-Alumina derived from böhmite	Product of calcination of böhmite at 500°	γ + little böhmite + little bayerite
	Product of calcination of böhmite at 500° rehydrated for 96 hr. at 170°, and subsequently calcined at 500°	γ + little böhmite

sequently a product was obtained which was a mixture of true κ-Al_2O_3 (derived from χ-Al_2O_3) and θ-Al_2O_3 (derived from δ and γ), both κ- and θ-Al_2O_3 ultimately yielding α-Al_2O_3.

It will be seen from Table IV that the böhmite/χ-Al_2O_3 mixture derived from the calcination of gibbsite at 300° yielded some bayerite on rehydration at 120°. On the other hand, above 140° böhmite only was produced. Since böhmite is unaffected by the treatments, it would seem that χ-Al_2O_3 is capable of rehydration to bayerite at temperatures below 140° and to böhmite at higher temperatures.

The γ-Al_2O_3 obtained by the calcination of either aluminum sulfate or the product of hydrolysis in boiling water of aluminum *s*-butoxide yielded only böhmite on rehydration at 130°. This is in accord with the scheme outlined in Fig. 1. However, the γ-Al_2O_3 derived from bayerite or commercial böhmite gave on rehydration böhmite mixed with a little bayerite. It seems likely that this apparent anomaly arises because, from the nature of their preparation, the starting materials in the last two cases could well be contaminated with a trace of gibbsite; this would yield χ-Al_2O_3 on calcination and bayerite on subsequent rehydration. Some support of this explanation is available from the results given in Table V. When γ-Al_2O_3 derived from bayerite or böhmite was rehydrated for a long time at 170° (to convert any χ-Al_2O_3 present to böhmite), recalcined at 500° and subsequently rehydrated at 130° no bayerite could be detected.

We therefore conclude that: (a) Bayerite and böhmite on calcination yield γ-Al_2O_3 which is highly adsorbent and which on further calcination passes through the δ- and θ-forms before finally yielding α-Al_2O_3. (b) γ-Al_2O_3 is capable only of rehydration to böhmite. (c) Gibbsite, ideally, yields χ-Al_2O_3 on dehydration which is also highly adsorbent. (d) χ-Al_2O_3, which has its own characteristic X-ray pattern at least one line of which coincides with one of the principal γ-Al_2O_3 lines, on further calcination yields κ-Al_2O_3 before conversion to α-Al_2O_3. (e) χ-Al_2O_3 is capable of rehydration below 140° to bayerite, and above 140° to böhmite. (f) In practice, calcination of gibbsite yields a product which is a mixture of χ-Al_2O_3 and böhmite derived from the secondary reaction of the highly active χ-Al_2O_3 with its adsorbed water. Subsequent calcination therefore gives rise to mixtures of the two series of anhydrous forms, *i.e.*, γ- → δ-, θ- → α-Al_2O_3 and χ- → κ- → α-Al_2O_3.

These conclusions are embodied in Fig. 1, from which it is apparent that the products obtained from the calcination of gibbsite are determined mainly by the conditions of dehydration. Thus, in a closed system where the water vapor is retained in contact with the χ-Al_2O_3, complete conversion to böhmite occurs, and at higher temperatures böhmite subsequently gives rise to the γ- → δ- → θ- → α-Al_2O_3 series of transformations. Under the conditions of the present experimental work, where the bulk of the water vapor was removed rapidly from the system although some adsorbed water must have remained for an appreciable time in close contact with the active alumina, only partial rehydration occurred and mixtures of the anhydrous aluminas characteristic of the two series were obtained. Similarly, partial rehydration of the γ-Al_2O_3 derived from bayerite occurs with the formation of böhmite.

We are indebted to Mr. H. P. Rooksby of the Research Laboratories of The General Electric Company for his interest and helpful discussion.

COAGULATION EFFECTS OF ALUMINUM NITRATE AND ALUMINUM SULFATE ON AQUEOUS SOLS OF SILVER HALIDES *IN STATU NASCENDI*. DETECTION OF POLYNUCLEAR COMPLEX ALUMINUM IONS BY MEANS OF COAGULATION MEASUREMENTS[1]

BY E. MATIJEVIĆ AND B. TEŽAK

Contribution from the Laboratory of Physical Chemistry of the University of Zagreb, Croatia, Yugoslavia

Received April 20, 1953

The effects of electrolytic coagulation of hydrophobic sols of silver halides *in statu nascendi* by aqueous solutions of aluminum nitrate and aluminum sulfate were investigated. It was found that the critical coagulation concentration of aluminum ions depends to a great extent on the age of the solution. Solutions of aluminum salts "artificially aged" by warming show a considerably lower critical coagulation concentration. *p*H of these solutions decreases also during this "aging." Experimental records indicate the formation of polynuclear tetravalent Al complexes in pure aqueous solutions of aluminum salts. A possible constitutional formula of these complexes is described.

The electrolytic coagulation of hydrophobic sols is decisively influenced by the surface of the solid phase (sol particles) on the one side, and by the structure of the electrolytic solution on the other side. If the conditions for the formation of the solid phase (temperature, sol concentration, chemical composition, the manner of mixing, the structure of particles, etc.) are defined to a sufficient extent, and remain constant, the rate of coagulation will depend on the nature of the electrolytic solution.

According to the Schulze–Hardy rule the charge of the ion which is of opposite sign to the charge of the sol (counter ion) plays the main role in the electrolytic coagulation of hydrophobic sols. The greater the charge the lower is the critical concentration of coagulation.[2] Thus if the sol is well defined it is possible to draw conclusions from the critical concentration of coagulation as to the charge of the counter ion. The concentration of coagulation is influenced also by the size of the counter ion[3] but this effect is considerably smaller.

The effects mentioned above offer the possibility for investigating the structure of electrolytic solutions especially the charge and the size of the counter ion by means of coagulation measurements on hydrophobic sols. The lack of real criteria for the determination of the "true" concentration of coagulation and of well defined sols are the chief reasons that this method has not so far been applied for such investigations.

We have shown on the example of coagulation of negative sols of silver halides by thorium ions[4] that the coagulation method is suitable for the determination of complex ions in the solution. Now we shall discuss the results of our investigations on the same sols with the solutions of Al salts where certain complexes are formed either by ordinary aging or by warming these solutions.

(1) Presented at the Meeting of Yugoslav Chemists and the First Croatian Congress of Pure and Applied Chemistry, October, 1952, Zagreb.

(2) B. Težak, E. Matijević and K. Schulz, THIS JOURNAL, **55**, 1567 (1951); E. Matijević and B. Težak, *Kolloid-Z.*, **125**, 1 (1952); B. Težak, E. Matijević, K. Schuls, M. Mirnik, J. Herak, V. B. Vouk, M. Slunjski, S. Babić, J. Kratohvil and T. Palmar, THIS JOURNAL, **57**, 301 (1953).

(3) B. Težak and E. Matijević, *Arhiv kem.*, **19**, 29 (1947).

(4) B. Težak, E. Matijević and K. Schulz, *J. Am. Chem. Soc.*, **73**, 1605 (1951).

Experimental

The rate of coagulation was followed by tyndallometric measurements as described previously.[5]

The forced "aging" of aluminum salt solutions was performed by warming always in the same manner. Fifty ml. of fresh diluted solutions of $Al(NO_3)_3$ or $Al_2(SO_4)_3$ (analytical reagent) of a fixed normality (0.02 *N*, 0.002 *N* or 0.0002 *N*) were kept in "Jena" glass stoppered bottles (erlenmeyer flasks) of 300 ml. in a thermostat at 90° (±1°) for a desired time. Subsequently the solutions were quickly cooled to 20° and then diluted to obtain the concentration gradient necessary for the coagulation of sols.

Figure 1 shows that for the coagulation of negatively charged sols of silver halides *in statu nascendi* in fresh acidified solutions of aluminum nitrate we obtained coagulation values which corresponded to those of trivalent ions. Fresh aluminum sulfate solutions gave the same effect.

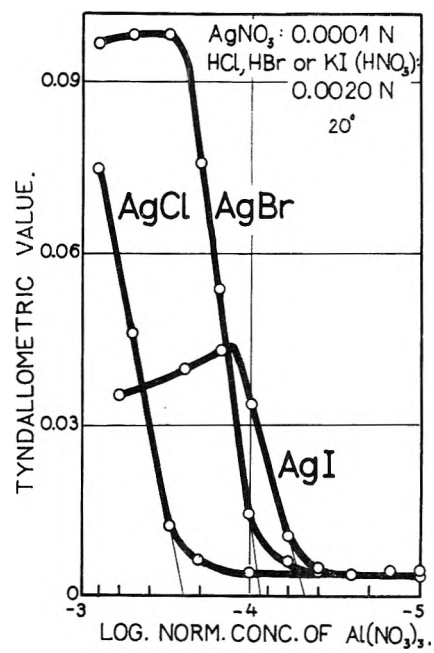

Fig. 1.—Concentration tyndallograms: coagulation effect of the concentration of freshly diluted aluminum nitrate solutions on silver chloride, silver bromide and silver iodide sols *in statu nascendi*, 10 minutes after mixing the reacting components.

If the coagulation was performed with solutions of aluminum salts without the addition of acid, the coagulation values were lower and uncertain. It was found that these values were for AgCl sol $\sim 5.5 \times 10^{-6}$ *N* and for AgBr and

(5) B. Težak, E. Matijević and K. Schulz, THIS JOURNAL, **55**, 1558 (1951).

AgI sol about $1.5 \times 10^{-6} N$. When a very small amount of free acid (HNO_3) was added to these systems, the coagulation limits shifted to their "normal" values. Figure 2 represents this effect on AgBr sol if coagulated with $Al(NO_3)_3$ and $Al_2(SO_4)_3$, respectively, without acid and with added nitric acid in total concentration of $5 \times 10^{-6} N$ and $5 \times 10^{-5} N$. Further addition of free acid did not influence the coagulation value. Therefore, we performed our experiments with acidified media using acids with lattice forming anions of the solid phase (HCl or HBr). Only when coagulating AgI sols we took mixtures of potassium iodide and nitric acid of the same normality. The concentration of added acids was always $2 \times 10^{-3} N$ to avoid other possible influences.

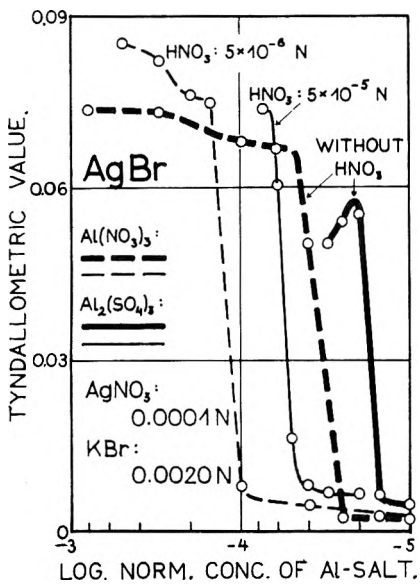

Fig. 2.—Concentration tyndallograms: the effect of the added nitric acid on the coagulation of silver bromide sol *in statu nascendi* in solutions of $Al(NO_3)_3$ and $Al_2(SO_4)_3$, 10 minutes after mixing the reacting components.

Aluminum salt solutions when kept for a longer time under usual room conditions gave entirely different coagulation values which were not reproducible. Therefore, we tried to induce the "aging" in an artificial way by keeping fresh solutions of Al salts at higher than room temperatures (but under 100°). When the rate of coagulation was measured with such solutions it was found the coagulation limits shifted to the lower concentrations of aluminum ion. Figures 3 and 4 show these shifts for sols of silver chloride and silver iodide in aluminum nitrate solutions. In these experiments the concentration of the original $Al(NO_3)_3$ solution (kept at 90°) was 0.002 N. It is worthwhile noting that after the Al salt solutions are kept at 90° for a certain time, the coagulation values reach a limit which is changed no more by longer heat treatment. The extreme limits obtained are shown in Fig. 5. It is evident that the shifts are considerably larger with the silver chloride sol than with the silver iodide sol. The silver bromide sol occupies a middle position. The sequence of sols is the reverse to that in Fig. 1. Maximal shifting amounts to more than one power of ten expressed in normality of Al salt solutions. Analogous effects were obtained with $Al_2(SO_4)_3$ solutions (Fig. 6).

When $Al(NO_3)_3$ solutions of lower initial concentration (0.0002 N) are kept at 90° for a short time (up to 30 minutes) the coagulation values of silver halide sols decrease. By longer heat treatment the coagulation value increases again and returns to higher concentrations as shown in Figs. 7 and 8.

At the same time measurements of hydrogen ion concentration in aluminum salt solutions were performed. Figure 9 is a graphical presentation of the functional relationship which exists between *p*H and the concentration of these solutions, while Fig. 10 shows that *p*H is considerably *decreased* by heat treatment. The Macbeth apparatus with glass electrode was used for *p*H measurements. Since no special measures of precaution with regard to the dissolved

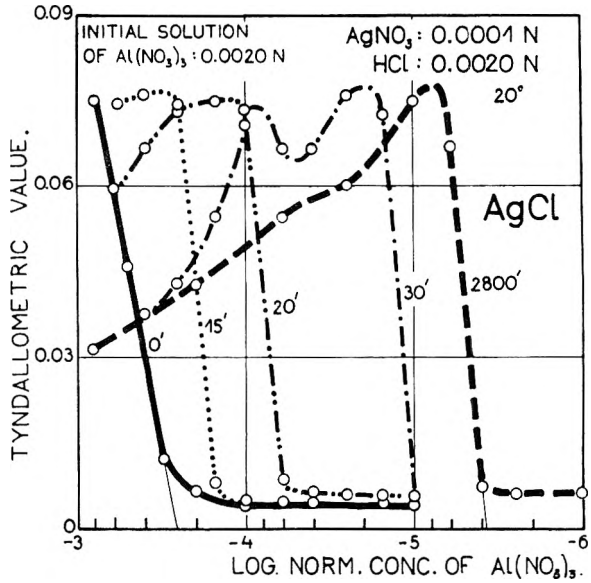

Fig. 3.—Concentration tyndallograms: the effect of "aging" of aluminum nitrate solution on coagulation curves of silver chloride sol *in statu nascendi*, 10 minutes after mixing the reacting components. Initial solution of aluminum nitrate (0.0020 N) kept at 90° for various times as marked on diagram.

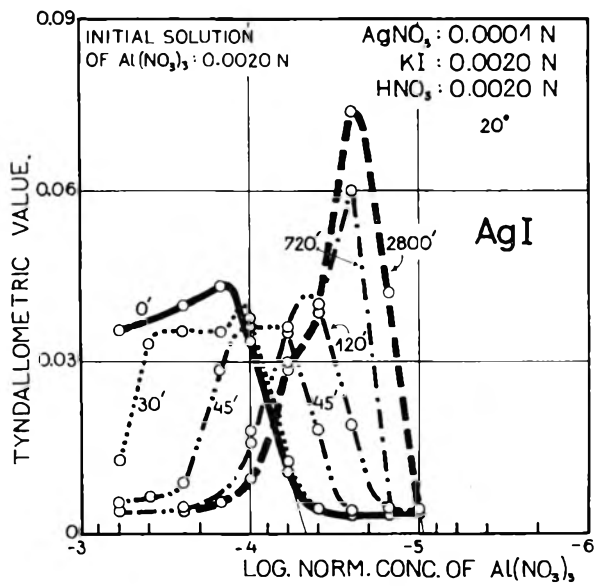

Fig. 4.—Same effects as in Fig. 3 on silver iodide sol.

gases were taken, the results cannot be regarded as entirely satisfactory, but the effects and the direction of the changes are without doubt significant.

Qualitative electrophoretic measurements proved that with the "aged" solutions of aluminum salts in larger concentration there is a *reversal of charge* of the negative silver halide sols thus showing similar effects as the solutions of thorium nitrate.

Discussion

It is well known that many metal ions are hydrolyzed in water solution forming polynuclear complexes. However it is neither easy to determine these complexes nor to explain their structure.

On the basis of the effects obtained by coagulation of silver halide sols in aluminum salt solutions it is possible to follow the changes of these solutions in a very obvious way.

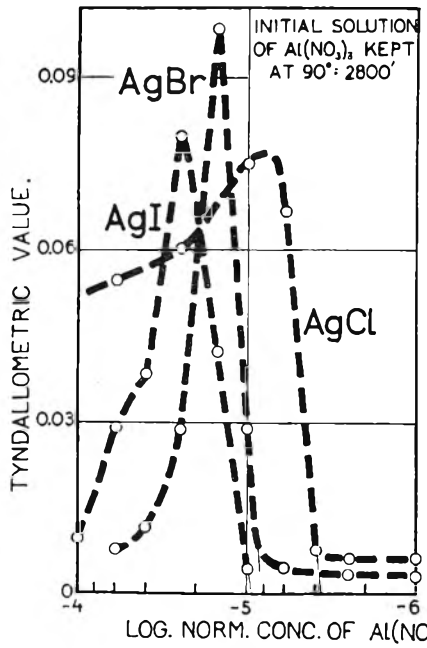

Fig. 5.—Concentration tyndallograms: coagulation effects of the concentration of aluminum nitrate solution kept 2800 minutes at 90° on silver chloride, silver bromide and silver iodide sols *in statu nascendi*, 10 minutes after mixing the reacting components.

Aluminum salts are very easily hydrolyzed. Recently, the reaction of Al ion with water was investigated by Brosset using potentiometric method but always in the presence of various concentrations of hydroxyl ions.[6] We intended to follow

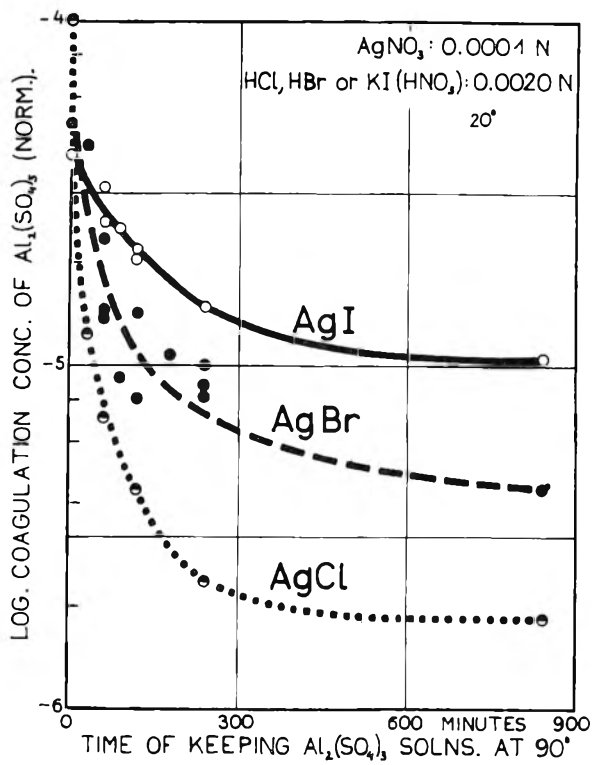

Fig. 6.—The effect of the time of keeping of aluminum sulfate solutions at 90° on the coagulation values of silver chloride, silver bromide and silver iodide sols *in statu nascendi*.

(6) C. Brosset, *Acta Chem Scand.*, **6**, 910 (1952).

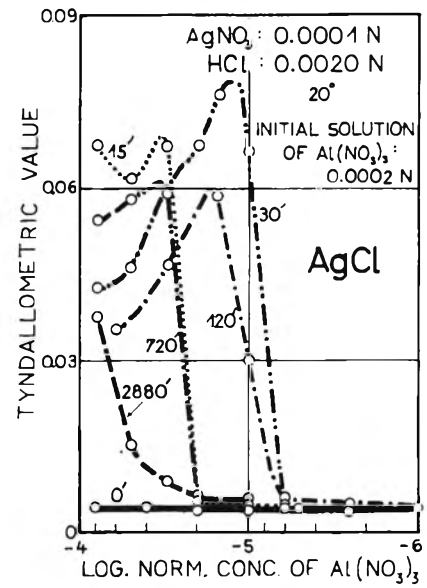

Fig. 7.—Effects as in Fig. 3 on silver chloride sol, when "aged" initial solution of $Al(NO_3)_3$ was 0.0002 *N*.

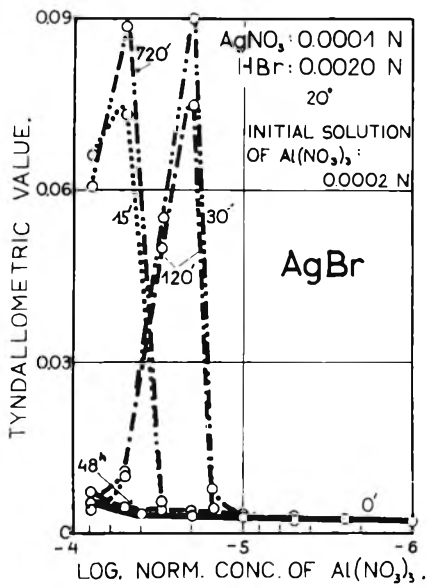

Fig. 8.—Same effects as in Fig. 7 on silver bromide sol.

the changes of Al ions in pure solutions of Al salts induced to "aging" by heat treatment. It was shown in the experimental part that the "aging" causes a decrease of the coagulating concentrations and simultaneously an increase of the hydrogen ion concentration. It is obvious that in aluminum salt solutions changes occur for which only aluminum ion forming aquo-complexes may be responsible.

If the size of the aluminum ion (in fresh solutions) is calculated from the coagulation data, one obtains a value which exceeds the radius of Al^{+++} as determined by X-ray analysis of crystals. Probably Al ions in solution are bound to a certain number of water molecules so that their general formula may be assumed as $Al(H_2O)_n^{+++}$.[7] It is very difficult to say something on the number of water molecules bound (n) and whether this number is

(7) J. N. Brönsted and K. Volqvartz, *Z. phys. Chem.*, **134**, 97 (1928); B. Težak and E. Matijević, *Arhiv kem.*, **19**, 29 (1947).

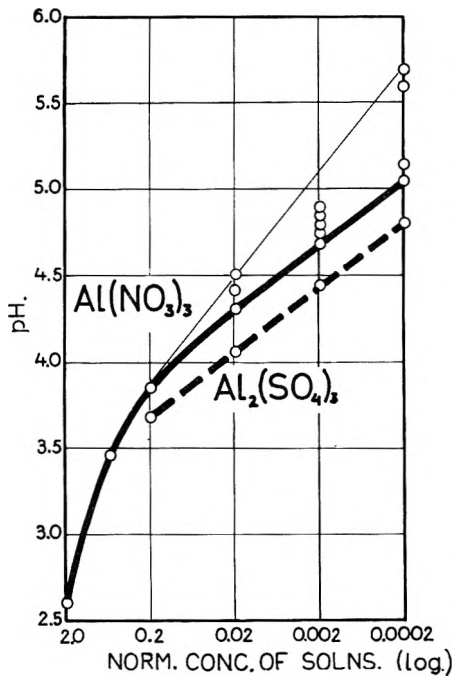

Fig. 9.—The dependence of *p*H on the concentration of $Al(NO_3)_3$ and $Al_2(SO_4)_3$ solutions. The increase of *p*H by "aging" of $Al(NO_3)_3$ solutions under normal room conditions is shown by circles between thick and thin line.

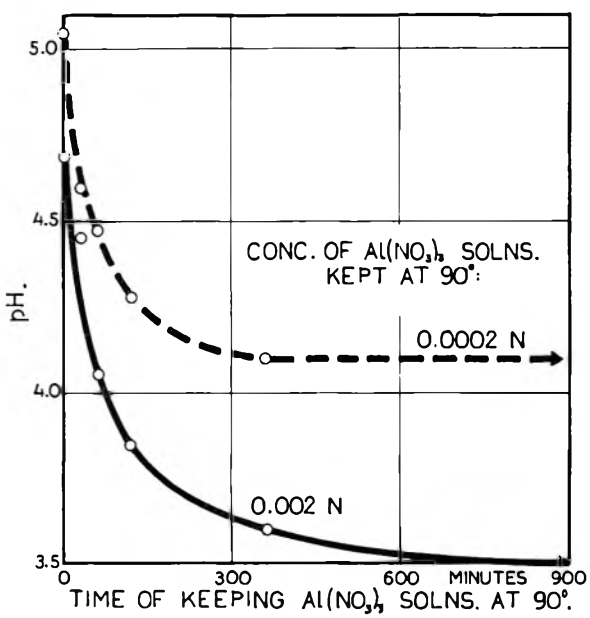

Fig. 10.—The change of *p*H in solutions of $Al(NO_3)_3$ when kept at 90°.

constant. By warming of Al salt solutions hydrogen ions are set free and polynuclear Al complexes are formed. From critical concentration of coagulation it clearly appears that these complexes are *tetravalent* (in comparison, *e.g.*, with coagulation data for Th^{++++}).[8] The proof for the tetravalent complexes follows also from the fact that these solutions reverse the charge of the sols, and that is the characteristic property of inorganic tetravalent ions in acidified media. Also, the sequence of coagulating limits for silver halide sols in "aged" solutions proves the tetravalent character of the Al complexes. On the basis of these data it is probable that by hydrolysis of moderately concentrated solutions of Al salts polynuclear ionic complexes are formed according to this simple reaction

$$2[Al(H_2O)_n]^{3+} + 2H_2O \longrightarrow [Al(OH)(H_2O)_{n-1}]_2^{4+} + 2H_3O^+$$

This equation is supported by our experimental results but the question of the inner constitution of such complexes and the kinetics of their formation remain open. One of the possible constitutional schemes could be, *e.g.*

$$\left[O\begin{matrix}Al(H_2O)_m \\ Al(H_2O)_m\end{matrix}\right]^{4+}$$

This formula agrees with the results of Granér and Sillén who investigated the hydrolysis of Bi^{+++} and came to the conclusion that by this process oxygen bridged polynuclear complexes are formed.[9]

We have seen that with more diluted "aged" solutions of $Al(NO_3)_3$ (0.0002 *N*) the coagulation values first decrease and then, if "aging" is continued, again increase (Figs. 7 and 8). This effect may be explained by the reduction of the valency of the complexes. It is probable that in such solutions bivalent complexes are formed either directly or by splitting of tetravalent complexes. We cannot prove the existence of bivalent complexes in this case by coagulation measurements because the critical coagulating concentration of bivalent ions is considerably higher than the concentration of the original Al salt solution used in these experiments. But our assumption agrees with Faucherre's results who showed that in Al salt solutions there exists a concentration limit above which the complexes are tetravalent and below which they are bivalent.[10]

General conclusions similar to ours were drawn by Hindman for plutonium ion (Pu^{+++}) when investigating the hydrolysis effects by spectral analysis.[11]

It is interesting to note that the existence of simple tetravalent complexes of Al ions was assumed also by Honda in a paper dealing with the separation of basic aluminum ions by means of ion exchangers.[12]

At the end we wish to mention that the complexes formed by our artificial aging of Al salt solutions are very stable. It is not easy to destroy these complexes either by subsequent dilution or by addition of various amounts of mineral acids.

(8) B. Težak, E. Matijević and K. Schulz, *J. Am. Chem. Soc.*, **73**, 1602 (1951).

(9) F. Granér and L. G. Sillén, *Acta Chem. Scand.*, **1**, 631 (1947).

(10) J. Faucherre, *Compt. rend.*, **227**, 1367 (1948).

(11) J. C. Hindman, "Natl. Nuclear Energy Ser., Div. IV, Transuranium Elements, Pt. 1," 1949, pp. 370, 388.

(12) M. Honda, *J. Chem. Soc. Japan, Pure Chem. Sect.*, **72**, 555 (1951); *C. A.*, **46**, 3458c (1952).

THE DISTORTION OF AEROSOL DROPLETS BY AN ELECTRIC FIELD[1]

BY CHESTER T. O'KONSKI AND HENRY C. THACHER, JR.

Contribution from the Department of Chemistry, University of California, Berkeley, Calif., and the Department of Chemistry, Indiana University, Bloomington, Ind.

Received May 1, 1953

An equation has been derived for the distortion of a liquid aerosol droplet under the influence of a parallel electric field. The equation, valid for static fields in insulating media, can be reduced to a simple form for many cases of interest. Numerical values of the distortion are computed for water and dioctyl phthalate droplets. The droplet becomes longer in the direction of the field, whether its dielectric constant is greater or less than that of the surrounding medium, because of the decrease in total electrostatic free energy of the system which accompanies this distortion in both cases. This effect is of interest in connection with size studies of aerosol droplets. It leads to predictions of an electric birefringence and of effects involving the scattering of electromagnetic radiation by liquid aerosol systems. A new method is proposed for studies of size distribution in aerosol systems containing large liquid droplets. It would employ the above effect to induce, by means of a periodic electric field, the natural resonant vibrations of the liquid droplets, which could be observed by the resulting modulation of the birefringence or of the light scattered by the aerosol. The distortion is also of interest for the study of dynamic surface tension by means of potentially very accurate measurements of the resonant frequencies of airborne or hanging drops.

I. Introduction

It is well known that anisometric isotropic dielectric bodies will tend to orient themselves in an electric field because the internal and external fields, and therefore the electrostatic free energy of the system, are functions of the orientation.[2] If the bodies are ellipsoids they will have the minimum free energy when the longest axis is in the direction of the field. Because spherical liquid droplets are deformable if forces operate against the effect of surface tension, it appeared reasonable that the same field considerations which explain preferential orientation of a rigid ellipsoidal body would cause the elongation of a liquid droplet. This is not an electrostrictive effect of the usual type. For example, the deformation would increase with droplet size, other factors being the same, because the electrostatic energy increases linearly with the volume, whereas the surface energy is proportional to the $^2/_3$ power of the volume. It is the purpose of this work to derive expressions from which to calculate the elongation, and to suggest ways in which the phenomenon may be of use in studies of liquid aerosol systems.

II. Theoretical Treatment

We consider a droplet of volume $4\pi r^3/3$, of a material of inductive capacity ϵ_2, suspended in a medium of inductive capacity ϵ_1, to which is applied a parallel electric field of strength E. For small droplets the effects of gravitation can be shown to be negligible and so will be ignored. If the resulting distortion is small, the shape of the droplet may be approximated by that of an ellipsoid of revolution of semimajor axis, a, in the direction of the field, and of semiminor axis, b. We can express the axes in terms of the eccentricity, e, and the radius, r, of the sphere of equal volume

$$a = r(1 - e^2)^{-1/3} \quad (1)$$

$$b = r(1 - e^2)^{+1/3} \quad (2)$$

When the field E is removed there will be in general a slight change in volume of the droplet because of electrostriction.[2] For cases of practical interest here this effect turns out to be very small. Hence the volume of the droplet in the field can be identified with the volume in zero field with negligible error. If the interfacial tension between the droplet and the medium is γ, the surface free energy of the droplet is

$$F_s = 2\pi r^2\gamma(1 - e^2)^{1/3}[1 + \sin^{-1} e/e(1 - e^2)^{1/2}] \quad (3)$$

The problem of the energy of a dielectric ellipsoid in a parallel electric field has been solved, and the solution is given by Stratton.[2] For the case in which we are interested the electrostatic free energy (in rationalized M.K.S. units) is

$$F_E = -2\pi ab^2E^2(\epsilon_2 - \epsilon_1)/3[1 + (\epsilon_2 - \epsilon_1)ab^2A/2\epsilon_1] \quad (4)$$

where A for this case is readily evaluated

$$A = \int_0^\infty ds/(s + b^2)(s + a^2)^{3/2} = [1 - e^2][\ln\{(1 + e)/(1 - e)\} - 2e]/e^3r^3 \quad (5)$$

Eliminating a and b by equations 1 and 2 we obtain

$$F_E = -2\pi r^3E^2(\epsilon_2 - \epsilon_1)/3[1 + (\epsilon_2 - \epsilon_1)(1 - e^2)(\ln<\{1 + e\}/\{1 - e\}> - 2e)/2\epsilon_1e^3] \quad (6)$$

The equilibrium eccentricity can be calculated by differentiating the sum of F_s and F_E, the only contributions to the free energy which depend upon e, with respect to e, and equating the result to zero. The result is

$$rE^2(\epsilon_2 - \epsilon_1)^2/2\gamma\epsilon_1 = \frac{[(3 - 2e^2)/(1 - e^2)^{2/3} - (3 - 4e^2)\sin^{-1} e/e(1 - e^2)^{1/2}]}{[\{3/e - e\}\{\ln<(1 + e)/(1 - e)>\} - 6]/e^2[1 + (\epsilon_2 - \epsilon_1)B/\epsilon_1]^2} \quad (7)$$

where B is defined by the expression

$$B = [1 - e^2][\ln\{(1 + e)/(1 - e)\} - 2e]/2e^3 = 1/3 - 2e^2/15 - 2e^4/35 - \ldots \quad (8)$$

Upon expanding in power series the numerator on the right turns out to be

$$16e^4(1 + 29e^2/21 + \ldots)/15 \quad (9)$$

while the denominator on the right is given by

$$8e^2(1/15 + 2e^2/35 + \ldots)/[1 + (\epsilon_2 - \epsilon_1)(1/3 - 2e^2/15 - \ldots)/\epsilon_1]^2 \quad (10)$$

Neglecting in each series the terms of higher order than e^2 and solving, we obtain

$$rE^2/\gamma = 4e^2[1 - (29\epsilon_2 - 194\epsilon_1)e^2/105(\epsilon_2 + 2\epsilon_1)][\epsilon_2 + 2\epsilon_1]^2/9\epsilon_1[\epsilon_2 - \epsilon_1]^2 \quad (11)$$

(1) Presented before the Division of Physical and Inorganic Chemistry, 123rd Meeting, American Chemical Society, March, 1953.

(2) J. A. Stratton, "Electromagnetic Theory," McGraw-Hill Book Co., Inc., New York, N. Y., 1941.

which is the expression for the case where $e^4 << 1$. If the eccentricity is smaller, so $e^2 << 1$, the expression simplifies to the limiting law

$$e = 3E(|\epsilon_2 - \epsilon_1|)(\epsilon_1 r/\gamma)^{1/2}/2(\epsilon_2 + 2\epsilon_1) \qquad (12)$$

In equation 7 it is seen that the difference $(\epsilon_2 - \epsilon_1)$ appears as a square term, so that the same values of e are obtained for equal positive and negative values of $(\epsilon_2 - \epsilon_1)$. Negative values of e have no physical significance, since $e = (1 - b^2/a^2)^{1/2}$, and imaginary values would correspond to an oblate spheroid. Examination of the right-hand side of the equation shows that solutions corresponding to an oblate spheroid are not allowed. It follows that *the droplet is elongated in the direction of the field whether its dielectric constant is greater or less than that of the surrounding medium* for the case where the surrounding medium can be regarded as perfect dielectric.

When the droplet is a conductor of electricity and the surrounding medium is a perfect insulator, the electric field within the droplet will be zero after transients have decayed following application of a steady field. In electrostatics, this is equivalent to the situation where the inductive capacity of the droplet is infinite.[3] To evaluate the equilibrium elongation for this case one therefore sets $\epsilon_2 = \infty$ in the expression 6 for the electrostatic free energy with the result

$$F_E = -2\pi r^3 E^2 \epsilon_1/3B \qquad (13)$$

Differentiating and expanding in series as above we obtain

$$rE^2/\gamma = 4e^2(1 - 29e^2/105)/9\epsilon_1 \qquad (14)$$

which applies for $e^4 << 1$. When $e^2 << 1$ this reduces to

$$e = 3E(\epsilon_1 r/\gamma)^{1/2}/2 \qquad (15)$$

By comparing 10 and 11 with 14 and 15, respectively, it is seen that the same results are obtained more quickly by setting $\epsilon_2 = \infty$ in 10 and 11.

We have followed Stratton's example in using rationalized M.K.S. units. For numerical calculations in c.g.s. units, γ is expressed in dyne cm.$^{-1}$, ϵ_2 and ϵ_1 are replaced by $K_2/4\pi$ and $K_1/4\pi$, where K_2 and K_1 are the respective dielectric constants of the two media, and E has the units statvolt cm.$^{-1}$.

To illustrate the magnitude of the effect, calculations have been made of the value of rE^2 necessary to produce varying degrees of distortion of the droplets in water clouds and in a dioctyl phthalate oil smoke. Tables I and II list the results obtained from the exact expression 7, as well as the approximate equations, to illustrate the range of applicability of the latter. It is seen that the first-order approximation, equation 15, is correct within 3% for values of e up to 0.30. For dioctyl phthalate the agreement is closer. For the case of water droplets in air the value infinity is used for k_2 in accordance with the discussion above because water has a finite conductivity whereas that of air is practically zero.

(3) J. A. Stratton, *ibid.*, p. 213. This will be clarified in a later publication, reference 5.

TABLE I

DISTORTION OF WATER DROPLETS BY AN ELECTRIC FIELD[a]

		Calcd. val. of rE^2, statvolts^2 cm.$^{-1}$		
e	a/b	Eq. 7	Eq. 14	Eq. 15
0.00	1.00000	0.00000	0.00000	0.00000
.01	1.00005	.04016	.04016	.04016
.02	1.00020	.16064	.16064	.16066
.05	1.00125	1.0034	1.0033	1.0041
.10	1.00503	4.005	4.004	4.016
.20	1.0206	15.883	15.888	16.066
.30	1.0483	35.200	35.249	36.148
.40	1.0911	61.127	61.423	64.262
.50	1.1547	92.27	93.48	100.41
.70	1.4003	158.91	170.17	196.80

[a] $\gamma = 71.97$ dyne cm.$^{-1}$; $K_1 = 1.00077$; $K_2 = \infty$; $t = 25.0°$.

TABLE II

DISTORTION OF DIOCTYL PHTHALATE DROPLETS BY AN ELECTRIC FIELD[a]

	Calcd. val. of rE^2, statvolts^2 cm.$^{-1}$		
e	Eq. 7	Eq. 10	Eq. 11
0.00	0.0000	0.0000	0.0000
.01	.0435	.0435	.0435
.02	.174	.174	.174
.05	1.088	1.088	1.088
.10	4.36	4.35	4.35
.20	17.45	17.45	17.41
.30	39.4	39.4	39.2
.40	70.4	70.3	69.7
.50	110.9	110.4	108.9
.70	224.6	219.3	213.2

[a] $\gamma = 26.4$ dyne cm.$^{-1}$; $K_1 = 1.000$; $K_2 = 5.18$.

To facilitate numerical calculations employing (7) this equation can be written

$$rE^2(\epsilon_2 - \epsilon_1)^2/2\gamma\epsilon_1 = C[1 + (\epsilon_2 - \epsilon_1)B/\epsilon_1]^2 \qquad (7')$$

where

$$C = \frac{[(3 - 2e^2)/(1 - e^2)^{2/3} - (3 - 4e^2)\sin^{-1} e/e(1 - e^2)^{1/6}]e^2}{[\{3/e - e\}\{\ln <(1 + e)/(1 - e)> - 6\}]} \qquad (16)$$

Values of the functions B and C have been computed and are given in Table III.

TABLE III

VALUES FOR THE FUNCTIONS B AND C

e	B	C
0.00	0.33333333	0.00000000
.01	.33332000	.00020001
.02	.33327999	.00080017
.03	.33321329	.00180085
.04	.33311985	.00320269
.05	.33299964	.00500656
.06	.33285259	.00721362
.07	.33267862	.00982526
.08	.33247765	.01284313
.09	.33224956	.01626920
.10	.33199425	.02010565
.20	.327906	.08173
.30	.320846	.18918
.40	.310392	.35104
.50	.295837	.58330
.60	.275992	.91710
.70	.248763	1.4208

III. Discussion

The results given in Table I show that the distortion of water droplets in natural clouds will be small even for the maximum sustainable fields in air. In the case of a cloud droplet of 10 microns radius, for example, a field of 30,000 volts per cm. will cause a fractional elongation, $(a - b)/r$, of about 0.01. For larger water droplets, around 1 mm. in radius, it is seen that large distortions will result for practicable values of E.

It should be noted that the equations given are rigorously valid only for small distortions because of the assumption regarding the shape. So far as we are aware, there exists no analytical proof that the droplet will be precisely an ellipsoid of revolution for large values of e. However, experiments at the University of California with small hanging drops indicate that the shape is very closely ellipsoidal, and also verify the equations for the magnitude of the distortion.[4]

The equations presented here apply only to static fields in insulating media, although the droplet may be conducting, as indicated above. A treatment of the more general case, where the medium may be conducting as well as the droplet, will be presented later.[5]

An interesting consequence of the distortion is its effect upon the properties of scattering of electromagnetic radiation by the aerosol. It is a well known result[6] that when the incident beam is plane polarized in a direction perpendicular to the plane of observation, the scattered radiation is polarized in the same direction if the scattering elements are isotropic, as is the case with spherical droplets. When the droplets are distorted by electric fields, the scattered radiation will become depolarized. This suggests that by suitable optical arrangements it should be possible to produce a modulation of the scattered light from an aerosol as the distorting electric field is turned on and off.

Another property of aerosol systems predicted by the above treatment is the existence of an electric birefringence, similar to the Kerr effect[7] for gases and solutions. The sign of the electric birefringence in static yields will be positive because the elongation of the aerosol droplet will place the longer axis of its polarization ellipsoid along the electric field. Sensitive apparatus similar to that previously developed[8] for studies of electric birefringence in macromolecular systems can be adapted for these studies.

Interpretations of these phenomena will be simplest if long wave infrared or microwave radiation is employed. It will be of interest to examine the polarization properties of microwave radiation scattered by electrified rain clouds, since this treatment predicts that relatively large droplets at the fringes of the charged cloud will be significantly distorted, and considerable depolarization should occur. Studies of this sort by means of modified radar techniques might yield useful meteorological data concerning electric field gradients and droplet sizes in certain types of rain clouds.

The distortion of droplets will also produce a slight change in the dielectric constant of the aerosol, which may be measurable by means of recently developed highly sensitive equipment. This possibility has been discussed by Thacher,[9] following the treatment given here.

Under favorable conditions, the above effects can be amplified by applying an alternating or pulsating field in synchronization with the natural vibration frequencies of the liquid droplets. Selective amplification is of particular interest in connection with size studies in aerosols since it offers a new approach to the problem of size distribution. Assuming for the moment that the magnitude of the distortion can be measured by some suitable electronic or electro-optical method, the technique as applied to a single droplet would be to apply an alternating or pulsating field of variable frequency, and to observe the frequency which gives maximum amplitude of vibration, which would be the resonance frequency of the droplet, determined primarily by its surface tension, size and density. For an aerosol system containing a large number of droplets within each size increment, the intensity of the derived signal, at any particular frequency, will be proportional to the number of droplets having the corresponding resonance frequency, if the motions are only slightly damped. When damping is appreciable, as will generally be the case in ordinary aerosols, contributions from the droplets with resonance frequencies other than the applied frequency will have to be considered. Thus, in principle, a recording of signal amplitude *versus* frequency could be converted to a plot of number concentration *versus* size. To investigate the feasibility of this method, we must consider the magnitude of the viscous damping in a typical aerosol.

The problem of the vibrations of a liquid droplet was first treated by Rayleigh.[10] His expression for the frequency of the nth mode of vibration is

$$\nu_n = [n(n-1)(n+2)\gamma/dr^3]^{1/2}/2\pi \qquad (17)$$

where d is the density, ν_n is the number of vibrations sec.$^{-1}$, other symbols have the usual meanings, and units are c.g.s. Since the droplet is considered as a surface of revolution which is expressed in terms of spherical harmonics, the symmetry corresponding to the mode n is given by the Legendre polynomial of that order. In our case the first mode of interest is $n = 2$. The treatment is only approximately correct when damping is present because it neglects the effect of viscosity upon the resonant frequency.

Following Rayleigh's treatment, Lamb[11] gave an equation for the modulus of the exponential decay, or the relaxation time, τ, for any mode of vibration, which can be written

$$\tau = dr^2/(n-1)(2n+1)\eta \qquad (18)$$

(4) C. T. O'Konski and R. L. Gunther, to be published.

(5) C. T. O'Konski and F. E. Harris, Jr., to be published.

(6) D. Sinclair, "Handbook of Aerosols," Atomic Energy Commission, 1950.

(7) M. Born, "Optik," J. Springer, Berlin, 1933.

(8) C. T. O'Konski and B. H. Zimm, *Science* **111**, 113 (1950).

(9) H. C. Thacher, Jr., THIS JOURNAL, **56**, 795 (1952).

(10) Rayleigh, John William Strutt, "The Theory of Sound," The Macmillan Co., Inc., New York, N. Y., 1896, Vol. II, Ch. XX, Sect. 364.

(11) H. Lamb, "Hydrodynamics," Dover Publications, New York, N. Y., 1945, Ch. XI, p. 641.

where η is the ordinary coefficient of viscosity. The product

$$\nu\tau = [n(n+2)d\gamma r/(n-1)(2n+1)^2]^{1/2}/2\pi\eta \quad (19)$$

is a convenient index of the sharpness of resonance of the vibration. It is equal to the number of vibrations required for the amplitude to decay to 1/2.7 of its initial value or to the reciprocal of the ordinary logarithmic decrement[12] for a damped system. For the primary mode of interest here, $n = 2$, and

$$\nu\tau = (2d\gamma r)^{1/2}/5\pi\eta \quad (20)$$

Values computed from the above equations are given in Table IV for liquid water aerosol droplets. It is seen that the resonance is strong for the large droplets, but rather weak for droplets around 10 microns in radius, and the system is heavily damped at 1 micron radius. Thus, the droplet resonance technique will be restricted to rather large aerosol particles, which constitutes a serious practical limitation on its general use in the laboratory, although it may be of some use in meteorological studies. Alternatively, it may be applicable for studies of surface tension by accurate measurement of the resonant frequency of a suspended droplet in conjunction with a separate measurement of the radius. By varying the droplet size, the surface tension can be measured as a function of frequency. Studies of this sort may lead to information regarding the rates of reorientation of surface active molecules in surface films.

(12) G. Joos, "Theoretical Physics," Hafner Publishing Co., Inc., New York, N. Y., 1934, p. 89.

TABLE IV

RESONANT FREQUENCIES AND VISCOUS DAMPING IN WATER DROPLETS AT 25°[a]

Radius, r, microns	Frequency, ν, cycles per second	Vibrational relaxation time, τ, sec.	Index of resonance, $\nu\tau = 1/\delta$
1000	1.2×10^2	2.2×10^{-1}	28.0
100	3.8×10^3	2.2×10^{-3}	8.5
10	1.2×10^5	2.2×10^{-5}	2.8
1	3.8×10^6	2.2×10^{-7}	0.85

[a] $\gamma = 72.0$ dyne cm.$^{-1}$; $\eta = 0.894 \times 10^{-2}$ poise.

LIGHT SCATTERING FROM NON-GAUSSIAN CHAINS[1]

BY H. BENOIT[2] AND P. DOTY

Gibbs Laboratory, Harvard University, Cambridge, Mass.

Received May 4, 1953

The first two terms, following unity, in the expansion of the particle scattering factor, $P(\theta)$, are examined with reference to non-Gaussian chains. The first term is always equal to one-third of the mean square radius of gyration. Since this term is readily determined from light scattering, it is the obvious choice for characterizing the size of non-Gaussian chains. The ratio of this mean square radius to the value it would have if the Gaussian relation was valid for all chain lengths is calculated for (1) the constant valence angle chain with free rotation, (2) the worm-like (Porod) chain, and (3) the constant valence angle chain with restricted rotation. In all cases the ratio decreases with decreasing chain length. The behavior of the worm-like chain is similar to the constant valence angle chain when the valence angle or the restriction on rotation is large. The effect of excluded volume is also noted. The second term in the expansion is evaluated for ellipsoids and cylinders as well as for the worm-like chain. In all cases it is found to be positive, numerically small and insufficient to characterize the angular distribution of the scattered light.

When the dimensions of a polymer molecule exceed a few hundred ångströms the intensity of scattered light is dependent on the scattering angle, θ, because of interference arising from light rays scattered from different parts of the same molecule. As in the case of X-rays, the angular intensity distribution is given explicitly by the expression[3]

$$P(\theta) = \frac{1}{(N+1)^2} \sum_i \sum_j \frac{\sin \mu r_{ij}}{\mu r_{ij}} \quad (1)$$

with $\mu = (4\pi/\lambda')\sin(\theta/2)$. The distance between pairs of the $N+1$ elements is denoted by r_{ij} and the summation extends over all pairs. It has been known for some time that this summation reduces to simple analytical expressions for particles having the shape of spheres, rods and Gaussian coils[4] and to power series for ellipsoids, cylinders and disks.[5,6] When particles are known to have one of these shapes, it is possible to deduce its dimensions from measurements of the angular intensity distribution. The existence of a size distribution or of anisotropy[7] complicates the problem somewhat but these effects are generally minor.

More recently light scattering investigations have been extended to several macromolecular substances, *e.g.*, sodium desoxyribonucleate[8,9] and sodium carboxymethyl cellulose,[10] which do not appear to be characterized by any of the above models, but have configurations lying between that of a rod and a Gaussian coil. Not being able to obtain a general solution for this case, our object in this paper is only to evaluate the first terms in the expansion of equation 1 for this case of stiff chains or non-Gaussian coils. This will show what information can be obtained about such macromolecules and will, in addition, lead to a consideration of the way in which the dimensions of a non-Gaussian

(1) Work supported by the Office of Naval Research under Contract No. N5ori-07654.

(2) Permanent address: Centre d'Étude de Physique Macromoleculaire, Strasbourg, France.

(3) P. Debye, *Physik. Z.*, 28, 135 (1927).

(4) (a) B. H. Zimm, R. S. Stein and P. Doty, *Polymer Bull.*, 1, 90 (1945); (b) T. Neugebauer, *Ann. Physik*, 42, 509 (1943); (c) P. Debye, THIS JOURNAL, 51, 18 (1947).

(5) L. C. Roess and C. G. Shull, *J. App. Phys.*, 18, 308 (1947).

(6) N. Saito and Y. Ikeda, *J. Phys. Soc. Japan*, 6, 305 (1951).

(7) P. Horn, H. Benoit and G. Oster, *J. chim. phys.*, 48, 1 (1951).

(8) P. Doty and B. H. Bunce, *J. Am. Chem. Soc.*, 74, 5029 (1952).

(9) M. E. Reichmann, B. H. Bunce and P. Doty, *J. Polymer Sci.*, 10, 109 (1953).

(10) P. Doty and N. S. Schneider, Abstracts, Los Angeles Meeting of the American Chemical Society, March 19, 1953.

chain depend on chain length. Following an introductory section, our discussion will be divided into two parts: the first is concerned with the first term, following unity, in the expansion of $P(\theta)$ and involves the dependence of the radius of gyration on chain length for several chain models. The second part deals with the next term in the expansion.

Section I

In the case of chain molecules, it is possible to simplify equation 1 upon recognizing that the distance r_{ij} between the ith and the jth element of the molecule is only a function of the difference $|i - j| = t$. In this way one can perform one of the two summations and equation 1 becomes

$$P(\theta) = \frac{1}{N+1} + \frac{2}{(N+1)^2} \sum_{t=1}^{N} \overline{(N+1-t)\frac{\sin \mu r_t}{\mu r_t}} \quad (2)$$

where r_t is the distance between segments separated by t elements. Expanding the sine in equation 1 and 2 gives

$$P(\theta) = 1 - \frac{1}{(N+1)^2} \sum_i \sum_j \overline{r_{ij}^2} \frac{\mu^2}{3!} + \frac{1}{(N+1)^2} \sum_i \sum_j \overline{r_{ij}^4} \frac{\mu^4}{5!} - \frac{1}{(N+1)^2} \sum_i \sum_j \overline{r_{ij}^6} \frac{\mu^6}{7!} + \ldots \quad (3)$$

and

$$P(\theta) = 1 - \frac{2}{(N+1)^2} \sum (N+1-t)\overline{r_t^2} \frac{\mu^2}{3!} + \frac{2}{(N+1)^2} \sum (N+1-t)\overline{r_t^4} \frac{\mu^4}{5!} - \ldots \quad (4)$$

These two equations which are equivalent can be put in the form

$$P(\theta) = 1 - A\frac{\mu^2}{3} + B\frac{\mu^4}{60} - C\frac{\mu^6}{2520} + \ldots \quad (5)$$

with

$$A = \frac{1}{2}\frac{1}{(N+1)^2} \sum\sum \overline{r_{ij}^2} = \frac{1}{(N+1)^2} \sum (N+1-t)\overline{r_t^2} \quad (6)$$

$$B = \frac{1}{2}\frac{1}{(N+1)^2} \sum\sum \overline{r_{ij}^4} = \frac{1}{(N+1)^2} \sum (N+1-t)\overline{r_t^4} \quad (6')$$

$$C = \frac{1}{2}\frac{1}{(N+1)^2} \sum\sum \overline{r_{ij}^6} = \frac{1}{(N+1)^2} \sum (N+1-t)\overline{r_t^6} \quad (6'')$$

We turn now to the evaluation of the coefficients A and B as functions of the molecular parameters of several models of polymer chains. It has been noted before that the coefficient A[4c,11,12] has a simple geometrical meaning: it is the radius of gyration of the molecule about its center of gravity. This can be shown easily; if as is shown in Fig. 1 we place the origin at the center of gravity of the molecule, G, and denote by $\vec{\rho_i}$ and $\vec{\rho_j}$ the vectors having their origin in G and terminating in i and j, respectively, one can write

$$r_{ij}^2 = (\vec{\rho_i} - \vec{\rho_j})^2 = \rho_i^2 + \rho_j^2 - 2\vec{\rho_i}\cdot\vec{\rho_j} \quad (7)$$

Substituting this value in equation 6 one obtains

$$A = \frac{1}{2}\frac{1}{(N+1)^2} \left\langle \sum_i \sum_j \rho_i^2 + \rho_j^2 - 2\vec{\rho_i}\cdot\vec{\rho_j} \right\rangle \quad (8)$$

where the sign $\langle\ \rangle$ indicates that this expression is averaged over all configurations. After a simple transformation one obtains

$$A = \left\langle \frac{1}{N+1} \sum_i \rho_i^2 - \frac{1}{(N+1)^2} \left(\sum_i \vec{\rho_i} \right)^2 \right\rangle \quad (9)$$

Since G is the center of gravity, the second part of the right hand side of this expression is zero and one recognizes immediately that the value for A

$$A = \frac{1}{N+1} \sum_i \overline{\rho_i^2} \quad (10)$$

is by definition the average radius of gyration of the particle which we shall designate as ρ^2.

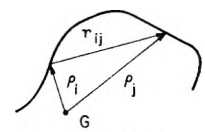

Fig. 1.

The conclusion that the first term in the expansion of $P(\theta)$ measures the radius of gyration for a particle of any shape is quite important, since this makes the radius of gyration accessible to direct experimental determination. Consequently, we have a new measure of particle size which is independent of specification of shape. Of course this represents no gain for particles known in advance to have simple shapes since the radius of gyration is readily related to their dimensions. Thus for Gaussian chains, $\rho^2 = \overline{r^2}/6$, and for rods, $\rho^2 = L^2/12$, where L is the length. But for stiff chains no simple relation exists. It is therefore natural to accept the radius of gyration as the quantity which measures the size of non-Gaussian coils.

Section II

In order to evaluate the relation between the molecular structure of the chain and its radius of gyration, we have to employ a model. In this section we will investigate the relation for four such models.

1. The Aliphatic Chain with Free Rotation.— This chain is formed with N monomeric units of length a, each making an angle, $\pi - \varphi$, with the extension of the preceding one such that its cosine is α. For the case of free rotation, *i.e.*, that all configurations being possible and equally probable, Eyring[13] calculated some time ago the mean end-to-end distance and Sadron[14] has given it a simpler form. The result is that for every value of N and α, r^2 is given by the expression

$$\overline{r^2} = a^2 \left[N\frac{1+\alpha}{1-\alpha} - 2\alpha\frac{1-\alpha^N}{(1-\alpha)^2} \right] \quad (11)$$

where $\alpha = \cos(\pi - \varphi)$, φ being the valence angle. To evaluate ρ^2 one uses equation 6 and obtains

$$\rho^2 = \frac{a^2}{(N+1)^2} \sum_{t=1}^{N} (N+1-t) \left\{ t\frac{1+\alpha}{1-\alpha} - 2\alpha\frac{1-\alpha^t}{(1-\alpha)^2} \right\} \quad (12)$$

The summation can be performed exactly giving the following result

(11) A. Guinier, *Ann. phys.*, 12, 161 (1939).

(12) B. H. Zimm and W. H. Stockmayer, *J. Chem. Phys.*, 17, 1301 (1949).

(13) H. Eyring, *Phys. Rev.*, 39, 746 (1932).

(14) C. Sadron, *Mem. services chim. état (Paris)*, 30, 92 (1943).

$$\frac{\rho^2}{a^2} = \frac{N}{6}\frac{N+2}{N+1}\frac{1+\alpha}{1-\alpha} - \frac{\alpha}{(1-\alpha)^4}\frac{N(N+1) - 2N(N+2)\alpha + (N+1)(N+2)\alpha^2 - 2\alpha^{N+}}{(N+1)^2} \quad (13)$$

If N is sufficiently large, the second part of this expression can be neglected and the well-known Gaussian approximation results[15]

$$\rho^2 = a^2\frac{N}{6}\frac{1+\alpha}{1-\alpha} \quad (14)$$

2. The "Worm-like" Chain.—Porod and Kratky[16,17] have introduced a useful model which requires only one parameter for its characterization assuming the contour length L to be fixed. In this model the contour length is kept fixed at L but the number of segments is increased indefinitely so that their length, $a = L/N$, approaches zero. In order to keep $\bar{r}^2$ finite, α must be set equal to 1. The parameter, q, is then introduced by the relation

$$\alpha = \exp(-a/q) = \exp(-L/Nq) \quad (15)$$

Substituting this value in the Eyring formula, one obtains

$$\bar{r}^2 = 2Lq - 2q^2(1 - \exp(-L/q)) \quad (15a)$$

The quantity q is called by Porod the "persistence length" since it characterizes the stiffness of the chain. When q is large the chain is very stiff and rod-like, when q is small the chain is Gaussian. Instead of using q as parameter it is often more convenient to use the new quantity $x = L/q$ and to write

$$\bar{r}^2/q^2 = 2x - 2(1 - \exp(-x)) \quad (15b)$$

For this model it is easy to evaluate ρ^2; one can either make the preceding substitution in equation 13 or use the definition 6 which can be written in this case as

$$\rho^2 = \frac{1}{L^2}\int_0^L (L-u)\,[2qu - 2q^2(1 - \exp(-u/q))]du \quad (16)$$

Either procedure gives

$$\frac{\rho^2}{q^2} = \frac{x}{3} - 1 + \frac{2}{x} - \frac{2}{x^2}(1 - \exp(-x)) \quad (17)$$

3. The Aliphatic Chain with Hindered Rotation.—Some time ago[18,19] it was taken into account that, in an aliphatic chain, the rotations are not free. For this purpose let us consider the plane defined by the three carbon atoms, t, $t-1$, $t-2$ in Fig. 2. The carbon atom $t+1$ is allowed to move on the circle C. But because of steric hindrance and potential energy barriers not all positions are equally probable: we can characterize this situation by means of the average value of the cosine of the angle φ shown in Fig. 2. We assume that sine $\psi = 0$. If $\eta = 1$ the chain is completely extended in zig-zag fashion; if $\eta = 0$ we have the case of free rotation. With this assumption $\bar{r}^2$ is given by the following expression

$$\frac{\bar{r}^2}{a^2} = \frac{\alpha - \lambda_2}{\lambda_1 - \lambda_2}S_1 - \frac{\alpha - \lambda_1}{\lambda_1 - \lambda_2}S_2 \quad (18)$$

where S_1 and S_2 are the values of

$$S = N\frac{1+\lambda}{1-\lambda} - 2\lambda\frac{1-\lambda^N}{(1-\lambda)^2}$$

when λ is equal to

$$\lambda_1 = \frac{1}{2}\left\{\alpha(1-\eta) - \sqrt{\alpha^2(1-\eta)^2 + 4\eta}\right\}$$

and

$$\lambda_2 = \frac{1}{2}\left\{\alpha(1-\eta) + \sqrt{\alpha^2(1-\eta)^2 + 4\eta}\right\}$$

respectively. Using equation 6 the value of ρ^2 is found to be

$$\rho^2 = \frac{\alpha - \lambda_2}{\lambda_1 - \lambda_2}S_1' - \frac{\alpha - \lambda_1}{\lambda_1 - \lambda_2}S_2' \quad (19)$$

where

$$S' = \frac{N}{6}\frac{N+2}{N+1}\frac{1+\lambda}{1-\lambda} - \frac{\lambda}{(1-\lambda)^4}\frac{N(N+1) - 2N(N+2)\lambda + (N+1)(N+2)\lambda^2 - 2\lambda^{N+2}}{(N+1)^2}$$

and λ has the same meaning as before.

4. The Effect of Excluded Volume.—The formulas given thus far have been derived on the assumption that each chain model becomes Gaussian when N becomes sufficiently large. Recent investigations of the excluded volume effect[20-23] indicate that this assumption is only valid in the special case of zero value of the second virial coefficient. There appears to be wide agreement that the general case can be expressed to a good approximation in the following way

$$\bar{r}^2 = b^2N(1 + kN^{1/2}) \quad (20)$$

where the constant k may have zero or positive values. The corresponding expression for ρ^2 then becomes

$$\rho^2 = \frac{Nb^2}{6}(1 + \frac{24}{35}kN^{1/2}) \quad (21)$$

If this effect of excluded volume is accepted, then the equations obtained for each of the foregoing models should be multiplied by the factor in brackets in equations 20 or 21.

5. Discussion.—We have now obtained precise expressions for the radius of gyration for three different chain models as a function of certain parameters. Since the most accessible of these is the degree of polymerization, let us examine the variation of ρ^2 with N or x, which is proportional to N in the case of the worm-like model. If we defer consideration of the excluded volume effect until later, the basic feature common to the three models is the proportionality between ρ^2 and N at large N. Consequently to study deviations from Gaussian behavior we can consider the ratio ρ^2/ρ_0^2 as a function of N. ρ_0^2 represents the value of the square of the radius for any value of N assuming that the behavior is Gaussian. This ratio is proportional to ρ^2/N, the square of the effective seg-

(15) P. Debye, *J. Chem. Phys.*, **14**, 636 (1946).
(16) G. Porod, *Monatsh.*, **80**, 251 (1949).
(17) O. Kratky and G. Porod, *Rec. trav. chim.*, **68**, 1106 (1949).
(18) W. J. Taylor, *J. Chem. Phys.*, **16**, 257 (1948).
(19) H. Benoit, *J. chim. phys.*, **44**, 18 (1947).
(20) P. J. Flory, *J. Chem. Phys.*, **17**, 303 (1949).
(21) F. Beuche, *ibid.*, **21**, 205 (1953).
(22) T. B. Grimley, *ibid.*, **21**, 185 (1952).
(23) B. H. Zimm, W. H. Stockmayer and M. Fixman, *ibid.*, (in press).

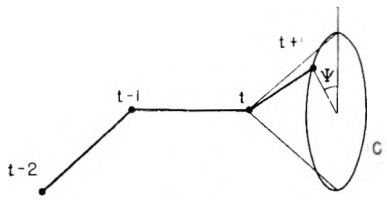

Fig. 2.

ment length, which is the most common representation of experimental data.

A simple consideration shows that the ratio, ρ^2/ρ_0^2, must always decrease downward from a value of unity for stiff, non-Gaussian chains. This is shown in Fig. 3 where ρ^2 is plotted against N. In the Gaussian range the direct proportionality corresponds to the diagonal. At low N values, however, rod-like behavior is approached and in this case ρ^2 must be proportional to L^2 and hence to N^2. The transition from the parabolic to linear behavior must be continuous in a manner qualitatively described by the full line. The ratio of the ordinates on this curve to that of the diagonal (Gaussian case) is the value of the ratio ρ^2/ρ_0^2: it is seen to rise from quite low values to a limiting value of unity.

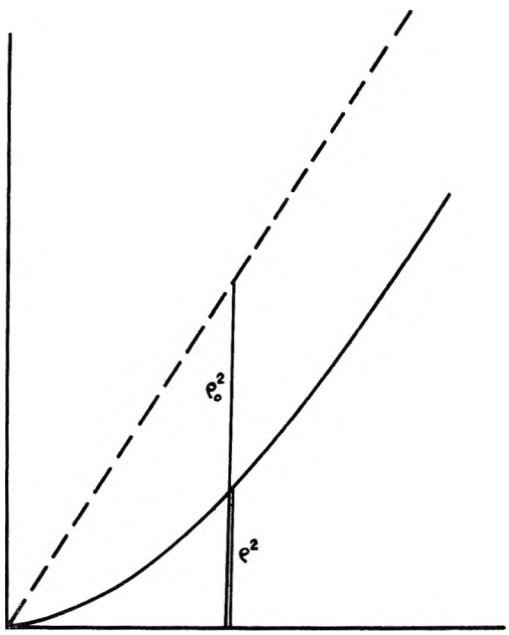

Fig. 3.—Qualitative representation of the mean square radius of gyration as a function of the number of elements.

To examine the quantitative relation consider first the fixed valence angle chain with free rotation where the cosine of the complement of the valence angle α is the parameter which will determine the value of the ratio for a given value of N. The results are shown in Fig. 4 for several values of α. From this one can see that value of N at which deviation from Gaussian behavior becomes significant for a given value of α. Of course, this value of N increases with α and becomes quite large when α approaches one. For an aliphatic chain ($\alpha = {}^1/_3$) the deviation from Gaussian behavior is not significant when N exceeds about 50. In an examination of the distribution of end-to-end lengths for

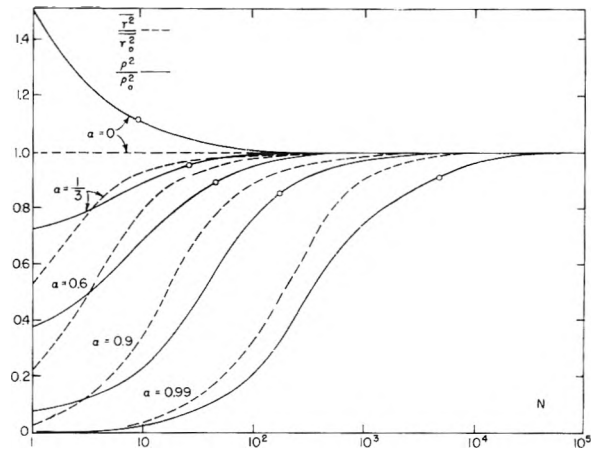

Fig. 4.—The ratio of the mean square radius of gyration for constant valence angle chains with free rotation to that for the Gaussian case as a function of number of elements.

aliphatic chains, Treloar[24] concluded that the deviation of the distribution from the Gaussian one becomes significant when the end-to-end distance exceeds one-third the contour length. Circles on each of the curves in Fig. 4 show the point where this criterion is met. We see that as a rough rule for fixed valence chains this is acceptable. For completeness the curves for the corresponding ratio $\overline{r^2}/r_0^2$ are also given (dashed lines in Fig. 4), even though there is no direct way at present to measure this ratio. One sees that the two sets of curves are comparable, the radius being a little more sensitive to the non-Gaussian behavior

In Fig. 5 a similar plot is made for the worm-like chain. As would be expected the curves are similar to the fixed-valence angle chain for large values of α. Indeed for this particular case the worm-like chain is the preferred model because of its simplicity. Several values of $Q = L/\sqrt{r^2}$ are plotted on the curve to indicate clearly the extent of deviation from Gaussian behavior that various values of this parameter represents.

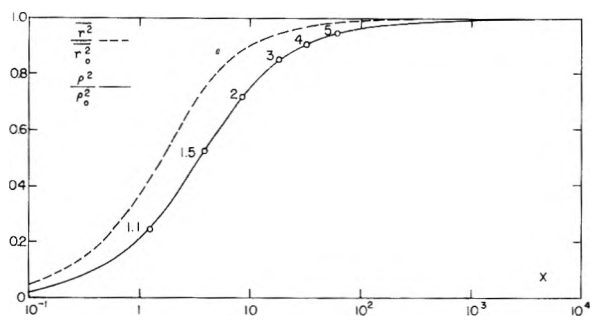

Fig. 5.—The ratio of the mean square radius of gyration for the worm-like chain to that for the Gaussian case as a function of the number of elements.

The series of curves in Fig. 6 shows the dependence of the ratio on log N for an aliphatic chain with steric hindrance. The values of $\eta = 0.73$ and 0.97 correspond approximately to polystyrene and cellulose trinitrate in relatively poor solvents as estimated from the values of $\overline{r^2}/N$ determined on high molecular weight samples. For any curve in Fig. 6 a very close match can be found in the family

(24) L. R. G. Treloar, *Proc. Roy. Soc.* (*London*), **55**, 345 (1943).

represented in Fig. 4 by a suitable choice of α. Thus, as would be expected, the relation between the ratio and N is affected in the same manner by either altering the valence angle or imposing steric hindrance.

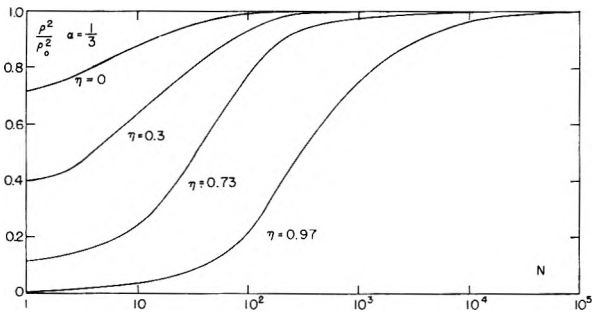

Fig. 6.—The ratio of the mean square radius of gyration for aliphatic chains with restricted rotation characterized by η to that for the Gaussian case as a function of the number of elements.

In view of the effect of excluded volume the examples given thus far would be expected to hold only for poor solvents for these are the ones in which the second virial coefficient approximates zero. The alterations produced by the excluded volumes effect in good solvents is best seen by considering two well studied polymer-solvent systems for which k in equation 20 can be estimated. Using the Flory–Fox[25] viscosity equation to determine $\overline{r^2}$ from intrinsic viscosity–molecular weight measurements on many polystyrene fractions[26,27] ranging over more than three decades in molecular weight, one finds a value of 8.4×10^{-3} for benzene. Somewhat similar data exist for polyisobutylene in benzene.[28] In this case one finds $k = 3.4 \times 10^{-3}$. Either of these values will cause a marked upward swing on the right side of Figs. 4–6. For example at $N = 10^4$ where Gaussian behavior has been reached in all the examples used the value of the ratio, ρ^2/ρ_0^2, is increased by 84 and 34%, respectively. On the other hand, the effect in the non-Gaussian range is for the most part negligible.

There is scarcely any experimental data yet available for comparison with Figs. 4–6. Ideally one should like measurements on fractions of a polymer in the range of $N = 10^4$ to 10^5 in order to determine k and η, α being known. Then with measurements on lower fractions it could be seen whether or not the predicted relation in the non-Gaussian region was satisfied. In order for the light scattering method to yield accurate values for the radius of gyration, the polymer would have to be relatively stiff. Cellulose derivatives appear to satisfy these requirements[10] and present work is directed toward such a comparison. It is interesting to note that earlier work,[29,30] the precision of which was not high, indicated a contrary result, *i. e.*, the ratio increased with decreasing N. If this result is borne out by the present experiments, one would have to conclude that the models employed here do not properly represent this particular polymer. For example, the steric hindrance may not occur symmetrically with respect to the plane determined by the two preceding elements.

(25) P. J. Flory and T. G Fox, *J. Am. Chem. Soc.*, **73**, 1904 (1951).
(26) P. Outer, C. I. Carr and B. H. Zimm, *J. Chem. Phys.*, **18**, 830 (1950).
(27) T. G Fox and P. J. Flory, *J. Am. Chem. Soc.*, **73**, 1915 (1951).
(28) T. G Fox and P. J. Flory, *ibid.*, **73**, 1909 (1951).
(29) R. M. Badger and R. H. Blaker, THIS JOURNAL, **53**, 1056 (1949).
(30) R. S. Stein and P. Doty, *J. Am. Chem. Soc.*, **68**, 159 (1946).

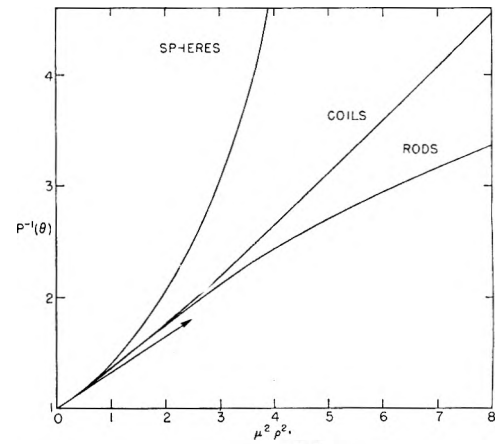

Fig. 7.—$P^{-1}(\theta)$ as function of $\mu^2\rho^2$ for spheres, Gaussian coils and rods.

Section III

We turn now to investigate the meaning of the second term in the expansion shown in equation 4. As a point of reference, we note that as a consequence of the interpretation of the first term, plots of $P(\theta)$ or $P^{-1}(\theta)$ as a function of $\mu^2\rho^2$ produce curves with a common initial slope numerically equal to one-third (Fig. 7). On the other hand, the shape of the curve depends only on the shape of the particle. Therefore one might expect the second term in the expansion to be a useful parameter characterizing particle shape.

If $\mu^2\rho^2$ is replaced by z the expansion, equation 5 becomes

$$P(\theta) = 1 - \frac{z}{3} + \frac{2}{5!}B'z^2 - \frac{2}{7!}C'z^3 + \ldots \qquad (5')$$

with $B' = B/(\rho^2)^2$ and $C' = B/(\rho^2)^3$. Since in evaluating experimental data it is preferable to deal with $P^{-1}(\theta)$ the corresponding expression in this case is noted

$$P^{-1}(\theta) = 1 + \frac{z}{3} + B''z^2 + \ldots \qquad (22)$$

with $B'' = 1/9 - (1/60)B'$.

Since it has been shown in the previous section that the worm-like chain is a good approximation for a stiff chain with a large number of elements, we select this model for use in the evaluation of B''. For this purpose an expression for $\overline{r^4}$, as shown in equation 6′, is required. Such a result has been obtained recently by Hermans and Ullman.[31] An alternative derivation is given in the Appendix. In either case the result is given in our notation by

$$\frac{\overline{r^4}}{q^4} = \frac{20}{3}x^2 - \frac{208}{9}x - 8xe^{-x} + 32(1 - e^{-x}) - \frac{8}{27}(1 - e^{-3x}) \qquad (23)$$

Using equation 6′ one can show that

$$B' = \frac{q^4}{(\rho^2)^2}\frac{1}{x^2}\int_0^x (x - u)\left[\frac{\overline{r^4}(u)}{q^4}\right]du \qquad (24)$$

(31) J. J. Hermans and R. Ullman, *Physica*, **18**, 951 (1952)

$$B' = \frac{\frac{5}{9}x^2 - \frac{104}{27}x + \frac{428}{27} - \frac{1}{x}\frac{3880}{81} + (1 - e^{-x})\left(\frac{48}{x^2} + \frac{8}{x}\right) - \frac{8}{243}(1 - e^{-3x})}{\left[\frac{x}{3} - 1 + \frac{2}{x} - \frac{2}{x^2}(1 - e^{-x})\right]^2} \quad (25)$$

For the purposes of comparison, we have evaluated B' for ellipsoids and cylinders. For rigid particles of any shape the general result may be written as

$$B' = 1 + \frac{1}{(\rho^2)^2}\left\{\frac{1}{V}\int(x^2 + y^2 + z^2)^2\,dv + \frac{2}{V^2}\left[(\int x^2 dv)^2 + (\int y^2 dv)^2 + (\int z^2 dv)^2\right]\right\} \quad (26)$$

In this expression the origin of the Cartesian coordinates is at the center of gravity and the axes lie along the principal axes of inertia. For ellipsoids of revolution with axial ratio $p = a/b$ one then obtains

$$B' = \frac{20}{9} + 48\left[\frac{p^2 - 1}{p^2 + 2}\right]^2 \quad (27)$$

in agreement with Debye.[32] For cylinders of length L and radius R ($p = L/2R$) the expression becomes

$$B' = \frac{90}{31} + \frac{244}{155}\left[\frac{p^2 - 5/7}{p^2 + 3/2}\right]^2 \quad (28)$$

The meaning of these expressions is most clear if they are plotted. In Fig. 8 B'' calculated from equations 25, 27 and 28 is plotted as a function of $1/x$ or the axial ratio. One sees that B'' is positive in all cases, that the behavior of ellipsoids and cylinders is very similar although B'' for cylinders is somewhat greater for high axial ratios. B'' for chains is considerably lower except in the rod-like limit where it meets the curve for long cylinders. The variation of B'' with the degree of coiling of the chain ($1/x$) is disappointingly small. When one considers that z is of the order of unity in most cases of interest, B'' cannot be determined with sufficient precision to be useful. Indeed it is clear that a number of terms in the expansion would have to be evaluated to adequately represent the actual state of affairs since in all the cases examined thus far the curvature of $P^{-1}(\theta)$ has been downward showing that the net effect of the higher terms in equation 22 is negative, not positive. Finally, one must note that we have dealt exclusively with monodisperse systems. When there is a distribution in molecular weight and hence in shape, it is reflected in $P^{-1}(\theta)$ generally by increasing the downward curvature.

As a result of these considerations, it becomes clear that only by evaluating a number of higher terms in the expansion could this approach become really useful. This would require a computational program which at the moment does not seem justified. However, the use of punched card methods already introduced in polymer statistics[33] could lead to useful, practical solutions in specific cases.

The alternative is to forego a rigorous solution in favor of approximations for the distribution function of r_{ij}. A major step in this direction has been taken by Peterlin[34] in terms of the worm-like chain. Other possibilities along these lines are open and when they are worked out the area in which each approximation is valid should become clear.

Appendix

In order to evaluate the sum appearing in equation 6' we evaluate first the differential $d(\overline{r^4})$. If α_{ij} represents the cosine of the angle between the ith and jth elements, we have

$$\overline{dr^4} = \overline{4r^3 dr} = \overline{4r^2 \cdot r \cdot dr}$$

$$= 4a^4 \overline{\sum_i \sum_j \alpha_{ij} \sum_k \alpha_{1k}} = 8a^4 \sum_i \sum_{i<j} \sum_k \overline{\alpha_{ij}\alpha_{1k}}$$

The mean products of the two α's have different values depending on the mutual arrangement of the i, j and kth elements. From the work of Porod[35] we have the following results for the three possible cases

$$\text{If } k \leqslant i, \quad \overline{\alpha_{ij}\alpha_{1k}} = \overline{\alpha_{ij}} \cdot \overline{\alpha_{1k}}$$

$$i < k \leqslant j, \quad = \overline{\alpha_{1i}} \cdot \overline{\alpha_{ik}^2} \cdot \overline{\alpha_{kj}}$$

$$j \leqslant k, \quad = \overline{\alpha_{1i}} \cdot \overline{\alpha_{jk}} \cdot \overline{\alpha_{ij}^2}$$

Moreover

$$\overline{a_{ij}^2} = \frac{1}{3} + \frac{2}{3}\beta^{j-i} \quad \text{with} \quad \beta = \frac{3\alpha^2 - 1}{2}$$

and $\overline{\alpha_{ij}} = \alpha^{|j-i|}$. Since $\alpha = e^{-a/q}$, we have for the value of $\overline{\alpha_{ij}\alpha_{1k}}$ in these three cases

$$e^{-(k-1+j-i)a/q}$$

$$e^{-(i-1+j-k)a/q}\left[\frac{1}{3} + \frac{2}{3}e^{-3a(k-i)/q}\right]$$

$$e^{-(i-1+k-j)a/q}\left[\frac{1}{3} + \frac{2}{3}e^{-2a(j-i)/q}\right]$$

Introducing the new variables, $w = ja/q$; $v = ia/q$; $u = ka/q$ and recalling that $x = Na/q$

$$\frac{\overline{dr^4}}{q^4} = \frac{a}{q} 8 \int_{w=0}^{x}\int_{v=0}^{w}\int_{u=0}^{v} e^{-u+v-w}\,du\,dv\,dw + \frac{8}{3}\int_{w=0}^{x}\int_{v=0}^{w}\int_{u=0}^{w} e^{-v-w+u}$$

$$(1 + 2e^{-2(u-v)})\,du\,dv\,dw + \frac{8}{3}\int_{w=0}^{x}\int_{v=0}^{w}\int_{u=0}^{x} e^{-u-v+w}(1 + 2e^{-2(w-v)})\,du\,dv\,dw$$

$$\frac{\overline{dr^4}}{q^4} = \frac{a}{q}\left[\frac{40}{3}x + we^{-x} - 3(1 - e^{-x}) + \frac{1}{9}(1 - e^{-3x})\right]$$

Consequently

$$\frac{\overline{r^4}}{q^4} = \int_0^x \overline{dr^4} = \frac{20}{3}x^2 - \frac{208}{9}x - 8xe^{-x} + 32(1 - e^{-x}) - \frac{8}{27}(1 - e^{-3x})$$

which is equation 23.

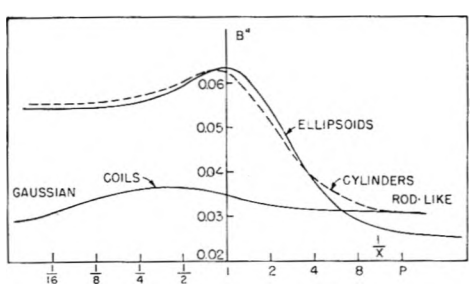

Fig. 8.—The value of the coefficient B'' for ellipsoids and cylinders as a function of axial ratio and for the worm-like chain as a function of $1/x$.

(32) Quoted by P. Doty and J. T. Edsall, *Advances in Protein Chem.*, 6, 35 (1951).

(33) G. King, private communication.

(34) A. Peterlin, *J. Polymer Sci.*, 10, 425 (1953).

(35) G. Porod, *J. Polymer Sci.*, 10, 157 (1953)

POLAROGRAPHIC STUDIES IN NON-AQUEOUS MEDIA. I. FORMAMIDE[1-3]

BY HARRY LETAW, JR.,[4] AND ARMIN H. GROPP

Chemistry Department, University of Florida, Gainesville, Florida

Received May 5, 1953

The polarographic half-wave potentials of acetophenone, anisaldehyde, benzalacetone, benzaldehyde, benzophenone, fluorenone, furfural, vanillin, lead(II), thallium(I) and zinc were determined in formamide solutions. Benzalacetone and furfural produced two waves. The diffusion currents of all species investigated were found to be proportional to their concentrations. Formamide was found to be a useful polarographic solvent at potentials less than −1.60 v. *vs.* S.C.E. because of its stability, solvent properties and the ease of removal of oxygen from its solutions.

Introduction

One previous study of the polarographic behaviors of formamide solutions has been reported. Zan'ko and Manusova[5] determined the half-wave potentials of Cd^{++}, Pb^{++}, Sn^{++}, Zn^{++} as the sulfate, nitrate and chlorides, respectively. They stated that no supporting electrolyte was added because of the presence of a sufficient quantity of NH_4Cl in the formamide. They attributed its presence to decomposition or to an impurity from the synthesis of the formamide. It was concluded that there is little change in the half-wave potential of a substance determined in formamide as compared to that determined in water. It was found that the diffusion current in formamide is less than that in water.

In an effort to extend the usefulness of this solvent in polarography, the present research was designed to study the conclusions of Zan'ko and Manusova with respect to inorganic compounds and to investigate the behavior of various reducible organic compounds in the same medium.

Experimental

Materials.—Ultra-pure $ZnSO_4$ supplied by the Mallinckrodt Chemical Works and Baker and Adamson reagent grade $Pb(NO_3)_2$ were used without further purification. Dr. F. H. Health of this Laboratory prepared and recrystallized Tl_2SO_4 for this research. Recrystallized fluorenone was provided by Dr. F. E. Ray, Director of the Cancer Research Laboratories of the University of Florida. Redistilled benzaldehyde, furfural and acetophenone and recrystallized benzalacetone, benzophenone and vanillin were given to us by Dr. C. B. Pollard of this Laboratory. Eastman Kodak anisaldehyde was used without further purification. Dried reagent grade KCl and KNO_3 were used as supporting electrolytes. Metal Salts Corporation triple-distilled mercury was used without further purification. Eimer and Amend chemically pure grade formamide, after being placed under a pressure of less than 1 mm. for two hours, was found to be polarographically pure in the range studied.

All solutions except those of Tl_2SO_4 were prepared in a stock solution of 0.1 *M* KCl in formamide. A 0.1 *M* KNO_3 solution in formamide was used for the Tl_2SO_4 solutions. Tl_2SO_4 and $ZnSO_4$ are sparingly soluble in formamide. Concentrations of these compounds were 0.0043 and 0.080 *M*, respectively. Dilutions were prepared from saturated solutions of each in formamide with the suitable supporting electrolytes.

Apparatus.—Polarograms were obtained using a Sargent–Heyrovsky Model XII Polarograph. Potentials were measured on a Gray "Queen" Potentiometer calibrated with a Weston Standard Cell. A 0.1 *N* calomel reference electrode equipped with an agar–KCl bridge was used in order that transference effects across the interface be minimized. All potentials are referred to the saturated calomel electrode.

The mercury reservoir was 60 cm. above the level of the solutions. It was attached by neoprene tubing to a glass capillary of Corning "marine barometer" tubing 5.4 cm. long with an internal diameter of 0.05 mm. The capillary constant was 2.81 $mg.^{2/3}$ $sec.^{-1/2}$ at −0.40, 2.78 $mg.^{2/3}$ $sec.^{-1/2}$ at −1.00, and 2.56 $mg.^{2/3}$ $sec.^{-1/2}$ at −1.40 applied volts in 0.1 *M* KCl in formamide.

Tank nitrogen was bubbled through a tower of alkaline pyrogallol and then through a tower of formamide before being introduced into the Heyrovsky-type electrolysis cell for the purpose of sweeping out atmospheric oxygen. The formamide tower eliminated errors in concentrations caused by the removal of solvent from the electrolysis cell by dry nitrogen. The temperature range throughout the experiments was 25 ± 1°.

Results

The supporting electrolyte solutions in formamide were found to have a polarographic decomposition potential of −1.69 ±0.02 v. This limited the half-wave potentials of materials studied in this solvent to a value less than −1.60 v.

The half-wave potentials found in this research are reported in Table I. The best values obtainable for half-wave potentials of these compounds determined in other solvents are also included in Table I. Average $i_d/Cm^{2/3}t^{1/6}$ values are reported

TABLE I

HALF-WAVE POTENTIALS

Compound or ion	Formamide $E_{1/2}$ *vs.* S.C.E., volts	No. determinations	Other media $E_{1/2}$, volts	Solvent
Acetophenone	−1.48 ± 0.02	7	−1.56	1:1 EtOH–HOH[a]
Anisaldehyde	−1.44 ± .01	6	−1.50	1:1 EtOH–HOH[a]
Benzalacetone	−1.08 ± .00	6	−1.12	1:1 EtOH–HOH[a]
	−1.28 ± .03	5	−1.36	1:1 EtOH–HOH[a]
Benzaldehyde	−1.34 ± .03	7	−1.34	1:1 EtOH–HOH[a]
Benzophenone	−1.26 ± .01	7	−1.48	1:1 Diox-HOH[b]
Fluorenone	−0.87 ± .02	7	−0.99	*i*-PrOH–HOH[c]
Furfural	−1.31 ± .02	6	−1.52	*p*H 6.50 (HOH)[d]
	−1.55 ± .02	5	−1.72	*p*H 6.50 (HOH)[d]
Vanillin	−1.44 ± .02	7	−1.73	1:1 EtOH–HOH[a]
Lead(II)	−0.38 ± .02	5	−0.396	HOH[e]
Thallium(I)	−0.35 ± .01	13	−0.46	HOH[e]
Zinc(II)	−0.97 ± .01	8	−0.995	HOH[a]

[a] H. Adkins and F. W. Cox, *J. Am. Chem. Soc.*, 60, 1151 (1938). [b] S. Wawzonek, H. A. Laitinen and S. J. Kwiatkowski, *ibid.*, 66, 827 (1944). [c] R. H. Baker and J. G. Schafer, *ibid.*, 65, 1675 (1943). [d] I. A. Korshunov and S. A. Ermolaeva, *J. Gen. Chem.* (*U. S. S. R.*), 17, 181 (1947). [e] I. M. Kolthoff and J. J. Lingane, "Polarography," Second Edition, Interscience Publishers, Inc., New York, N. Y., 1952.

(1) Abstracted from a thesis presented by Harry Letaw, Jr., to the Graduate Council of the University of Florida in partial fulfillment of the requirements for the M.S. degree, February, 1951.

(2) Supported in part by a grant from the Research Corporation.

(3) Presented in part at the meeting of the Florida Academy of Sciences on December 2, 1950, at Lakeland, Florida.

(4) A.E.C. Predoctoral Fellow, 1950–1952. Now at University of Illinois.

(5) A. M. Zan'ko and F. A. Manusova, *J. Gen. Chem.* (*U.S.S.R.*), 10, 1171 (1940).

in Table II. The concentration region studied for materials other than Tl^+ and Zn^{++} was 0.125–5.88 mm./l. These ions were investigated in the range of 0.0267 to 0.478 mm./l. and 0.114 to 13.36 mm./l., respectively.

TABLE II

AVERAGE $i_d/Cm^{2/3}t^{1/6}$ VALUES

Acetophenone	2.10	Furfural	1.26
Anisaldehyde	2.37		1.45
Benzalacetone	0.98	Vanillin	1.84
	0.97	Lead(II)	1.71
Benzaldehyde	1.63	Thallium(I)	4.92
Benzophenone	1.86	Zinc	1.38
Fluorenone	1.85		

Because of the ill-defined nature of the double waves obtained for furfural and benzalacetone, the half-wave potentials of those substances were considered to be the points of inflection as determined by the graphical method of Zimmerman and Gropp.[6]

Discussion

Kolthoff and Lingane[7] state that formamide is not reduced at the dropping mercury electrode. Formamide–KCl solutions continued to present reproducible decomposition potentials after standing for eight weeks in standard taper glassware. Although the agar bridge of the reference electrode was inserted into a given solution many times, the potentials were always reproducible. The introduction of water by means of the agar bridge would cause a gradual drift in this potential if the hydrolysis materials were not already present in reasonable concentration. Korshunov, Kuznetsova and Schennikova[8] have reported the half-wave potential of formic acid to be in the neighborhood of -1.80 v. They found that the absolute value of the half-wave potential decreases with decreasing concentration of formic acid. On the basis of these facts, it may be concluded that formic acid reduction constituted the limiting useful potential of the formamide used. This material would be expected to be present in excess of the ammonium formate because of the removal of ammonia in the purification procedure.

The half-wave potentials of Zn^{++} and Pb^{++} are in good agreement with the accepted values determined in aqueous solutions. The half-wave potentials of these ions previously determined in formamide are reported to be -0.51 and -1.03 v.[5]

(6) H. K. Zimmerman, Jr., and A. H. Gropp THIS JOURNAL, **54**, 764 (1950).

(7) I. M. Kolthoff and J. J. Lingane, "Polarography," Interscience Publishers, Inc., New York, N. Y., 1946, p. 361.

(8) I. A. Korshunov, Z. B. Kuznetsova and M. K. Schennikova, *Zhur. Fiz. Khim.*, **23**, 1292 (1949).

Comparison of the data obtained for the organic compounds to that available in other solvents is rather complex. Differences in dielectric constants, viscosities and solvation tendencies introduce numerous uncertainties. The dielectric constant of formamide at 25° is 109.5,[9] while that of water is 82. The viscosities of the two at 25° are 3.359 and 0.895 centipoises, respectively. On the basis of the data recorded in Table I for the inorganic ions, it would seem that these factors either cancel one another in an extremely fortuitous manner or that they do not affect half-wave potentials. It is likely that the general similarity of the two solvents results in differences in behavior which are too small to be considered significant, except in the somewhat anomalous case of Tl^+.

It is seen that the opposite situation pertains with respect to organic compounds in formamide as contrasted to those in water–alcohol solutions. Both the dielectric constants and the viscosities of the two systems differ greatly. The shifts in half-wave potentials in going from formamide to the other systems are all in the direction of more negative potentials except in the case of benzaldehyde in which there was no shift. The opposite direction of shift was observed by Sartori and Giacomello[10] in the case of Li^+ in water as contrasted to methanol solutions. The magnitudes of the shifts in the present research are apparently not subject to correlation.

In general, linearity was found in i_d *vs.* C graphs obtained in this research. A tendency for the i_d/C ratio to increase at concentrations in the neighborhood of 10^{-4} m./l. was observed. The latter phenomenon has been found in a large number of polarographic systems investigated in this Laboratory.

An analysis of the Tl^+ and Pb^{++} waves shows good agreement with the criteria of reversibility. The waves of Zn^{++}, however, do not indicate that a reversible process is occurring at the electrode.

It is believed that polarographic half-wave potentials obtained in formamide are of great theoretical value. It should be feasible to identify them, for comparative purposes, as the potentials which would be observed in water for organic materials which are insoluble in that medium. Although extension of the polarographic range of formamide is probably possible, it is extremely difficult to protect this solvent from hydrolysis by atmospheric moisture. This limits the classes of compounds which can be studied with ease in formamide. On the other hand, the ease of removal of oxygen from formamide constitutes a definite advantage over the commonly used alcohols for non-aqueous investigations near the polarographic zero of potential.

(9) G. R. Leader, *J. Am. Chem. Soc.*, **73**, 856 (1951).

(10) G. Sartori and G. Giacomello, *Gazz. chim. ital.*, **70**, 178 (1940).

VAPOR PRESSURES OF PERDEUTEROBENZENE AND OF PERDEUTEROCYCLOHEXANE[1a]

BY RAYMOND T. DAVIS,[1b] JR., AND ROBERT W. SCHIESSLER

Contribution from the Whitmore Laboratories of the School of Chemistry and Physics of the Pennsylvania State College, State College, Penna.

Received May 6, 1953

The vapor pressures of C_6D_6 and C_6D_{12} have been determined over the temperature range 10 to 85°. The Antoine Equation[2] has been fitted to the data from which equation the normal boiling point and molar heats of vaporization have been calculated. The vapor pressure of these deuterocarbons is greater than that of their hydrocarbon analogs.

For several years this Laboratory has been investigating the effect of chemical structure on the physical properties of liquids. Part of this study has dealt with the property changes resulting from increased molecular weight in homologous series. However, it has become increasingly evident that such a study is complicated by the fact that as one goes from one member of a series to the next, not only is there an increase in molecular weight but there is also an increase in molecular complexity. It was felt therefore that a study of the changes in physical properties which occur when heavy hydrogen (deuterium) is substituted for normal hydrogen (protium) in hydrocarbon molecules might permit an evaluation of the effect that increased mass alone has on physical properties, without the complications of increased molecular complexity. With this in mind, samples of perdeuterobenzene (C_6D_6) and perdeuterocyclohexane (C_6D_{12}) were prepared. The preparation of these materials, together with refractive index and density data have been reported.[3] Their viscosity behavior will be the subject of a separate publication. This paper presents the vapor pressure–temperature relation of these compounds.

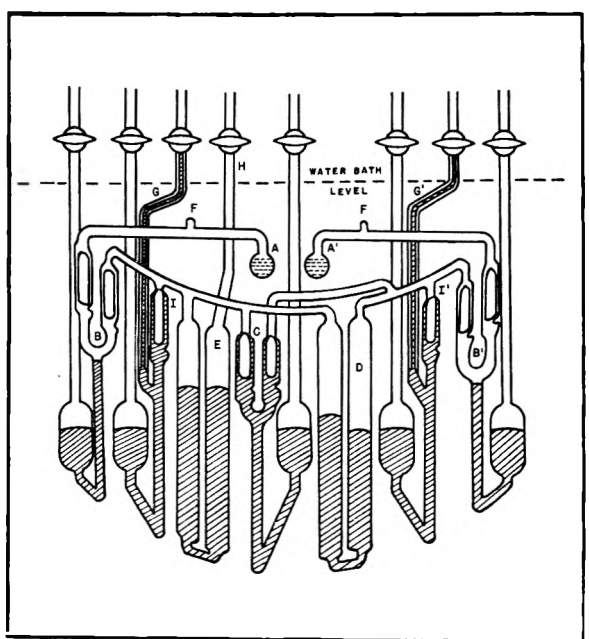

Fig. 1.—Schematic diagram of differential vapor pressure apparatus.

Experimental

Materials.—The preparation of the C_6D_6 and C_6D_{12}, together with the purification of samples of C_6H_6 and C_6H_{12}, have been described previously.[3] These materials had been stored under (99.9%) N_2 in sealed glass ampoules and before use were refluxed over calcium hydride and distilled directly into the apparatus. Careful experiment has shown the calcium hydride treatment to yield no H/D exchange. In C_6D_6, 99.3% of the protium had been replaced by deuterium and there was 98.8% replacement in the case of the C_6D_{12}, as determined by mass spectroscopic examination.[4]

Apparatus.—Figure 1 is a diagrammatic sketch of the apparatus. It consisted essentially of a differential mercury manometer D, and two sample bulbs A and A'. The normal protium compound was placed in A while the deuterium compound was placed in A'. B, B' and C, and I, and I' are mercury activated float cut-offs. E was a manometer which was kept at zero differential by means of an external system attached at H, such that the total vapor pressure of the liquid in A could be measured in a manner similar to the Menzies–Smith vapor pressure method.[5] The apparatus was small enough to fit into a small laboratory constant temperature bath and could be removed from the bath for filling purposes. The liquid and vapors made contact only with glass or mercury. Only 1 cc. of liquid was needed for the measurements.

The differential manometer D had an internal diameter of 15 mm. and was read with a precision of ±0.002 mm. by means of a Gaertner traveling microscope located outside of the constant temperature bath. The temperature bath was controlled to ±0.01°, the temperature being read with a total immersion, mercury in glass, thermometer calibrated by the National Bureau of Standards.

Procedure.—At points F on the apparatus the system for filling and drying the samples was attached. This consisted of a vertical tube about 10 cm. long, closed at its lower end, open initially at the top, and joined to F by a connecting tube which was sealed to the vertical tube at its mid-point. The entire system was first flushed with (99.9%) nitrogen. Approximately 0.5 g. of CaH_2 was introduced into the vertical tube and about 1 cc. of the sample was added. The sample was frozen in a Dry Ice–acetone-bath, and the open end of the vertical tube was sealed and the apparatus evacuated. Nitrogen was admitted and the sample refluxed over the CaH_2 by gentle heating for several minutes. The sample was again frozen, evacuated, and the above refluxing repeated. Next the sample was frozen, the system evacuated and the sample liquefied and distilled into A. After freezing the sample in A, the filling and drying portion of the system was sealed off at F and removed.

In practice, the above procedure for filling sample bulbs A and A' with hydrocarbon and deuterocarbon, respectively, was carried on simultaneously.

The whole unit was then placed in the constant temperature bath, the samples in A and A' melted, and the pressure differential measured in manometer D. The temperature of the constant temperature bath was raised in a stepwise fashion, with pressure differential measurements being taken at approximately 5° intervals. After a run the samples

(1) (a) American Petroleum Institute Project 42. (b) Department of Chemistry, Juniata College, Huntingdon, Pa.

(2) G. Thomson, *Chem. Revs.*, 38, 1 (1946).

(3) J. A. Dixon and R. W. Schiessler, *J. Am. Chem. Soc.*, **76**, in press (1954).

(4) The mass spectroscopic analyses were made by J. Y. Beach, California Research Corp., Richmond, California.

(5) A. Smith and A. W. C. Menzies, *J. Am. Chem. Soc.*, **32**, 1412 (1910).

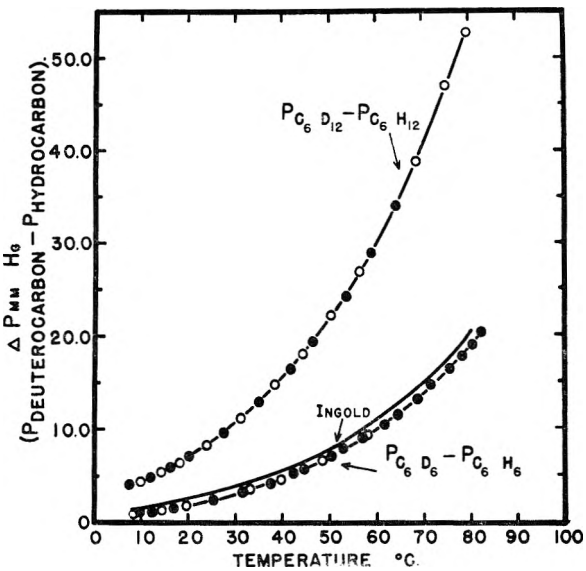

Fig. 2.—Differential vapor pressure of the C_6H_6/C_6D_6 and C_6H_{12}/C_6D_{12} pairs. Open and closed circles indicate results of different runs.

were again frozen in A and A′ and the system evacuated. Several runs were made with each liquid pair.

Treatment of Raw Data.—The height of meniscus rise in each arm of the manometer was determined for each reading, and meniscus capillarity depression corrections as given by Thomson[3] were applied. The differences in mercury height were also corrected for the change in mercury density with temperature and were converted to mercury densities at 0°. It is estimated that these data are accurate to ±0.01 mm. and ±0.03°.

The presence of the small amount of residual protium in the samples necessitates the correction of the data to the basis of 100.0% deuteration. The manner in which this small correction was made is outlined in an appendix.

Results

In all cases over the temperature range covered, the deuterocarbon has the higher vapor pressure. In Fig. 2, the corrected pressure difference between the compound pairs C_6D_6/C_6H_6 and C_6D_{12}/C_6H_{12} is plotted as a function of temperature. Smooth curves have been drawn through the points. For comparison purposes, the data of Ingold[7] also have been plotted.

From the smoothed curves, values of ΔP at ten or eleven different temperatures were taken. These were then added to the vapor pressure of the protium compound, at the given temperature. The vapor pressures of the protium compounds were calculated from the Antoine equation constants given by Willingham for cyclohexane[8] and by Forziati for benzene.[9] This procedure gives the vapor pressure of the deuterium compound at the designated temperatures. These data are listed in Table I. The constants of the Antoine equation

$$\log_{10} P_{mm} = A - \frac{B}{(C + t)} \qquad (1)$$

for the vapor pressure of the deuterocarbons were determined by the method of least squares. These constants together with the constants for the corresponding hydrocarbons are given in Table II. The boiling point at 760 mm. has been calculated and is likewise given in Table II.

TABLE I

Temp., °C.	ΔP_{mm} $C_6D_6-C_6H_6$	P_{mm}[a] C_6H_6	P_{mm} C_6D_6	ΔP_{mm} $C_6D_{12}-C_6H_{12}$	P_{mm}[b] C_6H_{12}	P_{mm} C_6D_{12}
10	1.10 (1.5)[c]	45.56	46.66	4.43	47.49	51.92
20	1.87 (2.4)	75.23	77.10	7.00	77.52	84.52
30	3.08 (3.6)	119.35	122.43	10.68	121.73	132.41
40	4.79 (5.2)	182.78	187.57	15.45	184.69	200.14
50	7.08 (7.7)	271.27	278.35	22.00	271.80	293.80
60	9.94 (10.8)	391.45	401.39	30.12	389.21	419.33
65	11.76 (12.6)	465.73	477.59	34.92	461.40	496.32
70	13.84 (14.6)	550.81	564.65	40.45	543.73	584.18
75	16.16 (17.2)	647.75	663.81	47.17	637.44	684.61
80	18.84 (20.0)	757.67	776.51	53.75	743.28	797.03
82	20.08	805.53	825.61			

[a] Calcd. from data of A. F. Forziati, W. R. Norris and R. D. Rossini.[9] [b] Calcd. from data of C. B. Willingham, W. J. Taylor, J. M. Pignocco and F. D. Rossini.[8] [c] Parenthetical values from Ingold.[7]

TABLE II

ANTOINE EQUATION CONSTANTS AND BOILING POINTS

Compound	A	B	C	B.p., °C., at 760 mm.
C_6D_6	6.88865	1196.383	219.205	79.31
C_6H_6[a]	6.91210	1214.645	221.205	80.099
C_6D_{12}	6.87038	1208.289	224.443	78.43
C_6H_{12}[b]	6.84498	1203.526	222.863	80.738

[a] Data from A. P. Forziati, W. R. Norris and R. D. Rossini.[9] [b] Data from C. B. Willingham, W. J. Taylor, J. M. Pignocco and F. D. Rossini.[8]

Discussion

For comparison purposes the only vapor pressure data available are those for C_6D_6 which have been reported by Ingold and co-workers.[7] The ΔP values reported herein were consistently lower than those of Ingold (see Fig. 2). The methods of measurement were essentially the same. The poor agreement may be due to (a) difference in the purities of the samples of C_6H_6 and C_6D_6 used in this study as compared to Ingold's samples, and (b) difference introduced by Ingold's use of a differential manometer of considerably smaller diameter without the application of meniscus corrections.

The heat of vaporization of C_6D_6 and C_6D_{12} may be calculated using the equation

$$\Delta H_{vap} = \frac{2.303\ RT^2\ B\Delta Z}{(C + t)^2} \qquad (2)$$

The B and C terms are those of the Antoine Equation and the ΔZ term takes into consideration the gas phase imperfection and the volume of the liquid phase. Without the actual P–V–T data for the deuterocarbons, the value of the ΔZ term can only be estimated. In this research the equation $\Delta Z = 1 - 0.97P_r/T_r$ as suggested by Thomson[2] was used. It was assumed that (a) in the evaluation of the reduced pressure the critical pressure of the deuterocarbon is the same as that of the hydrocarbon, (b) at their boiling points the hydrocarbon and deuterocarbon isomers have the same value of reduced temperature. With these assumptions the heats of vaporization at 25, 80° and at the boiling points have been calculated. The calculated

(6) G. Thomson, "Physical Methods of Organic Chemistry," Edited by Weissberger, 2nd Ed., Interscience Publishers, Inc., New York, N. Y., 1949, Chap. V.

(7) C. K. Ingold, C. G. Raisin, C. L. Wilson and C. R. Bailey, *J. Chem. Soc.*, 915 (1936).

(8) C. B. Willingham, W. J. Taylor, J. M. Pignocco and F. D. Rossini, *J. Research Natl. Bur. Standards*, **35**, 219 (1945).

(9) A. F. Forziati, W. R. Norris and F. D. Rossini, *ibid.*, 43 555 (1949).

values (Table III) are in good agreement with calorimetric values for the hydrocarbons, considering the uncertainty of about 0.5% in the ΔZ approximation.

TABLE III

HEAT OF VAPORIZATION IN CAL./G. MOLE

Compound	25°	80°	At b.p.
C_6H_6	8110	7394	7393
C_6D_6	8118	7367	7385
C_6H_6[a10]	..	..	7349
C_6H_6[a11]	..	..	7353
C_6H_6[7]	..	7639	..
C_6D_6[7]	..	7618	..
C_6H_{12}	7924	7214	7203
C_6D_{12}	7855	7149	7172

[a] Calorimetric values.

At the boiling point the heat of vaporization of C_6D_6 is less than that of C_6H_6, while at 25° the reverse is true. Substitution in suitable equations indicates that the heats of vaporization of C_6H_6 and C_6D_6 are equal at about 44°. The values of ΔH_{vap} are very sensitive to the values of the constants B, C and ΔZ; therefore, one can only conclude that the difference in the heat of vaporization of the isotopic pair is small, and any numerical value assigned to it will be of doubtful meaning.

For the C_6H_{12} and C_6D_{12} pair, equation 2 indicates that the heat of vaporization of C_6H_{12} is always greater than that of the C_6D_{12}.

In an appendix to the Ingold paper,[7] C. R. Bailey and B. Topley discussed the vapor pressure of C_6D_6. They attempted to explain, without success, the temperature dependence of the vapor pressure ratio $P_{C_6H_6}/P_{C_6D_6}$ which Ingold and co-workers had found could be represented by the equation

$$P_{C_6H_6}/P_{C_6D_6} = 1.00415 \exp(-20.96/RT)$$

The value -20.96 represents the difference between the heats of vaporization of the hydrocarbon and deuterocarbon calculated without the use of the ΔZ term. The present results indicate (a) that the ratio $P_{C_6H_6}/P_{C_6D_6}$ does not have a temperature dependence of the form reported by Ingold, even though the new values of the ratio only differ from those of Ingold by a maximum of 1%; and (b) that the uncertainty in the value of the heat of vaporization is considerable.

The data in the literature for the boiling points or vapor pressures of twenty-one other protium–deuterium isotopic pairs have been examined. These data have been compared with the available data for the dipole moment, polarizability and ionization potential of the normal protium molecules. Also the values of the dipole–dipole, induction and dispersion forces for the normal protium compounds have been calculated and compared with the vapor pressure data. It was hoped that an examination of these data might lead to some generalizations which would make it possible to predict which of two isotopic protium–deuterium compounds should have the higher vapor pressure. However, it was not found possible to draw any conclusions or generalizations other than the observation that in the absence of a dipole moment the deuterium compound will have the higher vapor pressure, and indeed there is one exception to this in the case of the H_2/D_2 pair.

Acknowledgment.—The authors express their appreciation to the American Petroleum Institute for the grant which made this research possible. They are also very grateful to Dr. J. Y. Beach of California Research Corporation for making possible the mass spectrometer analysis of the deuterium compounds.

Appendix

Raoult's Law Correction to Observed ΔP.—Mass spectrographic analysis[4] of the highest purity C_6D_6 and C_6D_{12}, together with analysis of intermediates which had been deuterated to a lesser degree, indicates a true statistical distribution of the partially deuterated products, *i.e.*, C_6H_5D, $C_6H_4D_2$, $C_6H_3D_3$, etc. For the materials used in this investigation (C_6D_6 of 99.3% deuteration, and C_6D_{12} of 98.8% deuteration) statistical distribution calculations indicate the presence of principally C_6HD_5, C_6D_6, and C_6HD_{11}, C_6D_{12}, respectively, and less than 0.2 mole per cent. of compounds containing lesser percentages of deuterium. Thus the vapor pressure measurements have been made on a solution of C_6HD_5 dissolved in C_6D_6, and of C_6HD_{11} dissolved in C_6D_{12}. Therefore, it is necessary to correct the observed vapor pressure differential ΔP_{obsd} to that which would have been obtained with the pure perdeuterocarbon.

It is assumed that Raoult's law is valid and further that $(P_5 - P_B) = X(P_6 - P_B)$ where P_5, P_6 and P_B refer to the vapor pressures of pure C_6HD_5, C_6D_6 and C_6H_6, respectively, and X is a constant less than unity. On the basis of these assumptions, it can be shown that for such a binary solution

$$\Delta P_{true} = (P_6 - P_B) = \frac{\Delta P_{obsd}}{X(1 - N_6) + N_6}$$

where N_6 is the mole fraction of perdeuterobenzene in the solution. It would also seem logical that X is the fraction of protium replaced by deuterium in the partially deuterated compound (*i.e.*, for C_6HD_5, $X = {}^5/_6$). A similar expression can be written for the case of C_6HD_{11} dissolved in C_6D_{12} for which $X = {}^{11}/_{12}$.

For the C_6D_6 sample used in this investigation, mass spectrographic data indicate 96 mole per cent. of perdeuterobenzene. Substitution of this value in the previous expression shows that all of the values of ΔP_{obsd} should be divided by 0.993 in order to give the correct value of ΔP_{true}. If this choice of X is in error by ±16%, the error in ΔP_{true} will be only ±0.7%.

For the C_6D_{12} sample, mass spectroscopic data indicate 86 mole per cent. of the perdeuterocyclohexane. Thus substitution of this value in the previous expression indicates that all of the values of ΔP_{obsd} should be divided by 0.988. If the choice of X is in error by 8%, then the error in ΔP_{true} will be ±1.2%.

(10) G. Waddington and D. R. Douslin, *J. Am. Chem. Soc.*, **69**, 2275 (1947).

(11) E. F. Fiock, D. C. Ginnings and W. B. Holton, *J. Research Natl. Bur. Standards*, **6**, 881 (1931).

STUDIES ON ION EXCHANGE RESINS. VI. WATER VAPOR SORPTION BY POLYSTYRENESULFONIC ACID[1]

BY MONROE H. WAXMAN,[2] BENSON R. SUNDHEIM AND HARRY P. GREGOR

Department of Chemistry, Polytechnic Institute of Brooklyn, Brooklyn, N. Y.

Received May 12, 1953

Linear polystyrenesulfonic acid and its salts sorb considerably less water, at the same relative humidities, than do their cross-linked analogs and sulfuric acid. Sorption is particularly low at relative humidities below 10%, where a strong hysteresis loop exists. The amount of water sorbed at a given relative humidity varies directly with the (hydrated) size of the exchange cation. This lowered sorption is interpreted as being due to polymer–polymer interactions, where van der Waals and other attractive forces act to prevent swelling and solution of the polymer chains. The free energies, heats and entropies of the sorption process were calculated. The considerable increase in entropy with sorption at low relative humidities is interpreted as being due to freeing of chains from positions of short range order. Freezing point data allow the calculation of osmotic coefficients for these systems. At concentrations of 0.1 normal (in terms of sulfonic groups), the value of $\phi\nu$ is approximately 0.3, which is considerably lower than corresponding values for monomeric electrolytes.

The sorption of water by linear polystyrenesulfonic acid and its salts was studied to allow a comparison with the cross-linked analogs, the ion-exchange resins. This paper describes sorption by polystyrenesulfonic acid and seven of its salts at two temperatures. The free energies, heats and entropies of sorption are calculated from these data. The next paper of this series will take up the effect of different degrees of cross-linking in the same chemical system.

Experimental Methods

Polystyrenesulfonic acid (PSA) was prepared by the sulfonation of linear polystyrene,[3] using the same general procedures described previously.[4] A mole of polystyrene was sulfonated with 15 moles of sulfuric acid, and the solution obtained diluted to 7500 ml.; pure PSA was obtained using ion-exchange methods to remove the excess sulfuric acid, as well as contaminating cations. Conventional purification techniques including fractional precipitation using lead and barium salts, and the use of mixed solvents were unsuccessful in removing the sulfuric acid impurity from the PSA solution.

The PSA solution, 0.13 *m* (molal) to PSA and 2 *m* to H_2SO_4, was passed through a 2-l. bed of hydroxide regenerated anion-exchange resin (Ionac A300, American Cyanamid Company) at a slow flow rate (85 ml./min.). Large resin particles (> 25 mesh) were used to decrease surface absorption of PSA. The column was rinsed with a small volume of water which was combined with the PSA solution. This entire process was then repeated three more times. After each pass, the total acid content of the solution was determined. The presence of sulfuric acid was shown by adding barium chloride solution to the effluent; a white precipitate which does not dissolve on heating shows the presence of sulfuric acid. This test was positive after each of the first three passes, negative after the fourth.

The total equivalents of acid originally present were 28.5. After each pass they were: 18.1; 8.6; 2.0; 0.87. Since one mole of polystyrene was used, assuming complete conversion to the monosulfonated form, it is seen that about 10% of the PSA was lost. This loss could have been reduced by more complete rinsing of the resin column after each pass, since the eluted material was largely PSA. The PSA solution contained small amounts of sodium, about 8×10^{-4} *m*. This was reduced to 3×10^{-4} *m* by passing the solution through a bed of cation-exchange resin in the hydrogen state.

The solution was concentrated to a volume of about one liter by vacuum distillation at 30°, then evaporated at this temperature under vacuum (1–2 mm.) to a tough lump of material which was broken up, ground to a fine powder, and dried at 110° to constant weight. A yield of 82.1% was obtained. The equivalent weight of PSA as determined by titration with base in the presence of sodium chloride was found to be 5.265 meq./g., while the calculated value for $C_8H_8O_3S$ is 5.430 meq./g.

The polystyrenesulfonic acid was soluble in water, methanol, ethanol and propanol; it was partially soluble in acetone and insoluble in methyl ethyl ketone, benzene, carbon tetrachloride, chloroform and hexane. The sodium and potassium salts were soluble in water, but insoluble in methanol and ethanol; the barium salt was insoluble in cold water, but soluble in hot water.

Salts of PSA were prepared by the addition of the appropriate hydroxides, using a *p*H meter to identify the end-point which was well defined. The salt solutions were evaporated slowly with stirring, and dried to constant weight in a vacuum oven at 40°. Care was taken to evaporate these solutions very slowly because the glass-like polymer tended to strip a thin layer of glass from the container.

Sorption was measured using the humidistat described previously.[5] Approximately half-gram samples were used. Freezing points of PSA solutions were determined in a Beckman apparatus, using standard techniques.[6] About one-half degree of super-cooling was encountered, following which the temperature rose to a value which remained constant (±0.001°) for 3 to 5 minutes. A modified procedure, which involved the addition of ice to the solution near its freezing point, and withdrawal of solution for analysis after constant temperature was reached, gave results which were not well reproducible, but whose averaged values agreed well with results obtained using the former technique.

Experimental Results

Sorption data for eight different polystyrenesulfonates are given in Tables I and II, referring to temperatures of 25 and 50°, respectively. The data are presented for n, the moles of water sorbed per equivalent of polystyrenesulfonic acid (189.93 g.), as a function of the relative humidity, $p/p^\circ = x$.

The samples required about three weeks to come to equilibrium at the higher relative humidities, and somewhat less at lower relative humidities. The dry powder, on sorbing water, was gradually converted into a very viscous liquid; examination showed that at all stages of the sorption process the system was homogeneous. After equilibrium was established, the samples were weighed daily for a two-week period. The standard relative deviations were five parts per thousand at relative

(1) The authors wish to thank the Office of Naval Research for the support given to this work.

(2) A portion of this work is abstracted from the dissertation of Monroe H. Waxman, submitted in partial fulfilment of the requirements for the degree of Doctor of Philosophy in Chemistry, Polytechnic Institute of Brooklyn, June, 1952.

(3) David E. Baldwin, Thesis, Polytechnic Institute of Brooklyn, June, 1950.

(4) H. P. Gregor, J. I. Bregman, F. Gutoff, R. D. Broadley, D. E. Baldwin and C. G. Overberger, *J. Colloid Sci.*, **6**, 20 (1951).

(5) H. P. Gregor, B. R. Sundheim, K. M. Held and M. H. Waxman, *ibid.*, **7**, 511 (1952).

(6) A. Weissberger, "Physical Methods in Organic Chemistry," Interscience Publishers, Inc., New York, 1949.

TABLE I

WATER SORPTION BY LINEAR POLYSTYRENE SULFONATES AT 25°

$x = p/p°$	H^+ n	Li^+ n	Na^+ n	K^+ n	NH_4^+ n	$(CH_3)_4N^+$ n	$(Et)_4N^+$ n	$(Bu)_4N^+$ n
0.05	0.115	0.383	0.307	0.251	0.251	0.210	0.174	0.210
.085	.393	.449	.607	.393	.291	.578	.909	.414
.094	.590	.490	.611	.412	.315	.800	1.003	.533
.117	.713	.504	.695	.513	.633	1.010	1.082	.601
.135	.898	.653	.745	.676	.700	1.118	1.151	.606
.201	1.065	.875	.994	.782	.870	1.236	1.459	.910
.287	1.170	.945	1.157	.816	.943	1.460	1.651	1.171
.443	2.102	1.708	1.650	1.299	1.091	2.081	2.195	1.348
.670	4.040	3.456	2.736	1.973	2.285	3.680	4.174	2.370
.761	5.351	4.630	3.592	2.143	3.144	5.057	5.968	3.290
.792	6.240	5.825	4.094	2.882	3.529	6.221	6.808	3.658
.849	7.517	6.881	5.391	3.101	4.667	7.532	8.210	4.492
.882	8.926	8.715	6.360	4.297	6.142	9.330	9.110	5.232
.921	11.826	11.863	8.750	5.845	8.423	11.925	12.237	7.081
.956	18.705	19.592	15.211	11.387	15.640	19.990	19.113	13.988
.974	25.956	26.440	19.953	16.117	19.310	25.039	26.153	19.485

TABLE II

WATER SORPTION BY LINEAR POLYSTYRENE SULFONATES AT 50°

$p/p°$	H^+ n	Li^+ n	Na^+ n	K^+ n	NH_4^+ n	$(CH_3)_4N^+$ n	$(C_2H_5)_4N^+$ n	$(C_4H_9)_4N^+$ n
0.0135	0.00	0.00	0.00	0.00	0.00	0.00	0.00	0.00
.0275	.00	.00	.00	.00	.00	.00	.00	.00
.0580	.106	.266	.211	.102	.049	.200	.034	.207
.1046	.438	.410	.447	.210	.226	.517	.640	.582
.254	1.21	.815	.953	.636	.679	.968	.945	.922
.501	2.28	1.673	1.582	1.112	1.286	1.861	2.159	1.522
.747	4.02	3.530	3.109	2.059	2.732	4.156	4.305	3.180
.920	9.69	9.304	7.318	5.336	6.547	10.378	9.829	5.150

humidities above 90%, and less than one part per thousand at the lower relative humidities.

To show the general character of the sorption curves, a representative curve (for the lithium salt) at the two temperatures is given in Fig. 1, together with similar data for sulfuric acid.

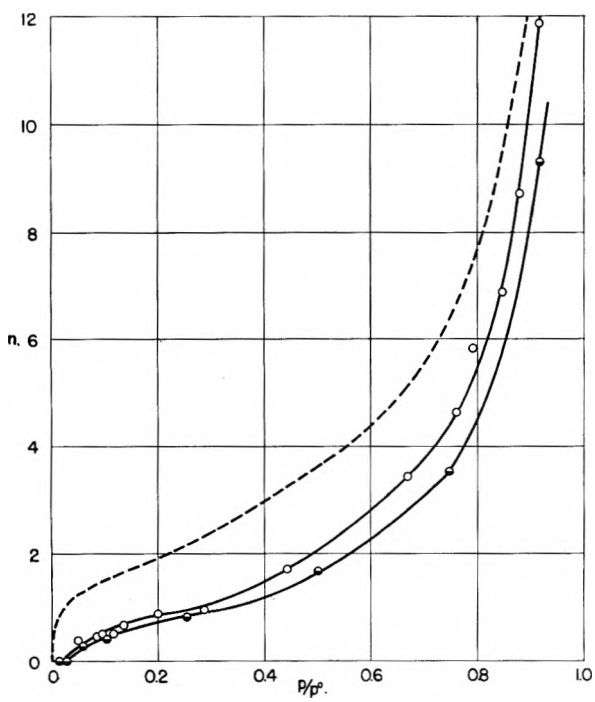

Fig. 1.—Sorption curves for the lithium salt of PSA at 25° (○) and 50° (◒), together with sorption curve for sulfuric acid at 25° (- -), presented as n, the moles of water sorbed per equivalent, as a function of $p/p°$.

Hysteresis effects were not observed (within experimental error) in the relative humidity range $0.1 < x < 1$. Below $x = 0.1$, a pronounced hysteresis effect was observed, where the descending loop was markedly higher than the ascending curve. Figure 2 shows this hysteresis effect for PSA at 25°. The data of Tables I and II are the ascending values in all cases.

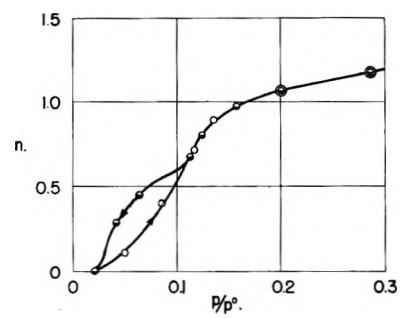

Fig. 2.—Hysteresis effects for PSA at 25°: ○, ascending curve; ◒, descending curve.

Freezing point measurements for PSA solutions are given in Table III; the freezing point depression θ is given for different values of m_2, the molality of the cationic species.

Discussion

A comparison of Figs. 1 and 2 shows that the hysteresis effect occurs over but a very small por-

TABLE III

CRYOSCOPIC DATA FOR POLYSTYRENESULFONIC ACID

m_2	θ in °C.	θ/m_2	m_2	θ in °C.	θ/m_2
1.135	1.265	1.114	0.196	0.116	0.592
0.710	0.600	0.845	.183	.108	.590
.664	.541	.815	.146	.082	.562
.464	.356	.767	.137	.075	.547
.446	.344	.771	.107	.060	.561
.343	.240	.670	.091	.050	.549

tion of the sorption curve. This effect is customarily interpreted as being due to short range order among the polymer chains. X-Ray powder diagrams of the dry PSA gave characteristic amorphous patterns, showing that any degree of order which did exist must have been very low. Thermodynamic functions were calculated using only the ascending values; the legitimacy of this selection has been thoroughly discussed, see, *e.g.*, White and Eyring.[7] In any event, the change in the thermodynamic functions introduced by the hysteresis is quite small.

An examination of Fig. 1 will serve to show the principal features of the sorption. The uptake of water as a function of relative humidity is quite similar to that for sulfuric acid with but one notable difference. At low (< 0.05) values of x, the sulfuric acid curve rises steeply and then quickly levels off while that of PSA shows almost no uptake until x becomes about 0.1, whereupon the sorption rises rapidly. Above this point the curves are very similar. One would not expect the curves to be identical, since there must be considerable differences in the activity coefficients of sulfuric acid and PSA by virtue of their chemical and structural differences. However, since they are both strong electrolytes, miscible in all proportions with water, it is expected that the shapes of these curves will be similar. Attempts to fit the PSA sorption curve or that of its salts to any of the BET type sorption curves were unsuccessful.

Among the various salts of PSA, the curves split into two definite groups. The first group contains, in order of the highest water sorption, those of tetraethylammonium, tetramethylammonium, hydrogen and lithium. All of these curves fall extremely close to one another. The next group includes the curves for the sodium, ammonium and tetrabutylammonium polymers, again spaced very closely. The potassium curve, surprisingly, falls distinctly below all the others for values of x greater than 0.3. These data are shown plotted in Fig. 3.

Ignoring the tetrabutylammonium curve for the moment, the sequence of curves is found to be approximately the sequence of activity coefficients of the corresponding halides, although ammonium is somewhat higher than anticipated. It is difficult to be sure of the correct activity coefficients of the quaternary salts but there is good reason to believe that they are placed in the same relative order as these sorption curves show.[8-10] The somewhat lower position of the tetrabutylammonium salt is doubtless due to its predominantly organic character. As the molecular weight of the organic portion is increased, the quaternary ammonium ions eventually become immiscible with water.

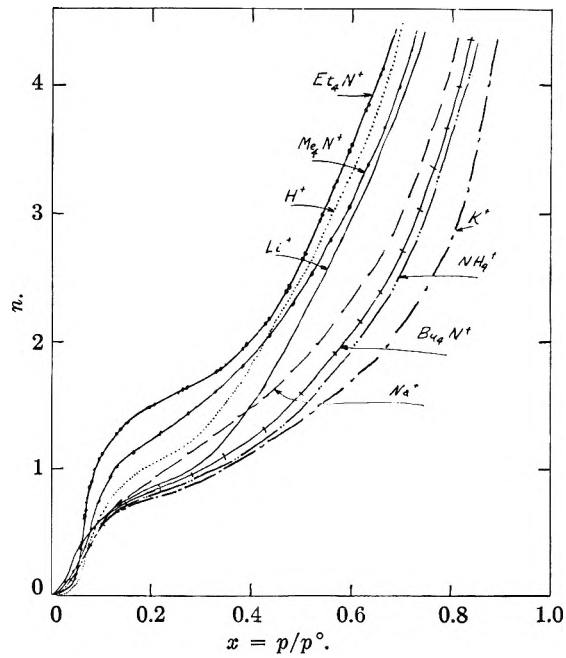

Fig. 3.—Sorption curves for PSA and its salts at 25°.

The sorption curves then proceed in the sequence of the largest (hydrated) ions. This behavior is characteristic of strong electrolytes in aqueous solutions and also may be inferred from the data of Stokes and Robinson.[11] Similar conclusions have been drawn from sorption studies of 10% cross-linked polystyrenesulfonic acid.[5]

The thermodynamics of the sorption of water vapor by polymers has been discussed in several papers.[12-15] The reaction considered is, taking as the source pure water, Polymer ($p = 0$) + $n\mathrm{H_2O}$ (p°) $\rightleftarrows$ Polymer·$n\mathrm{H_2O}$ (p). For this system the product is a homogeneous phase, and the calculation of thermodynamic quantities is the same as for other solution processes. It should be noted that the technique outlined below is not applicable to adsorption processes where a surface phase may be present.

The free energy change for the sorption process may be derived as follows: At constant temperature and pressure n_1 moles of water having a chemical potential of μ_1° (corresponding to $p = p^\circ$) and n_2 moles of dry polymer of chemical potential μ_2° react to form a solution where the solvent chemical potential is μ_1 and for the solute it is μ_2. For this process

$$\Delta F = n_1\mu_1 + n_2\mu_2 - n_1\mu_1^\circ - n_2\mu_2^\circ$$

But $\mu_1 - \mu_1^\circ = RT \ln x$. From the Gibbs–Duhem expression

(7) H. J. White and H. Eyring, *Textile Research J.*, **17**, 523 (1947).
(8) L. Ebert and J. Lange, *Z. physik. Chem.*, **A139**, 584 (1928).
(9) H. S. Harned and B. B. Owen, "The Physical Chemistry of Electrolytic Solutions," Reinhold Publ. Corp., New York, N. Y., 1950.
(10) J. Lange, *Z. physik. Chem.*, **A168**, 147 (1934).
(11) R. H. Stokes and R. A. Robinson, *J. Am. Chem. Soc.*, **70**, 1870 (1948).
(12) H. B. Bull, *ibid.*, **66**, 1499 (1944).
(13) S. Davis and A. D. McLaren, *J. Polymer Sci.*, **3**, 16 (1948).
(14) M. Dole and A. D. McLaren, *J. Am. Chem. Soc.*, **69**, 651 (1947).
(15) A. D. McLaren and J. W. Rowen, *J. Polymer Sci.*, **7**, 289 (1951).

$$d\mu_2 = -(n_1/n_2)d\mu_1, \text{ and}$$

$$\mu_2 - \mu_2^\circ = -\int_{-\infty}^{\mu_1} \frac{n_1}{n_2} d\mu_1 = -RT \int_{-\infty}^{\ln x} n_1 \, d \ln x$$

Then

$$\Delta F = -RT \int_{-\infty}^{\ln x} n_1 \, d \ln x + n_1 RT \ln x$$

The latter expression is equivalent to

$$\Delta F = \int_0^{n_1} \mu_1 \, d \, n_1 \qquad (13)$$

However, neither of these forms is convenient for carrying out graphical integrations since in both cases quantities which go to infinity are encountered. Therefore, the above expression is converted to

$$\Delta F = -RT \int_0^x \frac{n \, dx}{x} + nRT \ln x$$

When $-nRT/x$ is plotted against x, as $x \rightarrow 0$ Henry's law is obeyed, a straight line relationship

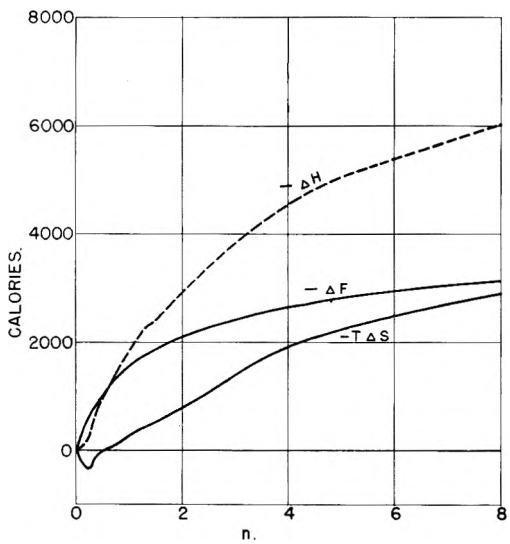

Fig. 4.—Thermodynamic properties ΔF, ΔH and $T\Delta S$ for the sorption process with the lithium salt of polystyrenesulfonic acid as a function of n.

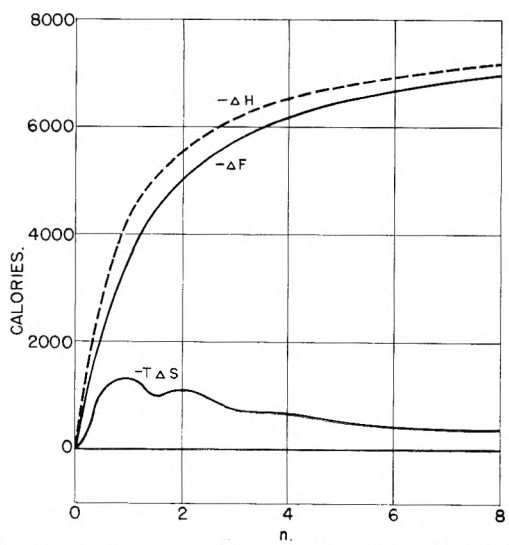

Fig. 5.—Thermodynamic properties ΔF, ΔH and $T\Delta S$ for the sorption process with sulfuric acid as a function of n.

becomes evident and the extrapolation can be made.

In order to calculate the heat or entropy of this reaction from the temperature coefficient of the free energy, it must be noted that different values of n are obtained for the same value of either p or x. The thermodynamic values desired must be calculated at the same value of n, giving the so-called "isosteric" heat.

The pertinent equations are

$$\left(\frac{\partial(\Delta F/T)}{\partial T}\right)_p = -\frac{\Delta H}{T^2}$$

$$\left[\frac{\partial(\Delta\mu/T)}{\partial T}\right]_{n,p} = -\frac{(\partial \Delta H/\partial n)_{T,p}}{T^2} = \left[\frac{\partial(R\Delta \ln x)}{\partial T}\right]_{n,p}$$

Then

$$\left(\frac{\partial \Delta H}{\partial n}\right)_{T,p} = \frac{RT_1T_2}{T_2 - T_1} \ln \frac{x_1}{x_2} = \Delta H^*$$

where ΔH^* is the isosteric heat, and is analogous to the differential heat of dilution. Here T_2 is the higher temperature, the amount of water sorbed, n, being the same at both x_1 and x_2. The integral heat ΔH is calculated by a graphical integration of the above equation. The entropy change ΔS is calculated from $(\Delta H - \Delta F)/T$.

The integral heats, free energies and entropies of sorption of representative salts of PSA were calculated as indicated above. A typical curve, that for lithium, is shown in Fig. 4. For comparison, the corresponding curves for sulfuric acid, calculated from vapor pressure data,[16] are given in Fig. 5. Similar calculations of the free energy[17,18] have previously appeared for sulfuric acid, but for a different process.

The curves for the free energy and heat content are not as informative or as interesting as the entropy curves. In evaluating the entropy change for this type of process, three types of contributions are important. There will be a so-called "ideal entropy of mixing" which will be positive in sign. In these electrolytic solutions there will also be important terms due to unsymmetrical interactions and these terms may be either positive or negative. In addition, there may be purely geometrical terms related to the shape, size and packing of the molecules. In the case of sulfuric acid, unsymmetrical interactions between solute and solvent molecules make for large negative entropy terms. In systems where the heat of solution is less negative or is positive, there may be a net positive entropy gain, which is, however, everywhere positive and shows no reversal of sign.

In the case of all of the PSA salts, there is a significant net positive entropy gain in the region $n \lesssim 1$, which changes sign and becomes negative as n increases. This striking behavior does not occur for ordinary electrolytes. For PSA salts, the ideal entropy of mixing term is, of course, the same as the corresponding term in the expression for sulfuric acid; from chemical considerations, the

(16) "International Critical Tables," Vol. III, McGraw-Hill Book Co., Inc., New York, N. Y., 1st Ed., 1928, p. 303.

(17) J. R. Katz, *Ergebn. exakten Naturwiss.*, **3**, 372 (1924); *ibid.*, **4**, 197 (1925).

(18) A. J. Stamm and W. K. Loughborough, THIS JOURNAL, **39**, 121 (1935).

second term, here primarily due to hydration, would be expected to be of comparable magnitude. It is, therefore, concluded that the unusual shape of the entropy curves for PSA salts is due to the presence of a positive entropy contribution arising from the configurational peculiarities of long chain molecules.

This argument is substantiated by a comparison between the curves for the lithium salt of PSA (Fig. 4) and sulfuric acid (Fig. 5). The ΔH curves of both are of about the same magnitude; for example, at $n = 7$, ΔH for the acid is -7000 cal. and for the salt is -5800. However, the curve for the acid is initially concave to the abscissa, while that for the salt is initially convex and later concave. The ΔF curves are quite different in their magnitudes, being -6800 cal. at $n = 7$ for the acid, and rising to only -3000 for the salt. Both curves are concave to the abscissa. The entropy curves are strikingly different. At $n = 0.25$, $T\Delta S$ for the acid is -200 cal., while for the salt it is $+350$. At $n = 7$, $T\Delta S$ is -200 cal. for the acid, and -2800 for the PSA salt. Thus the entropy difference between PSA and sulfuric acid is not a reflection of a heat of interaction, but rather of a purely geometrical phenomenon.

The only other instances of similar entropy curves known to the authors are those for some proteins.[12,13] In these papers positive net entropies and trends toward more positive net entropies are interpreted as "incipient solution." This interpretation clearly does not apply to the systems at hand, in view of the fact that sulfuric acid itself does not show a positive net entropy at any perceptible value of n. It seems much more likely that since this behavior has been observed only in polyelectrolyte systems, the entropy change is a reflection of configurational changes. This may be a freeing of polar groups for rotation,[13,19] or may be related to an untangling of chains.

Curves of the ΔF, ΔH and $T\Delta S$ functions for the other salts of PSA showed the same general shape as that for the lithium salt, but differed in magnitude. The sequence of ΔF values followed the sorption curves shown in Fig. 3. A numerical comparison of $-\Delta F$ values at $n = 12$ is as follows: tetraethylammonium, 4,450; tetramethylammonium, 3,950; hydrogen, 3,810; lithium, 3,360; sodium, 3,240; tetrabutylammonium, 2,830; ammonium, 2,750; potassium, 2,450 cal.

In order to examine the behavior of PSA solutions in the dilute range ($m_2 < 2$), corresponding to relative humidities above 97%, freezing point measurements were made. An alternative technique is the measurement of osmotic pressure. The product of the practical osmotic coefficient ϕ and the dissociation number ν at 25° was calculated from isopiestic data, and at the freezing point from freezing point data[9]; this is shown in Fig. 6.

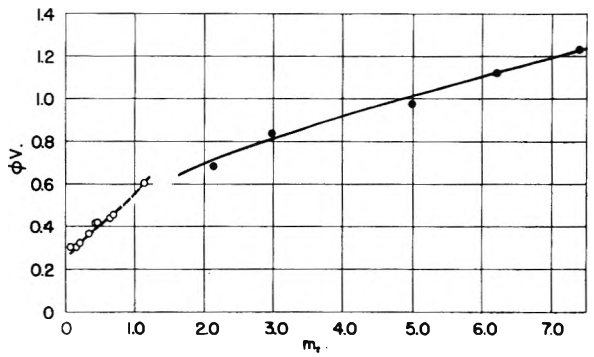

Fig. 6.—The product of the practical osmotic coefficient ϕ and the dissociation number ν plotted against m_2 for PSA solutions; ●, calculated from isopiestic data at 25°; ○, from freezing point measurements at the freezing point.

Ordinarily ν is determined by extrapolating to zero concentration where ϕ becomes unity. Extrapolation is obviously very uncertain for the PSA curve which is falling rapidly at low concentrations; it is not possible to tell where or how it will approach the axis. Also, the PSA curve is definitely unlike those for simple, strong electrolytes. For example, the values of $\phi\nu$ for sulfuric acid are about 2 in the dilute region, and then abruptly ascend to three as the secondary dissociation occurs. If it is postulated that activity effects of the Debye-Hückel type are somewhat the same in both cases, then the low value of $\phi\nu$ for PSA is due to the polyelectrolyte character of the anion. Unusual behavior for similar compounds is well known from viscosity, conductance, osmotic pressure and activity coefficient measurements.[20-23] No further conclusions can be drawn about this curve without extending the data to lower concentrations, beyond the limit of the freezing point method.

In view of the fact that the shape of the curve is uncertain as $m_2 \to 0$, it is impossible to calculate solute activity coefficients from these data unless an awkward and arbitrary standard state is chosen.

(19) G. King, *Nature*, **158**, 134 (1946).

(20) R. M. Fuoss and U. P. Strauss, *Ann. N. Y. Acad. Sci.*, **51**, 836 (1949).

(21) W. Kern, *Z. physik. Chem.*, **A181**, 249 (1938); **A184**, 302 (1939); **A184**, 197 (1939).

(22) A. Oth and P. Doty, THIS JOURNAL, **56**, 43 (1952).

(23) U. P. Strauss and R. M. Fuoss, *J. Polymer Sci.*, **4**, 457 (1949).

STUDIES ON ION EXCHANGE RESINS. VII. WATER VAPOR SORPTION BY CROSS-LINKED POLYSTYRENESULFONIC ACID RESINS[1a]

BY BENSON R. SUNDHEIM,[1b] MONROE H. WAXMAN AND HARRY P. GREGOR

Department of Chemistry, Polytechnic Institute of Brooklyn, Brooklyn, N. Y.

Received March 9, 1953

The sorption of water vapor by cross-linked polystyrene sulfonic acid has been studied in systems differing in ionic states and in degrees of cross-linking. The net free energies, heats and entropies of the sorption process are calculated and discussed. The sorption is interpreted in terms of the three important factors: polymer–polymer interaction, restraining cross-links and electrolytic effects.

The water sorption properties of linear polystyrene sulfonic acid and its salts, as well as preliminary studies on a variety of ion exchange resins have been described in two previous papers.[2,3] This paper presents a systematic study of the water sorption properties at two temperatures of a family of resins of variable degrees of cross-linking and in various ionic states. The free energies, heats and entropies of the sorption reaction are calculated and discussed.

Experimental Procedures and Results

Eight polystyrenesulfonic acid resins were prepared[4] using amounts of divinylbenzene, the cross-linking agent, varying from 0.4 to 23%. These resins were conditioned and the capacities measured.[4] Eight different ionic states of each resin were prepared and dried to constant weight in a vacuum oven at 40°. The resins are designated by giving the nominal percentage of cross-linking agent followed by the ionic state; *e.g.*, DVB 2-K refers to the potassium salt of a resin having 2% of divinylbenzene.

Isopiestic sorption studies were made at 25 and 50° using the humidistat described previously.[2] The dry samples weighed approximately 0.5 g. each; equilibrium was established within two to four days depending upon the DVB content and the relative humidity. Weight fluctuations for systems of this type have been studied and evaluated in a previous paper.[2] The weights at 100% relative humidity were determined by the centrifugation technique.[5,6] Reproducible results for the wet weight of DVB 0.4 could not be obtained because of its gelatinous nature. During the sorption process the resin particles do swell and increase in size as described previously,[2] but of course only a single phase is present at all times up to $x = p/p^\circ = 1.0$.

The capacities of the various resins, in meq. per dry g. of hydrogen resin, measured by titration of the hydrogen state vary from 6.85 for DVB 0.4 to 4.13 for DVB 23. The resin samples and capacities are very similar to ones described previously, but not identical with them.[4] Tables I and II present the sorption data for a representative ionic state, hydrogen, as n, moles of water sorbed per equivalent of resin as a function of x, the relative humidity at 25 and 50°, respectively. These data have been plotted in Figs. 1, 2 and 3; the curve for DVB 10-H appears in each for purposes of comparison.

The results for the hydrogen state are quite typical and, since the data are lengthy, numerical results for the other ionic states are given elsewhere[7]. Figures 4 and 5 compare the sorption of different ionic states at the same per cent. of cross-linking with resin DVB 10.

TABLE I

MOLES OF WATER SORBED PER EQUIVALENT OF CROSS-LINKED POLYSTYRENESULFONIC ACID RESINS AT 25° AS A FUNCTION OF p/p°

	DVB, %							
p/p°	0.4	2	4	8	10	13	17	23
0.006	0.41	0.40	0.61	0.73	0.90	1.08	1.05	0.51
.0218	0.69	0.77	1.05	1.17	1.43	1.54	1.30	0.87
.050	0.99	1.11	1.28	1.33	1.61	1.69	1.48	1.14
.0845	1.20	1.44	1.46	1.57	1.84	1.86	1.69	1.53
.0940	1.25	1.51	...	1.69	...	...	..	..
.1345	1.39	1.70	1.79	1.90	2.12	2.09	1.81	1.86
.201	1.67	2.04	2.06	2.25	2.49	2.34	1.98	2.20
.287	2.05	2.55	2.50	2.72	2.91	2.66	2.28	2.51
.443	2.97	3.58	3.38	3.64	3.90	3.41	3.04	2.98
.667	5.50	5.53	4.90	5.30	5.50	4.93	4.30	3.87
.759	7.06	7.10	6.06	6.14	6.40	5.60	4.98	4.26
.813	8.26	8.26	7.08	7.02	7.15	6.14	5.36	4.60
.827	8.70	8.59	7.41	7.30	7.32	6.31	5.42	4.76
.885	10.79	10.35	9.03	8.64	8.16	7.21	6.13	5.21
.924	13.70	12.93	11.39	9.69	9.08	7.97	6.60	5.62
.957	18.50	16.49	14.38	11.02	9.86	8.81	6.99	6.13
.976	23.21	20.20	16.77	12.21	10.66	9.30	7.37	6.40
1.000	...	55.17	28.43	14.05	11.79	10.38	7.61	7.01

TABLE II

MOLES OF WATER SORBED PER EQUIVALENT OF CROSS-LINKED POLYSTYRENESULFONIC ACID RESINS AT 50° AS A FUNCTION OF p/p°

p/p°	0.0135	0.0275	0.0580	0.1046	0.254	0.501	0.747	0.92
% DVB	n	n	n	n	n	n	n	n
0.4	0.35	0.47	0.75	1.06	1.75	3.42	6.50	13.28
2	.36	.61	0.92	1.31	2.12	3.61	6.22	12.51
4	.40	.73	1.02	1.25	2.06	3.42	5.65	10.99
8	.64	.83	1.07	1.34	2.05	3.61	5.54	9.69
10	.70	1.01	1.25	1.45	2.31	3.75	5.50	8.99
13	.85	1.14	1.38	1.60	2.08	3.38	5.19	7.81
17	.83	1.05	1.23	1.41	1.71	2.82	4.20	5.82
23	.46	0.69	0.94	1.31	1.94	2.92	4.08	5.35

Discussion

Hysteresis.—The importance of hysteresis was evaluated as follows: Two 0.6-g. samples of Dowex-50 (about 10% cross-linked) in the hydrogen state, carefully selected for uniformity of size and shape of the particles, and which had never been completely dried, were used. Each sample was run separately through a sorption curve at 50° from p/p° equal to 0.0135 to p/p° equal to one, using the humidistat previously described. The samples were weighed daily from 3 to 8 days after the attainment of equilibrium to permit the averaging of fluctuations. After the ascending loop of the curve was obtained, one sample was run back down the curve and then up again. The second sample was run through these three loops in the opposite directions. The maximum difference between ascending and descending curves is never more than 3 mg. ($p/p^0 = 0.7$), corresponding to a difference of 4–5%

(1) (a) The authors wish to thank the Office of Naval Research for the support given to this work. (b) New York University, New York, N. Y.

(2) H. P. Gregor, B. R. Sundheim, K. M. Held and M. H. Waxman, *J. Colloid Sci.*, **7**, 511 (1952).

(3) M. H. Waxman, B. R. Sundheim, and H. P. Gregor, THIS JOURNAL **56**, 969 1953.

(4) H. P. Gregor, J. I. Bregman, F. Gutoff, R. D. Broadley, D. E. Baldwin and C. G. Overberger, *J. Colloid Sci.*, **6**, 20 (1951).

(5) H. P. Gregor, F. Gutoff and J. I. Bregman, *ibid.*, **6**, 245 (1951).

(6) H. P. Gregor, K. M. Held and J. Bellin, *Anal. Chem.*, **23**, 620 (1951).

(7) M. H. Waxman, Thesis for the Ph.D., Polytechnic Institute of Brooklyn, 1952.

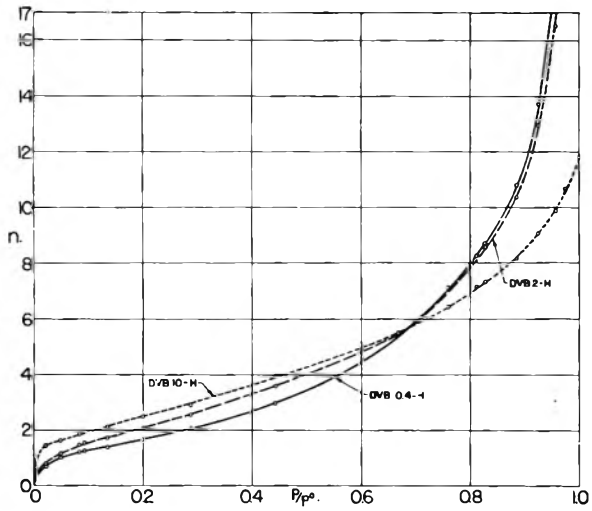

Fig. 1.—Sorption of water by resins DVB 0.4-H, 2-H, 10-H.

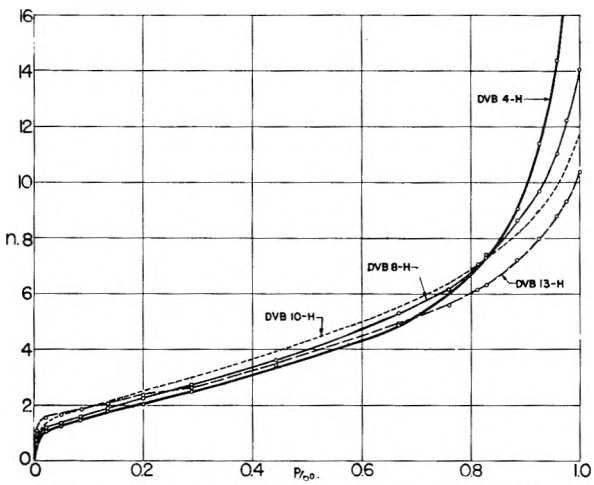

Fig. 2.—Sorption by DVB 4-H, 8-H, 10-H, 13-H.

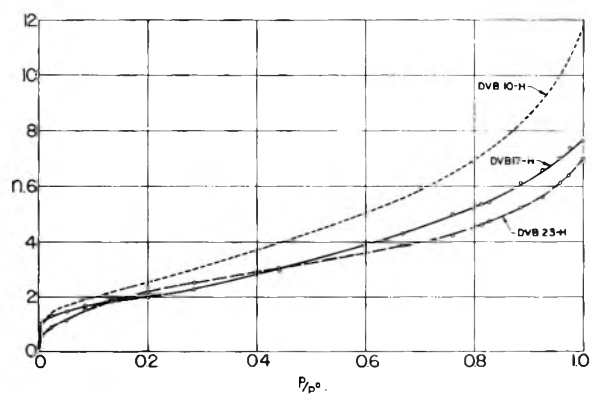

Fig. 3.—Sorption by DVB 10-H, 17-H, 23-H.

of the weight of water sorbed. Each curve reproduces itself accurately when the sorption is proceeding in the same direction. The data are presented in Fig. 6.

We conclude that there is a small amount of hysteresis in sorption by these systems. Since the loop in one direction can be reproduced accurately, there are no irreversible changes produced in the resin. Average values are reported in Tables I and II, obtained as a result of shifting samples

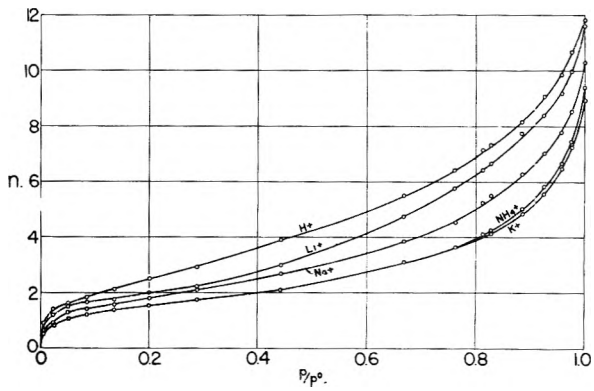

Fig. 4.—Sorption by DVB in 10 various ionic states.

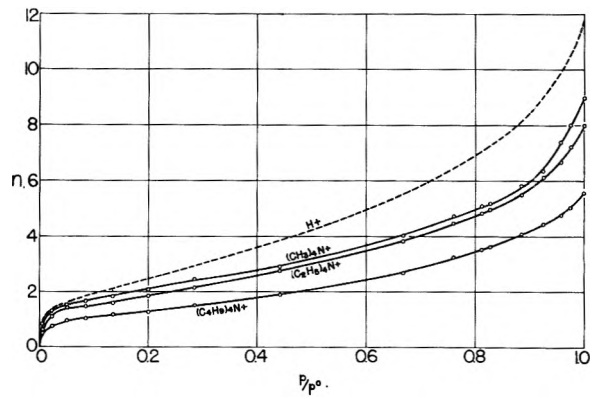

Fig. 5.—Sorption by DVB 10 in various ionic states.

randomly from one desiccator to another in the humidistat.

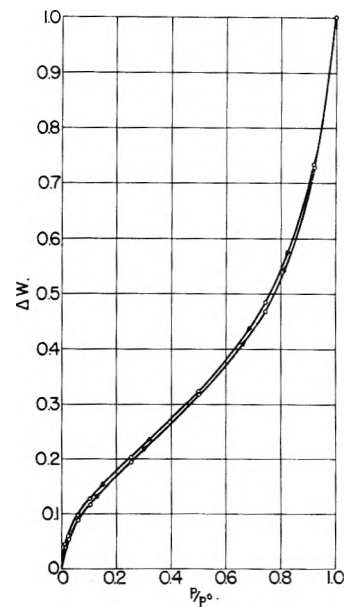

Fig. 6.—Hysteresis for DVB 10-H at 50°.

Effect of Cross-linking.—The sorption curves are all characteristically sigmoid in shape. The initial uptake of water becomes sharper as the percentage of divinylbenzene is increased and then falls off slightly at the very last with DVB 23. The central portions of all the curves are similar, and at high values of x the intercepts fall in the sequence of per cent, cross-linking, the lowest DVB resins sorb-

ing the largest amounts of water. Sorption curves for similar materials have been presented by Glueckauf and Duncan[8]; however, these authors do not appear to find the effects noted above at low values of the relative humidity.

Effect on Ionic State.—The effect of varying the ionic state has been discussed previously for a similar type of resin, approximately 10% cross-linked.[2] In that case, it was found that the sorption curves for different ionic states fell into two distinct families; the first including the H^+, Li^+, Na^+, NH_4^+ and K^+ states in the order of decreasing sorption, the second including the quaternary ammonium cations. This behavior is found in the present study as well for resins varying from DVB 2 to 23; Figs. 4 and 5 show typical results with resin DVB 10. The relative positions of the different ionic states and the separation into two general groups remains for all degrees of cross-linking. The first group follows the hydration sequence of the corresponding halides in aqueous solution. The group of quaternary ammonium salts differs from the first group in two respects. The curves invariably rise more sharply at low values of x. The horizontal portion is more extended with the result that the rise in the value of n in the latter portion of the curve does not occur until higher values of x. The difference between the quaternary ammonium group and the alkali group is attributed in the main to the organic nature of the former cations, which may lead to interaction with the organic portion of the resin,[9] and to activity coefficient effects of the type which occur in ordinary electrolytic solutions, which unfortunately are difficult to evaluate due to the lack of such data in the literature. It has been shown that the latter effect is of importance in evaluating the sorption curves of quaternary ammonium salts of linear polystyrenesulfonic acid.[3] An explanation of the sharp initial rise in the sorption curves of these organic resinates is advanced in following sections. The predominantly organic character of the tetrabutylammonium ion is undoubtedly responsible for the lower position of this curve relative to the other quaternary ammonium cations. This effect also has been observed with the linear material.

Calculation of Thermodynamic Functions.—From the water sorption data, the integral free energies, heats and entropies of the sorption process have been calculated for some of the various DVB's in the hydrogen state.[3,10–13] These quantities are presented in Figs. 7–10, plotted as a function of n, the moles of water sorbed. Because the change in sorption with temperature is not large, the calculated heats are less accurate than the calculated free energies of sorption. It is therefore felt that the absolute magnitudes of the entropy curves cannot be given great weight, but that relative magnitudes and the general shapes of these curves are of significance.

The net entropy changes for all the cross-linked resins are negative, the usual case for sorption, since the sorbed material is going into a more ordered state. It is to be noted that the entropy function becomes more negative with increasing amounts of cross-linking at constant values of the relative humidity. This is shown in Fig. 11 where the variation of $T\Delta S/n$ at $p/p^\circ = 0.957$ is plotted as a function of per cent. DVB. The entropy of sorption per mole of water is least negative for the linear polystyrene sulfonic acid at the same value of x.[3] This sequence is in agreement with the concept of entropic elasticity, where the increase of tension on isothermal swelling has been shown to be largely an entropy effect.[14] The increase in the number of entropy springs which oppose swelling with increased cross-linking should then be accompanied by a corresponding decrease in the entropy of sorption, and this is found to be the case.

The variation of the thermodynamic functions with ionic states for each percentage of DVB has been summarized by Waxman.[7] Since the data are very lengthy they will not be reproduced here.

Nature of Sorption Process.—The variation of the curves with per cent. cross-linking shows a very surprising feature. The resins with higher DVB's as 10, 13, 17 and 23% have initial rises similar to sulfuric acid,[15] and then, since the swelling is restricted, intercept the $x = 1.00$ ordinate at finite values of n. Resins with lower DVB's swell more highly at high values of x but have initial uptakes unexpectedly lower than the high DVB's. Thus each lower DVB curve crosses that of every higher DVB. Therefore, the effect of additional cross-linking seems to be the raising of the initial portion of the sorption curve and the depression of the final portion.

Comparison with sulfuric acid substantiates this interpretation. Sulfuric acid which is chemically similar to the resins shows an abrupt initial rise almost identical with that of DVB 10-H, and the two curves are very similar for the first 80% of the n *versus* x curve.[2] Thus one is led to consider the curves as divided into two regions. In the first, for low values of x, the water uptake is abnormally depressed for the resins having low values of DVB. In the second, for high values of x, the water uptake is depressed for resins with high DVB contents. This latter effect is clearly the result of increased restriction on swelling as has been discussed in terms of entropy springs. The former, however, requires a closer examination.

The question is what should be considered as normal behavior of an electrolyte of this chemical type at low values of x as distinguished from complications introduced by the high polymeric character of the material. Comparison with linear polystyrenesulfonic acid reveals that the amount of water sorbed falls below that for all the DVB's at low values of x, and above them at high values of x. The initial portion of the sorption curve is radically different from that for sulfuric acid and is

(8) E. Glueckauf and J. F. Duncan, "Atomic Energy Research Establishment Report," Ministry of Supply, Harwell, Berks., 1951.

(9) H. P. Gregor and J. I. Bregman, *J. Colloid Sci.*, **6**, 323 (1951).

(10) H. B. Bull, *J. Am. Chem. Soc.*, **66**, 1499 (1944).

(11) S. Davis and A. D. McLaren, *J. Polymer Sci.*, **3**, 16 (1948).

(12) M. Dole and A. D. McLaren, *J. Am. Chem. Soc.*, **69**, 651 (1947).

(13) A. D. McLaren and J. W. Rowen, *J. Polymer Sci.*, **7**, 289 (1951).

(14) E. Guth, H. M. James and J. Mark, "Advances in Colloid Science," Vol. II, John Wiley and Sons, Inc., New York, N. Y., 1946.

(15) "International Critical Tables, Vol." III, McGraw-Hill Book Co., Inc., New York, N. Y., 1st Ed., 1928, p. 303.

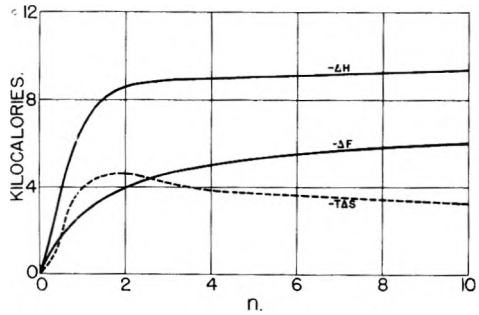

Fig. 7.—Thermodynamic functions for the water sorption process for DVB 0.4-H, as a function of n.

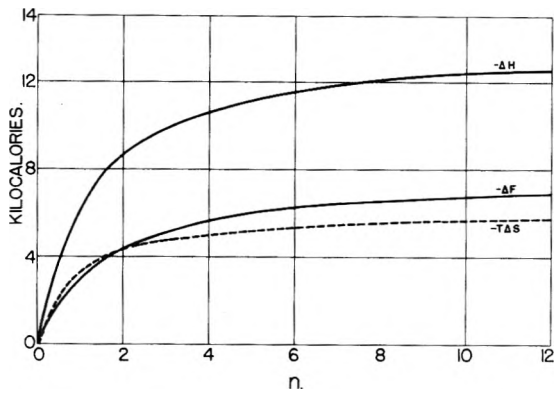

Fig. 8.—Thermodynamic functions for the water sorption process for DVB 2-H, as a function of n.

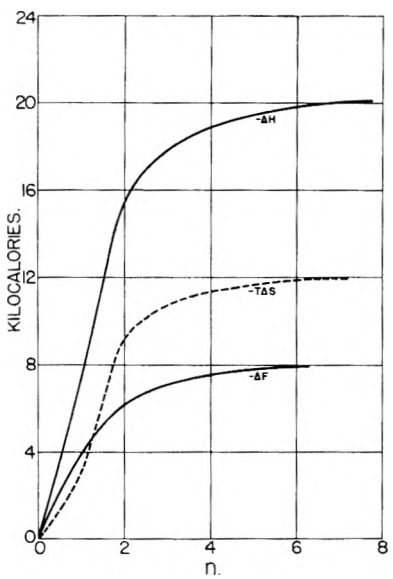

Fig. 9.—Thermodynamic functions for the water sorption process for DVB 13-H, as a function of n.

discussed more fully in a recent publication.[3] An inspection of the thermodynamic functions reinforces this opinion. As the degree of cross-linking is increased, the heat and free energy of hydration become markedly more negative. The heat of hydration of DVB 13-H, for instance, is almost the same as that for sulfuric acid through a corresponding range of concentration, whereas that for DVB 0.4 or the linear polymer is barely half of this value, despite the fact that the latter cases are more nearly dilute solutions. It is difficult to visualize any process which would lead to a more

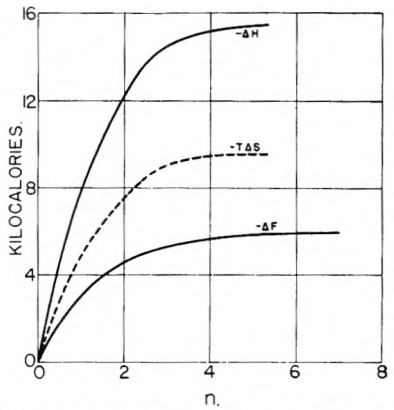

Fig. 10.—Thermodynamic functions for the water sorption process for DVB 23-H, as a function of n.

exothermic heat of hydration with increasing cross-linking. Rather, then, the high polymeric nature of the loosely cross-linked resins must introduce important changes, possibly increased van der Waals attractions, which disappear as the chains are held more rigidly at higher degrees of cross-linking.

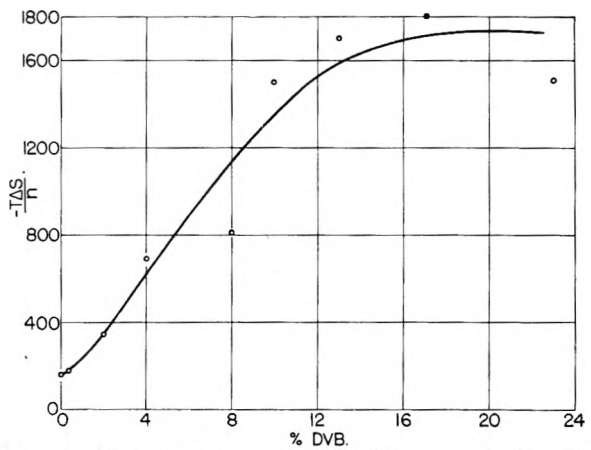

Fig. 11.—Variation in entropy function per mole of water sorbed at $p/p^\circ = 0.957$ for various DVB resins.

Another possibility is that the difference is primarily electrolytic in character. However, the equivalent volume and hence the average charge spacing is almost the same for all the different DVB's. It is therefore felt that electrical interactions should be similar except where long chain properties supervene.

A confirmation of the interpretation that the initial portion of the curve is depressed by polymeric interaction rather than electrolyte effects may be found in some work on the sorption of water by methacrylic acid–divinylbenzene copolymers of varying degrees of cross-linking agent.[16] Here also the sorption curves show the loosely cross-linked resins sorbing water to a lesser extent at the lower relative humidities, then crossing over and finally sorbing more water at high relative humidities. Since this system is chemically very different, being a weak carboxylic acid resin with a quite different chain structure, it appears that this effect

(16) N. Kadin, Thesis for the B.S. Degree, Polytechnic Institute of Brooklyn, June, 1952.

of varying cross-linking on the activity of a swelling solvent may be rather general.

It remains to speculate upon the mechanism of the depression of the sorption curve for low values of x. This, of course, represents elevation of the activity of the solvent at comparable concentrations, or less negative deviation from Raoult's Law. It may be worthwhile to emphasize again the unusual nature of this result. Water essentially becomes a better solvent for polystyrenesulfonic acid as the degree of cross-linking is increased at low relative humidities. This effect persists until the restraints upon the swelling become the most important factor.

A possible interpretation may be found in consideration of the effect of the polar groups in this matrix. The presence of the charge on the ionized sulfonate groups attached to a benzene ring would be expected to give rise to a strong dipole.[17] If the groups are relatively free to find the positions of lowest potential energy, then interactions of a polymer–polymer type will lead to more positive deviations from Raoult's Law. As the degree of cross-linking is increased, the charge density being kept approximately constant, then polymer–polymer contacts are reduced because of restrictions on free movements. The polymer–solvent interactions give large negative deviations from Raoult's Law and hence a crossing over on a Raoult's Law diagram can occur, as is actually observed. The heats of mixing will be less exothermic when there is polymer–polymer interaction in accord with the experimental data.

Another point which seems to be corroborative is the shape of the initial part of the sorption curve of the quaternary ammonium resinates. As was indicated, lack of information about the activity coefficients of these salts precludes a definite conclusion. However, it should be noted that the quaternary ammonium cations are very large. Thus the tetramethylammonium salt of DVB 10 in the dry state has a volume of 235.7 ml.,[2] corresponding to that of the hydrogen resinate swollen with five moles of water. The large size of the tetramethyl group distends the resin so that the polymer–polymer contacts are reduced on purely mechanical grounds. Therefore, in the process of swelling with water, less polymer–polymer interactions need be overcome and the initial uptake is then larger than for a small ion in the same resin. By the same token, at high degrees of swelling, the effect of the size of the ion is almost negligible and the latter part of the curve is shaped like those for smaller ions.

(17) F. London, THIS JOURNAL, **46**, 305 (1942)

PRESSURE DEPENDENCE OF THE DIELECTRIC CONSTANT OF WATER AND THE VOLUME CONTRACTION OF WATER AND *n*-BUTANOL UPON ADDITION OF ELECTROLYTE

BY F. E. HARRIS,[1] E. W. HAYCOCK AND B. J. ALDER

Department of Chemistry and Chemical Engineering, University of California, Berkeley, Calif.

Received June 2, 1953

The dielectric constant of water has been experimentally determined in the pressure range from 1 to 150 atmospheres and between 14 and 75°. From these data the volume contraction of water upon addition of electrolyte has been calculated and compared with previously reported density measurements. The agreement is satisfactory at temperatures below 30° but at temperatures above this the apparent molal volume of the salt is calculated to decrease with concentration. This decrease has not, as yet, been observed. A similar comparison has been attempted for *n*-butyl alcohol.

The variation of the dielectric constant of water with pressure has previously been reported at only one temperature[2] with no estimate of the inaccuracies involved. Since the derivative of the dielectric constant with pressure and also the change of this derivative with temperature is of interest in applications of the Debye–Hückel theory, we have measured the dielectric constant of water in the pressure range from 1 to 150 atmospheres and over a temperature interval from 14 to 75°.

Experimental Procedure and Results.—The apparatus used for these measurements has been described previously.[3] The water was purified by distillation from permanganate solution. The capacitance cell was calibrated at each temperature studied using literature values[4] of the dielectric constant of water at atmospheric pressure. The experimental values of the dielectric constant, measured at various temperatures and pressures, are given in Table I. The changes in the dielectric constant are relatively small over the pressure range studied and hence there is some scatter in the results obtained. A least square line was fitted to the data at each temperature and the resulting pressure derivative of the dielectric constant as a function of temperature is given in Table II and shown graphically in Fig. 1. The value of the derivative at 25° agrees within experimental error, which is estimated to be $\pm 0.5 \times 10^{-5}$ atm.$^{-1}$ at the lower temperatures, with the value of 4.6×10^{-5} determined by Falckenberg. Experimental errors at the three highest temperatures reported may be somewhat larger than $\pm 0.5 \times 10^{-5}$ because of the higher conductivity of the water. It will be noted from Fig. 1 that at about 60° the derivative passes through a minimum analogous to the variation of the compressibility with temperature. Both of these minima are manifestations of the fact that around this temperature the structure of water is the most rigid. Although the change in $(\partial\epsilon/\partial P)_T$ with temperature is somewhat dependent on the change in density with temperature, it can be shown[3] that it is primarily determined by the change in structure caused by the application of pressure.

(1) Predoctoral Fellow, National Science Foundation.

(2) G. Falckenberg, *Ann. Physik*, **61**, 145 (1920).

(3) F. E. Harris, E. W. Haycock and B. J. Alder, *J. Chem. Phys.*, in press.

(4) J. Wyman, Jr., and E. N. Ingalls, *J. Am. Chem. Soc.*, **60**, 1182 (1938).

TABLE I

PRESSURE DEPENDENCE OF THE DIELECTRIC CONSTANT OF WATER

14.5°		25.6°		35.9°		47.5°		60.7°		74.5°	
P_{atm}	ϵ	P_{atm}	ϵ	P_{atm}	ϵ	P_{atm}	ϵ	P_{atm}	ϵ	P_{atm}	ϵ
1.0	82.39	1.0	78.31	1.0	74.68	1.0	70.92	1.0	66.99	37.1	63.37
73.5	82.73	77.2	78.63	44.2	74.79	50.7	70.95	94.9	67.05	72.5	63.33
120.4	82.89	127.2	78.75	84.0	74.85	99.7	71.01	135.7	67.05	107.5	63.60
144.2	83.00			107.1	74.93	146.9	71.05	174.7	67.05	139.1	63.60
						188.1	71.08				

TABLE II

EVALUATION OF THE VOLUME CONTRACTION OF WATER

Temp., °C.	14.5	25.6	35.9	47.5	60.7	74.5
$\frac{1}{\epsilon}\left(\frac{\partial\epsilon}{\partial P}\right)_T \times 10^5$	5.11	4.53	3.00	1.26	0.54	4.47
K (eq. 2)	1.92	1.73	0.92	−0.14	−0.66	2.15
K (eq. 1)[a]	2.1	1.7		1.5		
K (eq. 1)	1.9[b]	1.86[c]				

[a] See ref. 8. [b] See ref. 6. [c] See ref. 7.

Discussion

By use of the pressure derivative of the dielectric constant in conjunction with the Debye–Hückel theory, it is possible to evaluate the volume contraction at infinite dilution when an electrolyte is added to water.[5] These contractions can then be compared with those determined by direct experiment. The volume contraction is expressed in terms of K, defined by

$$K = d\phi/dc^{1/2} \quad (1)$$

where ϕ is the apparent molal volume in cc. and c is the concentration in moles/liter. The Debye–Hückel theory yields for a 1–1 electrolyte

$$K = R\left(\frac{2e^2}{\epsilon k}\right)^{3/2}\left(\frac{\pi N}{1000T}\right)^{1/2}\left[\frac{1}{\epsilon}\left(\frac{\partial\epsilon}{\partial P}\right)_T - \beta/3\right] \quad (2)$$

where R is the gas constant, e the electronic charge, k the Boltzmann constant, N the Avogadro number, β the compressibility, and ϵ the dielectric constant. Values of K calculated using equation 2 are compared with the experimentally determined ones[6,7] in Table II. In view of the experimental uncertainties in $(\partial\epsilon/\partial P)_T$ and in the density measurements required for the determination of volume contraction, satisfactory agreement is obtained at the lower temperatures. At 47.5°, however, the value of K calculated from equation 2 is negative corresponding to an apparent molal volume contraction with concentration. This is in contradiction to the only reported result of direct density determination.[8]

The authors have previously determined the pressure dependence of the dielectric constant of n-butyl alcohol.[3] Since volume contraction measurements for this substance have also been reported,[9] a similar comparison to that made for water is possible for this system. Equation 2 yields a value of K of 38 at 25°, while the data of Vosburgh, *et al.*, give a value of 9. These latter data gave a good straight line when ϕ was plotted against $c^{1/2}$ in a range of c from 0.13 to 1.0 molar, as predicted by equation 1. This, however, is no criterion for assuming the applicability of the Debye–Hückel law in this concentration range, since in n-butyl alcohol, a medium of low dielectric constant, the number of associated ions at these concentrations must be large. The discrepancy in the values of K can be explained by assuming that at these concentrations not all of the ions are contributing fully to the volume contraction, thus decreasing the effective concentration and increasing K. That there is a large number of associated ions present at these concentrations was confirmed by conductivity measurements of solutions of lithium bromide in n-butanol at 24.8°. The conductivities were determined in a conductivity cell of standard design using bright platinum electrodes. Values of the equivalent conductance, Λ, at various concentrations of lithium bromide are given in Table III. Using these data, an association constant of 4×10^{-3} was determined from a graph of $1/\Lambda$ *vs.* Λc.[10] When this calculation was corrected for the effect of the activity coefficients an association constant of 6×10^{-4} was obtained. The magnitude of this association constant shows that volume contraction measurements must be performed at considerably lower concentrations than those studied by Vosburgh in order that a comparison with the Debye–Hückel theory can be justified.

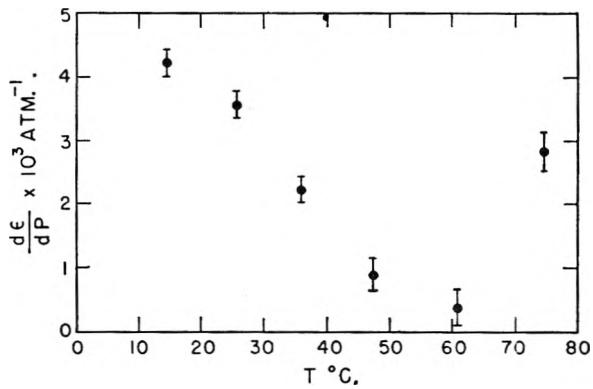

Fig. 1.—The pressure dependence of the dielectric constant of water as a function of temperature.

TABLE III

EQUIVALENT CONDUCTANCE OF LiBr IN n-BUTANOL

c, moles/l.	0.003276	0.005266	0.007685	0.01474	0.03409
Λ, cc./mole	7.71	6.75	6.06	5.00	3.70

We wish to acknowledge the interest shown by Dr. O. Redlich and the help of Mr. J. Konecny in the conductivity measurements. This work was supported in part by the Atomic Energy Commission.

(5) O. Redlich, *Z. physik. Chem.*, **A155**, 65 (1931).

(6) T. Batuecas, *ibid.*, **A182**, 167 (1938).

(7) O. Redlich and J. Bigeleisen, *Chem. Revs.*, **30**, 174 (1942).

(8) G. P. Baxter and C. C. Wallace, *J. Am. Chem. Soc.*, **38**, 70 (1916).

(9) W. C. Vosburgh, L. C. Connell and J. A. V. Butler, *J. Chem. Soc.*, 933 (1933).

(10) H. S. Harned and B. B. Owen, "The Physical Chemistry of Electrolytic Solutions," Reinhold Publ. Corp., New York, N. Y., 1950, p. 186.

ADDITIONS AND CORRECTIONS

Vol. 57, 1953

D. F. Peppard, J. P. Paris, P. R. Gray and G. W. Mason. Studies of the Solvent Extraction Behavior of the Transition Elements. I. Order and Degree of Fractionation of the Trivalent Rare Earths.

Page 298. In col. 2, line 33, for "500 ml." read "450 ml."

Page 299. In Table VII, note *a*, for "$R = 4.00$" read "$R = 0.24$."—D. F. PEPPARD.

M. H. Polley, W. D. Schaeffer and W. R. Smith. Development of Stepwise Isotherms on Carbon Black Surfaces.

Page 470. In Table I, note *a*, line 1 to read "B" and line 3 to read "are not linear for samples heated at 1500° and higher."—MYRTLE H. POLLEY.

Roger L. Jarry and Wallace Davis, Jr. The Vapor Pressure, Association, and Heat of Vaporization of Hydrogen Fluoride.

Page 600. To footnote (1) (b) add the Document No. "4069" and the cost of photostats and microfilm both as "$1.25."

Author Index to Volume LVII, 1953

ABERTH, E. R. See Maslan, F. D., 106.
ADAMS, C. R. See Milligan, W. O., 885.
ADLER, I., AND STEIGMAN, J. Interacn. of uranyl ions with $UX_1(Th^{231})$ in acid soln., 440; peptization of UX_1 by various metallic ions: a possible mechanism 443
ALDER, B. J. See Harris, F. E., 978.
ALEXANDER, G. B., AND ILER, R. K. Detn. of particle sizes in colloidal silica 932
ALLEN, H. C., JR. Pure quadrupole spectra of mol. crystals 501
ALLEN, J. A. Pptn. of Ni oxalate 715
ALLEN, J. A., AND SCAIFE, D. E. Dissocn. pressure of Ni oxalate dihydrate 863
ALTMAN, M. See Maslan, F. D., 106.
ALTSHULLER, A. P. Effect of dipolar ions upon activity coeffs. of neutral mols., 375; dipole moments of hydrocarbons 538
ANDERSON, R. B. See McCartney, J. T., 730.
ARNELL, J. C. Sorption of benzene by fatty acids 641
ARRINGTON, C. H., JR., AND PATTERSON, G. D. Colloidal properties of highly fluorinated alkanoic acids. 247
ASSARSSON, G. O. Equil. in aq. systems containing Sr^{2+}, K^+, Na^+ and Cl^- 207
ASSARSSON, G. O., AND BALDER, A. Equil. between 18 and 114° in aq. ternary system containing Ca^{2+}, Sr^{2+} and Cl^- 717

BAKER, L. L., JR. See Kilpatrick, M., 385.
BAKSHI, N. N. See Parthsarathy, S., 453.
BALDER, A. See Assarsson, G. O., 717.
BALLOU, E. V., AND ROSS, S. Adsorption of benzene and water vapor by MoS_2 653
BARRER, R. M. New approach to gas flow in capillary systems 35
BARTELL, F. E. See Ray, B. R., 49; Shepard, J. W., 458.
BARTELL, F. E., AND SHEPARD, J. W. Surface roughness as related to hysteresis of contact angles (I) system paraffin–water–air, 211; (II) systems paraffin–3 molar $CaCl_2$ soln.–air and paraffin–glycerol–air 455
BARTELL, F. E., AND SMITH, J. T. Alteration of surface properties of Ag and Au as indicated by contact angle measurements 165
BECKER, J. A., AND HARTMAN, C. D. Field emission microscope and flash filament techniques for study of structure and adsorption on metal surfaces 153
BEERS, R. F., JR., AND SIZER, I. W. Kinetics and thermodynamics of the steady state system of catalase with H_2O_2 290
BEHR, E. A., BRIGGS, D. R., AND KAUFERT, F. H. Diffusion of dissolved materials through wood 476
BEISCHER, D. E. Radioactive monolayers: new approach to surface research 134
BELL, E. E. See Burstein, E., 849.
BENDER, M. Mechanism by which Al ions alter electrokinetics of ZnS–H_2O interface 466
BENOIT, H., AND DOTY, P. Light scattering from non-Gaussian chains 958
BLEANEY, B. Paramagnetic resonance in the solid state 508
BLOCKER, H. G., CRAIG, S. L., AND ORR, C., JR. Dynamic gas adsorption methods of surface area detn. 517
BONDI, A. Penther, C. J., 540; Peterson, W. H., 30.
BONDI, A., AND PENTHER, C. J. Some elec. properties of colloidal suspensions in oils 72
BONNER, O. D., AND RHETT, V. Equil. studies of Ag–Na–H system on Dowex 50 254
BOUYOUCOS, G. J. Capillary rise of water in soils under field conditions 45
BRADLEY, R. S. Diffusion in a central field due to van der Waals attraction 307
BRADY, E. L. Chem. nature of silica carried by steam. 706
BRIGGS, D. R. See Behr, E. A., 476
BRIL, K., AND KRUMHOLZ, P. Polarographic detn. of relative formation consts. of metal complexes of ethylenediaminetetraacetic acid 874
BROMILOW, J., AND WINSOR, P. A. Structure and elec. conductivity of hydrocarbon-based solns. of "soluble oil" type—a comparable aq. system 889
BROOKSBANK, W. A., AND LEDDICOTTE, G. W. Ion-exchange sepn. of trace impurities 819
BROOKSBANK, W. A., LEDDICOTTE, G. W., AND MAHLMAN, H. A. Analysis for trace impurities by neutron activation 815
BUBE, R. H. Traps and trapping processes 785
BURSTEIN, E., BELL, E. E., DAVISSON, J. W., and LAX, M. Optical investigations of impurity levels in Si. 849
BURTON, J. A., HULL, G. W., MORIN, F. J., AND SEVERIENS, J. C. Effect of Ni and Cu impurities on recombination of holes and electrons in Ge 853
BYWATER, S. Thermal degradation of polymethyl methacrylates 879

CAGLE, F. W., JR., AND EYRING, H. Application of absolute rate theory to phase changes in solids 942
CAMERON, W. C., FARKAS, A., AND LITZ, L. M. Exchange of isotopic O between V_2O_5, gaseous O and H_2O 229
CAMPBELL, D. E. See Hirschfelder, J. O., 403.
CARMAN, P. C. Properties of capillary-held liquids. 56
CARRINGTON, T., AND DAVIDSON, N. Shock waves in chem. kinetics: rate of dissocn. of N_2O_4 418
CARROLL, B. H. See West, W., 797.
CHAMPION, W. M., AND HALSEY, G. D., JR. Phys. adsorption on uniform surfaces 646
CHARLWOOD, P. A. Estimation of heterogeneity from diffusion measurements 125
CHESSICK, J. J. See Healey, F. H., 178; Zettlemoyer, A. C., 649.
CHESSICK, J. J., HEALEY, F. H., AND ZETTLEMOYER, A. C. Adsorption studies on metals (II) abs. entropies of adsorbed mols. on Mo 912
CHOPPIN, G. R. See Watt, G. W., 567.
CHU, T. L., PAKE, G. E., PAUL, D. E., TOWNSEND, J., AND WEISSMAN, S. I. Paramagnetic resonance absorption of free radicals 504
CHWALOW, M. L. E. Electron microscopic studies of some paraffinic Na soaps 354
CINES, M. R., AND RUEHLEN, F. N. Selective adsorption—2,4-dimethylpentane–benzene–silica gel at 65.6° 710
COOK, M. A., CUTLER, I. B., HILL, G. R., AND WADSWORTH, M. E. Mechanism of cation and anion exchange capacity 1
COOKE, W. D. See Streuli, C. A. 824
COON, R. I. See Scholberg, H. M., 923.
CORCORAN, J. M., KRUSE, H. W., AND SKOLNIK, S. Thermal analysis of the systems N_2H_4–MeOH and N_2H_4–EtOH 435
CORYELL, C. D. See Spiegler, K. S., 687.
COULTER, L. V. Thermochemistry of alkali and alkaline earth metals and halides in liq. NH_3 at −33° 553
CRAIG, R. P. See Hansen, R. S., 215.
CRAIG, S. L. See Blocker, H. G., 517.
CROCKFORD, H. D. See Knight, S. B., 463.
CURTISS, C. F. See Hirschfelder, J. O., 403.
CUTLER, I. B. See Cook, M. A., 1.

DAILEY, B. P. Chem. significance of quadrupole spectra 490
DANFORTH, J. D. See Stright, P., 448.
DAVIDSON, A. W., AND KLEINBERG, J. Unfamiliar oxidn. states in liq. NH_3 571
DAVIDSON, N. See Carrington, T., 418.
DAVIS, J. W. See Johansen, R. T., 40.
DAVIS, R. T., JR., AND SCHIESSLER, R. W. Vapor pressures of perdeuterobenzene and of perdeuterocyclohexane 966
DAVIS, W., JR. See Jarry, R. L., 600, 905; Rutledge, G. P., 541.
DAVISSON, E. O., GIBSON, D. M., RAY, B. R., AND VESTLING, C. S. Rat liver lactic dehydrogenase (II) phys.-chem. studies on crystalline enzyme 609

DAVISSON, J. W. See Burstein, E., 849.
DAY, M. K. B., AND HILL, V. J. Thermal transformation of aluminas and their hydrates..... 946
DEAN, R. B. See Hayes, K. E., 80.
DECKER, B. F. See Hoffman, J. D., 520.
DIEPEN, G. A. M. See van Gunst, C. A., 578, 581.
DIEPEN, G. A. M., AND SCHEFFER, F. E. C. Soly. of naphthalene in supercrit. ethylene (II)..... 575
DIXON, J. K. See Judson, C. M., 916.
DODD, C. G. See Johansen, R. T., 40.
DOLE, M. See Wilhoit, R. C., 14.
DORFMAN, L. M., AND MATTRAW, H. C. Exchange reacn. of H and T., 723.
DOTY, P. See Benoit, H., 958.

EIRICH, F. R. See Simha, R., 584.
EL NADI, M. Variation of viscosity of EtCl vapor with temp..... 589
EL WAKKAD, S. E. S., AND HICKLING, A. Anodic behavior of Sb..... 203
ELLISON, A. H., FOX, H. W., AND ZISMAN, W. A. Wetting of fluorinated solids by H-bonding liqs..... 622
EMMETT, P. H. See Podgurski, H. H., 159.
EPSTEIN, L. F., AND POWERS, M. D. Liquid metals (I) viscosity of Hg vapor and potential function for Hg 336
EVERS, E. C., AND FINN, J. M., JR. Alkali metal phosphides (III) electrolysis studies in liq. NH_3..... 559
EWING, W. W., AND HERTY, C. H., III. Partial molal vols. of $Cd(NO_3)_2$ and H_2O in concd. aq. solns..... 245
EYRING, H. See Cagle, F. W., Jr., 942; Moore, R. J., 172.

FACKLER, W. V., JR. See Hansen, R. S., 634.
FARIS, J. P. See Peppard, D. F., 294.
FARKAS, A. See Cameron, W. C., 229.
FETSKO, J. M. See Healey, F. H., 186.
FINN, J. M., JR. See Evers, E. C., 559.
FLEISCHER, M. See Foote, H. W., 122.
FOERING, L. See Johnston, H. S., 390.
FONTANA, B. J. Relation of crystal habit to polymorphic behavior of long-chain paraffin hydrocarbons.. 222
FOOTE, H. W., AND FLEISCHER, M. Addn. of I to Me_4NI..... 122
FORDHAM, J. W. L., AND WILLIAMS, H. L. Copolymn. of butadiene and α-methylstyrene in emulsion at 12.8°..... 346
FOSTER, J. F. See Hanna, G. F., 614; Yang, J. T., 628.
FOWKES, F. M. Role of surface active agents in wetting..... 98
FOX, H. W. See Ellison, A. H., 622.
FRICKE, H. Maxwell-Wagner dispersion in a suspension of ellipsoids..... 934
FRISCH, H. L. See Simha, R., 584.

GEIGER, C. F. See Smith, R. N., 382.
GIBBS, P. See Moore, R. J., 172.
GIBSON, D. M. See Davisson, E. O., 609.
GIERST, L., AND JULIARD, A. L. Non-steady state electrolysis under const. current..... 701
GINZBARG, A. S. See James, H. M., 840.
GIRIFALCO, L. A. See Kraus, G., 330.
GLAMM, A. C., JR. See Hurd, C. B., 678.
GLOCKER, E. M. See Simpson, E. A., 529.
GOLDBERG, R. J. Sedimentation in the ultracentrifuge 194
GOLDHAGEN, S. See Svirbely, W. J., 597.
GRAHAM, D. Characterization of phys. adsorption systems (I) equil. function and standard free energy of adsorption..... 665
GRAHAME, D. C. Theory of faradaic admittance (II) analysis of current-interrupter method..... 257
GRAVEL, C. L. See Kahan, G. J., 239.
GRAY, P. R. See Peppard, D. F., 294.
GREEN, M., AND ROBINSON, P. H. Refractive index of germane..... 938
GREGOR, H. P. See Sundheim, B. R., 974; Waxman, M. H., 969.
GROPP, A. H. See Letaw, H., Jr., 964.
GUENTHNER, R. A. See Scholberg, H. M., 923.
GUMPRECHT, R. O., AND SLIEPCEVICH, C. M. Scattering of light by large spherical particles, 90; measurement of particle sizes in polydispersed systems by means of light transmission measurements combined with differential settling..... 95
VAN GUNST, C. A., SCHEFFER, F. E. C., AND DIEPEN, G. A. M. On crit. phenomena of satd. solns. in binary systems (II), 578; on crit. phenomena of satd. solns. in ternary systems..... 581
GUTMANN, J. R. Exchange reacn. between D and NH_3 on surface of metal powders..... 309
GUTOWSKY, H. S. See Meyer, L. H., 481.

HACKERMAN, N. See Hall, C. D., Jr., 262; Joncich, M. J., 674.
HACKERMAN, N., AND POWERS, R. A. Surface reacns. of Cr in dil. $Cr^{51}O_4^=$ solns..... 139
HALE, C. F. See Jarry, R. L., 905.
HALL, C. D., JR., AND HACKERMAN, N. Charging processes on anodic polarization of Ti..... 262
HALL, J. L. See Watt, G. W., 567.
HALL, R. N. Segregation of impurities during growth of Ge and Si crystals..... 836
HALLA, F. Simple general notations for systems of simultaneous reacns..... 599
HALSEY, G. D., JR. On the structure of micelles, 87; see Champion, W. M., 646.
HAMM, F. A. See Miller, L. E., 110.
HANNA, G. F., AND FOSTER, J. F. Streaming orientation studies on denatured proteins (IV) denaturation of ovalbumin with surface active ions..... 614
HANSEN, R. D. See Hansen, R. S., 215.
HANSEN, R. S., AND FACKLER, W. V., JR. Generalization of Polanyi theory of adsorption from soln..... 634
HANSEN, R. S., HANSEN, R. D., AND CRAIG, R. P. Effect of steam activation on multilayer adsorption from soln. by C..... 215
HARKINS, W. D. See Loeser, E. H., 251, 591.
HARNED, H. S., AND PAXTON, T. R. Thermodynamics of ionized water in $SrCl_2$ solns..... 531
HARRIS, F. E., HAYCOCK, E. W., AND ALDER, B. J. Pressure dependence of dielec. const. of H_2O and volume contraction of H_2O and n-BuOH upon addn. of electrolyte..... 978
HARTMAN, C. D. See Becker, J. A., 153.
HAWKINS, J. E., AND VOGH, J. W. Rate of thermal isomn. of β-pinene in the vapor phase..... 902
HAYCOCK, E. W. See Harris, F. E., 978.
HAYES, K. E., AND DEAN, R. B. Adsorption on monolayers (VI) adsorption of isomeric hexanes on condensed stearic acid monolayers and on clean water surfaces..... 80
HAZEL, J. F., MCNABB, W. M., AND SANTINI, R., JR. Formation and titration of colloidal vanadic acid.. 681
HEALEY, F. H. See Chessick, J. J., 912; Zettlemoyer, A. C., 649.
HEALEY, F. H., CHESSICK, J. J., AND ZETTLEMOYER, A. C. Adsorption studies on metals (I) phys. and chem. adsorption of gases on Mo..... 178
HEALEY, F. H., FETSKO, J. M., AND ZETTLEMOYER, A. C. Phys. adsorption on CdO..... 186
HELLER, C. A., JR., AND TAYLOR, H. A. Pyrolysis of $CdMe_2$..... 226
HERSH, S. L. See Suchow, L., 437.
HERTY, C. H., III. See Ewing, W. W., 245.
HICKLING, A. See El Wakkad, S. E. S., 203.
HILL, G. R. See Cook, M. A., 1.
HILL, T. L. Adsorption on proteins, the grand partition function and first-order phase changes, according to approximate statistical mechanical theories.. 324
HILL, V. J. See Day, M. K. B., 946.
HILLIER, J. See Turkevich, J., 670.
HIRSCHFELDER, J. O., CURTISS, C. F., AND CAMPBELL, D. E. Theory of flame propagation (IV)..... 403
HOERLIN, H. See Larson, E. T., 802.
HOFER, L. J. E. See McCartney, J. T., 730.
HOFFMAN, J. D., AND DECKER, B. F. Solid state phase changes in long chain compds..... 520
HOLMES, B. G. See Milligan, W. O., 11.
HONIG, J. M. Analysis of multilayer gas adsorption isotherms using concept of surface heterogeneity... 349
HOOVER, S. R. See Mellon, E. F., 607.
HOVORKA, F. See Yeager, E., 268
HUBBARD, W. D. See Kushner, L. M., 898
HUGHES, A. F. See Ross, S., 684.
HUGHES, V. L., AND MARTELL, A. E. Spectrophotometric detn. of stabilities of ethylenediaminetetraacetate chelates..... 694

HULL, G. W. See Burton, J. A., 853.
HUMENIK, M., JR. See Kingery, W. D., 359.
HUMPHREY, F. B. See Waugh, J. S., 486.
HURD, C. B., SMITH, M. D., WITZEI, F., AND GLAMM, A. C., Jr. Studies on silicic acid gels (XVII) dialysis of the gel mixt. and of the gels 678
HUTCHISON, C. A., JR. Paramagnetic resonance absorption in solns. of K in liq. NH_3 546

IBERS, J. A., AND SCHOMAKER, V. Structure of OF_2 .. 699
ILER, R. K. Polymn. of polysilicic acid derived from 3.3 ratio Na silicate, 604; see Alexander, G. B., 932.
INGHRAM, M. G. Trace element detn. by mass spectrometer 809

JAMES, F. W. See Knight, S. B., 463.
JAMES, H. M., AND GINZBARG, A. S. Band structure in disordered alloys and impurity semiconductors .. 840
JAMES, T. H., AND VANSELOW, W. Kinetics of reacn. between AgBr and an adsorbed layer of allylthiourea 725
JARRY, R. L. See Rutledge, G. P., 541.
JARRY, R. L., AND DAVIS, W., JR. Vapor pressure, assocn. and heat of vaporization of HF, 600, (corrn.) 980
JARRY, R. L., ROSEN, F. D., HALE, C. F., AND DAVIS, W., Jr. Liq.–vapor equil. in system UF_6–HF 905
JELLINEK, H. H. G., AND URWIN, J. R. Hydrolysis of picolinamide and isonicotinamide in concd. HCl solns. 900
JENSEN, L. H. See Lingafelter, E. C., 428.
JOHANSEN, R. T., LORENZ, P. B., DODD, C. G., PIDGEON, F. D., AND DAVIS, J. W. Permeation of water and isooctane through plugs of microscopic particles of crushed quartz 40
JOHNSON, M. F. L., AND RIES, H. E., JR. Structure of Co catalysts supported on diatomaceous earth 865
JOHNSTON, H. S., FOERING, L., AND THOMPSON, R. J. Kinetics of thermal decompn. of HNO_3 vapor (II) mechanism 390
JONCICH, M. J., AND HACKERMAN, N. Reacn. of H and O on submerged Pt electrode catalysts (I) effect of stirring, temp. and elec. polarization 674
JUDSON, C. M., LEREW, A. A., DIXON, J. K., AND SALLEY, D. J. Radiotracer study of sulfate ion adsorption at the air/soln. interface in solns. of surface-active agents 916
JULIARD, A. L. See Gierst, L., 701.

KAHAN, G. J., AND GRAVEL, C. L. Electrocapillarity in dielecs. and in poorly conducting systems 239
KAUFERT, F. H. See Behr, E. A., 476.
KENNEDY, M. L. See Ross, S., 684.
KILPATRICK. M., BAKER, L. L., JR., AND MCKINNEY, C. D., Jr. Studies of fast reacns. which evolve gases—reacn. of Na–K alloy with H_2O in presence and absence of O 385
KING, C. V., AND SCHOCHET, R. K. Adsorption of Ag salts on Ag 895
KINGERY, W. D., AND HUMENIK, M., JR. Surface tension at elevated temps. (I) furnace and method for use of sessile drop method; surface tension of Si, Fe and Ni 359
KLEINBERG, J. Symposium on liq. NH_3 chemistry—introductory remarks, 545; see Davidson, A. W., 571
KLICK, C. C. Emission and absorption in luminescent centers at low temps 776
KNIGHT, S. B., CROCKFORD, H. D., AND JAMES, F. W. E.m.f. studies in aq. solns. of HCl and glycerol from 0 to 40° 463
KOHL, J., AND ZENTNER, R. D. Prepn. and utilization of metallic aerosols for filter paper testing 68
KRAUS, G., AND ROSS, J. W. Surface area analysis by means of gas flow methods (II) transient state flow in porous media 334
KRAUS, G., ROSS, J. W., AND GIRIFALCO, L. A. Surface area analysis by means of gas flow methods (I) steady state flow in porous media 330
KRIMM, S. X-Ray studies of crystalline and amorphous order in high polymers 22
KRUMHOLZ, P. See Bril, K., 874.
KRUSE, H. W. See Corcoran, J. M., 435.
KUSHNER, L. M., AND HUBBARD, W. D. On detn. of crit. micelle concns. by a bubble pressure method .. 898

LAIDLER, K. J. Kinetics of surface reacns. in case of interacns. between adsorbed mols., 318; mechanisms of surface-catalyzed reacns. (I) parahydrogen conversion on W, 320; see Markham, M. C. 321, 363
LAITINEN, H. A. See McElroy, A. D., 564.
LARSON, E. T., MUELLER, F. W. H., AND HOERLIN, H. Sensitization of X-ray emulsions by very small quantities of a Pb salt 802
LAX, M. See Burstein, E., 849.
LAYTON, L. H. See Strauss, U. P., 352.
LECKY, J. A. See McCartney, J. T., 730.
LEDDICOTTE, G. W. See Brooksbank, W. A., 815, 819.
LEREW, A. A. See Judson, C. M., 916.
LETAW, H., JR., AND GROPP, A. H. Polarographic studies in non-aq. media (I) formamide 964
LEVY, H. A., AND PETERSON, S. W. Neutron diffraction studies on $ScVO_4$ and Sc_2O_3 535
LIANG, S. C. Study of phys. adsorption at low coverages, 84; on calcn. of thermal transpiration 910
LINGAFELTER, E. C., JENSEN, L. H., AND MARKHAM, A. E. Extent of hydration of some crystalline phases of Na 1-alkanesulfonates 428
LIPPINCOTT, E. R., MERCIER, P., AND TOBIN, M. C. Vibrational spectra of some Sn and Ge halogen metalorg. compds 939
LITZ, L. M. See Cameron, W. C., 229.
LIVINGSTON, R. Pure quadrupole spectra of solid Cl compds 496
LOESER, E. H., HARKINS, W. D., AND TWISS, S. B. Adhesion of liquids to solids—mol. interacn. between metal oxides and adsorbed vapors, 251; mol. interacn. between *n*-PrOH and Fe or Fe oxides 591
LORENZ, P. B. Electrokinetic processes in parallel and series combinations, 341; electrokinetic relations in quartz–acetone system, 430; see Johansen, R. T... 40
LUCKEY, G. W. Vacuum photolysis of AgBr 791
LUMB, R. F., AND MARTELL, A. E. Metal chelating tendencies of glutamic and aspartic acids 690

MAHLMAN, H. A. See Brooksbank, W. A., 815.
MARDOIAN, A. R. See Ross, S., 684.
MARKHAM, A. E. See Lingafelter, E. C., 428.
MARKHAM, J. J. Interacn. of color centers with their environment 762
MARKHAM, M. C., AND LAIDLER, K. J. Kinetic study of photo-oxidns. on surface of ZnO in aq. suspensions 363
MARKHAM, M. C., WALL, M. C., AND LAIDLER, K. J. Mol. kinetics and mechanism of CH_4–D exchange reacns. on Ni 321
MARSHALL, C. E., AND UPCHURCH, W. J. Free energy in cation interchange as illustrated by plant root–substrate relationships 618
MARTELL, A. E. See Hughes, V. L., 694; Lumb, R. F., 690.
MASLAN, F. D., ALTMAN, M., AND ABERTH, E. R. Prediction of gas-adsorbent equil 106
MASON, G. W. See Peppard, D. F., 294.
MATHIAS, S. Molar polarizations of isomeric Pr and Bu mercaptans 344
MATIJEVIĆ, E., AND TEŽAK, B. Coagulation effects of $Al(NO_3)_3$ and $Al_2(SO_4)_3$ on aq. solns. of Ag halides *in statu nascendi*—detection of polynuclear complex Al ions by means of coagulation measurements 951
MATTRAW, H. C. See Dorfman, L. M., 723.
MCCARTNEY, J. T., HOFER, L. J. E., SELIGMAN, B., LECKY, J. A., PEEBLES, W. C., AND ANDERSON, R. B. Electron and X-ray diffraction studies of Fe Fischer–Tropsch catalysts 730
MCELROY, A. D., AND LAITINEN, H. A. Polarography in liq. NH_3 (V) polarography of Pb, Cd, Zn, Ni, Co, Cr and Al ions 564
MCKINNEY, C. D., JR. See Kilpatrick, M., 385.
MCNABB, W. M. See Hazel, J. F., 681.
MELLON, E. F., VIOLA, S. J., AND HOOVER, S. R. Vapor pressure of acetylated amino acid Et esters .. 607
MERCIER, P. See Lippincott, E. R., 939.
MEYER, L. H., AND GUTOWSKY, H. S. Electron distribution in mols. (II) proton and F magnetic resonance shifts in halomethanes 481
MILLER, L. E., AND HAMM, F. A. Macromol. properties of polyvinylpyrrolidone: mol. wt. distribution 110
MILLIGAN, W. O. See Watt, L. M., 883.

MILLIGAN, W. O., AND ADAMS, C. R. Sorption–desorption studies in system $BeO–In_2O_3$ 885
MILLIGAN, W. O., AND HOLMES, B. G. X-Ray diffraction studies in system $Al_2O_3–SnO_2–TiO_2$ 11
MOOI, J., PIERCE, C., AND SMITH, R. N. Heats and entropies of adsorption on a homogeneous C surface. 657
MOORE, R. J., GIBBS, P., AND EYRING, H. Structure of liquid state and viscosity of hydrocarbons 172
MORIN, F. J. See Burton, J. A., 853.
MORRISON, S. R. Changes of surface conductivity of Ge with ambient 860
MUELLER, F. W. H. See Larson, E. T., 802.
MYSELS, K. J., AND STIGFER, D. New method of measuring diffusion coeffs. 104

NEZNAYKO, M. See Williams, F. J., 6.

OEY, T. S. See Yeager, E., 268.
O'KONSKI, C. T., AND THACHER, H. C., JR. Distortion of aerosol droplets by an elec. field 955
ORR, C., JR. See Blocker, H. G., 517.
ORR, R. J., AND WILLIAMS, H. L. Kinetics of reacns. between Fe(II) and some hydroperoxides based on cumene and cyclohexane 925

PAKE, G. E. See Chu, T. L., 504.
PARTHASARATHY, S., AND BAKHSHI, N. N. Velocity of sound in liquids and mol. wt. 453
PATCH, M. J. See Waugh, D. F., 377.
PATTERSON, G. D. See Arrington, C. H., Jr., 247.
PAUL, D. E. See Chu, T. L., 504.
PAXTON, T. R. See Harned, H. S., 531.
PEEBLES, W. C. See McCarney, J. T., 730.
PENTHER, C. J. See Bondi, A., 72.
PENTHER, C. J., AND BONDI, A. Apparatus for measurement of elec. properties of colloidal suspensions in oils 540
PEPPARD, D. F., FARIS, J. P., GRAY, P. R., AND MASON, G. W. Studies of solvent extraction behavior of transition elements (I) order and degree of fractionation of the trivalent rare earths 294 (corrn.) 980
PETERSON, S. W. See Levy, H. A., 535.
PETERSON, W. H., AND BONDI, A. Study of soap aerogels from lubricating greases 30
PIDGEON, F. D. See Johansen, R. T., 40.
PIERCE, C. Computation of pore sizes from phys. adsorption data, 149; see Mooi, J., 657; Smith, R. N., 382.
PIERCE, C., AND SMITH, R. N. Adsorption in capillaries 64
PLANK, C. J. Adsorption of ions from buffer solns. by silica, alumina and silica–alumina gels 284
PODGURSKI, H. H., AND EMMETT, P. H. Adsorption of H and CO on Fe surfaces 159
POLLEY, M. H., SCHAEFFER, W. D., AND SMITH, W. R. Development of stepwise isotherms on C black surfaces, 469, (corrn.) 980
POUND, R. V. Evidences of crystalline imperfections in nuclear magnetism 743
POWERS, M. D. See Epstein, L. F., 336.
POWERS, R. A. See Hackerman, N., 139.

RAMSAY, D. A. Absorption spectra of free NH and NH_2 radicals produced by flash photolysis of hydrazine 415
RAY, B. R. See Davisson, E. O., 609.
RAY, B. R., AND BARTELL, F. E. Wetting characteristics of cellulose derivs. (II) interrelations of contact angles 49
REID, W. P. Steady-state burning of a semi-infinite solid or liquid 242
RHETT, V. See Bonner, O. D., 254.
RHODIN, T. N. Phys. adsorption on single crystal Zn surfaces 143
RIES, H. E., JR. See Johnson, M. F. L., 865.
ROBINSON, P. H. See Green, M., 938.
ROSEN, F. D. See Jarry, R. L., 905.
ROSS, J. W. See Kraus, G., 330, 334.
ROSS, S. See Ballou, E. V., 653.
ROSS, S., HUGHES, A. F., KENNEDY, M. L., AND MARDOIAN, A. R. Inhibition of foaming (V) synergistic effects of antifoaming agents 684
RUEHLEN, F. N. See Cines, M. R., 710.
RUSSELL, E. R. See Shereshefsky, J. L., 660.
RUTLEDGE, G. P., JARRY, R. L., AND DAVIS, W., JR. F. p. diagram and liquid–liquid solys. of system UF_6–HF 541

SALLEY, D. J. See Judson, C. M., 916.
SANTINI, R., JR. See Hazel, J. F., 681.
SAXTON, P. M. See Wall, F. T., 370.
SCAIFE, D. E. See Allen, J. A., 863.
SCHAEFFER, W. D. See Polley, M. H., 469.
SCHEFFER, F. E. C. See Diepen, G. A. M., 575; van Gunst, C. A., 578, 581.
SCHELLMAN, J. A. Application of Bjerrum ion assocn. theory to binding of anions by proteins 472
SCHIESSLER, R. W. See Davis, R. T., Jr., 966.
SCHOCHET, R. K. See King, C. V., 895.
SCHOLBERG, H. M., GUENTHNER, R. A., AND COON, R. I. Surface chemistry of fluorocarbons and their derivs. 923
SCHOMAKER, V. See Ibers, J. A., 699.
SCHULMAN, J. H. Effects of impurities on coloration of solids by ionizing radiations 749
SCOTT, A. B., SMITH, W. A., AND THOMPSON, M. A. Alkali halides colored by colloidal metal 757
SEITZ, F. Survey of imperfections in nearly perfect crystals 737
SELIGMAN, B. See McCartney, J. T., 730.
SEVERIENS, J. C. See Burton, J. A., 853.
SHAPIRO, I., AND WEISS, H. G. Bound H_2O in silica gel 219
SHEPARD, J. W. See Bartell, F. E., 211, 455.
SHEPARD, J. W., AND BARTELL, F. E. Surface roughness as related to hysteresis of contact angles (III) systems paraffin–ethylene glycol–air, paraffin–Me cellosolve–air and paraffin–MeOH–air 458
SHERESHEFSKY, J. L., AND RUSSELL, E. R. Adsorption of EtOH vapor on glass spheres in systems of different porosities 660
SHULER, K. E. On the kinetics of elementary reacns. in flames and its relation to energy distribution of active species 396
SIMHA, R., FRISCH, H. L., AND EIRICH, F. R. Adsorption of flexible macromols 584
SIMPSON, E. A., AND GLOCKER, E. M. Soly. of NH_4, Mg and Zn fluosilicates from 2 to 68° 529
SIZER, I. W. See Beers, R. F., Jr., 290.
SKOLNIK, S. See Corcoran, J. M., 435.
SLIEPCEVICH, C. M. See Gumprecht, R. O., 90, 95.
SMITH, J. T. See Bartell, F. E., 165.
SMITH, M. D. See Hurd, C. B., 678.
SMITH, R. N. See Mooi, J., 657.
SMITH, R. N., GEIGER, C. F., AND PIERCE, C. Equil. exchange rates of adsorbed species with unadsorbed species in soln. 382
SMITH, W. A. See Scott, A. B., 757.
SMITH, W. R. See Polley, M. H., 469.
SPIEGLER, K. S., AND CORYELL, C. D. Electromigration in a cation-exchange resin (III) correlation of self-diffusion coeffs. of ions in a cation-exchange membrane to its elec. conductance 687
STEIGMAN, J. See Adler, I., 440, 443.
STEVENSON, P. C. See Turkevich, J., 670.
STIGFER, D. See Mysels, K. J., 104.
STRAIN, H. H. Paper chromatography of chloroplast pigments: sorption at a liq.–liq. interface 638
STRAUSS, U. P., AND LAYTON, L. H. Comparison of effects of several solubilized C_6-hydrocarbons on viscosity of a polysoap soln. 352
STREULI, C. A., AND COOKE, W. D. Application of polarized Hg pool electrodes to polarography 824
STRIGHT, P., AND DANFORTH, J. D. Effect of LiOH on activity of cracking catalysts 448
STRUTHERS, J. D. See Thurmond, C. D., 831.
SUCHOW, L., AND HERSH, S. L. Photothermal decompn. of mixed Ag and mercurous oxalates 437
SUNDHEIM, B. R. See Waxman, M. H., 969.
SUNDHEIM, B. R., WAXMAN, M. H., AND GREGOR, H. P. Studies on ion exchange resins (VII) H_2O vapor sorption by cross-linked polystyrenesulfonic acid resins. 974
SVIRBELY, W. J., AND GOLDHAGEN, S. Study of system *cis*- and *trans*-cyclohexanediol-1,2 597

TAYLOR, H. A. See Heller, C. A., Jr., 226.
TEŽAK, B. Mechanism of coagulation of lyophobic sols as revealed through investigations of Ag halide sols *in statu nascendi*, 301; see Matijević, E., 951.
THACHER, H. C., JR. See O'Konski, C. T., 955.
THOMPSON, M. A. See Scott, A. B., 757.
THOMPSON, R. J. See Johnston, H. S., 390.
THURMOND, C. D. Equil. thermochemistry of solid and liq. alloys of Ge and of Si (I) solv. of Ge and Si in elements of groups III, IV and V..... 827
THURMOND, C. D., AND STRUTHERS, J. D. Equil. thermochemistry of solid and liq. alloys of Ge and Si (II) retrograde solid solvs. of Sb in Ge, Cu in Ge, and Cu in Si..... 831
TOBIN, M. C. See Lippincott, E. R., 939.
TOWNSEND, J. See Chu, T. L., 504.
TURKEVICH, J., STEVENSON, P. C., AND HILLIER, J. Formation of colloidal Au..... 670
TWISS, S. B. See Loeser, E. H., 251, 591.

UHLIG, H. H., AND WOODSIDE, G. E. Anodic polarization of passive and non-passive Cr–Fe alloys.... 280
UPCHURCH, W. J. See Marshall, C. E., 618.
URWIN, J. R. See Jellinek, H. H. G., 900.

VAN RYSSELBERGHE, P. Electrode phenomena and thermodynamics of irreversible processes..... 275
VANSELOW, W. See James, T. H., 725.
VEIS, A. Interacn. of alkali ions with some linear polyelectrolytes..... 189
VESTLING, C. S. See Davisson, E. O., 609.
VIOLA, S. J. See Mellon, E. F., 607.
VOGH, J. W. See Hawkins, J. E., 902.
VOLD, M. J. Packing orientation of soap crystallites.. 26

WADSWORTH, M. E. See Cook, M.A., 1.
WAGNER, C. Phys. chemistry of ionic crystals involving small concns. of foreign substances..... 738
WALKER, W. C., AND ZETTLEMOYER, A. C. Active magnesia (V) adsorption in preferred positions.... 182
WALL, F. T., AND SAXTON, P. M. Electrolytic interacn. of nylon with NaOH solns. at different temps... 370
WALL, M. C. See Markham, M. C., 321.
WARD, F. Chemistry of phosphors..... 773
WATT, G. W., HALL, J. L., AND CHOPPIN, G. R. Potentiometric titration of halides of Al, Ga, In, and Tl with K in liq. NH_3..... 567
WATT, L. M., AND MILLIGAN, W. O. X-Ray diffraction studies in system BeO–In_2O_3..... 883
WAUGH, D. F., AND PATCH, M. J. Effects of ionic strength on interacn. of bovine fibrinogen and thrombin..... 377
WAUGH, D. F., AND YPHANTIS, D. A. Transient solute distributions from basic eq. of the ultracentrifuge.. 312
WAUGH, J. S., HUMPHREY, F. B., AND YOST, D. M. Magnetic resonance spectrum of a linear 3-spin system: configuration of bifluoride ion..... 486
WAXMAN, M. H. See Sundheim, B. R., 974.
WAXMAN, M. H., SUNDHEIM, B. R., AND GREGOR, H. P. Studies on ion exchange resins (VI) H_2O vapor sorption by polystyrenesulfonic acid..... 969
WEINTRITT, D. J. See Williams, F. J., 6.
WEISS, H. G. See Shapiro, I., 219.
WEISSMAN, S. I. See Chu, T. L., 504.
WEST, W., AND CARROLL, B. H. Effect of impurities on optical sensitization of photographic emulsion..... 797
WEYL, W. A. Metals in at. state in glasses..... 753
WILHOIT, R. C., AND DOLE, M. Sp. heat of synthetic high polymers—(II) polyhexamethylene adipamide and sebacamide..... 14
WILLARD, J. E. Application of radiotracers to study of surfaces..... 129
WILLIAMS, F. E. Theory of luminescence of impurity-activated ionic crystals..... 780
WILLIAMS, F. J., NEZNAYKO, M., AND WEINTRITT, D. J. Effect of exchangeable bases on colloidal properties of bentonite..... 6
WILLIAMS, H. L. See Fordhan, J. W. L., 346; Orr, R. J., 925.
WINSOR, P. A. See Bromilow, J., 889.
WITZEL, F. See Hurd, C. B., 678.
WOODSIDE, G. E. See Uhlig, H. H., 280.

YANG, J. T., AND FOSTER, J. F. Detn. of crit. micelle concn. by equil. dialysis..... 628
YEAGER, E., OEY, T. S., AND HOVORKA, F. Effect of ultrasonic waves on H overvoltage..... 268
YOST, D. M. See Waugh, J. S., 486.
YOUNG, G. J. See Zettlemoyer, A. C., 649.
YPHANTIS, D. A. See Waugh, D. F., 312.

ZENTNER, R. D. See Kohl, J., 68.
ZETTLEMOYER, A. C. See Chessick, J. J., 912; Healey, F. H., 178, 186; Walker, W. C., 182.
ZETTLEMOYER, A. C., YOUNG, G. J., CHESSICK, J. J., AND HEALEY, F. H. Thermistor calorimeter for heats of wetting; entropies from heats of wetting and adsorption data..... 649
ZISMAN, W. A. See Ellison, A. H., 622.

Subject Index to Volume LVII, 1953

ABSOLUTE rate theory, application to phase changes in solids 942
Acetone, electrokinetic relations in quartz–, system .. 430
Activity coefficients, effect of dipolar ions on, of neutral mols 375
Adipic acid, sp. heat of polyhexamethylene adipamide 14
Adsorption, surface heterogeneity in analysis of multilayer gas, isotherms, 349; of flexible macromols., 584; Polanyi theory of, from soln., 634; phys., on uniform surfaces, 646; heats and entropies of, on a homogeneous C surface, 657; of EtOH vapor on glass spheres, 660; characterization of phys., systems, 665; of A and O_2 on Mo, 912; radiotracer study of sulfate ion, at air/soln. interface in di-*n*-ocylsodium sulfosuccinate 916
Aerosol, prepn. and use of metallic, for filter paper testing, 68; analysis of an, produced by spraying kerosene from a conventional swirl-chamber nozzle, 95; distortion, droplets by an elec. field 955
Alloys, band structure in disordered, and impurity semiconductors 840
Allylthiourea, kinetics of reacn. between AgBr and an adsorbed layer of 725
Alumina, adsorption of gases on, 106; adsorption of ions from buffer solns. by, and silica–, gels, 284; LiOH effect on activity of, catalyst, 448; dynamic gas adsorption on, 517; heat of immersion for rutile, 649; thermal transformation of, and their hydrates. 946
Aluminum, cation and anion exchange capacity on, 1; X-ray diffraction studies in Al_2O_3–SnO_2–TiO_2 system, 11; effect of Al ions in electrokinetics of ZnS–H_2O interface, 466; potentiometric titration of, halides with K in liq. NH_3, 567; anodic oxidn. in liq. NH_3, 571; detection of polynuclear complex, ions by means of coagulation measurements 951
Ammonia, exchange reacn. between D and, on surface of metal powders, 309; introduction to symposium on liq., chemistry, 545; paramagnetic resonance absorption in K solns. in liq., 546; thermochemistry of alkali and alkaline earth metals in liq., 553; electrolysis of Na and K dihydrophosphides in liq., 559; polarography of metals ions in liq., 564; potentiometric titration of Al, Ga, In and Tl halides with K in liq., 567; unfamiliar oxidn. states in 571
Ammonium fluosilicate, soly. of 529
Ammonium iodide, addn. of I to Me_4NI 122
Ammonium ions, adsorption from buffer solns. by silica, alumina and silica–alumina gels 284
Anthracene, crit. phenomena of ethylene–, system 578
Antimony, anodic behavior of, 203; retrograde solid solys. in Ge 831
Arabic acid, interacn. of Na and K ions with 189
Argon, adsorption isotherms on glass spheres, 84; adsorption on Mo, 178, 912; phys. adsorption on CdO 186
Aspartic acid, metal chelating tendencies of 690

BANCROFT, W. D. Portrait of 480A
Band structure, in disordered alloys and impurity semiconductors 840
Bentonite, effect of exchangeable bases on colloidal properties of 6
Benzene, resonance line of *p*-dichloro-, 501; dipole moments of, 538; sorption by fatty acids, 641; adsorption by MoS_2, 653; selective adsorption of 2,4-dimethylpentane–,–silica gel, 710; vapor pressures of perdeutero– 966
Benzoic acid, equil. exchange rates of adsorbed radio Active, with non-radioactive, in soln 382
Beryllium, X-ray diffraction and sorption–desorption studies in system BeO–In_2O_3 ..... 883, 885
Bovine fibrinogen, effect of ionic strength on interacn. of thrombin and 377
Bromine, Br^{80} in study of surfaces, 129; intensity measurements of resonance of Br^{79} and Br^{81} 743
Burning, steady-state, of a semi-infinite solid or liquid 242
Butadiene, copolymn. of α-methylstyrene and 346
n-Butanol, volume contraction of H_2O and, on addn. of electrolyte 978
Butylcarbinol, synergistic effects of antifoaming agents 2-ethylhexanol and diiso- 684
Butyl mercaptans, molar polarizations of isomeric 344

CADMIUM, phys. adsorption on CdO, 186; pyrolysis of $CdMe_2$, 226; partial molal vols. of $Cd(NO_3)_2$ and H_2O in concd. aq. solns., 245; formation consts of, complexes of ethylenediaminetetraacetic acid 874
Calcium hysteresis of contact angles in system paraffin-air-3-molar $CaCl_2$ soln., 455; thermochemistry of, and, halides in liq. NH_3, 553; self-diffusion coeffs. of, ions in cation-exchange membranes, 687; equil. in aq. ternary system of Ca^{++}, Sr^{++} and Cl^- 717
n-Caproic acid, adsorption by C 215
Caprylic acid, sorption of benzene by 641
Carbon, properties of capillary-held liquids, 56; adsorption in capillaries, 64; adsorption of gases on, 106; computation of pore sizes from phys. adsorption data, 149; effect of steam activation on multilayer adsorption from soln. by, 215; desorption of radiocolloidal Th^{234} from graphite, 443; development of stepwise isotherms on, black surfaces, 469 (corrn.) 980; apparatus for measuring flocculation in oils, 540; adsorption on, from soln., 634; heat of immersion for graphon, 649; heats and entropies of adsorption on a homogeneous, surface 657
Carbon, C^{14}, monolayer of, sagged stearic acid in new approach to surface research, 134; equil. exchange rates of adsorbed radioactive benzoic acid with non-radioactive benzoic acid in soln 382
Carbon monoxide, adsorption on Fe surfaces, 159; phys. adsorption on CdO 186
Carotenes, sorption at a liq.–liq. interface 638
Catalase, kinetics and thermodynamics of, with H_2O_2. 290
Catalysts, electron and X-ray diffraction studies of Fe Fischer–Tropsch 730
Cellulose, wetting characteristics of, derivs 49
Cerium complex salts, paramagnetic resonance in solid state 508
Cetane, LiOH addn. to cracking catalysts for cracking of 448
Chelates, metal, tendencies of glutamic and aspartic acids, 690. spectrophotometric detn. of stabilities of ethylenediaminetetraacetate 694
Chloride ion, binding of, by serum albumin 472
Chlorine compounds, pure quadrupole spectra of solid 496
Chlorophyll, sorption at a liq.–liq. interface 638
Chromatography, paper, of chloroplast pigments 638
Chromium, anodic polarization of passive and non-passive Cr–Fe alloys, 280; polarography of, ions in liq. NH_3 564
Chromium, Cr^{51}, surface reacns. of Cr in dil. $Cr^{51}O_4^=$ solns 139
Clay, cation and ion exchange capacity on, 1; effect of exchangeable bases on colloidal properties of bentonite 6
Cobalt, structure of, catalysts supported on diatomaceous earth 865
Coloration, effects of impurities on, of solids by ionizing radiations 749
Color centers, interacn. of, with their environment 762
Contact angles, wetting characteristics of cellulose derivs. from interrelations of, 49; alteration of surface properties of Ag and Au as indicated by, measurements, 165; surface roughness as related to hysteresis of 211, 455, 458
Copper, retrograde solid solys. in Ge and Si, 831; effect of, impurities on recombination of holes and electrons in Ge, 853; formation consts. of, complexes of ethylenediaminetetraacetic acid 874
Cotton, mechanism for wetting of 98
Critical phenomena, of satd. solns. in binary systems .. 578
Critical phenomena, of satd. solns. in ternary systems. 581

Crystals, survey of imperfections in nearly perfect, 737; phys. chemistry of ionic, involving small concns. of foreign substances, 738; evidences of crystalline imperfections in nuclear magnetism, 743; effects of impurities on coloration of solids by ionizing radiations, 749; theory of luminescence of impurity-activated 780
Cumene hydroperoxide, kinetics of reacn. of Fe(II) and 925
Cyclohexane, effect of solubilized, on viscosity of polysoap solns., 352; kinetics of reacn. of Fe(II) and Ph⁻, hydroperoxide 925
Cyclohexanediol-1,2, system *cis*- and *trans*- 597

DECANE, mol. wt. of 172
n-Decanol, electrocapillarity in 239
Deuterium, exchange reacn. between NH_3 and, on surface of metal powders, 309; CH_4–, exchange reacns. on Ni, 321; vapor pressure of perdeutero-benzene and -cyclohexane 966
Diatomaceous earth, structure of Co catalysts supported on 865
Dielectric constant, pressure dependence of, of H_2O .. 978
Diffusion, new method of measuring, coeffs, 104; estimation of heterogeneity from, measurements, 125; in a central field due to van der Waals attraction, 307; consts. of rat liver lactic dehydrogenase 609
Dodecylbenzenesulfonic acid, crit. micelle concn. by Na salt of 628
n-Dodecyldimethylbenzylammonium chloride, crit. micelle concn. of 628
Dodecyl sulfate, crit. micelle concns. of Na, by a bubble pressure method 898
n-Dotriacontane, polymorphism of 222

ELECTRIC moment, of hydrocarbons 538
Electrode phenomena, and thermodynamics of irreversible processes 275
Electrokinetic processes, in parallel and series combinations 341
Electrolysis, non-steady state, under const. current .. 701
Ellipsoids, Maxwell-Wagner dispersion in suspension of 934
Ethanol, thermal analysis of hydrazine–, system, 435; adsorption of, vapor on glass spheres 660
Ethyl chloride, adsorption in capillaries, 64; variation of viscosity of, vapor with temp 589
Ethylene, X-ray studies of crystalline and amorphous order in high polymers, 22; solv. of naphthalene in supercrit., 575; crit. phenomena of anthracene–, stilbene–, and hexamethylbenzene–, systems, 578; crit. phenomena for naphthalene–hexachloroethane–, system, 581; wetting of solid polytetrafluoro-, by H-bonding liqs 622
Ethylenediaminetetraacetic acid, spectrophotometric detn. of stabilities of metal chelates of, 694; formation consts. of metal complexes of 874
Ethylene glycol, hysteresis of contact angles in paraffin–air–, system 458

FARADAIC admittance, theory of—analysis of current—interrupter method 257
Filter paper testing, prepn. and use of metallic aerosols for 68
Flame, kinetics of elementary, reacns., 396; theory of, propagation 403
Flocculation, apparatus for measurement of, of colloidal suspensions in oils 540
Fluorine, properties of capillary-held, fluorochloromethane, 56; colloidal properties of fluorocarboxylic acids, 247; magnetic resonance shifts in halomethanes, 481; configuration of bifluoride ion, 486; f. p. diagram of UF_6–HF system, 541; structure of OF_2, 699; surface chemistry of fluorocarbons and their derivs. 923
Foaming, inhibition of 684
Formamide, polarographic studies in 964
Free energy, in cation interchange, 618; equil. function and standard, of adsorption 665

GALLIUM, potentiometric titration of, halides with K in liq. NH_3, 567; anodic oxidn. in liq. NH_3 571
Gas flow, new approach to, in capillary systems 35
Germanium, solv. in elements of groups III, IV and V, 827; retrograde solid solv. of Sb and Cu in, 831; segregation of impurities during growth of, crystals, 836; effect of Ni and Cu impurities on recombination of holes and electrons in, 853; changes of surface conductivity of, with ambient, 860; refractive index of germane, 938; vibrational spectra of, halogen metalorg. compds 939
Glass, new approach to gas flow in capillary systems, 35; adsorption isotherms of K and A on 3 mm., spheres, 84; steady state flow rates measured on, 330; transient state flow rates measured on, 334; adsorption of EtOH vapor on, spheres, 660; metals in at. state in 753
Glutamic acid, metal chelating tendencies of 690
Glycerol, hysteresis of contact angles in paraffin–air–, system, 455; e.m.f. studies of aq. HCl and 463
Glycine, effect of dipolar ions on activity coeffs. of, 375; vapor pressure of, derivs 607
Gold, alteration of, surface properties, shown by contact angle measurements, 165; formation of colloidal 670

HEAT of reaction, of alkali and alkaline earth metals in liq. NH_3 553
Heat of wetting, thermistor calorimeter for 649
Helium, steady state flow in porous media 330
Heptane, adsorption isotherms of *n*-, on TiO_2, SnO_2 and Sn, 251; selective adsorption of 2,4-dimethylpentane–benzene–silica gel 710
1-Hexadecanesulfonic acid, extent of hydration of salts of 428
Hexanes, adsorption of isomeric, on condensed stearic acid monolayers, 80; effect of solubilized, on viscosity of polysoap solns 352
Hexanol, synergistic effects of antifoaming agents 2-Et-, and diisobutylcarbinol 684
Hydrazine, unimol. decompn. of, 403; absorption spectra of free NH and NH_2 radicals produced by flash photolysis of, 415; thermal analysis of MeOH–, and EtOH–, systems 435
Hydrochloric acid, e.m.f. studies of aq., and glycerol .. 463
Hydrogen, adsorption on Fe surfaces, 159; effect of ultrasonic waves on, overvoltage, 268; kinetics of surface reacns. in interacns. between adsorbed mols. with special reference to para-, conversion, 318; para-, conversion on W, 320; reacn. of O and, on submerged Pt electrode catalysts, 674; exchange reacn. of T and 723
Hydrogen fluoride, f.p. diagram of UF_6–HF system, 541; vapor pressure of, 600, (corrn.) 980; liq.–vapor equil. in system UF_6–HF 905
Hydrogen peroxide, kinetics and thermodynamics of catalase with, 290; kinetics of formation in aq. ZnO suspensions 363

INDIUM, potentiometric titration of, halides with K in liq. NH_3, 567; anodic oxidn. in liq. NH_3, 571; X-ray diffraction and sorption–desorption studies in system BeO–In_2O_3 ..... 883, 885
Iodine, addn. to Me_4NI, 122; active magnesia adsorption of 182
Iron, H and CO adsorption on, surfaces, 159; anodic polarization of passive and non-passive Cr–Fe alloys, 280; D–NH_3 exchange reacn. on surface of, powder, 309; surface tension by sessile drop method, 359; mol. interaction between *n*-PrOH and, or, oxides, 591; electron and X-ray diffraction studies of, Fischer–Tropsch catalysts, 730; kinetics of reacns. of Fe(II) and hydroperoxides based on cumene and cyclohexane 925
Iron carbonyl, aerosols for filter paper testing 68
Irreversible processes, electrode phenomena and thermodynamics of 275
Isonicotinamide, hydrolysis in HCl 900
Isooctane, permeation of water and, through crushed quartz 40

KEROSENE, analysis of an aerosol produced by spraying, from a swirl-chamber nozzle 95
Krypton, adsorption isotherms on glass spheres 84

LACTIC dehydrogenase, rat liver ... 609
Lead, polarography of, ions in liq. NH_3, 564; sensitization of X-ray emulsions by, salt ... 802
Light, scattering by large spherical particles, 90; measurement of particle sizes in polydispersed systems by, transmission measurements, 95; scattering from non-Gaussian chains ... 958
Lithium, thermochemistry of, and, halides in liq. NH_3 553
Lithium fluoride, crystalline imperfections in ... 743
Lithium hydroxide, effect on activity of cracking catalysts ... 448
Luminescence, theory of, of impurity-activated crystals ... 780
Luminescent centers, emission and absorption in ... 776

MACROMOLECULES, adsorption of flexible ... 584
Magnesia, active, adsorption in preferred positions ... 182
Magnesium fluosilicate, soly. of ... 529
Magnetic resonance, proton and F, shifts in halomethanes, 481; spectrum of a linear 3-spin system ... 486
Manganese, emission and absorption in luminescent centers in ... 776
Mass spectrometer, trace element detn. by ... 809
Maxwell–Wagner dispersion, in a suspension of ellipsoids ... 934
Mercury, electrocapillarity in dielecs. at dropping electrode, 239; viscosity of, vapor and potential function for, 336; photothermal decompn. of mixed Ag and mercurous oxalates, 437; application of polarized, pool electrodes to polarography ... 824
Methacrylic acid, thermal degradation of polymethyl methacrylates ... 879
Methane, mol. vol. of, 172; D–, exchange reacns. on Ni, 321; chem. significance of quadrupole spectra ... 490
Methanol, thermal analysis of hydrazine –, system ... 435
Micelles, structure of, 87; colloidal properties of highly fluorinated alkanoic acids, 247; detn. of crit., concn. by equil. dialysis, 628; detn. of crit., concns. by a bubble pressure method ... 898
Molal volume, partial, of $Cd(NO_3)_2$ and H_2O in concd. aq. solns ... 245
Molybdenum, adsorption of gases on, 178; adsorption of benzene and water vapor by MoS_2, 653; adsorption of A, N_2, O_2 and CO on ... 912
Monoethanolamine, conductivity of undecane-3 sodium sulfate with ... 889

NAPHTHALENE, diffusion through, 476; soly. in supercrit. ethylene, 575; crit. phenomena for ethylene–hexachloroethane–, system ... 581
Neutron, diffraction studies on $ScVO_4$ and Sc_2O_3, 535; analysis for trace impurities by, activation ... 815
Nickel, D–NH_3 exchange reacn. on surface of, powder, 309; CH_4–D exchange reacns. on, 321; surface tension by sessile drop method, 359; effect of, impurities on recombination of holes and electrons in Ge ... 853
Nickel oxalate, pptn. of 715; dissocn. pressure of, dihydrate ... 863
Nitric acid, kinetics of thermal decompn. of, vapor ... 390
Nitrogen, new approach to gas flow in capillary systems, 35; gas-adsorbent equil. on system O–NO activated C, 106; phys. adsorption on single crystal Zn surfaces, 143; computation of pore sizes from, desorption isotherms, 149; field emission microscope and flash filament techniques for, adsorption on W, 153; adsorption on Mo, 178; active magnesia adsorption of, 182; phys. adsorption on CdO, 186; steady state flow in porous media, 330; transient state flow in porous media, 334; adsorption on rutile, 349; dynamic, adsorption methods ... 517
Nitrogen oxides, bimol. reversible decompn. of NO, 403; rate of dissocn. of N_2O_4 ... 418
Nucleic acid, interacn. of Na and K ions with ... 189
Nylon, electrolytic interacn. with NaOH solns ... 370

n-OCTACOSANE, polymorphism of, ... 222
Octadecane, solid state phase changes in ... 520
n-Octylsodium sulfosuccinate, radiotracer study of sulfate ion adsorption at air/soln. interface in di- ... 916
Ovalbumin, denaturation with surface active ions ... 614
Oxygen, reacn. of Na–K alloy with H_2O in presence and absence of, 385; reacn. of H and, on submerged Pt electrode catalysts, 674; adsorption on Mo ... 912
Oxygen, O^{18}, exchange of isotopic O between V_2O_5, O_2 and H_2O ... 229
Oxygen fluoride, structure of ... 699
Ozone, 2-step chain mechanism in decompn. of ... 403

PALMITIC acid, packing orientation of soap crystallites ... 26
Paraffin, surface roughness and contact angles of water–air–, system, 211; hysteresis of contact angles in systems 3 molar $CaCl_2$ soln.–air–, and glycerol–air–, 455; hysteresis of contact angles in systems ethylene glycol–air–, Me cellosolve–air–, and MeOH–air– ... 458
Pentane, mol. vol. of, 172; surface tension of some fluoro– ... 923
Pentene-1, dipole moments of ... 538
Phase changes, application of absolute rate theory to, in solids ... 942
Phase rule, equil. in aq. ternary system of Ca^{++}, Sr^{++} and Cl^- ... 717
Phosphoric acid, distribution of rare earths in tributyl phosphate, 294, (corrn.) ... 980
Phosphoric acid, P^{32}, in study of surfaces ... 129
Phosphors, chemistry of ... 773
Phosphorus, electrolysis of Na and K dihydrophosphides in liq. NH_3 ... 559
Photographic emulsion, effect of impurities on optical sensitization of, 797; sensitization of X-ray, by very small quantities of a Pb salt ... 802
Photolysis, vacuum, of AgBr ... 791
Picolinamide, hydrolysis in HCl ... 900
β-Pinene, rate of thermal isomn. in vapor phase ... 902
Platinum, reacn. of H and O on submerged, electrode catalysts ... 674
Polarization, anodic, of passive and non-passive Cr–Fe alloys, 280; molar, of isomeric Pr and Bu mercaptans ... 344
Polarography, of Pb, Cd, Zn, Ni, Co, Cr and Al ions in liq. NH_3, 564; application of polarized Hg pool electrodes to, 824; detn. of relative formation consts. of metal complexes of ethylenediaminetetraacetic acid, 874; studies in formamide ... 964
Pore sizes, computation from phys. adsorption data ... 149
Potassium, interacn. of, ions with arabic, agar and nucleic acids, 189; equil. in aq. systems containing Sr^{2+}, K^+, Na^+ and Cl^-, 207; reacn. of Na–K alloy with H_2O, 385; paramagnetic resonance absorption in, solns. in liq. NH_3, 546; electrolysis of K dihydrophosphide in liq. NH_3 ... 559
Potassium chloride, colored by colloidal metal, 757; interacn. of color centers with environment, 762; activator system for Tl-activated, phosphor ... 780
Potential, thermodynamics of ionized H_2O in $SrCl_2$ solns. from e.m.f. measurements ... 531
n-Propyl alcohol, adsorption isotherms on TiO_2, SnO_2 and Sn, 251; mol. interacn. between Fe or Fe oxides and ... 591
Propyl mercaptans, molar polarizations of isomeric ... 344
Proteins, adsorption on, 324; streaming orientation studies on denatured ... 614
Proton, magnetic resonance shifts in halomethanes ... 481
Pyrrolidone, macromol. properties of polyvinyl- ... 110

QUARTZ, electrokinetic relations in acetone–, system 430

RAYS, Roentgen, diffraction studies in system BeO–In_2O_3 ... 883
Reaction velocity, and thermodynamics of catalase with H_2O_2, 290; of surface reacns. in interacns. between adsorbed mols., 318; of CH_4–D exchange reacns. on Ni, 321; of photo-oxidn. on surface of aq. ZnO, 363; of Na–K alloy with H_2O, 385; of thermal decompn. of HNO_3 vapor, 390; of elementary flame reacns., 396; of dissocn. of N_2O_4, 418; general notations for systems of simultaneous reacns., 599; of reacn. between AgBr and an adsorbed layer of allylthiourea, 725; of hydrolysis of picolinamide and isonicotinamide in concd. HCl, 900; of thermal isomn. of β-pinene in vapor phase, 902; of reacns. of Fe(II) and hydroperoxides based on cumene and cyclohexane ... 925
Resin, ion exchange, cation and anion exchange capacity on, 1; equil. studies of Ag–Na–H system on Dowex 50, 254; free energy in cation interchange,

618; electromigration in a cation, 687; sepn. of trace impurities, 819; H_2O vapor sorption by polystyrenesulfonic acid, 969; H_2O vapor sorption by cross-linked polystyrenesulfonic acid 974
Resonance, paramagnetic, in the solid state 508
Resonance absorption, paramagnetic, of free radicals, 504; paramagnetic, in K solns. in liq. NH_3 546
Rutile, N adsorption on 349

SCANDIUM, extraction of tracer, into tributyl phosphate, 294 (corrn.) 980; neutron diffraction of $ScVO_4$ and Sc_2O_3 535
Sebacic acid, sp. heat of polyhexamethylene sebacamide 14
Sedimentation, in the ultracentrifuge 194
Serum albumin, binding of chloride by 472
Silica, permeation of water and isooctane through crushed quartz, 40; properties of capillary-held liquids, 56; elec. properties of, particle suspensions in oils, 72; adsorption of gases on, gel, 106; bound H_2O in, gel, 219; adsorption of ions from buffer solns. by, and alumina-gels, 284; heat of immersion for, 649; chem. nature of, carried by steam, 706; selective adsorption of 2,4-dimethylpentane–benzene–, gel, 710; detn. of particle sizes in colloidal 932
Silicic acid, polymn. of poly–, 604; studies on, gels ... 678
Silicon, surface tension by sessile drop method, 359; soly. in elements of groups III, IV and V, 827; retrograde solid solys. of Cu in, 831; segregation of impurities during growth of, crystals, 836; optical investigations of impurity levels in 849
Silver, alteration of, surface properties as shown by contact angle measurements, 165; equil. studies of Ag–Na–H system on Dowex 50, 254; mechanism of coagulation of lyophobic sols as revealed through Ag halide sols, 301; photothermal decompn. of mixed Ag and mercurous oxalates, 437; kinetics of reacn. between AgBr and an adsorbed layer of allylthiourea, 725; decrease in soly. of Ag_2S in ZnS, 738; vacuum photolysis of AgBr, 791; adsorption of, salts on, 895; coagulation effects of $Al(NO_3)_3$ on aq. sols of, halides 951
Soap, packing orientation of, crystallites, 26; aerogels from lubricating greases, 30; elec. properties of, fiber suspensions in oils, 72; effect of C_6-hydrocarbons on viscosity of poly-, solns., 352; electron microscopic studies of paraffinic Na 354
Sodium, interacn. of, ions with arabic and nucleic acids, 189; equil. in aq. systems containing Sr^{2+}, K^+, Na^+ and Cl^-, 207; equil. studies of Ag–Na–H system on Dowex 50, 254; electrolytic interacn. of nylon with aq. NaOH, 370; reacn. of Na–K alloy with H_2O, 385; electrolysis of Na dihydrophosphide in liq. NH_3, 559; self-diffusion coeffs. of, ions in cation-exchange membranes 687
Sodium, Na^{24}, in study of surfaces 129
Sodium chloride, diffusion through wood, 476; colored by colloidal metal 757
Soils, capillary rise of water in, under field conditions. 45
Sorption, of carotenes at a liq.–liq. interface 638
Sound, velocity in liquids 453
Specific heat, of synthetic polyhexamethylene adipamide and sebacamide 14
Spectra, absorption, of free NH and NH_2 radicals produced by flash photolysis of hydrazine 415
Spectra, quadrupole, chem. significance of, 490; pure, of solid Cl compds., 496; pure, of mol. crystals 501
Spectra, vibrational, of Sn and Ge halogen metalorg. compds 939
Stearic acid, packing orientation of soap crystallites, 26; adsorption of isomeric hexanes on condensed, monolayers, 80; monolayer of C^{14}-tagged, in new approach to surface research, 134; electron microscopy of paraffinic Na soaps, 354; sorption of benzene by. 641
Stilbene, crit. phenomena of ethylene–, system 578
Strontium, equil. in aq. systems containing Sr^{2+}, K^+, Na^+ and Cl^-, 207; equil. in aq. ternary system of Ca^{++}, Sr^{++} and Cl^- 717
Strontium chloride, thermodynamics of ionized H_2O in, solns. from e.m.f. measurements, 531; distribution between solid and liq. KCl 738
Styrene, X-ray studies of crystalline and amorphous order in high polymers, 22; copolymn. of butadiene and α-Me–, 346; H_2O vapor sorption by polystyrenesulfonic acid, 969; H_2O vapor sorption by cross-linked polystyrenesulfonic acid resins 974
Sulfate ion, radiotracer study of, adsorption at air/soln. interface in di-*n*-octylsodium sulfosuccinate .. 916
Sulfur, S^{33}, radiotracer study of sulfate ion adsorption at air/soln. interface 916
Surface, applications of radiotracers to study of, 129; new approach to, research, 134; reacns. of Cr in dil. $Cr^{51}O_4^=$ solns., 139; area analysis by means of gas flow methods, 330, 334; dynamic gas adsorption methods of, area detn. 517
Surface tension, of Si, Fe and Ni by sessile drop method, 359; of fluorocarbons and their derivs. 923

THALLIUM, potentiometric titration of, halides with K in liq. NH_3, 567; anodic oxidn. in liq. NH_3, 571; activator system for, activated KCl phosphor 780
Thermal transpiration, calcn. of 910
Thorium, Th^{234}, interacn. of uranyl ions with UX_1-(Th^{234}) in acid soln., 440; peptization of UX, by metallic ions 443
Thrombin, effect of ionic strength on bovine fibrinogen–, interacn. 377
Tin, X-ray diffraction studies in Al_2O_3–SnO_2–TiO_2 system, 11; adsorption isotherms of *n*-heptane, *n*-PrOH and H_2O on SnO_2 and, 251; vibrational spectra of, halogen metalorg. compds. 939
Titanium, X-ray diffraction studies in Al_2O_3–SnO_2–TiO_2 system, 11; adsorption isotherms of *n*-heptane, *n*-PrOH and H_2O on TiO_2, 251; charging processes on anodic polarization of 262
Trace element, detn. by mass spectrometer, 809; analysis for, impurities by neutron activation, 815; ion-exchange sepn. of, impurities 819
Trapping processes in ZnS 785
Tritium, exchange reacn. of H and 723
Tungsten, field emission microscope and flash filament techniques for N adsorption on, surfaces, 153; parahydrogen conversion on 320
Tyrosine, vapor pressure of, derivs. 607

ULTRACENTRIFUGE, sedimentation in, 194; transient solute distribution from basic, eq. 312
Ultrasonic waves, effect on H overvoltage 268
Undecane-3 sodium sulfate, conductivity of, with monoethanolamine laurate 889
Undecanoic acid, wetting of adsorbed monolayers of ω-monohydroperfluoro- 622
Uranium, interacn. of uranyl ions with UX_1(Th^{234}) in acid soln., 440; f. p. diagram of UF_6–HG system, 541; liq.–vapor equil. in system UF_6–HF 905

n-VALERIC acid adsorption by C 215
Valine, vapor pressure of, derivs. 607
Vanadium, exchange of isotopic O between V_2O_5, gaseous O and H_2O, 229; neutron diffraction of $ScVO_4$, 535; formation and titration of colloidal vanadic acid 681
Vapor pressure, of HF, 600 (corrn.) 980; of acetylated amino acid Et esters 607
Vinyl compds., macromol. properties of polyvinylpyrrolidone 110
Viscosity, of hydrocarbons, 172; of Hg vapor, 336; effect of C_6 hydrocarbons on, of polysoap solns., 352; variation of, of EtCl vapor with temp. 589

WATER, capillary rise of, in soils under field conditions, 45; pressure dependence of dielec. const. of .. 978
Wetting agents, role of surface active agents in wetting 98
Wood, diffusion of dissolved materials through 476

YTTRIUM, extraction of tracer, into tributyl phosphate, 294, (corrn.) 980

ZINC, phys. adsorption on single crystal, surfaces, 143; kinetics of photo-oxidn. on surface of ZnO, 363; effect of Al ions in electrokinetics of H_2O–ZnS interface, 466; soly. of zinc fluosilicate, 529; polarography of, ions in liq. NH_3, 564; self-diffusion coeffs. of, ions in cation-exchange membranes, 687; emission and absorption in luminescent centers in ZnS, 776; traps and trapping processes in ZnS 785

New Schedule

BACK ISSUE PRICES

AMERICAN CHEMICAL SOCIETY JOURNALS

Effective January 1, 1953

Single copies or complete volumes of nearly all the ACS journals listed below may be purchased at these prices.

Journal	Current Year		Back Years			
	Member	Non-Member	Member	Non-Member	Foreign Postage	Canadian Postage
AGRICULTURAL AND FOOD CHEMISTRY	$0.40	$0.50	...	...	$0.15	$0.05
ANALYTICAL CHEMISTRY	.40	.50	$0.60	$0.75	.15	.05
Analytical Edition (I&EC)						
Volumes 1–4	...	...	1.60	2.00	.15	.05
Volumes 5–8	...	...	1.00	1.25	.15	.05
Volumes 9 et seq.	...	...	.60	.75	.15	.05
CHEMICAL ABSTRACTS, Volumes 11–44						
Numbers 1–22	...	...	1.00	1.25	.15	.05
Numbers 23 and 24	...	...	2.40	3.00*	.45	.15
CHEMICAL ABSTRACTS, Vol. 45 et seq.						
Numbers 1–22	1.00**	2.00	1.60**	2.00	.15	.05
Number 23 (Author Index)	6.00**	12.00	9.60**	12.00	free	free
Number 24 (Subject, Patent, Formula Indexes, complete)	12.00**	24.00	19.20**	24.00	free	free
CHEMICAL AND ENGINEERING NEWS	.15	.15	.15	.15	.05	free
INDUSTRIAL AND ENGINEERING CHEMISTRY	.60	.75	.80	1.00	.15	.05
Industrial Edition (I&EC)	...	...	.80	1.00	.15	.05
JOURNAL OF THE AMERICAN CHEMICAL SOCIETY, Vols. 32–73	...	...	1.00	1.25	.15	.05
JOURNAL OF THE AMERICAN CHEMICAL SOCIETY, Vol. 74 et seq.	.50	.75	.80	1.00	.15	.05
JOURNAL OF PHYSICAL CHEMISTRY	1.00	1.25	1.20	1.50	.15	.05

RATES FOR VOLUMES OF BACK NUMBERS

	Member	Non-Member	Foreign Postage	Canadian Postage
ANALYTICAL CHEMISTRY (formerly Analytical Edition)	$6.00	$7.50	$0.75	$0.25
CHEMICAL ABSTRACTS				
Volumes 11–44	20.00	25.00	2.40	.80
Volume 45 et seq.	50.80**	63.50	2.40	.80
CHEMICAL AND ENGINEERING NEWS (Volumes 1–24)	2.80	3.50	2.25	.75
CHEMICAL AND ENGINEERING NEWS (Vol. 25 et seq.)	5.60	7.00	2.25	.75
INDUSTRIAL AND ENGINEERING CHEMISTRY	8.80	11.00	2.25	.75
JOURNAL OF THE AMERICAN CHEMICAL SOCIETY (Vol. 32 et seq.)	12.00	15.00	1.50	.50
JOURNAL OF PHYSICAL CHEMISTRY (Vol. 56 et seq.)	10.00	12.50	1.20	.40

(Prior Volumes—Order from Walter Johnson, 125 East 23rd Street, New York 10, N. Y.)

* Each part, when divided.

** The member discount for Volume 45 et seq. applies only if purchase is for personal use and not for resale.

●

AMERICAN CHEMICAL SOCIETY

Back Issue Department

1155 Sixteenth St., N.W. Washington 6, D. C.